



Elaboration of New Layer by Layer (LbL) Fluorescent thin films and their functionalization for the sensitive detection of bacteria

Yayang Tian

► To cite this version:

Yayang Tian. Elaboration of New Layer by Layer (LbL) Fluorescent thin films and their functionalization for the sensitive detection of bacteria. Organic chemistry. Université Paris Saclay (COMUE), 2018. English. NNT : 2018SACLN029 . tel-01867306

HAL Id: tel-01867306

<https://theses.hal.science/tel-01867306>

Submitted on 4 Sep 2018

HAL is a multi-disciplinary open access archive for the deposit and dissemination of scientific research documents, whether they are published or not. The documents may come from teaching and research institutions in France or abroad, or from public or private research centers.

L'archive ouverte pluridisciplinaire **HAL**, est destinée au dépôt et à la diffusion de documents scientifiques de niveau recherche, publiés ou non, émanant des établissements d'enseignement et de recherche français ou étrangers, des laboratoires publics ou privés.

Elaboration of new layer-by-layer (LbL) fluorescent thin films and their functionalization for the sensitive detection of bacteria

Thèse de doctorat de l'Université Paris-Saclay
préparée à l'École Normale Supérieure Paris-Saclay

École doctorale n°571 Sciences Chimiques : Molécules, Matériaux,
Instrumentation et Biosystèmes (2MIB)
Spécialité de doctorat: Chimie

Thèse présentée et soutenue à Cachan, le 16 Juillet 2018, par

M^{lle} Yayang TIAN

Composition du Jury :

Mme Marie ERARD	
Professeure, Université Paris-Sud (Laboratoire de Chimie Physique)	Président
Mme Eléna ISHOW	
Professeure, Université de Nantes (Laboratoire CEISAM)	Rapporteur
M. Andrey KLYMCHENKO	
Directeur de Recherche, CNRS, Université de Strasbourg (Laboratoire de Bioimagerie et Pathologies)	Rapporteur
M. Donal O'SHEA	
Professeur, Royal College of Surgeons in Ireland (Pharmaceutical & Medicinal Chemistry)	Examineur
Mme Bianca SCLAVI	
Directrice de Recherche CNRS, École Normale Supérieure Paris-Saclay (LBPA)	Examinatrice
M. Gilles CLAVIER	
Directeur de Recherche, CNRS, École Normale Supérieure Paris-Saclay (PPSM)	Directeur de thèse
Mme Rachel MEALLET-RENAULT	
Professeure, Université Paris-Sud (ISMO)	Co-Directrice de thèse







Nothing happens until something moves.
When something vibrates, the electrons of the entire universe resonate with it.
Everything is connected.

Albert Einstein

Table of content

Abbreviations	vii
General introduction.....	1
Chapter 1 Introduction: bibliographical background.....	3
1.1 Introduction of bacteria detection	3
1.1.1 Introduction of bacteria	3
1.1.2 Antimicrobial resistance (AMR)	4
1.1.3 Current methods for bacteria detection.....	6
1.1.4 Discussion on the detection methods	10
1.2 Layer-by-Layer (LbL) self-assembly	11
1.2.1 Layer-by-Layer (LbL) self-assembly	11
1.2.2 Main factors in LbL self-assembly process.....	12
1.3 Fluorescent polymers.....	14
1.3.1 The principle of molecular fluorescence.....	14
1.3.2 BODIPY	16
1.3.3 Fluorescent polymers.....	18
1.3.4 Reversible addition fragmentation transfer (RAFT) polymerization.....	19
1.3.5 Click chemistry	21
1.3.6 Combination of click chemistry and RAFT polymerization	23
References	25
Chapter 2 BODIPY-based Fluorescent Polymer Chains Thin Film Devices for Bacteria Detection	39
2.1 The synthesis and features of the three pairs of fluorescent polymer chains (FPCs)	41
2.1.1 Synthesis of three pairs of fluorescent polymer chains (FPCs).....	41
2.1.2 The features of three pairs of fluorescent polymer chains (FPCs).....	42
2.2 Characterization of FPCs in solution	44
2.2.1 Photophysical properties of FPCs in solution	44
2.2.2 Zeta potential of FPCs in solution	44
2.2.3 Isoelectric point of SW FPCs in H ₂ O	45
2.3 Layer-by-layer assembly deposition process investigation with SW FPCs.....	46

2.4 Photophysical and surface characterizations of the three types of FPC LbL films	48
2.5 Stability and toxicity assessments of the three types of FPC LbL films	51
2.5.1 Stability study of the FPC LbL film.....	51
2.5.2 Toxicity assessments	52
2.6 <i>E. coli</i> bacteria detection with FPC LbL films.....	53
2.6.1 Effect of the concentration of the deposition solution on <i>E. coli</i> bacteria detection with SW FPC LbL films	53
2.6.2 Effect of the nature of fluorescent polymers on <i>E. coli</i> bacteria detection.....	55
2.7 Mechanism of <i>E. coli</i> bacteria detection with LW FPC LbL films	57
2.7.1 FPC localization with methylene blue (MB).....	57
2.7.2 Dead-alive assay with propidium iodide (PI)	57
2.8 Conclusions	58
Experimental Section	60
References	64
Chapter 3 Single fluorescent layer LbL film based on metal-enhanced fluorescence (MEF) for bacteria detection	67
3.1 Au nanoparticles (Au NPs) and modified Au NPs preparation	69
3.1.1 Au nanoparticles (Au NPs) synthesis.....	69
3.1.2 Polymer coating of Au NPs (Au NPs@PAH)	69
3.2 Characterization of Au NPs and Au NPs@PAH	70
3.2.1 Photophysical study of Au NPs and Au NPs@PAH in solution.....	70
3.2.2 Zeta potential of Au NPs and Au NPs@PAH in solution	71
3.3 Synthesis of polycation, polyanion and fluorescent GFPC ⁻	71
3.3.1 Synthesis of fluorescent P(APEG-co-GBDPMA-co-AA) (GFPC ⁻)	71
3.3.2 Synthesis of P(APEG-co-DMEA) (PC ⁺)	73
3.3.3 Synthesis of P(APEG-co-AA) (PC ⁻).....	73
3.4 Characterization of the polyelectrolytes	74
3.4.1 Spectroscopic properties of BDPMA and GFPC ⁻	74
3.4.2 Zeta potential of polyelectrolytes.....	75
3.5 Preparation and characterization of Au NPs@PAH surfaces.....	76
3.6 Fabrication and spectroscopic study of Au NPs/PCs/GFPC ⁻ LbL surfaces	77
3.6.1 Fabrication of Au NPs/PCs/GFPC ⁻ LbL films.....	77

3.6.2 Spectroscopy study of Au NPs/PCs/GFPC ⁻ LbL films	78
3.7 The Au NPs/PCs/GFPC ⁻ LbL surfaces for bacteria detection	83
3.8 Conclusion	85
Materials and methods	86
References	91
Chapter 4 “Click”-based Layer-by-Layer Antibody Nanostructured Surface for Selective Bacteria	
Detection	93
4.1 Synthesis of 4-dibenzocyclooctynol functionalized poly(acrylic acid-co-poly(ethylene glycol) methyl ether acrylate) (DIBO-PC ⁻) and poly(2-(dimethylamino)ethyl acrylate-co-poly(ethylene glycol) methyl ether acrylate) (PC ⁺)	94
4.1.1 Synthesis of DIBO-PC ⁻	94
4.1.2 Synthesis of PC ⁺	96
4.2 Preparation and characterization of DIBO-PC ⁻ surface	97
4.3 Specific bacteria detection based on immunoassay between anti- <i>E. coli</i> antibody surface and <i>E. coli</i>	98
4.4 Azide-modified antibody preparation and anti- <i>E. coli</i> antibody surface preparation in a microfluidic set up	99
4.5 Surface passivation with bovine serum albumin (BSA)	101
4.6 Effect of fluidic conditions on the stability and sensitivity of the anti- <i>E. coli</i> antibody surface for <i>E. coli</i> detection	102
4.7 Effect of the concentration of anti- <i>E. coli</i> antibody on the sensitivity of the anti- <i>E. coli</i> antibody surface for <i>E. coli</i> detection	103
4.8 Specificity evaluation	104
4.9 Conclusion	105
Materials and methods	106
References	111
Chapter 5 pH sensitive Layer-by-Layer film surface for bacteria growth detection	
5.1 Synthesis of fluorescein azide, polyanion and polycation	118
5.1.1 Synthesis of fluorescein azide (FA)	118
5.1.2 Synthesis of polyanion	118
5.1.3 Synthesis of poly(2-(dimethylamino)ethyl acrylate-co-poly(ethylene glycol) methyl ether acrylate) (PC ⁺)	122
5.2 Characterization of fluorescein azide, polyanion and polycation	122

5.2.1 Spectroscopic properties of fluorescein azide and RFPC ⁻ in solution	122
5.2.2 Zeta potential of DIBO-SW PC ⁻ , DIBO-LW PC ⁻ and RFPC ⁻	123
5.3 pH sensitive surface preparation	124
5.3.1 DIBO-SW PC ⁻ / fluorescein surface preparation by click chemistry	124
5.3.2 DIBO-LW PC ⁻ / fluorescein surface preparation by click chemistry	125
5.3.3 (DIBO-LW PC ⁻ + RFPC ⁻) / fluorescein surface preparation by click chemistry	125
5.4 Characterization of DIBO-SW PC ⁻ /FA, DIBO-LW PC ⁻ /FA and (DIBO-LW PC ⁻ + RFPC ⁻)/FA surface	126
5.4.1 Fluorescence emission analysis of the LbL films	126
5.4.2 Fluorescence imaging of LbL films	127
5.5 Study of surface pH sensitivity	128
5.5.1 pH effect on DIBO-SWPC ⁻ /fluorescein surface	128
5.5.2 pH effect on RFPC ⁻ /fluorescein surface	129
5.6 Study of bacterial growth on the pH sensitive surfaces	129
5.6.1 Real-time detection of <i>E. coli</i> growth in modified M9 minimal medium	129
5.6.2 Study of <i>E. coli</i> growth on pH sensitive DIBO-SW PC ⁻ /fluorescein surface	130
5.6.3 Study of <i>E. coli</i> growth on pH sensitive DIBO-LW PC ⁻ /fluorescein surface	133
5.6.4 Study of <i>E. coli</i> growth on pH sensitive RFPC ⁻ /fluorescein ratiometric surface	134
5.7 Conclusion	135
Materials and methods	137
References	144
General conclusion and perspectives	147
Acknowledgements	151

Abbreviations

AA	Acrylic acid
ACPA	4,4'-azobis(4-cyanopentanoic acid)
AFM	Atomic force microscopy
AIBN	2,2'-azobis(2-methylpropionitrile)
AMR	Antimicrobial resistance
APEG	Poly(ethylene glycol) methyl ether acrylate
ATRP	Atom transfer radical polymerization
Au NPs	Spherical gold Nanoparticles
B	Brightness
BDPMA	BODIPY methacrylate
BODIPY	4,4-difluoro-4-bora-3a,4a-diaza-s-indacene
BSA	Bovine serum albumin
<i>B. subtilis</i>	<i>Bacillus subtilis</i>
CFU	Colony forming unit
CDs	Carbon dots
CRP	Controlled/living radical polymerization
CTA	Chain transfer agent
CuAAC	Copper-catalyzed azide-alkyne cycloaddition
DBU	1,8-diazobicyclo[5,4,0]undec-7-ene
DCC	N,N'-dicyclohexylcarbodiimide
DCM	Dichloromethane
DEG	Diethylene glycol
DIBO	4-dibenzocyclooctynol
DIBO-PC⁻	Negatively charged polymer chain with DIBO moiety
DIBO-SWPC⁻	Negatively charged short polymer chain with DIBO moiety
DIBO-LWPC⁻	Negatively charged long polymer chain with DIBO moiety
DMAP	4-dimethylaminopyridine
DMEA	2-(Dimethylamino)ethyl acrylate
DMF	Dimethylformamide
DMSO	Dimethyl sulfoxide

<i>E. coli</i>	<i>Escherichia coli</i>
EIS	Electrochemical impedance spectroscopy
EM	Electromagnetic
Et₃N	Triethylamine
FA	Fluorescein azide
FPC	Fluorescent polymer chain
FRP	Free radical polymerization
GFPC⁻	Green fluorescent long chains and weak polyanion
FRET	[2-(Acryloyloxy)ethyl]trimethylammonium
FITC	Fluorescein isothiocyanate
IgG	Immunoglobulin G
IR	Infrared
K_d	Dissociation constant
LbL	Layer-by-Layer
LW PFC	Relatively long chains and weak polyelectrolytes
LW FPC⁺	Positively charged long chains and weak polyelectrolytes
LW FPC⁻	Negatively charged long chains and weak polyelectrolytes
M9 medium	M9 Minimal growth medium
MB	Methylene blue
MEF	Metal-enhanced fluorescence
M_w (NMR)	NMR estimated number-average molar mass
NMP	Nitroxide mediated polymerization
NMR	Nuclear magnetic resonance
NPs	Nanoparticles
OD	Optical density
OD₆₀₀	Optical density at 600 nm
PAH	Poly(allylamine hydrochloride)
PBS buffer	Phosphate buffered saline buffer
PC⁺	Positively charged polymer chains
PC⁻	Negatively charged polymer chains
PCR	Polymerase Chain Reaction
PEO	Poly(ethylene oxide) (see PEG)

PEOA	Poly(ethylene oxide) methyl ether acrylate
PEG	Polyethylene glycol (see PEO)
pH	Hydrogen ions
PI	Propidium iodide
pKa	Acid dissociation constant
PMMA	Poly(methyl methacrylate)
[(PPh₃)₃CuBr]	Bromotris(triphenylphosphine)copper(I)
QDs	Quantum dots
RAFT	Reversible addition-fragmentation chain transfer
RI	Refractive index
RFPC⁻	Negative red fluorescent polymer chain
RPM	Revolutions per minute
RT	Room temperature
SEM	Scanning electron microscope
SPAAC	Strain promoted alkyne-azide cycloaddition
SPR	Surface Plasmon Resonance
SS FPC	Relatively short chains and strong polyelectrolytes
SS FPC⁺	Positively charged chains and strong polyelectrolytes
SS FPC⁻	Negatively charged chains and strong polyelectrolytes
SW FPC	Relatively short chains and weak polyelectrolytes
SW FPC⁺	Positively charged short chains and weak polyelectrolytes
SW FPC⁻	Negatively charged short chains and weak polyelectrolytes
TCSPC	Time-correlated single photon counting
TFA	Trifluoroacetic acid
THF	Tetrahydrofuran
TMS	Tetramethylsilane
TTCA	2-methyl-2-[(dodecylsulfanylthiocarbonyl)sulfanyl] propanoic acid
SPM	3-Sulfopropyl methacrylate
TMEA	Fluorescence resonance energy transfer
UV	Ultraviolet
WHO	World health organization
vis.	Visible

λ_{abs}	Absorption wavelength
λ_{ex}	Excitation wavelength
λ_{em}	Fluorescence emission wavelength
λ_{max}	Maximum absorption or emission wavelength
Φ_{F}	Fluorescence quantum yield
τ	Fluorescence lifetime
ζ	Zeta potential

General introduction

General introduction

Antibiotics have been used for the treatment of bacterial infections for over 70 years, saving millions of lives. The current antibiotic resistance crisis has been attributed to the overuse and misuse of these medications. Therefore, the prevention of infection transmission by the rapid and sensitive detection of antibiotic resistant strains is needed in managing this crisis. Fluorescent polymers show great potential for bacteria detection, because they are easy to functionalize and graft. Compared with the methods used for bacterial detection in liquid, bacterial detection on a film surface is more convenient, easier to handle and is amenable to device development that can be easily reused. The goal of my PhD work is to develop fluorescent and sensitive nanostructured polymer films on surface for bacterial detection.

In chapter 2, we describe how a first generation of nanostructured fluorescent LbL films were designed and fabricated for bacterial detection (*E. coli*). Firstly, green BODIPY methacrylate (BDPMA) as the fluorescent monomer was synthesized. Subsequently, the water-soluble and biocompatible poly(ethylene oxide) acrylate (PEOA) was selected as another monomer. Different types of basic (ammoniums) and acidic (carboxylates or sulfonates) groups were available for the positively and negatively charged units, respectively. Three pairs of BODIPY-based fluorescent polyelectrolytes (FPC) with different features were synthesized based on reversible addition-fragmentation transfer (RAFT) polymerization: relatively Short chains and Weak polyelectrolytes (SW FPCs), Short chains and Strong polyelectrolytes (SS FPCs) and Long chains and Weak polyelectrolytes (LW FPCs). Subsequently, FPC LbL films were fabricated on activated glass slides by means of electrostatic attraction. The photophysical and surface properties of FPC LbL films were controlled by adjusting the deposition conditions. The effects of the concentration of the deposition solution and the nature of FPCs on *E. coli* bacteria detection were evaluated. Finally, the possible mechanism of *E. coli* bacteria detection on FPC LbL film surface was proposed.

Chapter 3 describes the effort to increase the films' sensitivity by using the metal-enhanced fluorescence (MEF) principle. A MEF based LbL film was prepared and tested for bacteria detection. Firstly, spherical gold nanoparticles (Au NPs) were synthesized and coated with positively charged poly(allylamine hydrochloride) (PAH). Modified Au NPs were deposited on activated glass slides. Based on the previous results, described in Chapter 2, the green fluorescent long chains and weak polyanion (GFPC⁻) was selected as the fluorescent layer. Different films containing Au NPs and GFPC⁻ were fabricated and the distance between the Au NPs and GFPC⁻ was adjusted by changing the numbers of layers with two oppositely charged "blank" polymers (PC⁺ and PC⁻). The surface morphologies of Au NPs surfaces and photophysical properties of all Au NPs/ PCs/LW FPC⁻ surfaces were carried out. Finally, these Au NPs/ PCs/LW FPC⁻ surfaces were employed for *E. coli* detection.

In Chapter 4, we describe how the selectivity of LbL films was added by introducing an antibody on the surface of the film to provide specific recognition of a chosen bacterial strain. This LbL surface was designed to achieve a rapid, effective and specific detection of *E. coli* bacteria. The polyanion and polycation with a 4-dibenzocyclooctynol (DIBO) functional group were assembled on the activated glass slides and an anti-*E. coli* antibody containing a clickable azide group was introduced on the surface in a single step based on the strain-promoted azide-alkyne cycloaddition (SPAAC) reaction. After the surface passivation, the antibody surface was used for bacteria detection. The influence of various parameters such as fluidic condition and concentration of antibody on the sensitivity of the antibody surface for bacteria detection was investigated. Finally, the selectivity of anti-*E. coli* antibody surface was tested with *E. coli* and *B. subtilis*.

In the last chapter, chapter 5, an alternative approach to detect bacterial growth on thin LbL film by introducing pH sensitive fluorophore (fluorescein) is presented. The growth of bacteria is often associated with a decrease in pH of the growth medium due to a release of acidic metabolites. Two single-signal pH sensitive surfaces containing fluorescein with different features and one ratiometric pH sensitive surface combining fluorescein with insensitive BODIPY were designed and prepared for the detection of bacterial growth. First, the synthesis of different functionalized polyanions (short and long chain of DIBO-PC⁻ and red fluorescent polymer) was carried out. Three types of pH sensitive surfaces containing fluorescein (DIBO-SWPC/fluorescein, DIBO-LWPC/fluorescein and ratiometric RFPC/fluorescein surfaces) were prepared based on the combination of LbL assembly and copper-free click chemistry. Their photophysical and surface properties were studied. Finally, the bacterial growth detection was performed on each surface.

Chapter 1

Introduction: bibliographical background

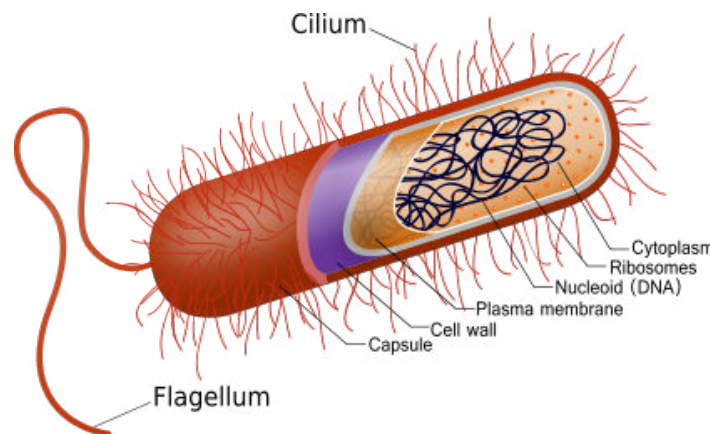
Chapter 1 Introduction: bibliographical background

1.1 Introduction of bacteria detection

Bacteria were among the first life forms on our Earth. The production of oxygen from photosynthetic bacteria made the existence of humans and multiple varieties of species possible. We can find microbes everywhere (soil, water, the Eiffel Tower, on the skin and in gut of the human body, *etc.*), they are extremely adaptable to different environmental conditions. Many of bacteria are beneficial to our everyday life. In industry, bacteria are important in sewage treatment [1, 2] and the breakdown of oil spills [3]. Our favorite cheese, yogurt and wine are produced through bacterial fermentation. In addition, the vast majorities of the bacteria in the body are harmless and even have positive effects on the immune system, though many are beneficial particularly in the gut flora [4].

1.1.1 Introduction of bacteria

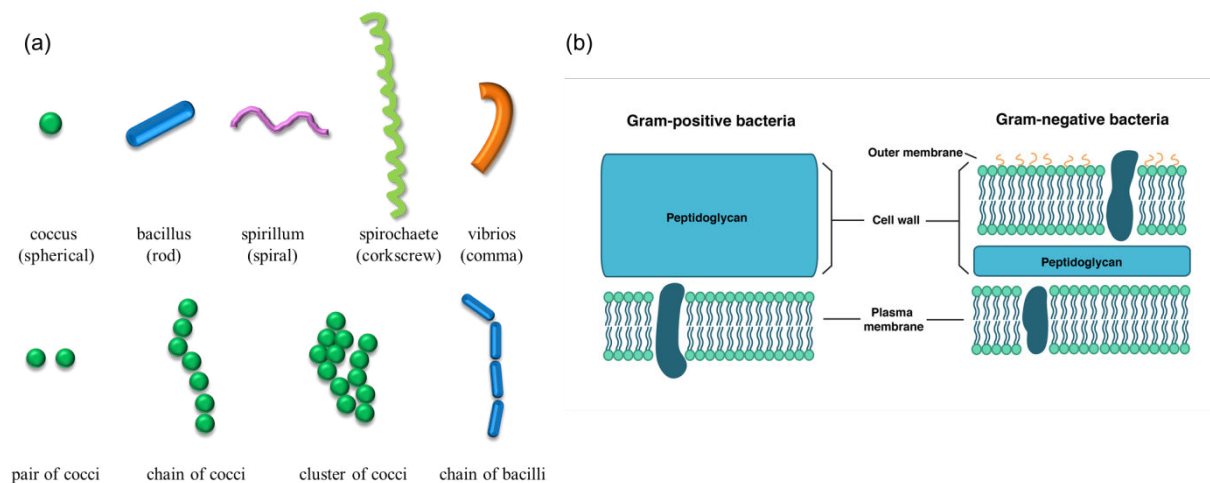
Bacteria are single-celled microbes (Scheme 1.1). The cell structure is simple, containing a single circular genome with the genetic information. Some bacteria have a plasmid as an extra set of genetic material, and normally genes contained in the plasmid give the bacterium more advantages than other bacteria. For instance, it may contain genes that provide antibiotic resistance to bacteria [5]. In addition, they have flagella, which can be used for motility [6].



Scheme 1.1. Structure of typical bacteria (from [7]).

Bacteria can be divided into five groups based on their basic shapes and sizes: spherical (cocci), rod (bacilli), spiral (spirilla), corkscrew (spirochaetes) and comma (vibrios). After cell division, they can exist in different morphologies: single cells, in pairs, chains or clusters (Scheme 1.2a). Moreover, bacteria can be classified into two major groups on the basis of cell wall composition: gram-positive and gram-negative (Scheme 1.2b). The difference between two

cell wall is that gram-positive bacteria has only one membrane and thick peptidoglycan while there are an inner cell membrane, a thin layer of peptidoglycan and an outer cell membrane in gram-negative bacteria. Some receptors (*e.g.*, antigen) as the components of bacteria cell wall can be specifically bound with the recognition elements (*e.g.*, aptamer, antibody and phage) [8]. In general, the surface antigens have different classification [9]: the O-antigen is the external component of the lipopolysaccharide located in the cell wall [10]; the H-antigen is determined based on flagellar proteins [11] and the capsule's K antigen [12]. In addition, the composition of antigens varies between different bacterial strains and antigens can be detected using immunological tests [13].



Scheme 1.2. (a) The different bacterial shapes. (b) The cell wall composition of gram-positive and gram-negative bacteria (from [14]).

1.1.2 Antimicrobial resistance (AMR)

However, the most common serious and even fatal diseases are caused by bacterial infections. The Black Death, the most devastating pandemic in human history, which was caused by the bacterium *Yersinia pestis*, killed 30-60% of Europe's total population in the medieval period [15]. Generally, the majority of pathogenic bacteria can cause disease because pathogens attach to host cells for nutrients and produce toxins and virulence factors that affect host cells in different ways [16].

For the treatment of bacterial infections, the use of microorganisms for the management of microbial infections in ancient Egypt, Greece and China is well-documented [17]. The American microbiologist Selman Waksman and his colleagues first coined the term “antibiotics” to describe chemical substances produced by microorganisms and having the capacity to inhibit the growth of other microorganisms [18]. The modern era of antibiotics started with the discovery of penicillin by Alexander Fleming in 1928 [17, 19]. Since then, antibiotics have transformed modern medicine and have led to intense research [20]. Antibiotics were first prescribed to treat

serious infections and saved millions of lives since the 1940s [21]. At the beginning of the use of antibiotics, penicillin was successful in controlling bacterial infections among World War II soldiers. However, penicillin has become less effective very soon and penicillin resistant strains began to appear in infected patients [22]. In response, new antibiotics were studied, developed, and marketed. Only 3 years later, however, the first case of methicillin-resistant *Staphylococcus aureus* (MRSA) was identified and during that same decade, in the United Kingdom in 1962 and in the United States in 1968 [23]. Repeating the cycle, multiple new antibiotics were once again discovered and introduced into commercial use since the 1960s. Unfortunately, bacterial resistance continued to spread and has been seen for nearly all antibiotics that have been developed (Figure 1.1). As a result, in 2018, more than 70 years after the first patients were treated with antibiotics, bacterial infections have again become a threat.

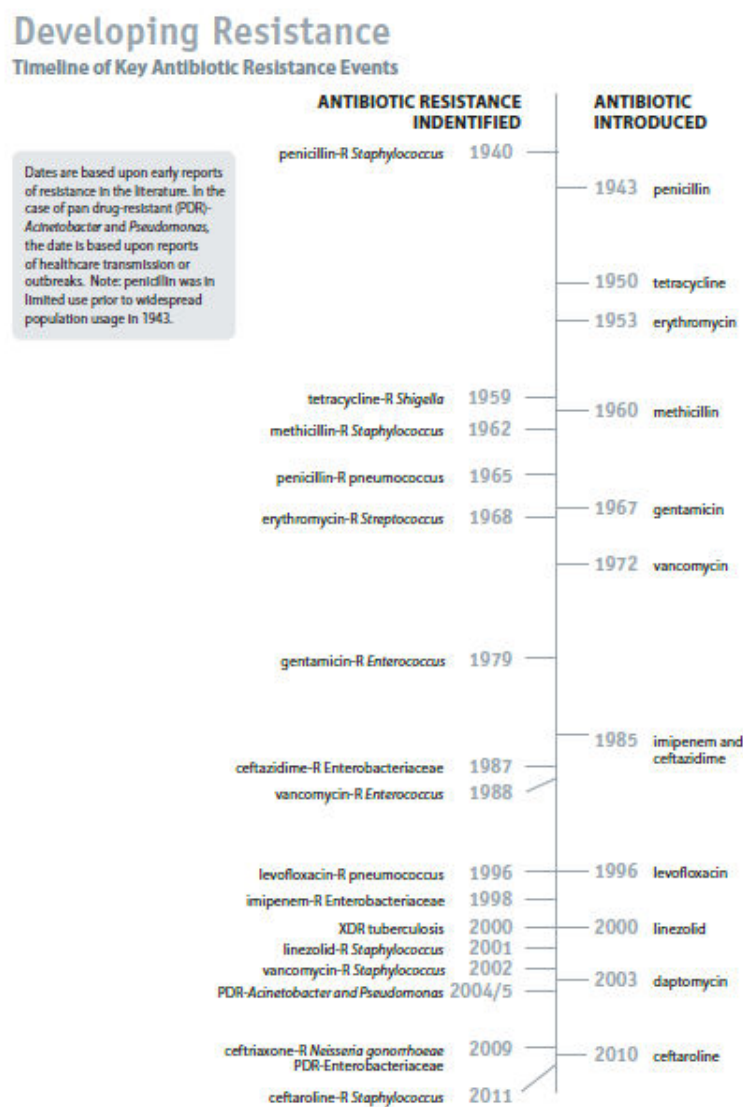


Figure 1.1. Developing antibiotic resistance: a timeline of key events. (from [24])

There are many causes of the emergence of antibiotic resistance. (i) Overuse, the direct relationship between the overuse of antibiotic and the emergence of resistant bacteria strains has been demonstrated in epidemiology [25]. On one hand, there are still a large number of antibiotics prescribed in the U.S. [26], and in many other countries, the use of antibiotics without a doctor's prescription is also a very big problem [27]. (ii) Inappropriate prescribing, incorrectly prescribed antibiotics, like stopping the treatment too early, can make the promotion of resistant bacteria [28]. (iii) Extensive agricultural use, they are also used in farming and for farm animals in many countries to produce larger yields and higher quality product or promote growth and prevent infection of animals [29].

Antibiotic resistance phenomenon reflects evolutionary processes of bacteria that take place during the above use of antibiotic. The emergence of resistant bacteria, especially multidrug-resistant bacteria, is already widespread and endangers the efficacy of antibiotics in therapy [30]. Therefore, beside the development of new antibiotics [31], preventing infection transmission is also expected to be effective in managing this crisis. Rapid and sensitive bacteria detection is significant not only to prevent contamination of food, air and water [32, 33] but also for medical diagnostics to identify bacterial contamination in medical settings [34, 35].

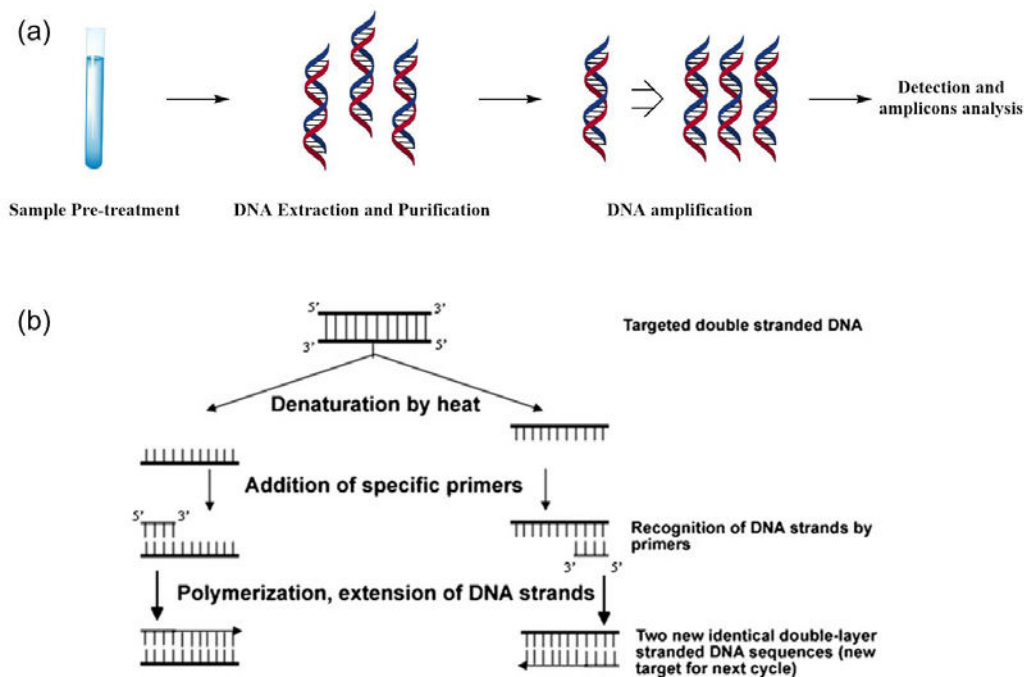
1.1.3 Current methods for bacteria detection

Colony forming unit (CFU) counting is one of the conventional bacteria detection methods relying on pre-enrichment in non-selective culture broth, selective enrichment, plating on agar, and counting of colonies after 37-48 h or more. This is time-consuming and requires large amounts of samples and materials and may miss most types of bacteria [36-38]. This is clearly insufficient, and the development of rapid detection methods has been a focus for many researchers. Alternative methods have been developed based on nucleic acid amplification and on biosensors based on different sensing technologies [39].

1.1.3.1 Nucleic acid amplification based technologies

Detection methods based on nucleic acid amplification include Polymerase Chain Reaction (PCR), Loop Mediated Isothermal Amplification (LAMP) and Nucleic Acid Sequence Based Amplification (NASBA). All of these technologies involve four main steps: sample preparation, DNA extraction, nucleic acid amplification and amplicons analysis (Scheme 1.3a). PCR is the most popular in bacterial detection since it was developed in 1986 [40]. It is based on the isolation, amplification and quantification of a short DNA sequence including the targeted bacteria's genetic material. Different PCR methods have been developed for bacterial detection: the classic end point PCR (epPCR) [41], quantitative or real time PCR (qPCR) [42], multiplex PCR (mPCR) [43], reverse transcriptase PCR (rtPCR) [44] and viability PCR (vPCR) [45]. Scheme 3b illustrates the PCR method, consisting in different cycles of denaturation by heat of the extracted and purified DNA, followed by an extension phase using specific primers and a

thermostable DNA polymerization enzyme. In the following step, each new double-stranded DNA acts as starting material for a new cycle and exponential amplification is thus obtained [36]. The amplicon products are subsequently detected by gel electrophoresis. Among the different PCR variants, qPCR is based on fluorescent detection enabling amplicon quantification in real time and quicker results [46]. mPCR allows multiple and simultaneous detection of several organisms by introducing different primers to amplify DNA regions coding for specific genes of each targeted bacterial strain [47]. The user cannot discriminate between viable and dead cells from the above PCR techniques due to the presence of DNA in all cells. rtPCR targets RNA transcripts in order to detect viable cells only. This method must be performed quickly due to the fast degradation of RNA [48]. vPCR has also been developed to discriminate between viable and dead cells. Prior to the DNA extraction, free DNA that has been released from dead cells is blocked with an impermeable nucleic acid binding dye, which will prevent the amplification of such DNA during the PCR [49].

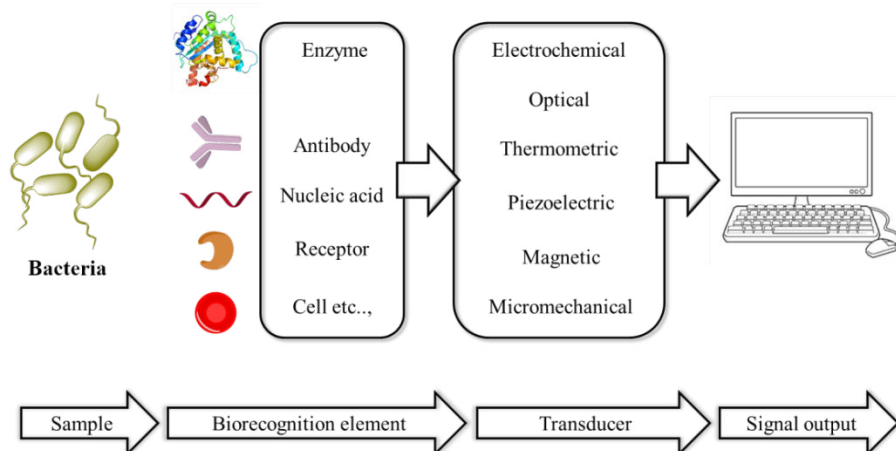


Scheme 1.3. (a) The main steps of the nucleic acid amplification based technologies; (b) Schematic representation of one PCR cycle taking place in thermocycler (from [36]).

LAMP is a technique developed by Notomi *et al.* in 2000, which is based on DNA amplification under isothermal conditions [50]. LAMP shows high specificity because six different regions of a gene are targeted by independent sequences for a selective identification. Four different primers are subsequently used in combination to amplify the target gene segment, thus offering higher sensitivity and shorter analysis time. NASBA is based on enzymatic activity of reverse transcriptase that amplifies RNA templates into complementary DNA under

isothermal conditions which was developed by Compton in 1991 [51]. This technique is able to detect viable cells.

1.1.3.2 Biosensors



Scheme 1.4. Schematic representation of a biosensor.

Biosensors are defined as analytical devices combining a biological element (*e.g.* enzymes, antibodies, nucleic acids, receptors, cell, tissue, *etc.*), a biologically derived component (*e.g.*, aptamers, engineered proteins, *etc.*) or a biomimic material (*e.g.*, combinatorial ligands and synthetic catalysts) intimately integrated within or associated with a physicochemical transducer, which may be electrochemical, optical, thermometric, piezoelectric, micromechanical or magnetic [52]. Enzymes, antibodies and nucleic acids are three main classes of biological recognition elements which are applied to biosensor applications (Scheme 1.4). The following parts discuss biosensors classified according to their transduction methods.

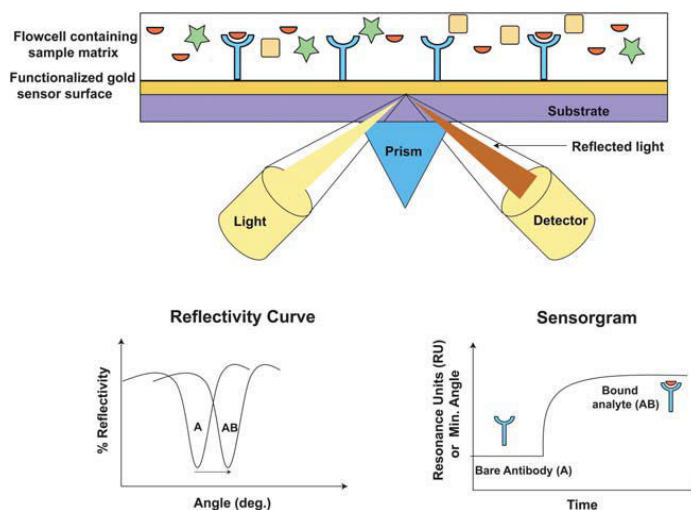
(1) Electrochemical biosensors

This kind of devices are mainly based on the detection of changes in electrical current or potential when the target analyte is involved in the reaction that takes place at the sensor sample matrix interface. According to the observed parameter in the reaction, electrochemical biosensors are generally classified into three categories: amperometric (current), potentiometric (potential) and impedimetric (impedance) [53]. Amperometric methods are based on an existing linear relationship between analyte, concentration and current, the produced current at the electrode is measured at a fixed potential. In amperometric detection, the current signal is generated due to the reduction or oxidation of an electroactive metabolic product or intermediate on the surface of a working electrode [54]. Potentiometric methods are the least common of all biosensors maybe because a highly stable and accurate reference electrode is always required and challenging to

maintain. A potentiometric biosensor yields a logarithmic concentration response with a high dynamic range at zero current; therefore, it enables the detection of extremely small concentration changes [55]. Electrochemical impedance spectroscopy (EIS) represents a powerful method for the study of conducting materials and interfaces. A cyclic function of small amplitude and variable frequency is applied to a transducer, and the resulting current is used to calculate the impedance at each of the frequencies probed in this technique [56]. Although this methodology is widely accepted due to its ease of operation and simple sensor preparation, extreme care must be taken to ensure the equivalent circuit obtained makes physical sense, because the same impedance data may well be fit by several different circuits [57]. One of the advantages of electrochemical biosensing is that it can be performed with turbid samples, such as milk.

(2) Optical biosensors

Optical biosensors are another commonly used technique in bacterial detection. Surface plasmon resonance (SPR) and fluorescence-based methods have been widely studied because of their high sensitivity. SPR biosensors measure the changes in refractive index occurring at a thin film metal surface caused by the interaction between the bacteria and the biorecognition species [58]. SPR has successfully been employed for bacterial detection by introducing antibodies as biorecognition elements [59]. A typical SPR biosensor instrument is depicted in Scheme 1.5 [60]. A substrate functionalized by a gold thin film is irradiated from the backside of the sample by p-polarized light through a prism. In the meantime, the reflectivity is recorded as a function of the angle of incidence. The observed SPR from the surface is a curve with a narrow dip. The angle of reflection is determined by the mass of material at the biosensor surface. When bacteria bind to the biorecognition elements on the surface and the mass of the surface layer is changed, the SPR angle shifts (from A to AB in Scheme 1.5). Hence, the change in SPR angle, and the binding reaction, can be measured in real time.



Scheme 1.5. A typical SPR biosensor set-up from Linman et al [60].

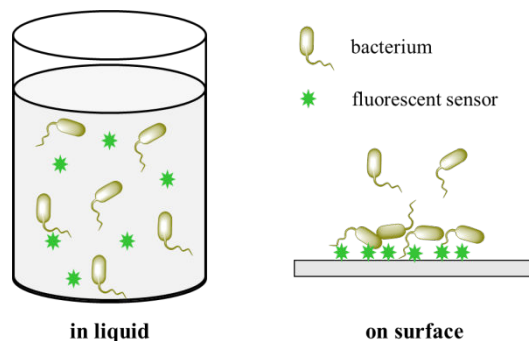
Fluorescence based biosensors are based on monitoring the fluorescence intensity which is related to the target bacteria, *e.g.* the concentration of the fluorescence sensor binding with bacteria or environment of bacteria changed by metabolite. The biorecognition element (antibody) may be conjugated to fluorescent probes. According to the types of fluorescent probes, this technique can be divided into three classes: organic dyes, nanoparticles, rare-earth elements [61]. Concerning the organic dyes, they are frequently used to target the bacteria *in vivo* through membrane permeability or detect the fluorescence intensity change in the environment surrounding bacteria. Fluorescein isothiocyanate (FITC) is one of the most common used dyes due to its higher quantum yield [62]. New multicolor fluorescent probes to target protein or DNA of bacteria are also developed by researchers. In order to decrease the signal from the background, the fluorescent probes with longer emission wavelength are studied [63]. Quantum dots (QDs) are the most popular nanoparticles owing to their good photostability and narrow photoluminescence spectra. The fluorescence emission wavelength of QDs can be tunable from blue to red by changing the particle size and chemical composition. Recently, fluorescent carbon dots (CDs) have emerged because they keep the same favorable photophysical characteristics than QDs but are more environmentally friendly since they do not contain any heavy metals [64]. For rare-earth elements, lanthanide-based fluorescent probes have gained extensive attention owing to the exclusion of light scattering, long fluorescence lifetime and red emission [65].

1.1.4 Discussion on the detection methods

Several alternative methods for bacteria detection have been developed to reduce the amount of sample necessary and the analysis time. Although nucleic acid amplification based technologies show high sensitivity and selectivity, the complex sample preparation (DNA extraction and purification), time needed (the extraction method takes around 5 hours [39]) and sophisticated and costly instruments limit their utilization. Electrochemical biosensors are highly sensitive and can work with turbid samples, however these techniques make data acquisition and interpretation complex and well-trained personnel is necessary. In optical biosensors SPR can detect bacteria within a short time and deliver sensitive and reliable data in a noninvasive manner. The main drawbacks of this technique are the complexity of the device and expensive equipment. Fluorescence based biosensor not only achieves sensitive and nondestructive detection, but also can provide rapid response. Hence, we proposed to design fluorescent sensors for bacteria detection.

Two pathways for bacteria detection are possible (Scheme 1.6). If we detect bacteria in liquid with a fluorescent material (Scheme 1.6 left), we need to introduce first the fluorescent probe into the sample suspension and then wait for a long incubation time to obtain sufficient interaction between bacteria and the fluorescent probe. The mixture of bacteria and probe must

then be concentrated through centrifugation before microscope observation. While in the case of film surface detection (Scheme 1.6 right), we can introduce the bacteria suspension onto the sample surface directly. The film surface can be used to capture the bacteria from the bacteria suspension. Compared with the method in bulk solution, a film for bacteria detection appears more effective, convenient, easier to operate and potentially recyclable. Moreover, the nanostructured fluorescent films have the potential for large specific surface area, leading to a high bacterial adsorption capacity [66]. Therefore, the goal of my PhD project is to develop fluorescent and sensitive nanostructured film on surfaces for bacteria detection.



Scheme 1.6. Comparison of fluorescent probe for bacteria detection in solution and on surface.

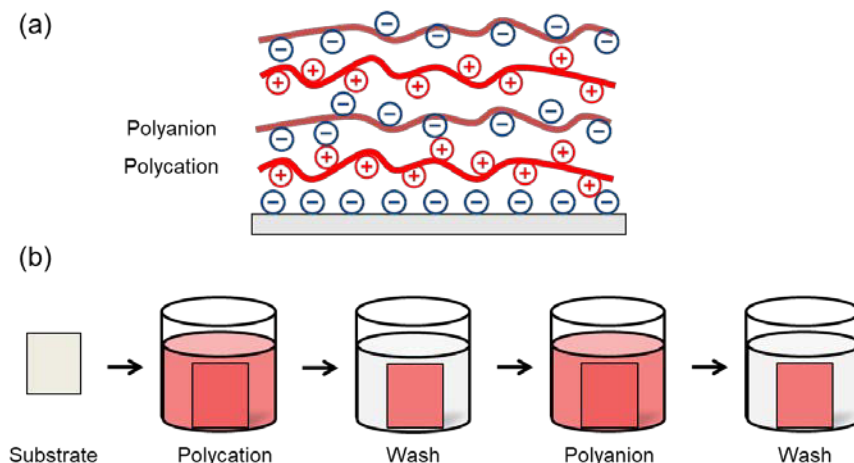
To our knowledge, bacterial detection on fluorescent nanostructured film surfaces is rarely considered. A first generation sensor will be designed and studied in our work. We select *Escherichia coli* (*E. coli*) as the model for bacteria detection instead of pathogenic bacteria. *E. coli* are gram-negative bacteria. They are typically rod-shaped and around 3.0 μm long and 0.5 μm in diameter. They also have flagella, which can be used for motility [6]. *E. coli* bacteria are one of the most widely utilized and investigated model organisms in microbiology and biotechnology because they can be cultured easily and divide quickly and have been intensively studied for over many years. For my research, we used *E. coli* strains K12 BW25113 which are well adapted to the laboratory environment and not pathogenic.

1.2 Layer-by-Layer (LbL) self-assembly

1.2.1 Layer-by-Layer (LbL) self-assembly

Layer-by-Layer (LbL) assembly was first introduced by Iler in 1966 [67]. The concept as a diverse bottom-up nanofabrication technique has been of considerable interest since its development by Decher in the 1990s [68-70]. The major advantage of the LbL assembly is its simple and low cost equipment: tweezers and beakers are the only apparatus required [71]. Another advantage of this method is that a large variety of materials can be used as LbL building blocks. Besides polymers (various functional polyelectrolytes, *e.g.*, poly(allylamine)

hydrochloride), poly(acrylic acid), *etc.*) [72-75], inorganic nanoparticles (clay, nanosheets, colloidal nanoparticles and modified zeolite crystals, *etc.*) [76, 77] and biological materials (polypeptides, nucleic acids and protein, *etc.*) [78-80] can also be assembled. In addition, the multilayer assemblies achieved by LbL technique are not always films depending on the templates. For instance, coating on planar templates yields thin films [81, 82]. Removing the templates leads to freestanding membranes. Performing the material modification on 3D templates, like nanoparticle, fiber, tubular structures, *etc.*, gives different corresponding nano-architectures [83-85].



Scheme 1.7. (a) Layer-by-layer film fabrication based on electrostatic attraction. (b) Immersive LbL assembly basic deposition process.

Since we will focus on nanostructured film preparation in my research, polyelectrolytes have been chosen as the suitable material. A brief principle of the layer-by-layer self-assembly is shown in Scheme 1.7a. Two oppositely charged polymers are deposited alternatively on a substrate by means of electrostatic attraction [86]. Other driving forces can be used such as hydrogen bonding [87], π - π interaction [88], click chemistry [89] or Van der Waals forces [90]. A typical LbL process is shown in Scheme 1.7b. A substrate is dipped into an aqueous solution of positively charged polymers for around 10 min, allowing polymers to deposit on the substrate, washed with water for few minutes, dried and subsequently dipped into an aqueous solution of negatively charged polymers. Multilayer thin films are prepared by simply repeating the basic deposition process [91]. Following this process, films are deposited on both sides of substrate.

1.2.2 Main factors in LbL self-assembly process

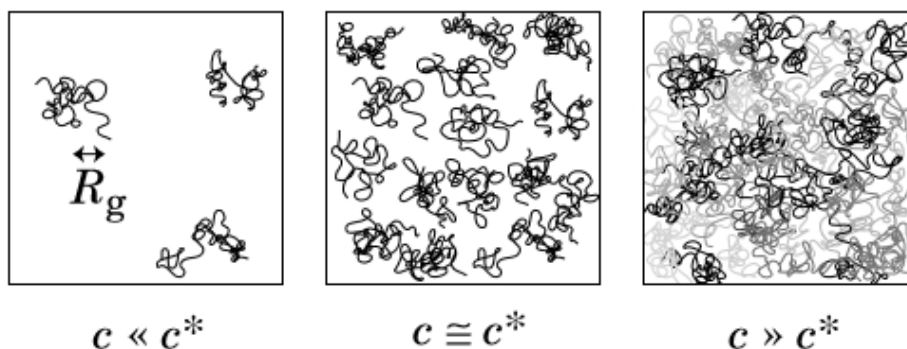
The quality of nanostructured films depends on the ionic properties of the polyelectrolytes in solution that is mainly affected by the molecular structure and concentration of polyelectrolytes, pH and ionic strength of the solution [92]. Herein, these factors will be discussed.

1.2.2.1 Nature of the polyelectrolytes

Many different natural and synthetic polyelectrolytes can be selected as building blocks in the LbL self-assembly process. The basic features required for the polyelectrolytes in bacterial detection are no/low toxicity and hydrophilicity. Polyelectrolytes with different charge densities, degrees of hydrophilicity and molecular weight will significantly affect the assembly behavior. The charge density of the polyelectrolytes depends on the type of polymer. Strong polyelectrolytes can be fully ionized when they dissociate in solution, whereas weak polyelectrolytes are partially ionized. Generally, the electrostatic interaction between polycation and polyanion for strong polyelectrolytes is stronger than in the case of weak polyelectrolytes, and probably there is a different interaction between the bacteria and LbL films. Moreover, the more hydrophobic the polyelectrolytes, the more compressed the structure of the multilayers, due to the contribution of strong hydrophobic electrostatic interaction between polycation and polyanion. On the other hand, the growth behavior of the LbL self-assembled polyelectrolytes multilayer is related to the molecular weight of the polyelectrolytes. For polyelectrolytes with higher molecular weight, the interaction among each chain is more complex and induces more stable and higher roughness multilayer films.

1.2.2.2 Effect of concentration of the polyelectrolytes

Besides the nature of polyelectrolytes, their concentration is also a crucial factor for the construction of multilayer films. More concentrated polyelectrolytes solutions are able to provide more electrostatic adsorption of polycation and polyanion (Scheme 1.8). It equals to say that the concentration might affect up to a certain point the percent coverage of the surface and then the thickness and roughness of the layer, which might influence the stability of the following layer. So one would expect that as the concentration increases the stability of the interaction with the following layer will at first increase and then start to decrease.



Scheme 1.8. The interaction of polyelectrolytes among each chain in dilute and concentrated solutions (from [93]).

1.2.2.3 Effect of pH

Modulating pH in the weak polyelectrolytes solutions can affect multilayer film construction as well as cross-link density and morphology owing to changes in degree of ionization with pH. Normally, the polycations are partially ionized in high pH solution ($\text{pH} \geq 8$) and the thin layer can be formed through adsorption, while polyanions ionization increases and thick layer will be deposited.

1.2.2.4 Effect of ionic strength

Ionic strength can affect the thickness and roughness of the layer because the addition of salt to the deposition solutions can shield the charges of the polyelectrolytes and then can change the conformation of polyelectrolytes in solution. Upon charge screening, the conformation of polyelectrolytes is transformed from an extended form to a more globular or coiled one, resulting in thicker layers.

The quality of the multilayer films is affected by the combination of each factor.

1.3 Fluorescent polymers

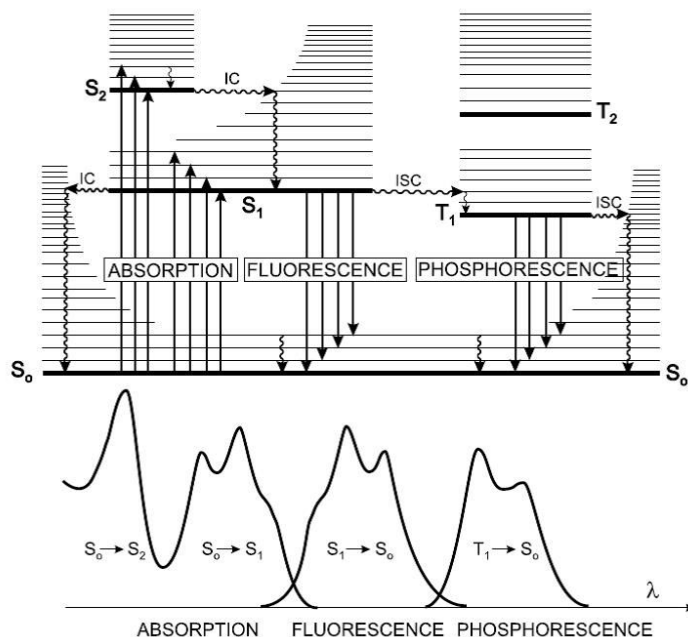
In order to prepare fluorescent nanostructured films with the LbL assembly technique, fluorescent polyelectrolytes should be designed and synthesized. First examine what is fluorescence.

1.3.1 The principle of molecular fluorescence

What happens when light meets matter? It depends on the property of matter and it is also related to the wavelength of light. The light can be reflected, transmitted, scattered or absorbed. There is a special kind of matter that can emit longer wavelength light when it absorbs an appropriate wavelength of light. We term the longer wavelength light as photoluminescence. Fluorescence is one type of photoluminescence where light is quickly emitted (< 10 ns) after absorption. Materials that can emit light upon excitation are called fluorophores.

Scheme 1.9 is a classic Perrin-Jablonski diagram that illustrates electronic energy levels of fluorophore molecules and the transitions between them. The various types of radiative (absorption, fluorescence emission and phosphorescence) and non-radiative (internal conversion and intersystem crossing) processes that occur in fluorophore molecules are clearly shown in the diagram. Absorption refers to the physical process of absorbing light. An electron of fluorophore molecules in the singlet ground state (S_0) can absorb a photon and be excited to a higher energy orbital, *e.g.*, S_1 , S_2 *etc.* The electron at the excited state of the horizontal multiplicity of spin can

release energy as non-radiative processes and arrive at the lower vibrational level of S_1 , which is called internal conversion (IC). When the electron at an excited state (S_1) returns to the ground state (S_0), fluorescence emission is radiated. The excited molecule (S_1) can also undergo an electronic state of different multiplicity of spin T_1 through an intersystem crossing (ISC). Emission from the T_1 state to S_0 is termed phosphorescence, which is generally shifted to longer wavelengths compared to the fluorescence [95].



Scheme 1.9. A classic Perrin-Jablonski diagram and illustration of the relative positions of absorption, fluorescence and phosphorescence spectra (from [94]). IC: internal conversion, ISC: intersystem crossing, S_i : singlet electronic state, T_i : triplet electronic state.

From the Perrin-Jablonski diagram, we can notice that the fluorescence emission wavelength is red shifted compared to the absorption wavelength, due to the energy loss through the non-radiative processes. This energy gap is called Stokes shift. In the fluorescence process, quantum yield (Φ_F) and lifetime (τ_F) are considered to be the most important characteristics. Fluorescence quantum yield is defined by the ratio of emitted photons to the absorbed photons. Commonly, the fluorescence quantum yield is less than 1 due to the non-radiative processes. The fluorescence quantum yield is given by

$$\Phi_F = \frac{\kappa_r}{\kappa_r + \kappa_{nr}}$$

where κ_r is the radiative rate constant and κ_{nr} the non-radiative rate constant.

The fluorescence lifetime is defined as the average time that the molecule spends in the excited state S_1 prior to returning to the ground state S_0 . The lifetime is

$$\tau_F = \frac{1}{\kappa_r + \kappa_{nr}}$$

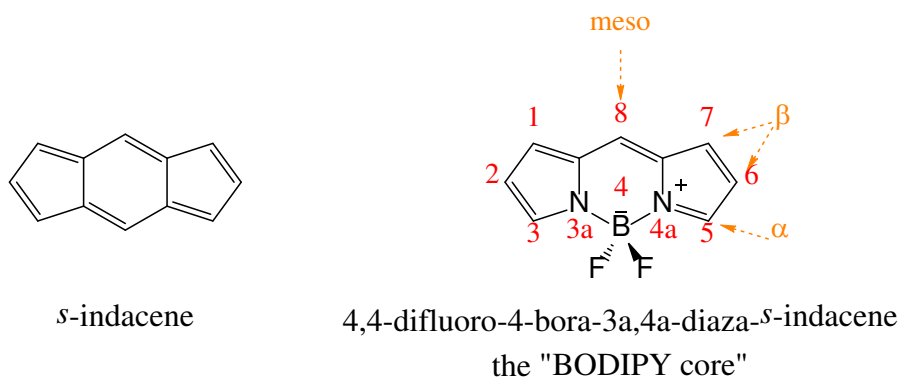
For the visual phenomenon, brightness of the fluorescent molecules is always an evaluation standard for the quality of a fluorophore. The brightness (B) of a fluorophore is proportional to the molar extinction coefficient (accounts for the quantity of light absorbed) at the excitation wavelength ($\epsilon(\lambda)$) and the fluorescence quantum yield (account for the emission efficiency) (Φ_F). It is defined by the following relationship [96]:

$$B = \epsilon(\lambda) \times \Phi_F$$

An ideal fluorescent molecule should carry out sharp excitation and emission peaks, strong brightness and good chemical and photo stability.

1.3.2 BODIPY

Chemical structures determine the properties of the compounds. Fluorescence typically occurs from aromatic molecules because an electron at the ground state of the molecular orbital (π) can be excited to an unoccupied orbital (π^*) with relatively low energy.

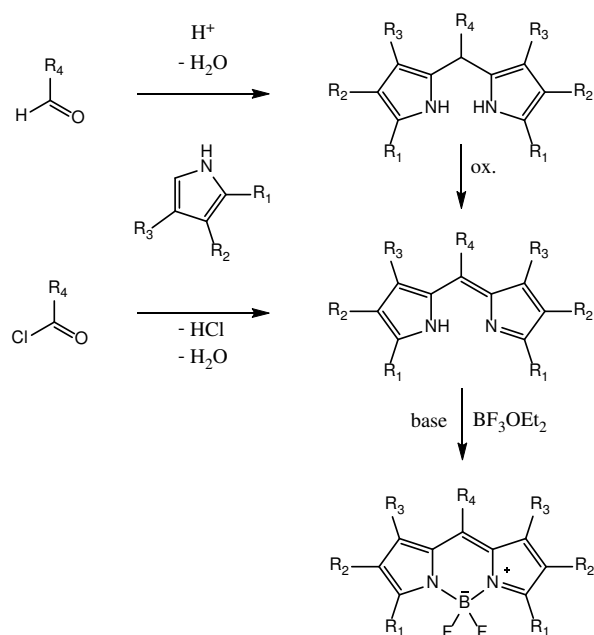


Scheme 1.10. Numbering scheme used for the BODIPY framework derived from indacene. The 8-position is often called meso; the 3,5-positions are sometimes denoted by α , while β is used to refer the 2,6- and 1,7-positions.

4,4-difluoro-4-bora-3a,4a-diaza-*s*-indacene [97, 98] (better known as BODIPY [99] or difluoroboron *dipyrromethene*) has a conjugation of the π -electrons running along the organic backbone and can be fluorescent (Scheme 1.10). Although Treibs and Kreuzer reported the first member of this family as early as 1968 [100], the various applications of BODIPY-based dyes were only fully studied since the mid-1990s [101, 102]. BODIPY shows many excellent features: good chemical and photo stability, intense absorption/emission profiles, relatively high molar absorption coefficient $\epsilon(\lambda)$ and fluorescence quantum yield, and relatively insensitivity to the pH and polarity of the environment. Moreover, the fluorescence properties can be fine-tuned by

introducing different electron donating/withdrawing substituents at the suitable positions of the BODIPY core. In addition, the synthetic pathways to the BODIPY-based dyes are relatively straightforward starting from pyrrole heterocycles and they are easily post-functionalized on various positions.

The conjugated π -electrons on the BODIPY core can be extended by attachment of conjugated groups to one or both pyrrole fragments [103, 104] or condensation of appropriate units onto the periphery [105, 106] to obtain red-shifted absorption and emission spectra of BODIPY-based fluorophore [107]. A typical synthesis of symmetric BODIPY fluorophores is based on the well-known pyrrole condensation reaction (Scheme 1.11), which is derived from the synthesis of certain types of porphyrin [108]. In order to avoid polymerization and/or porphyrin formation, pyrroles are generally substituted at one of the positions adjacent to the nitrogen atom. The other position adjacent to the nitrogen atom on pyrroles is used to form the methene bridge with a highly electrophilic carbonyl compound (*e.g.*, aldehyde, acyl chloride or acid anhydride) [109, 110]. Moreover, the aldehyde is very often an aromatic one in the condensation reaction with pyrrole because oxidation tends to fail in other cases.



Scheme 1.11. A typical synthesis of symmetric BODIPY fluorophores (from [98]).

Once BODIPY-based fluorophores with the expected photophysical properties are obtained, a post-modification for the polymerization is desired with negligible changes of the optical properties. Many post-synthetic modifications on the *meso*-position (8-position) of BODIPY dyes do not perturb the geometry of the chromophore and without significant decomposition of the electron density on the BODIPY unit [111, 112]. This kind of strategies can also avoid problems arising from steric hindrance.

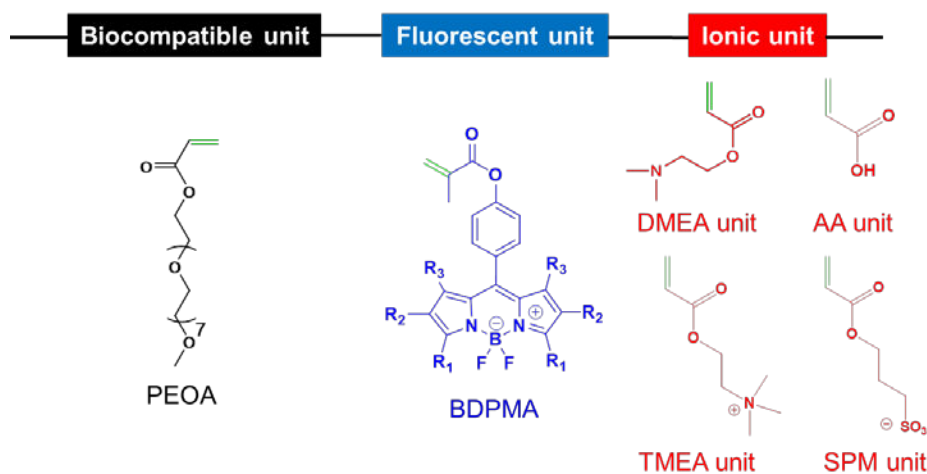
1.3.3 Fluorescent polymers

In general, organic fluorophores are toxic and hydrophobic compounds which limit the applications in biology and medicine. They can be functionalized by introducing some hydrophilic moieties onto the aromatic fluorescent core [113]. However, in most cases they result in a dramatic drop of the fluorescence quantum yield. Fluorescent polymers show great potential in bioimaging and biosensor applications due to the variety of available monomers with good water solubility, biocompatibility and compatibility with organic fluorophores. Modified organic fluorophores can be fluorescent monomers building blocks for fluorescent polymers preparation.

Contrary to fluorescent π -conjugated polymers, when side-chain pendant fluorophores are covalently introduced to a polymeric backbone, the photophysical properties are mostly independent from the number of repeating units and the degree of polymerization. In addition, fluorescent monomers that carry polymerizable moieties (*e.g.*, double bonds in terms of (meth)acrylate-, vinyl- or styrene units) can be directly polymerized by various polymerization techniques [114]. Besides the direct copolymerizing of dyes approach, post-polymerization modification is an alternative method to introduce reactive fluorophores onto functionalized side chains using highly efficient reactions.

Some fluorescent polymers were synthesized and applied as labels or sensors for cell imaging. Charreyre's team reported a new class of lipid-ended polymer conjugates as bright far-red fluorescent lipid probes and the probes were able to efficiently label the lipid bilayer of liposomes of various sizes [115]. Raymo's group recently addressed seven bright and non-cytotoxic BODIPY-based polymers incorporating with hydrophobic decyl and hydrophilic oligo-(ethylene glycol) side chains which allow the imaging of living organisms (*Caenorhabditis elegans* and *HeLa* cells) [116]. A cationic BODIPY-based fluorescent polymeric thermometer was synthesized by Uchiyama's group and applied for the sensing of intracellular temperature (MOLT-4 (human acute lymphoblastic leukaemia) and HEK293T (human embryonic kidney) cells) [117]. However, to our knowledge, fluorescent polymers for bacterial detection are rarely considered.

In order to introduce BODIPY dyes into polymer backbones as side chains by direct polymerization, BODIPY methacrylate (BDPMA), which carries double bonds in the methacrylate unit, was selected as the fluorescent monomer (Scheme 1.12) [118]. Fluorescent polymers can maintain the features of the individual monomers. The water-soluble and biocompatible fluorescent polymers are expected to be used for biological applications; therefore poly(ethylene oxide) acrylate (PEOA) is used to introduce this feature. In order to carry out the Layer-by-Layer assembly, different types of basic (ammoniums) and acidic (carboxylates or sulfonates) monomers are used as positively and negatively charged units, respectively.



Scheme 1.12. Different BODIPY-based fluorescent polyelectrolytes.

1.3.4 Reversible addition fragmentation transfer (RAFT) polymerization

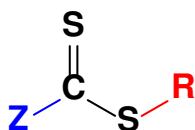
Monomers carrying double bonds can be directly polymerized either through a straightforward free radical polymerization (FRP) approach or through living/controlled radical polymerization (CRP) techniques. However, conventional uncontrolled free radical polymerization generally leads to polydisperse polymers because of unavoidable radical-radical terminations. CRP methods allow the synthesis of well-defined polymers with a narrow molecular weight distribution, diverse chain composition, and controlled chain lengths. They are thus convenient for the synthesis of block copolymers [119].

“Living” polymerization was first introduced by Michael Szwarc in 1956, starting with living anionic chain-growth polymerizations [120]. In the standard polymerization process, polymeric molecules are created in an initiation step, and then grow by a propagation step, and finally they “die” in a termination step. The death is regulated by the reaction conditions. Whereas, in the concept of living polymerizations, there is no termination step, the polymeric molecules then “live” for an indefinite period of time and the growth is not interrupted until the supply of monomers is exhausted. In addition, the living ends are potentially able to grow further if an additional amount of monomer is available [121]. This approach was extended to vinyl monomers after around 30 years [122, 123], however, anionic polymerizations are only suitable for several types of monomers (*e.g.*, aprotic, apolar) with high purity under harsh reaction conditions [124]. More interesting studies on living polymerization have been subsequently reported. Controlled radical polymerization (CRP) approaches, including the nitroxide mediated polymerization (NMP), the atom transfer radical polymerization (ATRP), and the reversible addition-fragmentation transfer (RAFT) polymerization, have received great attentions for polymer synthesis due to the easy procedures, less stringent reagent purity and setup and tolerance to a wide range of chemical groups. It is also suitable for various polymerizable

monomers under mild reaction conditions [125].

In 1986, Solomon *et al.* reported the first example of NMP [126]. NMP is relatively tolerant to impurities and primarily suited for styrenic monomers [127]. Based on the NMP investigations, ATRP and RAFT became the most popular techniques during the 90s. In ATRP, various monomers (except unprotected acids) can be used and many initiators including multifunctional and hybrid systems are commercially available under a wide range of temperatures in the presence of transition metal catalyst [128]. A wide range of monomers including unprotected acids are able to be polymerized with RAFT. Considering the fluorescent polyelectrolytes preparation involves the anions that includes acidic groups and the toxicity of transition metals in biological system, RAFT polymerization was chosen in our work.

The RAFT technique was firstly described by the group of Rizzardo and Moad in 1998 [129]. As is generally the case in CRP, RAFT relies on the kinetic equilibrium between active and dormant chains [130, 131]. The efficient reversible activation-deactivation process in RAFT is conferred by a special kind of chain transfer agent (CTA)/or RAFT agent that generally contains a thiocarbonylthio moiety (Scheme 1.13). When a radical species attack the thiocarbonylthio moiety of the CTA, the double bond (C=S) that can be activated by Z groups, cleaves and a radical adduct forms [132, 133]. The stability of the radical adduct can also be controlled by the Z segments during the process and the R group is leaving as a radical species, that achieves the kinetics of addition and fragmentation of this agent. Therefore, the selection of R and Z groups is crucial.



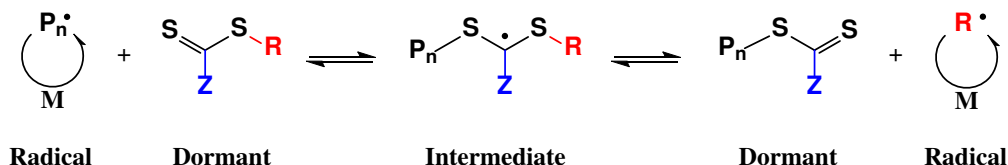
Scheme 1.13. General structure of RAFT chain transfer agents (CTA).

In RAFT polymerization (Scheme 1.14), a small quantity of initiating radicals (I^\bullet) reacts with the monomers and growing radical species (P_n^\bullet) form. These radical species attack the C=S double bonds of CTA, the stabilized radical intermediates are formed, and then R segments fragment leave as another propagating radicals (R^\bullet). Meanwhile, other transfer agents ($P_n-S(C=S)Z$) are obtained and then new initiators (R^\bullet) are able to reinitiate monomers to give growing radicals ($R-P_m^\bullet$). The growing radicals (P_m^\bullet) react with the transfer agents ($P_n-S(C=S)Z$) again and yield new propagating radicals (P_n^\bullet) and large amount of polymeric transfer agents ($P_m-S(C=S)Z$). In the final step, which is undesirable but terminations may occur in all CRP process, dead chains ($(D_{n+m}$ or D_n and $D_m)$) are formed. Fortunately, the above equilibria are still living. RAFT markedly reduces the probability of termination. Thermal initiators (azobisisobutyronitrile (AIBN) or 4,4'-azobis(4-cyanopentanoic acid) (ACPA)) have been selected for the initiation [135]. A commercial carboxyl-terminated trithiocarbonate based

transfer agent was used in our work due its good efficiency in RAFT [136]. Furthermore, the carboxyl groups at the end are available for further functionalization.



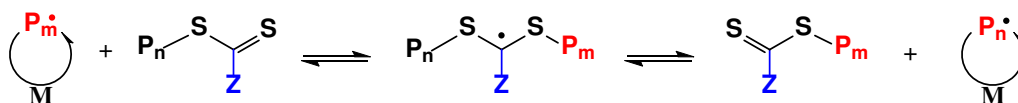
RAFT pre-equilibrium:



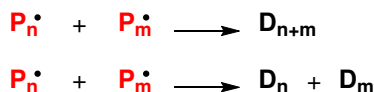
Propagation:



RAFT main equilibrium:



Termination:



Scheme 1.14. General mechanism of the RAFT polymerization (from [134]).

1.3.5 Click chemistry

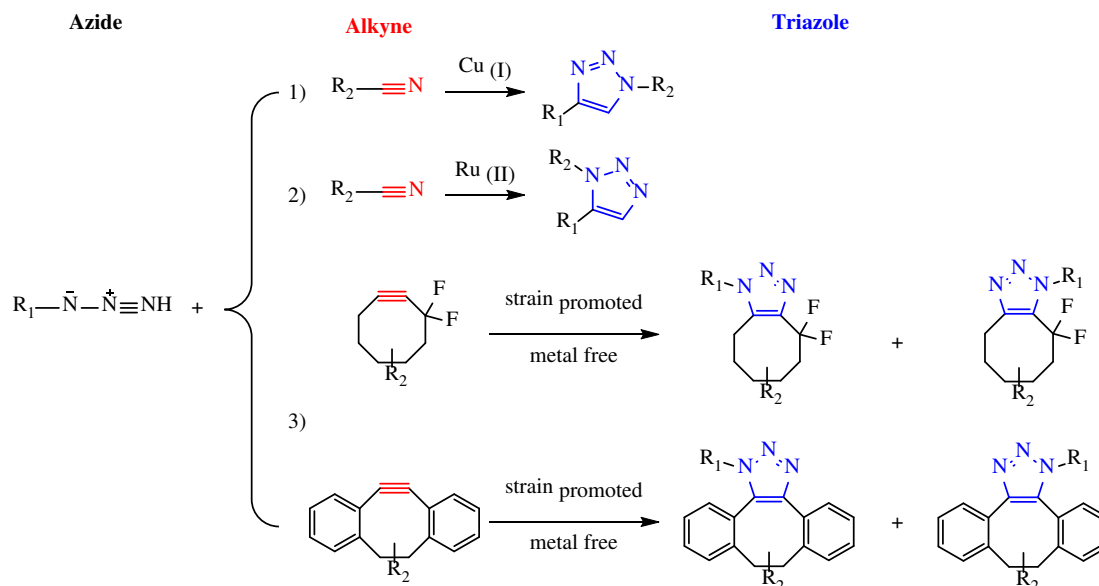
Click chemistry is a very powerful tool not only for the post modification of polymers [137, 138] but also for surface modification [139, 140], extending the applications of functional polymers.

1.3.5.1 Introduction of click chemistry

The concept of “click” chemistry was first introduced by Sharpless and coworkers in 2001 and they defined the term as “*the reaction must be modular, stereospecific, give very high yields, readily available starting materials, simple and mild reaction conditions in multiply solvents (including water), simple purification procedures and the product must be stable under physiological conditions*” [141]. Among these reactions, 1, 3-dipolar cycloadditions between azides and terminal alkynes catalyzed by copper (I) (termed CuAAC) meet the above criteria due to a very high thermodynamic driving force and have been classified as “click” reactions since 2002 [142, 143]. CuAAC can be classified into three categories based on the catalyst (Scheme

1.15). The 1,4-disubstituted 1,2,3-triazole regioisomer products are generated in the presence of Cu (I) (Scheme 1.15, entry 1). Cu (I) is needed for the CuAAC reaction, however, the Cu (I) coordination complexes and salts are always unstable when they are utilized directly [144, 145] or there are large amounts of undesired side products appearing in the presence of Cu (I) halides [146]. Consequently, the required Cu (I) is prepared in site either by the comproportionation of Cu (0) and Cu (II), or *via* a reduction reaction between Cu (II) and a reducing agent (*e.g.*, ascorbate) [142]. One of the remarkable advantages is that CuAAC enable the incorporation of even very dilute functional groups because of relative independence of the reaction rate on the azide and alkyne concentration and the lack of side products. Although CuAAC has been successfully used in polymer chemistry owing to the high efficiency and excellent functional group tolerance, the Cu (I) catalyst is cytotoxic and limits its biological applications. Several groups have tried to minimize the quantity of catalysis under high reaction rates [147].

Azide-Alkyne Cycloaddition



Scheme 1.15 General scheme of azide-alkyne cycloaddition reactions (from [143]).

An alternative catalyst for azide-alkyne cycloaddition is ruthenium (II) and results in the 1,5-regioisomer (Scheme 1.15, entry 2) [148, 149]. Furthermore, it is possible to obtain completely substituted 1,2,3-triazoles with Ru (II) catalyzed azide-alkyne cycloaddition because Ru (II) can engage internal alkynes in catalysis. Other transition metals (*e.g.*, Ni, Pd, Pt and Fe) and different ligands (*e.g.*, bipyridine derivatives) have also been investigated [150-152].

1.3.5.2 Strain promoted alkyne-azide cycloaddition (SPAAC)

Recently, more practical metal-free click chemistry reactions have been developed. The most

significant development of copper-free alkyne-azide cycloaddition is probably the use of a ring strained alkynyl moieties that reacts at room temperature (SPAAC) [153]. Bertozzi *et al.* achieved the effective [3+2] cycloaddition between fluoro-substituted cyclooctynes containing ring strain and electron-withdrawing fluorine substituents and azides in the absence of catalysts (Scheme 1.15, entry 3) [154-156]. Conversely, Boons *et al.* utilized dibenzocyclooctynes instead of fluoro-substituted cyclooctynes to perform strain-promoted cycloaddition with similar reaction rates, based on increase strain by adding sp^2 centers to the cyclooctyne ring (Scheme 1.15, entry 3) [157, 158]. Electron-deficient alkynes (*e.g.*, alkynyl esters [159, 160]) have also been used in catalyst-free azide-alkyne cycloaddition.

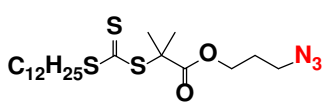
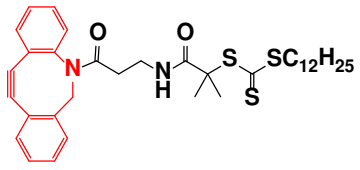
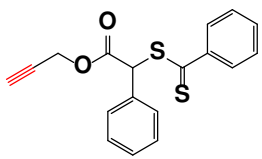
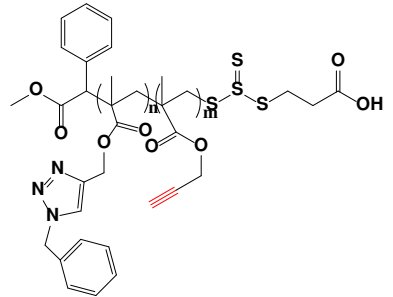
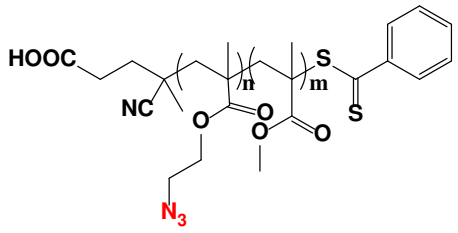
SPAAC reactions have been widely employed in biological systems to target azido-biomolecules (*e.g.*, sugars [161], peptides [162], nucleic acids [163] and proteins [164]) and cells [165] without observable cytotoxicity. Furthermore, functional groups (*e.g.*, hydroxyl group) on cyclooctyne derivatives provide a handle for the incorporation of functional polymers.

1.3.6 Combination of click chemistry and RAFT polymerization

As previously introduced, RAFT polymerization is an efficient and convenient technique for the preparation of well-defined polymers. In order to extend their applications, polymers bearing functional groups at terminal positions are required for further functionalization [166]. Hence, the functional group tolerance is very important for the post-polymerization modification. Azides and terminal alkynes received great attentions for post-polymerization modification owing to their excellent tolerance in a broad range of reaction conditions [167]. Moreover, click chemistry between azides and terminal alkynes can be carried out simply, effectively and selectively under mild conditions to give stable triazoles. Consequently, the combination between click chemistry and RAFT polymerization not only simply and efficiently adds the properties and functions to the original polymers but also expands the versatility of polymer synthesis. Clickable polymers can be further conjugated with various compounds ranging from small tracers [168], drugs [169] to other polymers [170], even on solid surface [171, 172].

In general, there are two approaches to introduce alkynyl or azido groups into RAFT-generated polymers (Table 1.1). (1) Clickable functional groups can be introduced into RAFT agents or (2) incorporated as pendant units. As mentioned above, the commercial RAFT agent we selected carry carboxyl groups at the end, therefore clickable functional groups can be introduced based on condensation reactions. In the second method, the clickable functional groups can be incorporated to the polymer backbone through either post-polymerization onto functional polymers or as monomers that participate to the polymerization. Subsequently, the clickable polymers are conjugated with alkyne (or azide)-terminated molecules based on click reactions.

Table 1.1 Brief overview of “click” reactions with RAFT-generated polymers.

Entry	Polymer/substrate	Catalyst/conditions	Comments	Ref.
1		CuBr/PMDET DMF, rt	RAFT agent	[173]
2		/	RAFT agent	[174]
3		/	RAFT agent	[175]
4		/	monomer	[176]
5	 <p>/glass slides</p>	/	monomer	[177]

References

- [1] M. C. M. van Loosdrecht and D. Brdjanovic. Anticipating the next century of wastewater treatment. *Science*, 2014, **344** (6191), 1452-1453.
- [2] B. Kartal, J. G. Kuenen and M. C. M. van Loosdrecht. Sewage Treatment with Anammox. *Science*, 2010, **328** (5979), 702-703.
- [3] T. C. Hazen, E. A. Dubinsky, T. Z. DeSantis, G. L. Andersen and O. U. Mason, et al. Deep-Sea Oil Plume Enriches Indigenous Oil-Degrading Bacteria. *Science*, 2010, **330** (6001), 204-208.
- [4] C. L. Sears. A dynamic partnership: celebrating our gut flora. *Anaerobe*, 2005, **11**, 247-251.
- [5] <http://microbiologyonline.org/about-microbiology/introducing-microbes/bacteria>.
- [6] N. C. Darnton, L. Turner, S. Rojevsky and H. C. Berg. On Torque and Tumbling in Swimming. *Escherichia coli. J. Bacteriol.*, 2007, **189**, 1756-1764.
- [7] <http://thebiologyprimer.com/cell/>
- [8] I. Lerouge and J. Vanderleyden. O-antigen structural variation: mechanisms and possible roles in animal/plant-microbe interactions. *FEMS Microbiol. Rev.*, 2001, **26**, 17-47.
- [9] P. R. Murray. Manual of clinical microbiology. (DC:ASM Press Washington, 1995).
- [10] European Food Standards Agency. Scientific opinion on monitoring and assessment of the public health risk of “*Salmonella* Typhimurium-like” strains. *EFSA Journal*, 2010, **8**, 7-8.
- [11] P. I. Fields, K. Blom, H. J. Hughes, L. O. Helsel and B. Swaminathan, et al. Molecular characterization of the gene encoding H antigen in *Escherichia coli* and development of a PCR-restriction fragment length polymorphism test for identification of *E. coli* O157:H7 and O157:NM. *J. Clin. Microbiol.*, 1997, **35**, 1066-1070.
- [12] B. Kaijser. Immunology of *Escherichia coli*: K antigen and its relation to urinary-tract infection. *J. Infect. Dis.*, 1973, **127**, 670-677.
- [13] C. S. Cummins. Chemical composition and antigenic structure of cell walls of corynebacterium, mycobacterium, nocardia, actinomyces and arthrobacter. *J. gen. Microbiol.*, 1962, **28**, 35-50.
- [14] <http://www.onlinebiologynotes.com/bacterial-cell-wall-structure-composition-types/>
- [15] D. Zhou, Z. Tong, Y. Song, Y. Han and R. Yang, et al. Genetics of Metabolic Variations between *Yersinia pestis* Biovars and the Proposal of a New Biovar, microtus. *J. Bacteriol.*, 2004, **186** (15), 5147-5152.
- [16] J. Zhou, A. L. Loftus, G. Mulley and A. T. A. Jenkins. A Thin Film Detection/Response System for Pathogenic Bacteria. *J. Am. Chem. Soc.*, 2010, **132**, 6566-6570.

- [17] S. Sengupta, M. K. Chattopadhyay and H. Grossart. The multifaceted roles of antibiotics and antibiotic resistance in nature. *Front Microbiol*, 2013, **4**, 1-13.
- [18] “*Streptomycin: background, isolation, properties, and utilization*,” *Nobel Lectures, Physiology or Medicine 1942-1962*. (Amsterdam: Elsevier Publishing Company, 1964), p. 372.
- [19] L. J. Piddock. The crisis of no new antibiotics—what is the way forward? *Lancet Infect Dis*, 2012, **12(3)**, 249-253.
- [20] I. M. Gould and A. M. Bal. New antibiotic agents in the pipeline and how they can help overcome microbial resistance. *Virulence*, 2013, **4(2)**, 185-191.
- [21] C. L. Ventola. The Antibiotic Resistance Crisis: Part 1: Causes and Threats. *Pharmacy&Therapeutics*, 2015, **40(4)**, 277-283.
- [22] H. F. Chambers. The changing epidemiology of *Staphylococcus aureus*? *Emerg Infect Dis.*, 2001, **7(2)**, 178-182.
- [23] B. Spellberg and D. N. Gilbert. The Future of Antibiotics and Resistance: A Tribute to a Career of Leadership by John Bartlett. *Clin Infect Dis.*, 2014, **59 suppl 2**, S71-S75.
- [24] Centers for Disease Control and Prevention, Office of Infectious Disease. Antibiotic resistance threats in the United States, 2013. <https://www.cdc.gov/drugresistance/threat-report-2013/pdf/ar-threats-2013-508.pdf#page=14>
- [25] The antibiotic alarm. *Nature*, 2013, **495 (7449)**, 141.
- [26] M. Gross. Antibiotics in crisis. *Curr. Biol.*, 2013, **23(24)**, R1063- R1065.
- [27] C. A. Michael, D. Dominey-Howes and M. Labbate. The antibiotics resistance crisis: causes, consequences, and management. *Front. Public Health*, 2014, **2**, 145(1) - 145(8).
- [28] J. G. Bartlett, D. N. Gilbert and B. Spellberg. Seven ways to preserve the miracle of antibiotics. *Clin. Infect. Dis.*, 2013, **56(10)**, 1445-1450.
- [29] B. Chen, L. Lin, Y. Yang, E. Chen and T. Luan, *et al.* Complex pollution of antibiotic resistance genes due to *beta*-lactam and aminoglycoside use in aquaculture farming. *Water Res.*, 2018, **134**, 200-208.
- [30] T. S. Crofts, A. J. Gasparrini and G. Dantas. Next-generation approaches to understand and combat the antibiotic resistome. *Nat. Rev. Microbiol.*, 2017, **15**, 422-434.
- [31] M. O. A. Sommer, C. Munck, R. V. Toft-Kehler and D. I. Andersson. Prediction of antibiotic resistance: time for a new preclinical paradigm? *Nature Reviews Microbiology*, 2017, **15**, 689-696.
- [32] N. J. Ashbolt. Microbial contamination of drinking water and disease outcomes in developing regions. *Toxicology*, 2004, **198**, 229-238.

- [33] J. A. Crump, P. M. Griffin and F. J. Angulo. Bacterial contamination of animal feed and its relationship to human foodborne illness. *Clin. Infect. Dis.*, 2002, **35**, 859-865.
- [34] E. L. Palavecino, R. A. Yomtovian and M. R. Jacobs. Detecting bacterial contamination in platelet products. *Clin. Lab.*, 2006, **52**, 443-456.
- [35] M. E. Brecher and S. N. Hay. Bacterial contamination of blood components. *Clin. Microbiol. Rev.*, 2005, **18**, 195-204.
- [36] O. Lazcka, F. J. D. Campo and F. X. Muñoz. Pathogen detection: A perspective of traditional methods and biosensors. *Biosens. Bioelectron.*, 2007, **22**, 1205-1217.
- [37] M. Nayak, A. Kotian, S. Marathe and D. Chakravorty. Detection of microorganisms using biosensors-A smarter way towards detection techniques. *Biosens. Bioelectron.*, 2009, **25**, 661-667.
- [38] P. K. Mandal, A. K. Biswas, K. Choi and U. K. Pal. Methods for rapid detection of foodborne pathogens: An overview. *Am. J. Food Technol.*, 2011, **6**, 87-102.
- [39] A. Mortari and L. Lorenzelli. Recent sensing technologies for pathogen detection in milk: A review. *Biosens. Bioelectron.*, 2014, **60**, 8-21.
- [40] K. Mullis, F. Faloona, S. Scharf, R. Saiki and H. Erlich, *et al.* Specific Enzymatic Amplification of DNA in Vitro: the Polymerase Chain Reaction. *Cold spring harbor symposia on quantitative biology*, 1986, **51**, 263-273.
- [41] S. Q. Jin, B. C. Yin and B. C. Ye. Multiplexed bead-based mesofluidic system for detection of food-borne pathogenic bacteria. *Appl. Environ. Microbiol.*, 2009, **75**, 6647-6654.
- [42] D. Rodríguez-Lázaro, M. D'Agostino, A. Herrewegh, M. Pla and J. Ikononopoulos. Real-time PCR-based methods for detection of *Mycobacterium avium* subsp. *paratuberculosis* in water and milk. *Int. J. Food Microbiol.*, 2005, **101**, 93-104.
- [43] K. Lee, J. Lee, S. Wang, L. Liu and C. Chi, *et al.* Development of a novel biochip for rapid multiplex detection of seven mastitis-causing pathogens in bovine milk samples. *J. Vet. Diagn. Investig.*, 2008, **20**, 463-471.
- [44] A. K. Deisingh, M. Thompson. Strategies for the detection of *Escherichia coli* O157:H7 in foods. *J. Appl. Microbiol.*, 2004, **96**, 419-429.
- [45] H. Falentin, F. Postollec, S. Parayre, N. Henaff and D. Sohier. Specific metabolic activity of ripening bacteria quantified by real-time reverse transcription PCR throughout Emmental cheese manufacture. *Int. J. Food Microbiol.*, 2010, **144**, 10-19.
- [46] M. Paul, D. L. Van Hekken, J. D. Brewster. Detection and quantitation of *Escherichia coli* O157 in raw milk by direct qPCR. *Int. Dairy J.*, 2013, **32**, 53-60.
- [47] A. Touron, T. Berthe, B. Pawlak and F. Petit. Detection of *Salmonella* in environmental

water and sediment by a nested-multiplex polymerase chain reaction assay. *Res. Microbiol.*, 2005, **156**, 541-553.

[48] S. H. Choi and S. B. Lee. Development of reverse transcriptase-polymerase chain reaction of *filmA* gene to detect viable *Salmonella* in milk. *J. Anim. Sci. Technol.*, 2004, **46**, 841-848.

[49] S. Sheu, W. Hwang, Y. Chiang, W. Lin and H. Tsen, *et al.* Use of *Tuf* Gene-Based Primers for the PCR Detection of Probiotic *Bifidobacterium* Species and Enumeration of Bifidobacteria in Fermented Milk by Cultural and Quantitative Real-Time PCR Methods. *J. Food. Sci.*, 2010, **75**, M521-M527.

[50] T. Notomi, H. Okayama, H. Masubuchi, T. Yonekawa and T. Hase, *et al.* Loop-mediated isothermal amplification of DNA. *Nucleic Acids Research*, 2000, **28**, e63 i-vii.

[51] J. Compton. Nucleic acid sequence-based amplification. *Nature*, 1991, **350**, 91-92.

[52] <http://www.biosensors-congress.elsevier.com/about.htm>

[53] L. Su, W. Jia, C. Hou and Y. Lei. Microbial biosensors: A review. *Biosens. Bioelectron.*, 2011, **26**, 1788-1799.

[54] L. Ding, D. Du, X. Zhang and H. Ju. Trends in cell-based electrochemical biosensors. *Curr. Med. Chem.*, 2008, **15**, 3160-3170.

[55] J. Bobacka, A. Ivaska and A. Lewenstam. Potentiometric Ion Sensors. *Chem. Rev.*, 2008, **108**, 329-351.

[56] E. Barsoukov and J. R. Macdonald. Impedance spectroscopy theory, experiment, and applications. 2005, John Wiley & Sons Ltd., Hoboken, New Jersey.

[57] P. L. Bonora, F. Deflorian and L. Fedrizzi. Electrochemical impedance spectroscopy as a tool for investigating underpaint corrosion. *Electrochimica Acta*, 1996, **41**, 1073-1082.

[58] M. A. Cooper. Label-free screening of bio-molecular interactions. *Anal. Bioanal. Chem.*, 2003, **377**, 834-842.

[59] M. J. Linman, A. Abbas and Q. Cheng. Interface design and multiplexed analysis with surface plasmon resonance (SPR) spectroscopy and SPR imaging. *Analyst*, 2010, **135**, 2759-2767.

[60] M. J. Linman and Q. J. Cheng. Surface Plasmon Resonance: New Biointerface Designs and High-Throughput Affinity Screening. *Optical Guided-Wave Chemical and Biosensors I*, 2010, **7**, 133-153.

[61] B. Li, Q. Yu and Y. Duan. Fluorescent labels in biosensors for pathogen detection. *Crit. Rev. Biotechnol.*, 2015, **35**, 82-93.

[62] Y. Li, W. A. Dick and O. H. Tuovinen. Fluorescence microscopy for visualization of soil

microorganisms-a review. *Biol. Fertility Soils*, 2004, **39**, 301-311.

[63] P. Zhu, D. R. Shelton, J. S. Karns, A. Sundaram and C. M. Tang, *et al.* Detection of water-borne *E. coli* O157 using the integrating waveguide biosensor. *Biosens. Bioelectron.*, 2005, **21**, 678-683.

[64] B. S. B. Kasibabu, S. L. D'souza, S. Jha, R. K. Singhal and S. K. Kailasa, *et al.* One-step synthesis of fluorescent carbon dots for imaging bacterial and fungal cells. *Anal. Methods*, 2015, **7**, 2373-2378.

[65] K. Ai, B. Zhang and L. Lu. Europium-based fluorescence nanoparticle sensor for rapid and ultrasensitive detection of an anthrax biomarker. *Angew. Chem.*, 2009, **121**, 310-314.

[66] J. Chen, S. M. Andler, J. M. Goddard, S. R. Nugen and V. M. Rotello. Integrating recognition elements with nanomaterials for bacteria sensing. *Chem. Soc. Rev.*, 2017, **46**, 1272-1283.

[67] R. K. Iler. Multilayers of colloidal particles. *J. Colloid Interface Sci.*, 1966, **21**, 569-594.

[68] G. Decher, J. D. Hong and J. Schmitt. Buildup of ultrathin multilayer films by a self-assembly process: III. Consecutively alternating adsorption of anionic and cationic polyelectrolytes on charged surfaces. *Thin Solid Films*, 1992, **210-211**, 831-835.

[69] G. Decher and J. D. Hong. Buildup of ultrathin multilayer films by a self-assembly process: II. Consecutive adsorption of anionic and cationic bipolar amphiphiles and polyelectrolytes on charged surfaces. *Ber. Bunsenges. Phys. Chem.*, 1991, **95**, 1430-1434.

[70] G. Decher, J. MacLennan, J. Reibel and U. Sohling. Highly-Ordered Ultrathin LC Multilayer Films on Solid Substrates. *Adv. Mater.*, 1991, **3**, 617-619.

[71] K. Ariga, J. P. Hill and Q. Ji. Layer-by-layer assembly as a versatile bottom-up nanofabrication technique for exploratory research and realistic application. *Phys. Chem. Chem. Phys.*, 2007, **9**, 2319-2340.

[72] H. Liu, X. Gu, M. Hu. Y. Hu and C. Wang. Facile fabrication of nanocomposite microcapsules by combining layer-by-layer self-assembly and Pickering emulsion templating. *RSC. Adv.*, 2014, **4**, 16751-16758.

[73] K. Szczepanowicz, H. J. Hoel, L. Szyk-Warszynska, E. Bielańska and P. Warszynski, *et al.* Formation of Biocompatible Nanocapsules with Emulsion Core and Pegylated Shell by Polyelectrolyte Multilayer Adsorption. *Langmuir*, 2010, **26**, 12592-12597.

[74] J. J. Richardson, M. Björnmalm, F. Caruso. Technology-driven layer-by-layer assembly of nanofilms. *Science*, 2015, **348**, aaa2491-1-aaa2491-11.

[75] S. W. Lee, J. Kin, S. Chen, P. T. Hammond and Y. Shao-Horn. Carbon Nanotube/Manganese Oxide Ultrathin Film Electrodes for Electrochemical Capacitors. *ACS Nano*, 2010, **4**, 3889-3896.

- [76] C. B. Bucur, M. Jones, M. Kopylov, J. Spear and J. Muldoon. Inorganic-organic layer by layer hybrid membranes for lithium-sulfur batteries. *Energy Environ. Sci.*, 2017, **10**, 905-911.
- [77] U. Chakraborty, T. Singha, R. R. Chianelli, C. Hansda and P. K. Paul. Organic-inorganic hybrid layer-by-layer electrostatic self-assembled film of cationic dye Methylene Blue and a clay mineral: Spectroscopic and Atomic Force microscopic investigations. *J. Lumin.*, 2017, **187**, 322-332.
- [78] A. V. Staeten, A. Bratek-Sicki, L. Germain, C. D'Haese and C. Dupont-Gillain, *et al.* Protein-polyelectrolyte complexes to improve the biological activity of proteins in layer-by-layer assemblies. *Nanoscale*, 2017, **9**, 17186-17192.
- [79] R. R. Costa and J. F. Mano. Polyelectrolyte multilayered assemblies in biomedical technologies. *Chem. Soc. Rev.*, 2014, **43**, 3453-3479.
- [80] Q. He, Y. Tian, Y. Cui, H. Möhwald and J. Li. Layer-by-layer assembly of magnetic polypeptide nanotubes as a DNA carrier. *J. Mater. Chem.*, 2008, **18**, 748-754.
- [81] K. Kang, K. Lee, Y. Han, H. Gao and J. Park, *et al.* Layer-by-layer assembly of two-dimensional materials into wafer-scale heterostructures. *Nature*, 2017, **550**, 229-233.
- [82] N. Joseph, P. Ahmadiannamini, R. Hoogenboom and I. F. J. Vankelecom. Layer-by-layer preparation of polyelectrolyte multilayer membranes for separation. *Polym. Chem.*, 2014, **5**, 1817-1831.
- [83] E. Donath, G. B. Sukhorukov, F. Caruso, S. A. Davis and H. Möhwald. Novel Hollow Polymer Shells by Colloid-Templated Assembly of Polyelectrolytes. *Angew. Chem. Int. Ed.*, 1998, **37**, 2202-2205.
- [84] A. Nishiguchi, H. Yoshida, M. Matsusaki and M. Akashi. Rapid construction of three-dimensional multilayered tissues with endothelial tube networks by the cell-accumulation technique. *Adv. Mater.*, 2011, **23**, 3506-3510.
- [85] B. Jiang, C. Li, H. Qian, M. Shahriar and Y. Yamauchi. Layer-by-layer motif architectures: programmed electrochemical syntheses of multilayer mesoporous metallic films with uniformly sized pores. *Angew. Chem. Int. Ed.*, 2017, **56**, 7836-7841.
- [86] G. Decher. Fuzzy nanoassembled: toward layered polymeric multicomposites. *Science*, 1997, **277**, 1232-1237.
- [87] A. Laschewsky, E. Wischerhoff, S. Denzinger, H. Ringsdorf and P. Bertrand, *et al.* Molecular recognition by hydrogen bonding in polyelectrolyte multilayers. *Chem. Eur. J*, 1997, **3**, 34-38.
- [88] T. Tang, J. Qu, K. Müllen and S. E. Webber. Molecular layer-by-layer self-assembly of water-soluble perylene diimides through π - π and electrostatic interaction. *Langmuir*, 2006, **22**,

26-28.

[89] D. E. Bergbreiter and B. S. Chance. "Click"-based covalent layer-by-layer assembly on polyethylene using water-soluble polymeric reagents. *Macromolecules*, 2007, **40**, 5337-5343.

[90] A. K. Geim and I. V. Grigorieva. Van der Waals heterostructures. *Nature*, 2013, **499**, 419-425.

[91] P. Bertrand, A. Jonas, A. Laschewsky and R. Legras. Ultrathin polymer coating by complexation of polyelectrolytes at interfaces: suitable materials structure and properties. *Macromol. Rapid Commun.*, 2000, **21**, 319-348.

[92] Y. Xiang, S. Lu and S. Jiang. Layer-by-layer self-assembly in the development of electrochemical energy conversion and storage devices from fuel cells to supercapacitors. *Chem. Soc. Rev.*, 2012, **41**, 7291-7321.

[93] I. Teraoka. Polymer solutions: an introduction to physical properties. (Wiley, 2002).

[94] B. Valeur. Molecular Fluorescence. (Wiley-VCH Verlag GmbH, 2001).

[95] J. R. Lakowicz. Principles of Fluorescence Spectroscopy. (Springer US, 2006).

[96] S. E. Braslavsky. Glossary of terms used in photochemistry, 3rd edition (IUPAC Recommendations 2006). *Pure Appl. Chem.*, 2007, **79**.

[97] A. Loudet and K. Burgess. BODIPY Dyes and Their Derivatives: Syntheses and Spectroscopic Properties. *Chem. Rev.*, 2007, **107**, 4891-4932.

[98] G. Ulrich, R. Ziessel and A. Harriman. The Chemistry of Fluorescent Bodipy Dyes: Versatility Unsurpassed. *Angew. Chem. Int. Ed.*, 2008, **47**, 1184-1201.

[99] R. P. Haugland. The Handbook. A Guide to Fluorescent Probes and Labeling Technologies, (Molecular Probes. Invitrogen. Carlsbad, 10th edn, 2005).

[100] A. Treibs and F. H. Kreuzer. Difluorboryl-Komplexe von Di-und Tripyrrylmethenen. *Justus Liebigs Ann. Chem.*, 1968, **718**, 208-223.

[101] A. C. Benniston and G. Copley. Lighting the way ahead with boron dipyrromethene (Bodipy) dyes. *Phys. Chem. Chem. Phys.*, 2009, **11**, 4124-4131.

[102] N. Boenes, V. Leen and W. Dehaen. Fluorescent indicators based on BODIPY. *Chem. Soc. Rev.*, 2012, **41**, 1130-1172.

[103] T. T. Vu, S. Badré, C. Dumas-Verdes, J. Vachon and R. Méallet-Renault, *et al.* New Hindered BODIPY Derivatives: Solution and Amorphous State Fluorescence Properties. *J. Phys. Chem. C*, 2009, **113**, 11844-11855.

[104] E. Y. Schmidt, B. A. Trofimov, A. I. Mikhaleva, N. V. Zorina and R. B. Pansu, *et al.* Synthesis and optical properties of 2-(Benzo[b]thiophene-3-yl)pyrroles and a new BODIPY

fluorophore (BODIPY=4,4-Difluoro-4-bora-3*a*,4*a*-diazas-indacene). *Chem. Eur. J.*, 2009, **15**, 5823-5830.

[105] E. Y. Schmidt, N. V. Zorina, M. Y. Dvorko, N. I. Protsuk and B. A. Trofimov, *et al.* A general synthetic strategy for the design of new BODIPY fluorophores based on pyrroles with polycondensed aromatic and metallocene substituents. *Chem. Eur. J.*, 2011, **17**, 3069-3073.

[106] O. Galangau, C. Dumas-Verdes, R. Méallet-Renault and G. Clavier. Rational design of visible and NIR distyryl-BODIPY dyes from a novel fluorinated platform. *Org. Biomol. Chem.*, 2010, **8**, 4546-4553.

[107] J. Chin and H. Kin. Near-infrared fluorescent probes for peptidases. *Coordin. Chem. Rev.*, 2018, **354**, 169-181.

[108] T. E. Wood and A. Thompson. Advances in the chemistry of dipyrins and their complexes. *Chem. Rev.*, 2007, **107**, 1831-1861.

[109] B. J. Littler, M. A. Miller, C. Hung, R. W. Wagner and J. S. Lindsey, *et al.* Refined synthesis of 5-substituted dipyrromethanes. *J. Org. Chem.*, 1999, **64**, 1391-1396.

[110] M. Baruah, W. Qin, N. Basarić, W. M. De Borggraeve and N. Boens. BODIPY-based hydroxyaryl derivatives as fluorescent pH probes. *J. Org. Chem.*, 2005, **70**, 4152-4157.

[111] C. Dumas-Verdes, F. Miomandre, E. Lépiciér, O. Galangau and P. Audebert, *et al.* BODIPY-Tetrazine Multichromophoric Derivatives. *Eur. J. Org. Chem.*, 2010, **13**, 2525-2535.

[112] C. Gazon, J. Rieger, R. Méallet-Renault, B. Charleux and G. Clavier. Ultrabright fluorescent polymeric nanoparticles made from a new family of BODIPY monomers. *Macromolecules*, 2013, **46**, 5167-5176.

[113] A. Romieu, C. Massif, S. Rihn, G. Ulrich and P. Renard, *et al.* The first comparative study of the ability of different hydrophilic groups to water-solubilise fluorescent BODIPY dyes. *New. J. Chem.*, 2013, **37**, 1016-1027.

[114] A. M. Breul, M. D. Hager and U. S. Schubert. Fluorescent monomers as building blocks for dye labeled polymers: synthesis and application in energy conversion, biolabeling and sensors. *Chem. Soc. Rev.*, 2013, **42**, 5366-5407.

[115] S. Adjili, A. Favier, J. Massin, Y. Bretonnière and M. T. Charreyre, *et al.* Synthesis of multifunctional lipid-polymer conjugates: application to the elaboration of bright far-red fluorescent lipid probes. *RSC Adv.*, 2014, **4**, 15569-15578.

[116] E. R. Thapaliya, Y. Zhang, P. Dhakal, A. S. Brown and F. M. Raymo, *et al.* Bioimaging with macromolecular probes incorporating multiple BODIPY fluorophores. *Bioconjugate Chem.*, 2017, **28**, 1519-1528.

[117] S. Uchiyama, T. Tsuji, K. Ikado, A. Yoshida and N. Inada, *et al.* A cationic fluorescent

polymeric thermometer for the ratiometric sensing of intracellular temperature. *Analyst*, 2015, **140**, 4498-4506.

[118] C. Gazon, J. Rieger, R. Méallet-Renault, G. Clavier and B. Charleux. One-pot synthesis of pegylated fluorescent nanoparticles by RAFT minoemulsion polymerization using a phase inversion process. *Macromo. Rapid. Commun.*, 2011, **32**, 699-705.

[119] J. Lutz, J. Lehn, E. Meijer and K. Matyjaszewski. From precision polymers to complex materials and systems. *Nat. Rev. Mater.*, 2016, **1**, 16024.

[120] M. Szwarc. 'Living' Polymers. *Nature*, 1956, **178**, 1168-1169.

[121] R. Faust, J. P. Kennedy. Living carbocationic polymerization - III. Demonstration of the living polymerization of isobutylene. *Polym Bull*, 1986, **15**, 317-323.

[122] M. Miyamoto, M. Sawamoto and T. Higashimura. Living polymerization of isobutyl vinyl ether with hydrogen iodide/iodine initiating system. *Macromolecules*, 1984, **17**, 265-268.

[123] S. Beyazit, B. T. S. Bui, K. Haupt and C. Gonzato. Molecularly imprinted polymer nanomaterials and nanocomposites by controlled/living radical polymerization. *Prog. Polym. Sci*, 2016, **62**, 1-21.

[124] W. A. Braunecker and K. Matyjaszewski. Controlled/living radical polymerization: features, developments and perspectives. *Prog. Polym. Sci*, 2007, **32**, 93-146.

[125] D. H. Solomon, E. Rizzardo and P. Cacioli. Polymerization process and polymers produced thereby. *US4581429*, 1986.

[126] N. Ballard, M. Aguirre, A. Simula, J. R. Leiza and J. M. Asua, *et al.* High solids content nitroxide mediated miniemulsion polymerization of *n*-butyl methacrylate. *Polym. Chem.*, 2017, **8**, 1628-1635.

[127] O. Garcia-Valdez, P. Champagne and M. F. Cunningham. Graft modification of natural polysaccharides via reversible deactivation radical polymerization. *Prog. Polym. Sci*, 2018, **76**, 151-173.

[128] J. Chiefar, Y. K. Chong, F. Ercole, J. Krstina and S. H. Thang, *et al.* Living free-radical polymerization by reversible addition-fragmentation chain transfer: the RAFT process. *Macromolecules*, 1998, **31**, 5559-5562.

[129] G. Conzatti, S. Cavalie, C. Combes, J. Torrisani and A. Tournette, *et al.* PNIPAM grafted surfaces through ATRP and RAFT polymerization: Chemistry and bioadhesion. *Colloids Surf. B*, 2017, **151**, 143-155.

[130] M. Uchiyama, K. Satoh and M. Kamigaito. Cationic RAFT polymerization using ppm concentrations of organic acid. *Angew. Chem. Int. Ed.*, 2015, **54**, 1924-1928.

[131] D. H. R. Barton and S. W. McCombie. A new method for the deoxygenation of secondary

alcohols. *J. Chem. Soc. Perkin Trans. I*, 1975, **0**, 1574-1585.

[132] D. Crich and L. Quintero. Radical chemistry associated with the thiocarbonyl group. *Chem. Rev.*, 1989, **89**, 1413-1432.

[133] G. Moad, J. Chiefari, Y. K. Chong, J. Krstina and S. H. Thang, *et al.* Living free radical polymerization with reversible addition-fragmentation chain transfer (the life of RAFT). *Polym. Int.*, 2000, **49**, 993-1001.

[134] A. Favier and M. Charreyre. Experimental requirements for an efficient control of free-radical polymerizations via the reversible addition-fragmentation chain transfer (RAFT) process. *Macromol. Rapid. Commun.*, 2006, **27**, 653-692.

[135] J. T. Lai, D. Filla and R. Shea. Functional polymers from novel carboxyl-terminated trithiocarbonates as highly efficient RAFT agents. *Macromolecules.*, 2002, **35**, 6754-6756.

[136] V. T. G. Tan, D. H. T. Nguyen, R. H. Utama, M. Kahram and J. J. Gooding, *et al.* Modular photo-induced RAFT polymerized hydrogels *via* thiol-ene click chemistry for 3D cell culturing. *Polym. Chem.*, 2017, **8**, 6123-6133.

[137] L. Qu, P. Sun, Y. Wu, K. Zhang and Z. Liu. Efficient homodifunctional bimolecular ring-closure method for cyclic polymers by combining RAFT and self-accelerating click reaction. *Macromol. Rapid. Commun.*, 2017, **38**, 1700121-1700127.

[138] L. Wu, U. Glebe and A. Böker. Synthesis of polystyrene and poly(4-vinylpyridine) mixed grafted silica nanoparticles via a combination of ATRP and Cu^I-catalyzed azide-alkyne click chemistry. *Macromol. Rapid. Commun.*, 2017, **38**, 1600475-1600482.

[139] O. Roling, K. D. Bruycker, B. Vonhören, L. Stricker and F. E. D. Prez, *et al.* Rewritable polymer brush micropatterns grafted by triazolidione click chemistry. *Angew. Chem. Int. Ed.*, 2015, **54**, 13126-13129.

[140] H. C. Kolb, M. G. Finn and K. B. Sharpless. Click chemistry: diverse chemical function from a few good reactions. *Angew. Chem. Int. Ed.*, 2001, **40**, 2004-2021.

[141] V. V. Rostovtsev, L. G. Green, V. V. Fokin and K. B. Sharpless. A stepwise Huisgen cycloaddition process: copper (I)-catalyzed regioselective “Ligation” of azides and terminal alkynes. *Angew. Chem. Int. Ed.*, 2002, **41**, 2708-2711.

[142] C. W. Tornøe, C. Christensen and M. Meldal. Peptidotriazoles on solid phase: [1, 2, 3]-triazoles by regiospecific copper (I)-catalyzed 1, 3- dipolar cycloadditions of terminal alkynes to azides. *J. Org. Chem.*, 2002, **67**, 3057-3064.

[143] W. Xi, T. F. Scott, C. J. Kloxin and C. N. Bowman. Click chemistry in materials science. *Adv. Funct. Mater.*, 2014, **24**, 2572-2590.

[144] J. E. Hein and V. V. Fokin. Copper-catalyzed azide-alkyne cycloaddition (CuAAC) and

- beyond: new reactivity of copper (I) acetylides. *Chem. Soc. Rev.*, 2010, **39**, 1302-1315.
- [145] M. Meldal and C. W. Tornøe. Cu-catalyzed azide-alkyne cycloaddition. *Chem. Rev.*, 2008, **108**, 2952-3015.
- [146] P. Siemsen, R. C. Livingston and F. Diederich. Acetylenic coupling: a powerful tool in molecular construction. *Angew. Chem. Int. Ed.*, 2000, **39**, 2632-2657.
- [147] A. E. Speers, G. C. Adam and B. F. Cravatt. Activity-based protein profiling *in vivo* using a copper (I)-catalyzed azide-alkyne [3+2] cycloaddition. *J. Am. Chem. Soc.*, 2003, **125**, 4686-4687.
- [148] L. Zhang, X. Chen, P. Xue, H. H. Y. Sun and G. Jia, *et al.* Ruthenium-catalyzed cycloaddition of alkynes and organic azides. *J. Am. Chem. Soc.*, 2005, **127**, 15998-15999.
- [149] B. C. Boren, S. Narayan, L. K. Rasmussen, L. Zhang and V. V. Fokin, *et al.* Ruthenium-catalyzed azide-alkyne cycloaddition: scope and mechanism. *J. Am. Chem. Soc.*, 2008, **130**, 8923-8930.
- [150] W. H. Binder and R. Sachsenhofer. "Click" chemistry in polymer and materials science. *Macromol. Rapid Commun.*, 2007, **28**, 15-54.
- [151] C. N. Urbani, C. A. Bell, M. R. Whittaker and M. J. Monteiro. Convergent synthesis of second generation AB-type miktoarm dendrimers using "Click" chemistry catalyzed by copper wire. *Macromolecules*, 2008, **41**, 1057-1060.
- [152] S. Chassaing, A. S. S. Sido, A. Alix, M. Kumarraja and J. Sommer, *et al.* "Click chemistry" in zeolites: copper (I) zeolites as new heterogeneous and ligand-free catalysts for the Huisgen [3+2] cycloaddition. *Chem. Eur. J.*, 2008, **14**, 6713-6721.
- [153] J. F. Lutz. Copper-free azide-alkyne cycloadditions: new insights and perspectives. *Angew. Chem. Int. Ed.*, 2008, **47**, 2182-2184.
- [154] C. G. Gordon, J. L. Machey, J. C. Jewett, E. M. Sletten, K. N. Houk and C. R. Bertozzi. Reactivity of biarylazacyclooctynones in copper-free click chemistry. *J. Am. Chem. Soc.*, 2012, **134**, 9199-9208.
- [155] J. M. Baskin, J. A. Prescher, S. T. Laughlin, N. J. Agard and C. R. Bertozzi, *et al.* Copper-free click chemistry for dynamic *in vivo* imaging. *Proc. Natl. Acad. Sci. USA*, 2007, **104**, 16793-16797.
- [156] N. J. Agard, J. A. Prescher and C. R. Bertozzi. A strain-promoted [3+2] azide-alkyne cycloaddition for covalent modification of biomolecules in living systems. *J. Am. Chem. Soc.*, 2004, **126**, 15046-15047.
- [157] A. A. Poloukhine, N. E. Mbua, M. A. Wolfert, G. J. Boons and V. V. Popik. Selective labeling of living cells by a photo-triggered click reaction. *J. Am. Chem. Soc.*, 2009, **131**, 15769-15776.

- [158] X. Ning, J. Guo, M. A. Wolfert and G. J. Boons. Visualizing metabolically labeled glycoconjugates of living cells by copper-free and fast Huisgen cycloadditions. *Angew. Chem. Int. Ed.*, 2008, **47**, 2253-2255.
- [159] X. Deng, C. Friedmann and J. Lahann. Bio-orthogonal “Double-click” chemistry based on multifunctional coatings. *Angew. Chem. Int. Ed.*, 2011, **50**, 6522-6526.
- [160] C. R. Becer, R. Hoogenboom and U. S. Schubert. Click chemistry beyond metal-catalyzed cycloaddition. *Angew. Chem. Int. Ed.*, 2009, **48**, 4900-4908.
- [161] J. Shie, Y. Liu, J. Hsiao, J. Fang and C. Wong. A cell-permeable and triazole-forming fluorescent probe for glycoconjugate imaging in live cells. *Chem. Commun.*, 2017, **53**, 1490-1493.
- [162] W. Tang and M. Becker. “Click” reactions: a versatile toolbox for the synthesis of peptide-conjugates. *Chem. Soc. Rev.*, 2014, **43**, 7013-7039.
- [163] M. Shelbourne, T. B. Jr, A. H. El-Sagheer and T. Brown. Fast and efficient DNA crosslinking and multiple orthogonal labelling by copper-free click chemistry. *Chem. Commun.*, 2012, **48**, 11184-11186.
- [164] C. A. DeForest and D. A. Tirrell. A photoreversible protein-patterning approach for guiding stem cell fate in three-dimensional gels. *Nat.e Mater.*, 2015, **14**, 523-531.
- [165] J. Dommerholt, S. Schmidt, R. Temming, L. J. A. Hendriks and F. L. van Delft. Readily accessible bicyclononynes for bioorthogonal labeling and three-dimensional imaging of living cells. *Angew. Chem. Int. Ed.*, 2010, **49**, 9422-9425.
- [166] S. Hilf and A. F. M. Kilbinger. Functional end groups for polymers prepared using ring-opening metathesis polymerization. *Nat. Chem.*, 2009, **1**, 537-546.
- [167] R. Fu and G. D. Fu. Polymeric nanomaterials from combined click chemistry and controlled radical polymerization. *Polym. Chem.*, 2011, **2**, 465-475.
- [168] C. Fu, A. Bongers, K. Wang, B. Yang and L. Tao, *et al.* Facile synthesis of a multifunctional copolymer *via* a concurrent RAFT-enzymatic system for theranostic applications. *Polym. Chem.*, 2016, **7**, 546-552.
- [169] W. Yang, T. Zhao, P. Zhou, S. Chen and L. Wang, *et al.* “Click” functionalization of dual stimuli-responsive polymer nanocapsules for drug delivery systems. *Polym. Chem.*, 2017, **8**, 3056-3065.
- [170] T. Tsutsuba, H. Sogawa and T. Takata. Preparation of a highly reactive polymer click reagent, PEG nitrile *N*-oxide, and its application in block and star polymer synthesis. *Polym. Chem.*, 2017, **8**, 1445-1448.
- [171] H. Taneda, A. Shundo, H. Matsuno and K. Tanaka. Design of a well-defined polyrotaxane

structure on a glassy polymer surface. *Langmuir*, 2018, **34**, 709-714.

[172] M. Szuwarzyn'ski, K. Wolski, A. Pomorska, T. Uchacz and S. Zapotoczny, *et al.* Photoactive surface-grafted polymer brushes with phthalocyanine bridging groups as an advanced architecture for light-harvesting. *Chem. Eur. J.*, 2017, **23**, 11239-11243.

[173] J. A. Alfurhood, P. R. Bachler and B. S. Sumerlin. Hyperbranched polymers *via* RAFT self-condensing vinyl polymerization. *Polym. Chem.*, 2016, **7**, 3361-3369.

[174] H. Lai, M. Lu, H. Lu, M. H. Stenzel and P. Xiao. pH-triggered release of gemcitabine from polymer coated nanodiamonds fabricated by RAFT polymerization and copper free click chemistry. *Polym. Chem.*, 2016, **7**, 6220-6230.

[175] M. A. Harvison and A. B. Lowe. Combining RAFT radical polymerization and click/Highly efficient coupling chemistries: a powerful strategy for the preparation. *Macromol. Rapid Commun.*, 2011, **32**, 779-800.

[176] J. Wang, X. Wang, W. Xue, G. Chen and X. Zhu. Initiator and photocatalyst-free visible light induced one-pot reaction: concurrent RAFT polymerization and CuAAC click reaction. *Macromol. Rapid Commun.*, 2016, **37**, 799-804.

[177] L. A. Canalle, S. S. *van* Berkel, L. T. *de* Haan and J. C. M. *van* Hest. Copper-free clickable coatings. *Adv. Funct. Mater.*, 2009, **19**, 3464-4370.

Chapter 2

BODIPY-based Fluorescent Polymer Chains Thin Film Devices for Bacteria Detection

Chapter 2 BODIPY-based Fluorescent Polymer Chains Thin Film Devices for Bacteria Detection

Every year over 300 million cases of serious and even fatal diseases are caused by bacterial infections or contaminations with the loss of over 2 million lives [1, 2]. Since 1940s, antibiotics became responsible for saving countless human and other lives, as well as transforming modern medicine [3]. However, due to the intensive use of antibiotics, human pathogens have become resistant to many antibiotics. Therefore, the rapid emergence of resistant bacteria is occurring worldwide in the last few decades [4, 5]. Especially, resistance of important bacterial pathogens to common antimicrobial therapies and rise of multidrug-resistant bacteria are increasing at an alarming rate [6]. Long-time scale is needed to go from fundamental research in the laboratory to clinical trials on humans before placing on the market. Furthermore, any new antibiotics have a limited lifespan of utility, and it is likely that new drug resistance in bacteria will appear [7]. Disease prevention is the most effective, affordable way to reduce risk of infectious bacterial pathogens.

Current methods for the identification of pathogenic bacteria are very slow and take several days to report the correct information [8]. The common assay is CFU (colony forming unit) counting which relies on plating the sample on agar and counting the colonies after at least 18 hours of incubating time. This method is time-consuming and may miss most types of bacteria [9]. Alternative methods have been developed to reduce the amount of time and sample necessary for a reliable measurement, such as surface plasmon resonance (SPR). Although SPR can detect bacteria within a short time, issues like the complexity of the device and expensive equipment, make SPR detection difficult to be applied in the market so far [10]. Another effective method is electrochemical impedance spectroscopy. This technology is highly sensitive; however it requires well-trained personnel to analyze the result [11]. This demands an urgent need for the development of rapid, sensitive, reliable, convenient and low cost bacteria detection approaches. One promising method, which is currently in the infant stage, is the development of fluorescent polymers enabled detection strategies. They are easier to functionalize, graft and get reproducible results.

To date, several attempts have been made to effectively detect bacteria with functionalized fluorescent polymers. Since many pathogens that infect humans use cell surface carbohydrates as receptors to facilitate cell-cell adhesion, P. H. Seeberger's group designed carbohydrate-functionalized fluorescent polymers which display many carbohydrate ligands on a single polymer chain to allow for multivalent detection of pathogens [12]. U. H. F. Bunz's team demonstrated that non-covalent conjugates of gold nanoparticles and poly (*para*-phenyleneethynylene) (PPE) *via* nanoparticle-bacteria interactions allow the release of bound fluorescent polymer from the gold-nanoparticle quencher, turning on the polymer fluorescence:

this allows the identification of bacteria effectively within minutes [13]. D. Zhang *et al.* addressed the issue of avoiding the interference of q-MNP (quaternized magnetic nanoparticles)-fluorescent polymer constructs in the measurement system and designed a magnetic nanoparticle and fluorescent polymer system for bacteria detection based on the above work [14]. Although these approaches for bacteria detection are sufficiently sensitive and selective, all of them were performed on liquid phases (solution phases), to our knowledge so far there are almost no efficient fluorescent sensors reported on solid support (e.g. thin-films). In comparison with fluorescent sensors based on solution phase, thin-film sensors are more convenient and applicable in operation. Moreover, the fluorescent thin film can capture the bacteria from the bacteria suspension and then detect them.

Layer-by-Layer (LbL) self-assembly is an easy and inexpensive process for multilayer formation and allows different types of materials to be incorporated in the film structures [15, 16]. Two oppositely charged polymers are alternatively deposited on the substrate by means of electrostatic attraction and multilayer thin films are prepared *via* simply repeating the basic deposition process [17]. Functional LbL thin films can easily be prepared from fluorescent polymer chains due to their versatility depending on functionalized units. In this study, the BODIPY derivative was chosen as the fluorescent unit owing to its attractive spectroscopic features such as an emission spectrum tunable from green to red and a high fluorescence quantum yield [18, 19]. Our group's recent work has proved that the reversible addition-fragmentation transfer (RAFT) polymerization is an easy and efficient tool to synthesize fluorescent polymer chains [20, 21]. Positively and negatively charged BODIPY-based fluorescent polymer chains (FPC) were synthesized thanks to this approach. BODIPY methacrylate was chosen as the fluorescent monomer. Poly (ethylene oxide) was selected as a steric stabilizer owing to its biocompatibility and stealth properties [22], and different types of basic and acidic groups are available for the positively and negatively charged units, respectively (see scheme 2.1 §2.2).

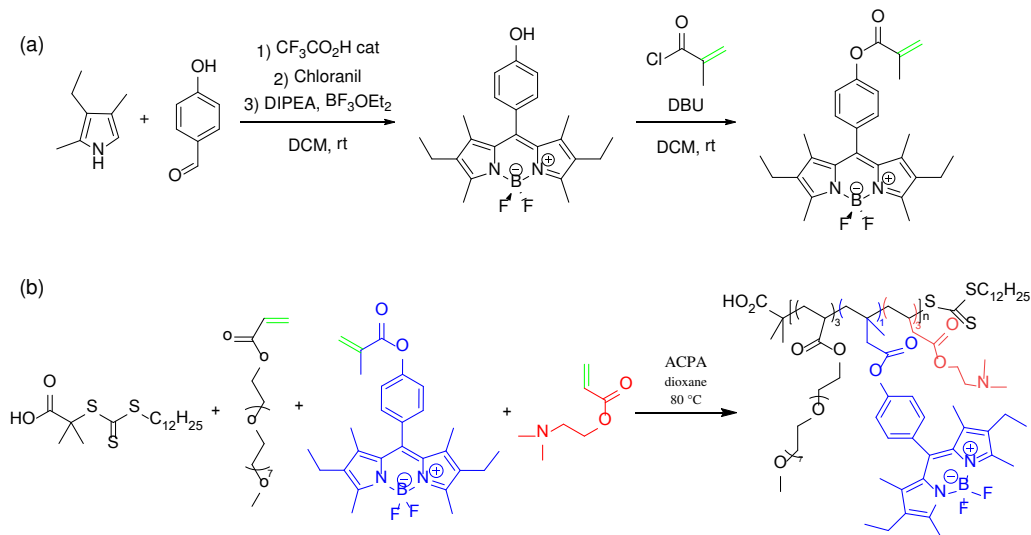
In this chapter, three pairs of BODIPY-based FPCs were synthesized with RAFT polymerization. Their features are:

- i) relatively **S**hort chains and **W**weak polyelectrolytes (we call them **SW** FPCs),
- ii) relatively **S**hort chains and **S**trong polyelectrolytes (**SS** FPCs),
- iii) relatively **L**ong chains and **W**weak polyelectrolytes (**LW** FPCs), respectively.

Then the characterization of three pairs (negative and positive chains) of FPCs will be introduced. The optimal deposition condition of the three pairs of FPCs for the FPC LbL films preparation will be described. After photophysical and surface properties investigation of each FPC LbL film, bacteria detection on these three types of FPC LbL films will be performed.

2.1 The synthesis and features of the three pairs of fluorescent polymer chains (FPCs)

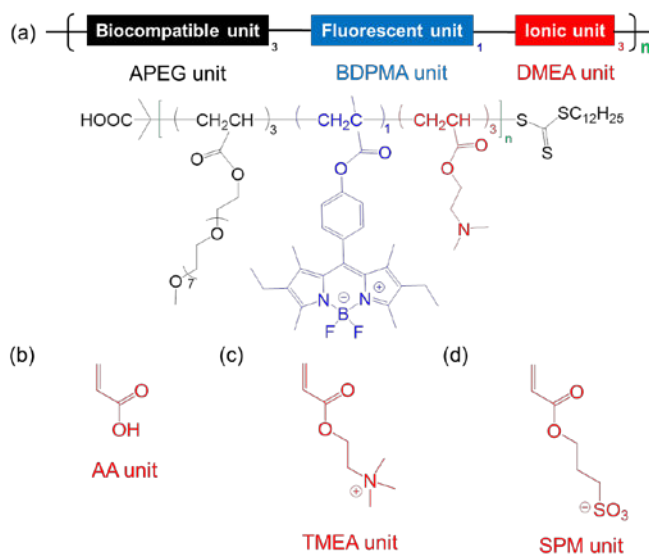
2.1.1 Synthesis of three pairs of fluorescent polymer chains (FPCs)



Scheme 2.1. (a) The synthetic route of green BODIPY methacrylate (BDPMA) and (b) an example preparation of green fluorescent polycation, different types of fluorescent polyelectrolytes can be synthesized using the other ionic units instead of DMEA (2-(Dimethylamino)ethyl acrylate) and changing the number of repeat units (n).

Green BODIPY phenol was chosen as the model fluorophore due to the simple synthetic route and the functionalization can be carried out on the hydroxyl group to introduce the polymerizable functional group (Scheme 2.1a). The polymerizable methacrylate group was introduced in BODIPY phenol by esterification with methacryloyl chloride and obtained BODIPY monomer. Different hydrophilic fluorescent polymer chains (FPC) containing polyethylene glycol, functionalized BODIPY and DMAEA (or AA) or TMEA (or SPM) (with molar ratios of PEG/BODIPY/charged units = 3/1/3) were synthesized at 80°C in dioxane solution (for AA and DMEA monomers) or a mixture of dioxane and ethanol (for TMEA and SPM monomers) in the presence of TTCA as a chain transfer agent and ACPA as initiator (Scheme 2.1b). The reaction progress was followed by NMR and the conversion rates of each FPCs were determined by ^1H NMR analysis of the disappearance of the ethylenic protons in the crude mixture. These polymers were purified by Bio-Gel® P polyacrylamide gel (10 media for relatively high molecular weight polymers and 6DG media for the others) column chromatography.

2.1.2 The features of three pairs of fluorescent polymer chains (FPCs)



Scheme 2.2. Chemical structures of (a) short chains and weak cationic fluorescent polymer chain (SW FPC⁺) where molecular weight is around 5 kg/mol ($n=2$) or long chains and weak cationic fluorescent polymer chain (LW FPC⁺) where molecular weight is around 30 kg/mol ($n=14$); (b) AA, (c) TMEA and (d) SPM monomers used instead of DMEA to modulate the charge of the FPC. APEG, poly(ethylene glycol) methyl ether acrylate; BDPMA, 4,4-difluoro-4-bora-3a, 4a-diaza-s-indacene derivative monomer; DMEA, 2-(Dimethylamino)ethyl acrylate; AA, acrylic acid; TMEA, [2-(Acryloyloxy)ethyl]trimethylammonium; SPM, 3-Sulfopropyl methacrylate.

As shown in scheme 2.2, in each polymer chain, four features are present: the number of repeating units, hydrophilic units, the fluorescent part and cationic or anionic part. Thus, FPCs are versatile and tunable since they benefit from different functional units. The length of polymer chains is different depending on the radical initiator concentration controlling the numbers of repeating units. The polyethylene glycol moiety plays the role of the hydrophilic unit. The fluorescent unit is a BODIPY derivative with a phenyl methacrylate polymerizable function, named BDPMA. The charged units come from the ionization of DMAEA or AA in the aqueous solution at proper pH or the use of TMEA or SPM. The three pairs of FPCs were designed with, hydrophilic and fluorescent units in constant numbers, whereas the total number of repeating units and charged monomers were tuned. SW FPC⁺ carrying positively charged unit are composed of about 16 repeating units (short chain), and DMAEA (weak polyelectrolyte) -which is partially ionized in aqueous solution- as the charged unit. SW FPC⁻ carrying a negatively charged unit are composed of about 18 repeating units (short chain), and AA which is partially ionized in aqueous solution (named weak polyelectrolytes). Following the same naming rule, SS FPC stand for short chains and strong polyelectrolytes with fully ionized moieties in aqueous solution. Meanwhile, LW FPC is long chains and weak polyelectrolytes. All the chemical structure characterizations of SW FPCs, SS FPCs and LW FPCs were performed with by NMR (Table 2.1).

Table 2.1. The composition of the different FPCs

FPC	total repeating unit	ionic monomer	estimated M_w (NMR) g/mol
<p>SW FPC⁺</p>	16	DMEA	5800
<p>SW FPC⁻</p>	18	AA	5700
<p>SS FPC⁺</p>	19	TMEA	6 700
<p>SS FPC⁻</p>	19	SPM	6 800
<p>LW FPC⁺</p>	100	DMEA	31 700
<p>LW FPC⁻</p>	82	AA	23 600

2.2 Characterization of FPCs in solution

2.2.1 Photophysical properties of FPCs in solution

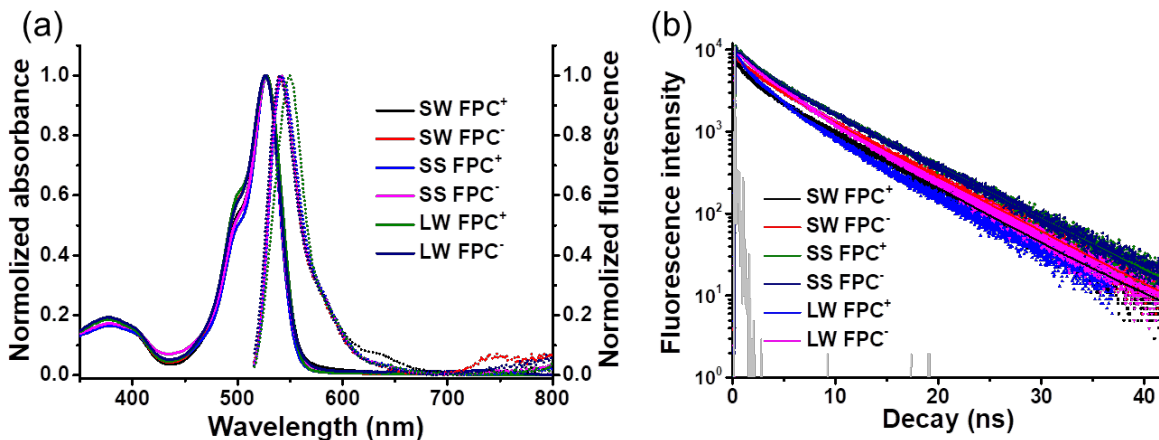


Figure 2.1. (a) Normalized absorption (full lines) and fluorescence emission (dotted lines, $\lambda_{ex} = 495$ nm) spectra and (b) fluorescence decays ($\lambda_{ex} = 495$ nm, $\lambda_{em} = 540$ nm) of (1) SW FPC⁺ ($[SW FPC^+] = 4.5 \times 10^{-7}$ M), (2) SW FPC⁻ ($[SW FPC^-] = 4.5 \times 10^{-7}$ M), (3) SS FPC⁺ ($[SS FPC^+] = 4.5 \times 10^{-7}$ M), (4) SS FPC⁻ ($[SS FPC^-] = 3.6 \times 10^{-7}$ M), (5) LW FPC⁺ ($[LW FPC^+] = 4.5 \times 10^{-7}$ M) and (6) LW FPC⁻ ($[LW FPC^-] = 3.7 \times 10^{-7}$ M) recorded in water.

Absorption and fluorescence emission spectra of all synthesized FPCs are shown in Figure 2.1a. Spectra of FPCs are almost identical in shape and position. The main fluorescent properties of BODIPY monomer (BDPMA) and FPCs are summarized in Table 2.2. The absorption and emission maxima of BDPMA and FPCs are all similar; they are located at around 527 nm and 540 nm, respectively. Only for the LW FPC⁺, the emission band is red shifted by 8 nm. One hypothesis is that LW FPC⁺ is folded and the BODIPY units are slightly aggregated. The determination of the fluorescence quantum yield and lifetime of BDPMA in toluene and FPCs in H₂O were also carried out. The fluorescence decays of the BDPMA in toluene and FPCs in H₂O were recorded at 540 nm ($\lambda_{ex} = 495$ nm) (Figure 2.1b). The fluorescence quantum yield of FPCs decreased due to the solvent effect [23]. The monomer's decay could be fitted by a single-exponential function in contrast to the FPC decay. The lifetimes of FPCs were slightly increased. This is likely due to the BODIPY fluorophore protection from solvent interactions by polymer chains.

2.2.2 Zeta potential of FPCs in solution

In addition, the zeta potentials (ζ) of FPCs were all recorded in pure distilled water (Table 2.2). Strong polyelectrolytes, both SS FPC⁺ and SS FPC⁻, are fully ionized in aqueous solution. The

zeta potentials of SS FPC⁺ and SS FPC⁻ are 44.9 ± 1.35 and -67.7 ± 0.35 mV, respectively. For the weak polyelectrolytes, the same charged groups of SW FPC⁺ and LW FPC⁺ partially dissociate. Therefore, the zeta potentials of SW FPC⁺ and SS FPC⁺ are similar. The zeta potential of LW FPC⁺ is lower than SW FPC⁺, probably because the ammonium groups are screened by the long chains. This is in agreement with the emission spectrum of LW FPC⁺ [16]. Concerning the polycations SW FPC⁻ and LW FPC⁻, they are partially ionized in distilled water due to carrying carboxyl groups. Their zeta potentials are both around -38 mV.

Table 2.2. Spectroscopic properties and zeta potentials (ζ) of the BDPMA and FPCs

	BDPMA	SW FPC ⁺	SW FPC ⁻	SS FPC ⁺	SS FPC ⁻	LW FPC ⁺	LW FPC ⁻
solvent	toluene	water	water	water	water	water	water
λ_{\max} (abs) / nm	528	527	527	527	527	527	526
λ_{\max} (em) / nm	540	541	540	542	541	549	540
Φ_F ^a	70 %	17 %	11 %	27 %	20 %	16 %	14 %
$\langle\tau\rangle$ ^b / ns	4.9	5.6	5.9	6.0	6.0	4.8	5.2
ζ ^c / mV	/	44.4±0.4	-38.4±0.8	44.9±1.4	-67.7±0.4	21.2±0.3	-38.9±0.8

^aThe relative fluorescence quantum yields were determined using Rhodamine 590 ($\Phi_F = 0.95$ in ethanol) as a reference. ^bAverage fluorescent lifetime recorded for the FPCs in water and BDPMA in toluene ($\lambda_{\text{ex}} = 495$ nm, $\lambda_{\text{em}} = 540$ nm); decay fitted with a monoexponential function for BDPMA and multiexponential function for FPCs. ^cZeta potentials (ζ) were recorded in Milli-Q water at 25 °C.

2.2.3 Isoelectric point of SW FPCs in H₂O

The isoelectric points of SW FPC⁺ and SW FPC⁻ were determined in H₂O. The neutral polymers were equilibrated with deionized water, and then the pH was adjusted by adding 1M HCl or 1M NaOH. The zeta potentials of different pH polymer solutions were measured, as shown in Figure 2.2. The value of the isoelectric point of SW FPC⁺ is around 8.55. For SW FPC⁻, the isoelectric point is about 3.35.

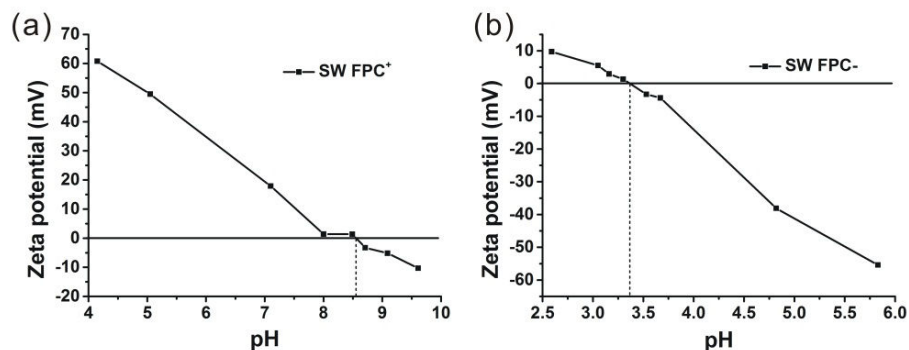


Figure 2.2. Zeta-potential of SW FPC⁺ (a) and SW FPC⁻ (b) solution as a function of pH. The concentrations of SW FPC⁺ solution is 7.8×10^{-4} M and SW FPC⁻ is 7.4×10^{-4} M, 1.0 M aqueous HCl and NaOH solutions were used to adjust the pH of the FPC solutions.

The above discussions of the photophysical properties and zeta potential measurements on each FPCs in solution indicate that FPCs are fluorescent polyelectrolytes due to the BODIPY units, and they can be charged in water. Moreover, pH of the deposition solution can be selected according to the isoelectric point of weak polyelectrolytes.

2.3 Layer-by-layer assembly deposition process investigation with SW FPCs

Table 2.3. The parameters of deposition solution

Solution	Concentration (mol/L)	pH	Ionic strength (mol/L)
SW FPC ⁺	1.3×10^{-4} ^a	5.46	0.1
SW FPC ⁻	1.3×10^{-4} ^a	5.48	0.1

^a for the optimization of concentration of SW FPC, the concentration of SW FPCs are 1.3×10^{-4} M, 1.3×10^{-5} M, 1.3×10^{-6} M, 8.0×10^{-7} M, 5.0×10^{-7} M and 1.3×10^{-7} M, respectively.

Self-assembled layer-by-layer (LbL) films were prepared by alternatively depositing the two oppositely charged SW FPCs on glass by means of electrostatic interactions. After the piranha solution treatment, the glass slides are highly hydrophilic and negatively charged. The surface structure and quality of the LbL films depend on the experimental conditions during deposition: concentration, pH and ionic strength. For both kinds of polyelectrolytes, the concentration of the deposition solution is the crucial factor in the LbL film fabrication. SW FPCs were selected as the model to investigate the concentration effect. pH of SW FPCs deposition solution was set according to the zeta potential results, both of the SW FPCs are almost fully ionized when pH

values are around 5.5 (Figure 2.2). In addition, in order to enhance the adsorption of polyelectrolytes onto surface to clearly observe the deposition process, ionic strength was set at 0.1 M [24]. Under the deposition condition (Table 2.3), we recorded the absorption and emission spectra after each layer deposition for each concentration to help us understand and optimize the LbL assembly deposition process.

Before the investigation of the concentration effect on SW FPCs, the layer-by-layer assembly process was studied under the above mentioned deposition condition when the concentration of SW FPCs was 0.95×10^{-5} M. During layer-by-layer assembly, the UV-vis. spectra of LbL film were measured after the construction of each layer (Figure 2.3a). The absorbance increment at 529 nm dependent on the number of layers is linear (Figure 2.3b). This indicates that the deposition process is going on as expected.

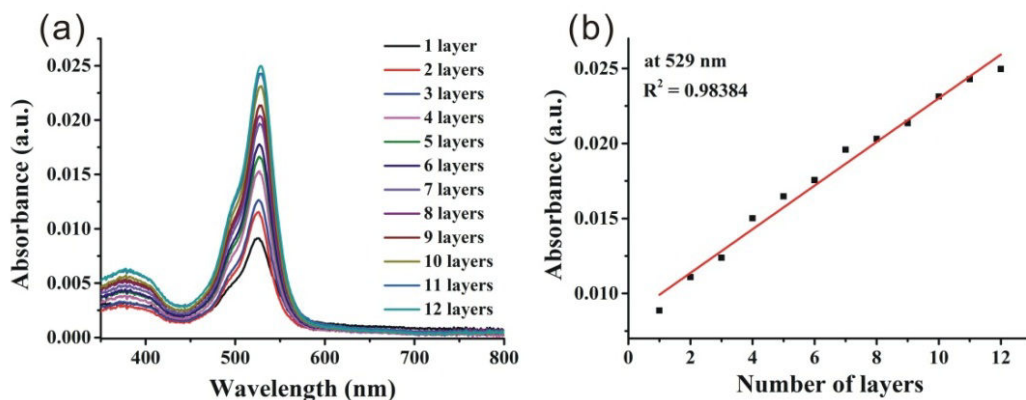


Figure 2.3. (a) UV-Vis absorption spectra of LbL self-assembly of FPC layers on activated glass slide with SW FPC⁺ and SW FPC⁻. (b) The dependence of the intensity of BDP absorbance at 529 nm as a function of number of layers. The LbL assembly was performed at [SW FPCs] = 0.95×10^{-5} M.

As shown in Figure 2.4, when the concentration of the deposition solution is higher ([SW FPCs] = 1.3×10^{-4} mol/L), the absorbance increment as a function of the number of layers is non-linear (Figure 2.4a). It is possible that an explanation could be found from the corresponding emission spectrum (Figure 2.4e). At the beginning of LbL deposition, there were two BODIPY aggregates bands. This means that there were some aggregates on the first bilayer film surface inducing an inhomogeneous layer. The concentrated deposition solution forces the FPCs to contract and form compact coils due to the self-shielding [25]. When the deposition is carried further, the number of FPCs are random, which depends on the binding sites from the underlying surface layer [26]. Only when the concentration of the deposition solution is reduced to 1.3×10^{-6} mol/L, there is a single emission band at the first bilayer (Figure 2.4f). In addition, the corresponding absorbance was below to 0.01. For the purpose of reducing the amount of sample, we decreased the concentration of the deposition solution until a homogeneous and fluorescent

film surface could still be obtained. When the concentration of the deposition solution is reduced to 1.3×10^{-7} mol/L, the absorption spectrum is very noisy. This means that in this case, SW FPCs were hard to deposit on the substrate. Therefore, the optimum concentration of the deposition solution seems to be 5.0×10^{-7} mol/L. However, it was very clearly seen that when the number of bilayers increased, the fluorescence intensity of the LbL film decreased. This could be attributed to the formation of aggregates during LbL deposition process [27]. In summary, homogeneous films were obtained by the layer-by-layer assembly from low concentration solutions of SW FPCs (5.0×10^{-7} mol/L).

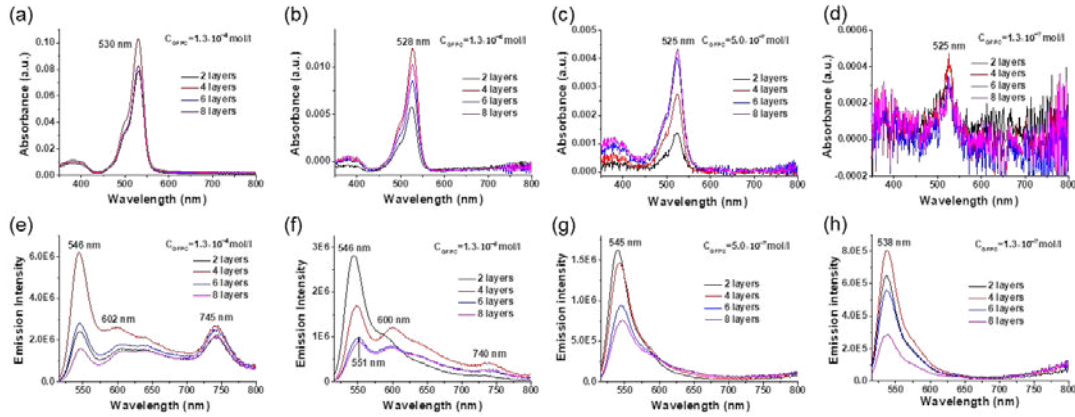


Figure 2.4. The effect of the concentration of deposition solutions (SW FPC⁺ and SW FPC⁻) (a, e) 1.3×10^{-4} M; (b, f) 1.3×10^{-6} M; (c, g) 5.0×10^{-7} M; (d, h) 1.3×10^{-7} M on the absorption and emission spectra of each bilayer (SW FPC⁺/SW FPC⁻) of SW FPC LbL films.

2.4 Photophysical and surface characterizations of the three types of FPC LbL films

Table 2.4. The parameters of deposition solution

Solution	Concentration (mol/L)	pH	Ionic strength (mol/L)
SW FPC ⁺	5.0×10^{-7}	5.49	0.1
SW FPC ⁻	5.0×10^{-7}	5.56	0.1
SS FPC ⁺	5.0×10^{-7}	5.46	0.1
SS FPC ⁻	5.0×10^{-7}	5.44	0.1
LW FPC ⁺	5.0×10^{-7}	5.41	0.1
LW FPC ⁻	5.0×10^{-7}	5.51	0.1

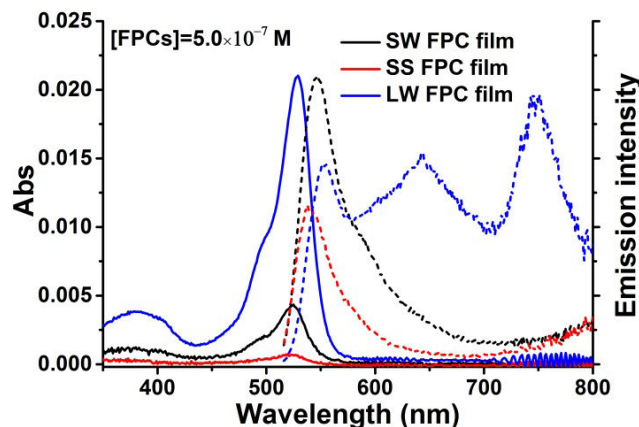


Figure 2.5. Effect of the nature of polymer (SW, SS and LW FPCs) on absorption and emission spectra of FPC LbL films with 8 layers ($[FPCs] = 5.0 \times 10^{-7} M$).

As shown above, the greater the number of layers is, the thicker the FPC LbL films will be. Considering that the adsorption of FPCs on surface will afford more active sites on the film surface, it might result in more efficient bacteria detection. FPC LbL films were thus prepared with four bilayers (eight layers) for the following studies. SW, SS and LW FPC LbL films were fabricated using the optimum concentration of the deposition solutions (Table 2.4). Figure 2.5 shows the absorption and emission spectra of the three FPC LbL films with four bilayers. The UV-vis. spectra show that the amount of absorbed LW FPCs was the maximum, compared with the SW and SS FPCs. However, the fluorescence intensity of the SW FPC film was the strongest. The aggregate bands at 645 and 745 nm were observed in the emission spectrum of LW FPC film.

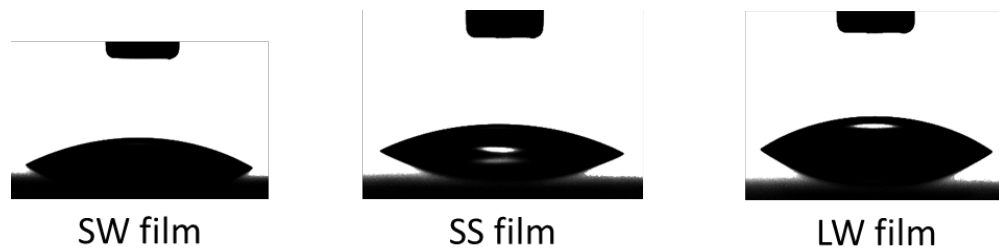


Figure 2.6. The contact angle images of the SW, SS and LW LbL FPC film surfaces.

Besides the photophysical properties, we also studied the morphologies of the three types of FPC LbL film surfaces. Firstly, the surface wettability of these three films was determined by measuring the contact angle of water drops on the surface (Figure 2.6). The water contact angle of the blank “piranha” treated glass slide was measured to be $4^\circ \pm 2^\circ$. The contact angle results confirmed that the SW, SS and LW FPC LbL film surfaces were hydrophilic with $32.7^\circ \pm 2^\circ$,

$27.2^\circ \pm 2^\circ$ and $33.7^\circ \pm 2^\circ$, respectively.

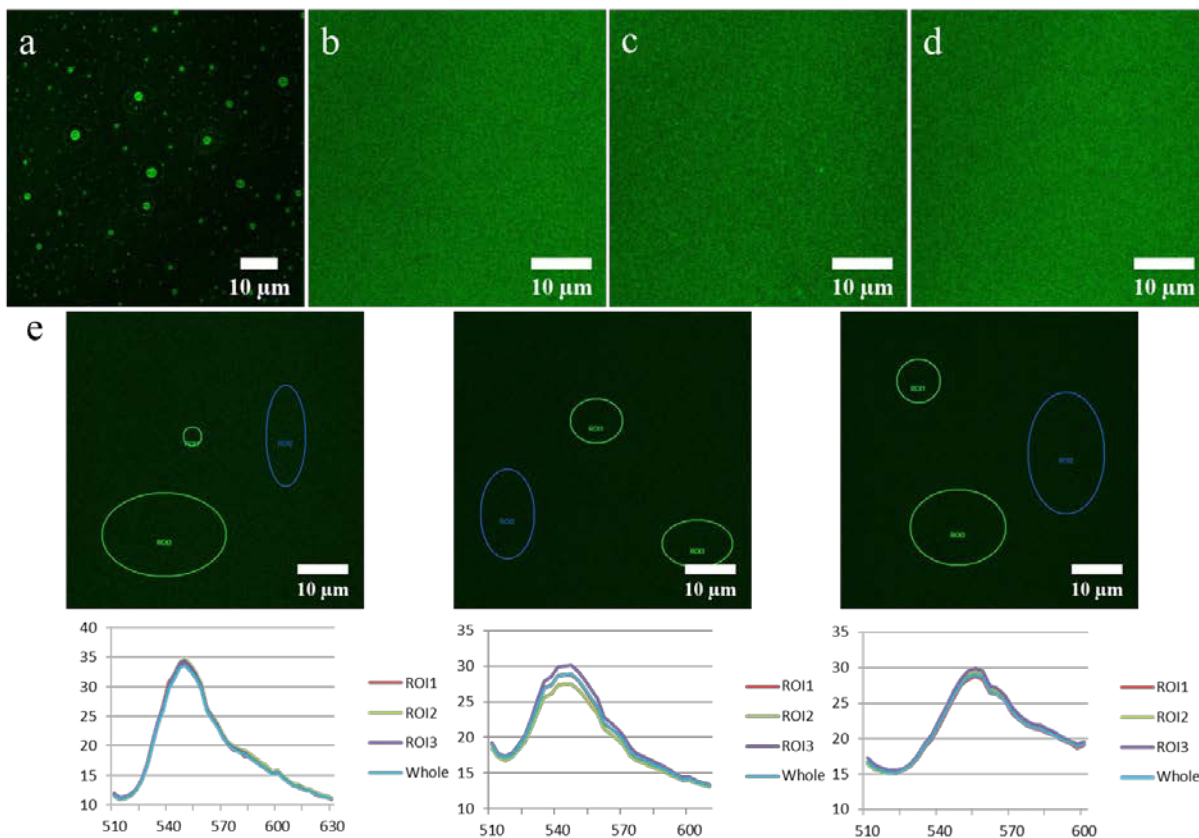


Figure 2.7. Confocal fluorescence microscope images of (a) SW ($[SW\ FPCs] = 1.3 \times 10^{-4}\ M$), (b) SW ($[SW\ FPCs] = 5.0 \times 10^{-7}\ M$), (c) SS ($[SS\ FPCs] = 5.0 \times 10^{-7}\ M$) and (d) LW FPC ($[LW\ FPCs] = 5.0 \times 10^{-7}\ M$) LbL film surfaces, respectively. (e) Fluorescence intensity images of SW, SS and LW FPC LbL films (from left to right) and the corresponding spectra of different ROIs on the films recorded with a confocal microscope ($\lambda_{ex} = 496\ nm$).

Fluorescence images of SW, SS and LW FPC LbL films were recorded under a confocal microscope (Figure 2.7). The results indicate that the film surfaces are quite homogeneous without large aggregation spots (Figure 2.7b, c and d), compared with the SW FPC LbL film surface with many aggregations that prepared in high concentration of the deposition solutions ($[SW\ FPCs] = 1.3 \times 10^{-4}\ M$) (Figure 2.7a). In addition, the spectra of different zones of FPC LbL films were recorded (Figure 2.7e). For each FPC LbL film, the emission maximum of all spectra locates at the same position, which means that the films are uniform.

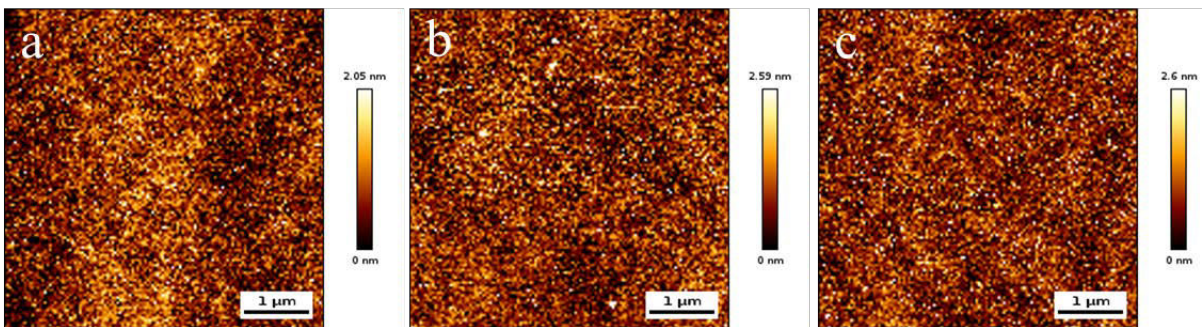


Figure 2.8. AFM images of SW (a), SS (b) and LW (c) FPC LbL film surfaces, respectively.

Furthermore, the nanometer scale topologies of SW, SS and LW FPC LbL film surfaces were measured by AFM (Figure 2.8a, b and c). The AFM images confirm that the SW, SS and LW FPC LbL film surfaces are uniform with around 2.05, 2.59 and 2.6 nm in height, respectively.

2.5 Stability and toxicity assessments of the three types of FPC LbL films

2.5.1 Stability study of the FPC LbL film

Before testing them for detection of biological samples, the stability of the FPC LbL films was investigated. We suspected that FPC LbL films in contact with solutions might detach from the substrate or re-disperse into the solution. Therefore, we measured the UV-vis. spectra of the SW FPC LbL film wetted by different solutions: H_2O , 0.1M NaCl solution and M9 culture medium (Figure 2.9). The absorbance of the SW FPC LbL film in the presence of different solutions shows no significant change. This means that FPC LbL films have good stability in different solutions and are able to apply to bacteria detection.

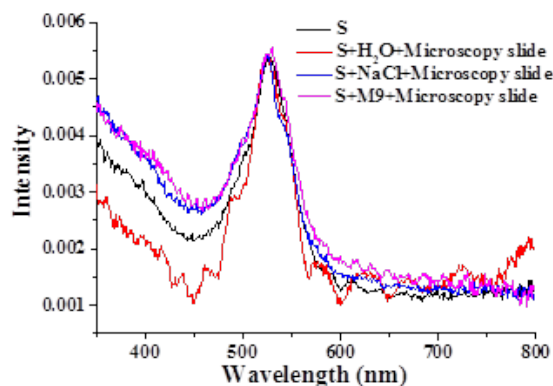


Figure 2.9. UV-vis spectra of the SW FPC LbL film in the presence of different solutions (H_2O , 0.1M NaCl and M9).

2.5.2 Toxicity assessments

The possible toxic effect of the three pairs of FPCs on *E. coli* was measured by monitoring the growth rates of bacteria in the presence of each type of FPC in M9 culture medium (the final concentration of the FPC solutions are all 4.0×10^{-6} M). The growth rate of *E. coli* bacteria in the M9 culture medium was measured in the same conditions as control. For over 18 hours incubation, the growth curve of bacteria with SW FPC⁻ was very similar to the growth curve of bacteria in M9 culture medium (Figure 2.10a) while the growth rate of bacteria with SW FPC⁺ was decreased over the same time period. For the other types of FPC solutions (Figure 2.10b and c), the growth curves of bacteria have the same trend. This means that, on one hand, the three types of FPC⁻ solutions have no toxic effect on bacteria growth over a time scale of several hours. On the other hand, the three types of FPC⁺ solutions slightly inhibit *E. coli* growth. This might be due to the ammonium group of FPC⁺ which are known to be bactericides [28].

Following this observation, FPC LbL films with FPC⁻ as the outermost layer were prepared. In order to confirm that the FPC LbL films where FPC⁻ was the outermost layer were non-toxic, we immersed SW, SS and LW FPC LbL films into *E. coli* bacteria suspension and incubated them at 37 °C. For over 3.5 hours incubation time, the growth curves of bacteria with SS, SW and LW FPC film were almost the same as the growth curve of bacteria alone (Figure 2.10d). This means that the three types of FPC LbL films with FPC⁻ as the external layer show good biocompatibility.

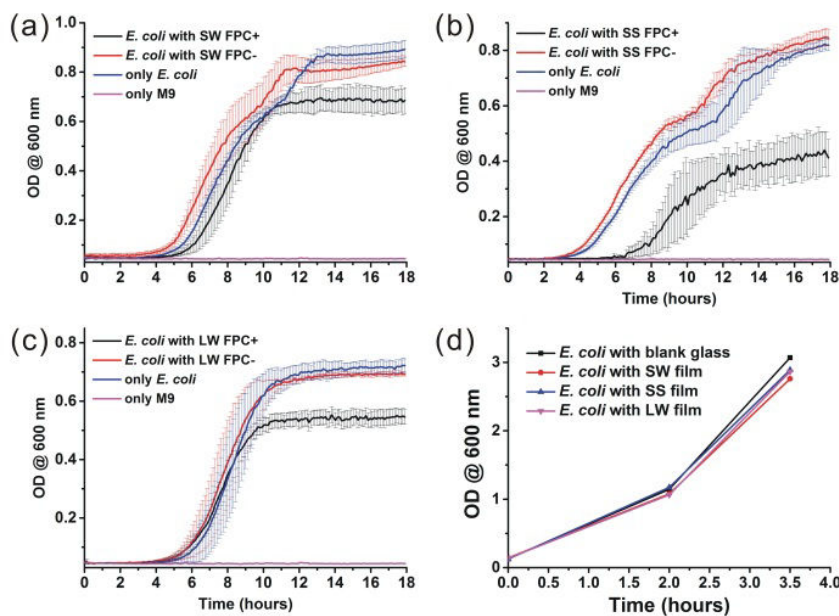


Figure 2.10. *E. coli* bacteria growth rates incubated with (a) SW, (b) SS and (c) LW FPCs solutions by measuring the OD@600 nm as a function of time in M9 medium ($[FPCs] = 4.0 \times 10^{-6}$ M). (d) Growth curves of *E. coli* bacteria in the presence of SW, SS and LW FPC LbL films with 8 layers and glass in M9 medium.

2.6 *E. coli* bacteria detection with FPC LbL films

2.6.1 Effect of the concentration of the deposition solution on *E. coli* bacteria detection with SW FPC LbL films

Before studying the interaction of bacteria with the FPC LbL films, the interaction of *E. coli* bacteria with FPC molecules as fluorescent dyes in solution were investigated. The water-soluble and biocompatible SW FPC⁻ was chosen as the model. The sample was observed under a wide-field fluorescence microscope after the addition of SW FPC⁻ (final concentration 6.6×10^{-5} M) to M9 growth medium containing bacteria at 37 °C in the dark for one hour, followed by two washing steps with PBS to remove the free SW FPC⁻. The fluorescence images show that most of *E. coli* cells were targeted with green fluorescence (Figure 2.11a).

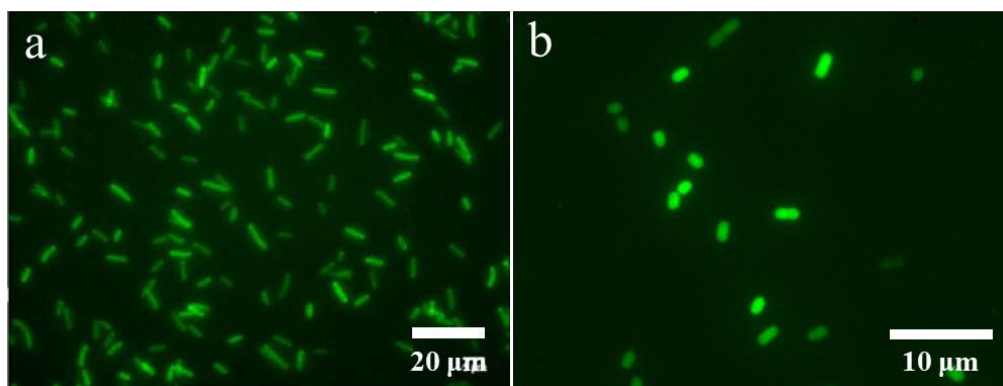


Figure 2.11. (a) The fluorescence microscope image of *E. coli* bacteria in the presence of SW FPC⁻ after 1 hour incubation. (b) The image after adding MB.

In order to determine whether the SW FPC⁻ are inside the bacteria or target the membrane of the bacteria cells, methylene blue (MB), which is a quencher of BODIPY fluorescence, was introduced in the solution. The working principle is that since MB does not enter the bacteria, only the fluorescent molecules outside the cells can be quenched while the polymers inside the bacteria will be protected by the membrane and remain fluorescent (Figure 2.12). In other words, if the bacteria remain fluorescent after adding MB, this means that FPCs are inside while if the SW FPC⁻ molecules are on the membrane their emission will be quenched. After adding MB, the *E. coli* cells were still green fluorescent (Figure 2.11b). This means that SW FPC⁻ entered the *E. coli* cells.

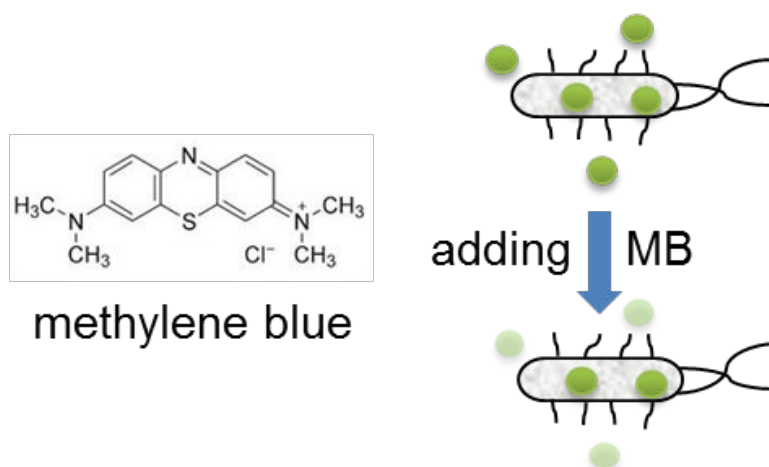


Figure 2.12. Chemical structure of methylene blue (left) and schematic diagram of the determination for fluorescence internalization of *E. coli* bacteria in the presence of fluorescent polymer (right).

The polymer chains have free mobility in solution, after the polymer chains are assembled as a film, are they arranged in a particular way or self-assembled? We studied the effect of the concentration of the FPC solutions during deposition and the effect of the nature of FPCs on the detection of *E. coli* bacteria.

Figure 2.13 shows that when the concentration of the deposition solution is increased from 5.0×10^{-7} M to 1.3×10^{-4} M, the *E. coli* bacteria became labeled on the SW FPC film (Figure 2.13a and b). While at the lower concentration, bacteria cells are less fluorescent (Figure 2.13c and d). We hypothesized that the bacteria are able to extract and internalize the outermost SW FPC⁻ in the first case (high concentration of the deposition solution) while they could not in the second. This can be explained by the fact that when the concentration of the SW FPC solution is lower, the thickness of the outermost SW FPC⁻ layer is likely to be thinner. It means the electrostatic adsorption between the top SW FPC⁻ molecule and the next to last SW FPC⁺ layer is stronger than in the case of the higher concentration (figure 2.13e). Therefore, for the bacteria it is more difficult to detach the top SW FPC⁻ of “low concentration” LbL films and they are less fluorescent.

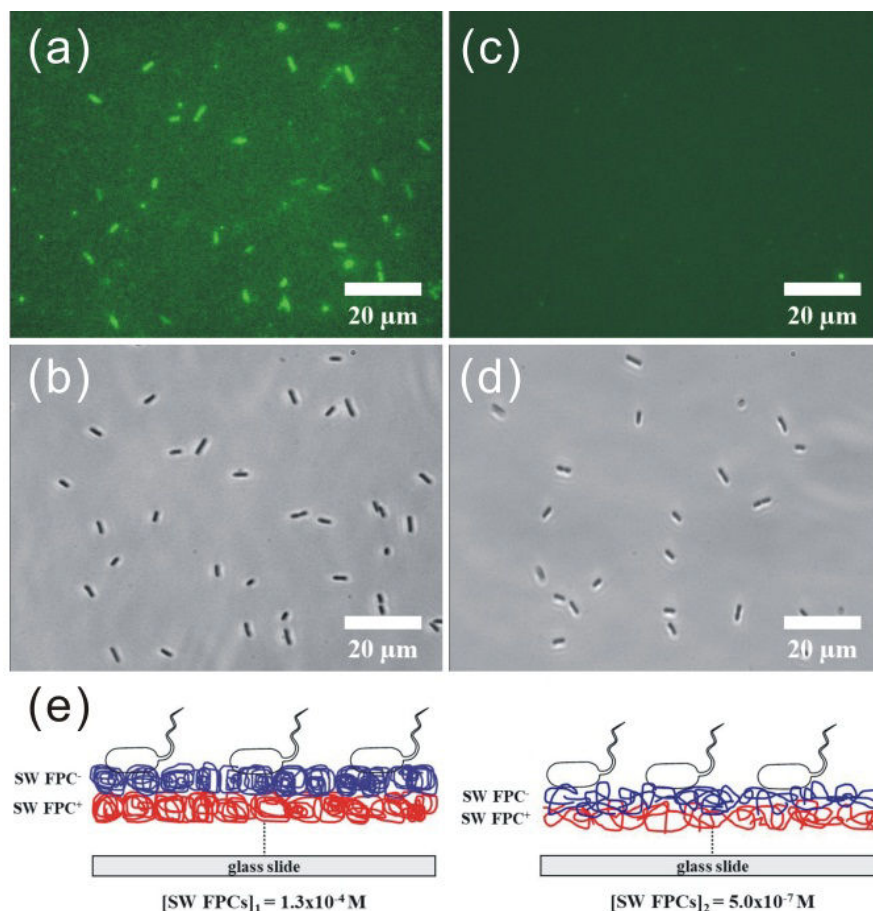


Figure 2.13. Wide field microscope fluorescence (a, c) and phase contrast images (b, d) of *E. coli* bacteria on SW FPC LbL films prepared under different concentrations of SW FPCs solutions: (a, b) $[SW FPCs] = 1.3 \times 10^{-4} M$; (c, d) $[SW FPCs] = 5.0 \times 10^{-7} M$. (e) Schematic diagram of the effect of the concentration of the FPCs solutions during deposition on film morphology and *E. coli* bacteria detection.

2.6.2 Effect of the nature of fluorescent polymers on *E. coli* bacteria detection

All the FPC LbL films were obtained under the lower concentration of the FPCs solutions ($5.0 \times 10^{-7} M$). After incubation of *E. coli* bacteria on these three kinds of FPC LbL film surfaces (SW, SS and LW) for only 10 mins, we found that only in the case of LW FPC film, almost every bacterium was stained with green fluorescence (Figure 2.14a-f).

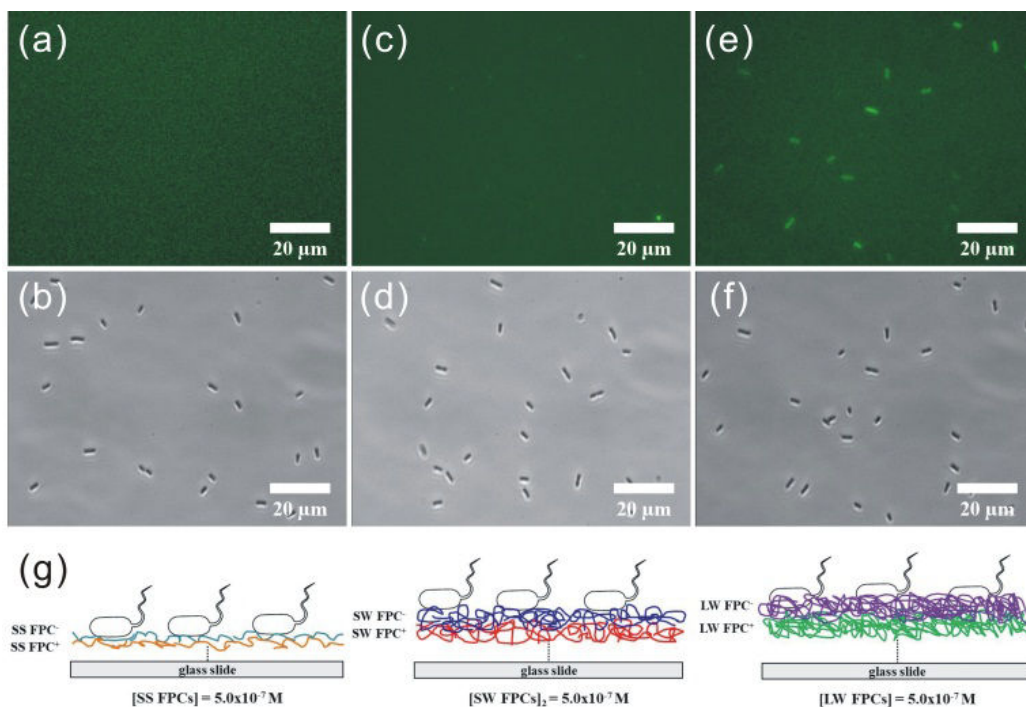


Figure 2.14. Microscope images of *E. coli* bacteria on SS FPC LbL film (a and b), SW FPC LbL film (c and d) and LW FPC LbL film (e and f) which prepared under the concentration of FPCs solutions was 5.0×10^{-7} M. (g) The schematic diagram of the effect of the nature of the FPCs on the *E. coli* bacteria detection.

It is likely that at the same concentration of the FPCs solutions (Figure 2.14g), the two SW FPC and SS FPC LbL films, which are both short chains polyelectrolytes, have a similar thickness of the outermost FPC⁻ layer. However, the interaction forces between strong polyelectrolytes (SS FPC⁺ and SS FPC⁻) is stronger than for the weak polyelectrolytes (SW FPC⁺ and SW FPC⁻). Therefore, for the SS FPC LbL film, the film has a compact morphology and SS FPC⁻ molecules are more difficult to detach from the surface structure, compared to the SW FPC LbL film. Meanwhile, when comparing the two weak polyelectrolytes films at the same concentration of the FPCs solutions, the outermost long chain FPC⁻ layer should be thicker due to the longer chains. This means that the electrostatic adsorption between the top LW FPC⁻ molecule and the next to last LW FPC⁺ layer is weaker. That is to say, the interaction force in the case of the LW FPC surface is the weakest and therefore, the *E. coli* bacteria can catch the LW FPC⁻ molecule easily.

In summary the study of the effect of the concentration of the FPCs solutions during deposition and of the nature of FPCs on the detection of *E. coli* bacteria shows that the LW FPC LbL film can detect *E. coli* more effectively under quite low concentration of the FPCs solutions compared to the others.

2.7 Mechanism of *E. coli* bacteria detection with LW FPC LbL films

2.7.1 FPC localization with methylene blue (MB)

The methylene blue (MB) method was used as described previously (see §2.6.1) in order to investigate the mechanism of detection of *E. coli* bacteria on the LW FPC LbL film. The quencher was added to the film surface to determine whether the LW FPCs were inside *E. coli* or on the membrane. The results show that the bacteria are still with fluorescent in the presence of MB (Figure 2.15a and b). This means that LW FPCs⁻ entered the *E. coli* cells.

2.7.2 Dead-alive assay with propidium iodide (PI)

Propidium iodide (PI) is a membrane impermeable dye and therefore does not enter viable cells with intact membranes. On the other hand, when cells are dead, their membrane is damaged and PI does gain access to nucleic acids and intercalates resulting in a dramatic red fluorescence increase. PI is therefore used to identify dead cells [29]. After incubating *E. coli* bacteria on the LW FPC LbL film in the presence of the PI solution ([PI] = 0.1 mg/mL), the results indicate that the *E. coli* bacteria were labeled by LW FPC LbL film (Figure 2.15d) as well as stained with red fluorescence coming from PI (Figure 2.15e). This means that the *E. coli* bacteria on the LW FPC films have damaged cell membranes when they were detected on the film by green fluorescence.

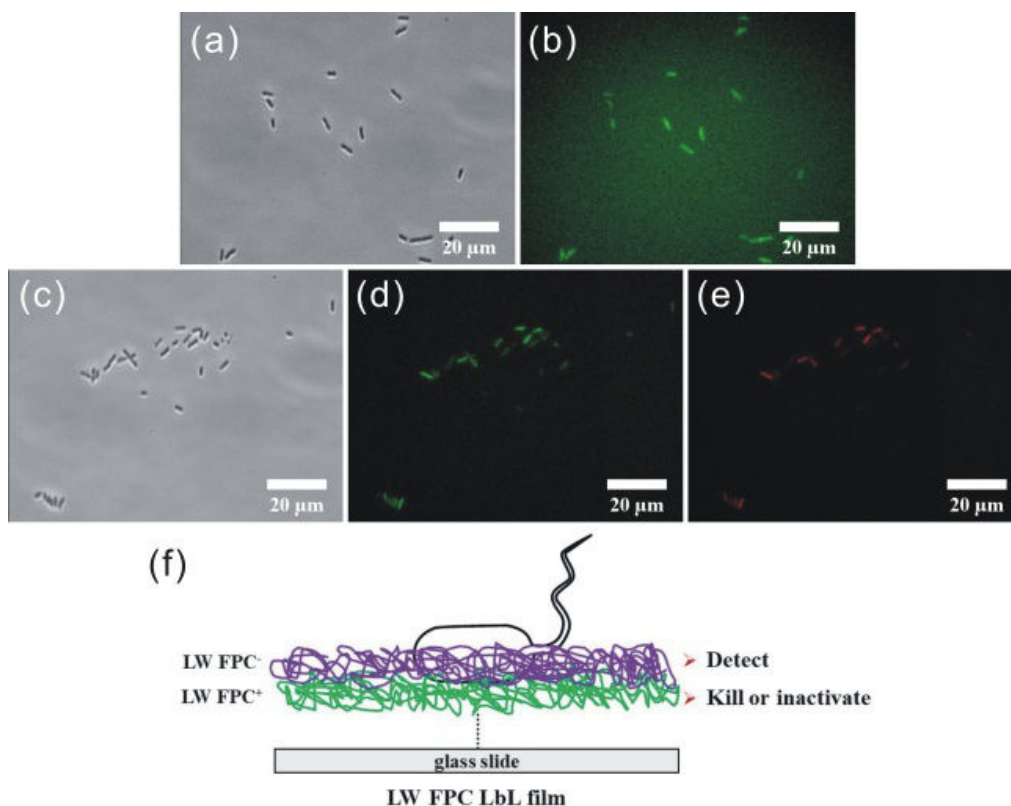


Figure 2.15. Microscope images of *E. coli* bacteria on LW FPC LbL film after adding methylene

blue (a and b), in the presence of propidium iodide (c, d ($\lambda_{ex}=482$ nm) and e ($\lambda_{ex}=543$ nm)). (f) The schematic diagram of the mechanism of *E. coli* bacteria detection with LW FPC LbL films.

Based on the MB and PI assessments of the *E. coli* detection on the LW FPC LbL films, we propose a mechanism for the labeling of *E. coli* bacteria by LW FPC LbL films (Figure 2.15f). Upon interaction between *E. coli* bacteria and the outermost LW FPC⁻ layer, the LW FPC⁻ chains detach from the surface and enter the *E. coli* cells which then became fluorescent. Therefore, the bacteria can be detected on the outermost LW FPC⁻ layer. The *E. coli* bacteria are then in contact with the next to last layer containing LW FPC⁺. As demonstrated by toxicity assessment (see §2.5.2), the LW FPC⁺ is toxic for *E. coli* bacteria due to the DMEA unit [28]. The bacterial growth curve in a more concentrated LW FPCs⁺ solution (8.0×10^{-5} M) also confirmed this point (Figure 2.16). It is possible that the *E. coli* bacteria were killed or inactivated by the concentrated LW FPC⁺ layer. This means that the controllable FPC LbL film not only can detect but also kill or inactivate bacteria which will lead to more future advances for the pathogenic bacteria detection.

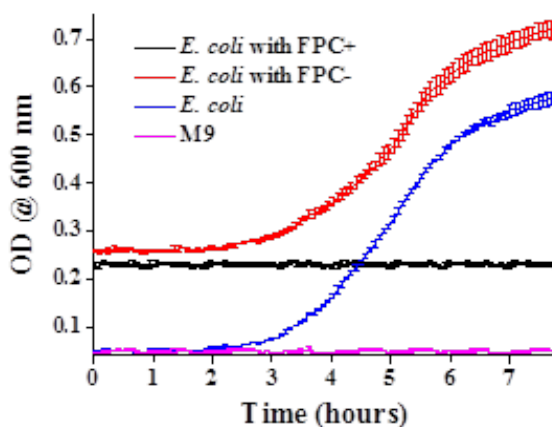


Figure 2.16. The growth rates of bacteria with concentrated LW FPC⁺ and LW FPC⁻, respectively.

2.8 Conclusions

In conclusion, water-stable BODIPY-based FPC LbL thin films have been successfully developed by LbL self-assembly and used as a functional first-generation sensing device for *E. coli* bacteria detection. The spectroscopic and surface properties of FPC LbL films were easily controlled by adjusting the deposition conditions, such as the concentration of the FPCs solution and the nature of FPCs. When the concentrations of the FPCs solution were 5.0×10^{-7} M, the FPC LbL film surfaces were homogenous. In addition, we also demonstrated that the *E. coli* bacteria detection can be carried out with the LW FPC LbL film surfaces. In the following we will aim at

first increasing the sensitivity of the films using the metal enhanced fluorescence principle (chapter 3) and then their selectivity by introducing a specific recognition site on the surface of the film (chapter 4).

Experimental Section

Materials

4-hydroxybenzaldehyde (98%, Aldrich), 2,4-Dimethyl-3-ethylpyrrol (97%, Aldrich, Kryptopyrrol), boron trifluoride diethyletherate (2M in diethyl ether, Aldrich), tetrachloro-1,4-benzoquinone (99%, Aldrich, Chloranil), N,N-diisopropylethylamine (99.5%, Sigma-Aldrich, DIPEA), 1,8-diazobicyclo[5, 4, 0]undec-7-ene ($\geq 98\%$, Fluka, DBU), trifluoroacetic acid (99%, Sigma-Aldrich, TFA), Poly(ethylene glycol) methyl ether acrylate (Sigma-Aldrich, $M_n = 454$ g.mol⁻¹, APEG), 2-methyl-2-[(dodecylsulfanylthiocarbonyl)sulfanyl] propanoic acid (97%, Strem, TTCA), acrylic acid (99%, Aldrich, AA), 2-(Dimethylamino)ethyl acrylate (98%, Sigma, DMEA), [2-(Acryloyloxy)ethyl]trimethylammonium chloride (80 wt. % in H₂O, Sigma, TMEA), 3-Sulfopropyl methacrylate potassium (98%, Sigma, SPMP) were used as received without further purification. Solvents were of synthetic grade and purified according to standard procedures. 2,2'-Azobis(2-methylpropionitrile) (98%, Sigma, AIBN) was recrystallized from chloroform containing a few drops of petroleum ether. 18 M Ω Millipore water was used throughout and further pH-adjusted with either 0.1M HCl or NaOH.

M9 minimal medium: 4mL 5 \times Salts, 4 mL 5 \times complementary salts, 0.4 mL glucose 20%, 0.5 mL CAA 20% and 11.1 mL H₂O.

Characterization techniques

All nuclear magnetic resonance (NMR) spectra were recorded in CDCl₃ on a JEOL ECS (400 MHz) spectrometer. All chemical shifts are in ppm and referenced to tetramethylsilane (TMS).

Zeta potentials (ζ) were performed on a Zetasizer Nanoseries (Malvern) apparatus. The dispersant RI value was 1.330. Samples were analyzed in DTS 1060 plastic cells, at 25 °C. Three measurements of at least ten scans were performed for each sample.

pH measurements were performed using a glass electrode connected to PHM210 Standard pH meter from Mettler Toledo.

Absorption measurements were performed using Varian Cary 100 and Cary 500 from Agilent Technologies.

Emission spectra were performed using Fluorolog FL3-221 spectrofluorimeter from Horiba Jobin-Yvon. A front-face configuration was used.

The fluorescence decay curves were obtained with a time-correlated single-photon-counting method using a titanium-sapphire laser (82 MHz, repetition rate lowered to 4 MHz thanks to a pulse-peaker, 1 ps pulse width, a doubling crystals is used to reach 495 nm excitation) pumped by an argon ion laser from Spectra Physics (Mountain View, CA, USA). The Levenberg-Marquardt algorithm was used for non-linear least square fit as implemented in the Globals

software (Globals Unlimited, Villa Grove, USA). In order to estimate the quality of the fit, the weighted residuals were calculated. In the case of single photon counting, they are defined as the residuals, i.e. the difference between the measured value and the fit, divided by the square root of the fit. χ^2 is equal to the variance of the weighted residuals. A fit was said appropriate for χ^2 values between 0.8 and 1.2.

Contact angles were performed on an advanced surface technology (AST) video contact angle measuring device. A 1 μ L droplet of deionized water was deposited on the samples.

Microscope images were taken on an epifluorescence microscopy (Nikon inverted microscope ECLIPSE TI-E) or a confocal laser scanning microscope (Leica TCS SP5).

Atomic force microscopy (AFM) images were recorded by JPK Nanowizard3 instrument.

Synthesis

Synthesis of BODIPY (BODIPY phenol) [30]. A few drops of trifluoroacetic acid were added to a dichloromethane solution of kryptopyrrole (1.0 g, 2 equiv.) and 4-hydroxybenzaldehyde (500 mg, 1 equiv.). The dark reaction mixture was stirred at room temperature until total disappearance of the aldehyde. The oxidising agent (chloranil, 1 equiv.), then 5 min later DIPEA (7 equiv.) and finally trifluoroborate etherate (11 equiv.) were successively added. The mixture was filtered through a pad of silica or used crude. The filtrate was concentrated and the residue purified by chromatography on silica gel or by automatic chromatography to afford BODIPY.

^1H NMR (400 MHz, CDCl_3): $\delta(\text{ppm}) = 0.98$ (t, $J = 7.5$, 6H, CH_2CH_3), 1.35 (s, 6H, CH_3), 2.31 (q, $J = 7.5$ Hz, 4H, CH_2CH_3), 2.53 (s, 6H, CH_3), 6.95 (d, $J = 8.24$ Hz, 2 H_{ar}). ^{13}C NMR (100 MHz, CDCl_3): $\delta(\text{ppm}) = 12.12, 12.76, 14.90, 17.35, 116.29$ (C_{ar}), 128.17, 129.93 (C_{ar}), 131.39, 132.97, 138.64, 140.54, 153.79, 156.48. ^{19}F NMR (376 MHz, CDCl_3): $\delta(\text{ppm}) = -145.68$ (q, $J = 32$ Hz, BF_2). ^{11}B NMR (128 MHz, CDCl_3): $\delta(\text{ppm}) = -0.13$ (t, $J = 32$ Hz).

Synthesis of BODIPY Methacrylate [21]. BODIPY phenol (1 equiv. 1.2 mmol, 475 mg) is dissolved in 50 mL of anhydrous dichloromethane under argon. Then DBU (2 equiv., 2.4 mmol, 365 mg) is slowly added with a syringe to the solution and methacryloyl chloride (1.5 equiv., 1.8 mmol, 190 mg) is added to the dark solution. The mixture is stirred at room temperature during 24 h, until disappearance of the BODIPY phenol trace on TLC. The mixture is concentrated and the residue purified by chromatography on silica gel (dichloromethane/petroleum ether: 70/30), affording 432 mg of product.

^1H NMR (400 MHz, CDCl_3): $\delta(\text{ppm}) = 0.97$ (t, $J = 7.6$ Hz, 6H), 1.33 (s, 6H), 2.08 (s, 3H), 2.29 (q, $J = 7.6$ Hz, 4H), 2.52 (s, 6H), 5.80 (s, 1H), 6.39 (s, 1H), 7.27 (d, $J = 8.7$ Hz, 2H), 7.32 (d, $J = 8.7$ Hz, 2H); ^{13}C NMR (100 MHz, CDCl_3): $\delta(\text{ppm}) = 165.69, 154.01, 151.44, 139.22, 138.45, 135.78, 133.32, 133.00, 130.90, 129.53, 127.68, 122.58, 18.46, 17.15, 14.68, 12.60, 11.92$. ^{19}F

NMR (376 MHz, CDCl_3): $\delta(\text{ppm}) = -145.68$ (q, $J = 32.9$ Hz, BF_2). ^{11}B NMR (128 MHz, CDCl_3): $\delta(\text{ppm}) = -0.15$ (t, $J = 32.9$ Hz).

Synthesis of three types of fluorescent polymer chains (FPC). Reversible addition-fragmentation transfer (RAFT) polymerization of BODIPY methacrylate is performed in the presence of APEG and different charged units in a one-pot process. In a typical experiment, TTCA agent (0.047 g, 0.13 mmol), APEG (0.506 g, 1.15 mmol), BODIPY methacrylate (0.179 g, 0.38 mmol), AA (0.083 g, 1.15 mmol) and DMF (as an internal reference for the ^1H NMR determination of the monomer consumption in deuterated chloroform) (0.047 g, 0.64 mmol) are dissolved in 5 ml of 1,4-dioxane at room temperature. Then 0.0427 mL of a 0.33 M solution of ACPA in 1,4-dioxane is added. The mixture is purged with nitrogen for 30 min in an ice bath, and then placed in an oil bath thermostated at 80°C to initiate the polymerization. After 90 min, the reaction is stopped by immersion of the flask in iced water. In this case, we obtained the short chain and weak polyelectrolytes negatively charged FPC (SW FPC $^-$). In addition, when changing the charged units (DMEA, TMEA or SPMP), the short chain and weak polyelectrolytes positively charged FPC (SW FPC $^+$), the short chain and strong polyelectrolytes positively charged FPC (SS FPC $^+$) or the short chain and strong polyelectrolytes negatively charged FPC (SS FPC $^-$) were formed, respectively. Furthermore, increasing the amount of AIBN in the polymerization, the long chain and weak polyelectrolytes positively charged FPC (LW FPC $^+$) and the long chain and weak polyelectrolytes negatively charged FPC (LW FPC $^-$) were prepared, respectively.

Preparation of the FPCs multilayers

The glass slides were treated with Piranha solution (70% H_2SO_4 +30% H_2O_2) for 30 min, washed three times with deionized water, and then dried under a gentle stream of nitrogen gas. (*CAUTION: "Piranha" solution reacts violently with organic materials; it must be handled with extreme care.*). The polycations (FPC $^+$) and polyanions (FPC $^-$) were dissolved in pure water. Adjust the pH and ionic strength of the dipping solution with HCl (or NaOH) and NaCl, respectively. In the deposition process, the substrates were dipped in a polyelectrolyte solution for 10 min and washed with pure water that was adjusted to be the same pH as the polyelectrolyte dipping solution. After each deposition and washing, the samples were blown dry with a flow of compressed air. Substrates were then dipped in the oppositely charged solution for an equal amount of time followed by the same washing and drying procedures. The FPCs multilayer thin films were prepared by repeating the above deposition process.

Bacteria culture

Bacteria strain used in this research was *Escherichia coli* (K-12, BW25113). The strain was

firstly streaked onto Luria-Bertani (LB) agar plates, and then incubated at 37 °C for overnight. An isolated colony of each strain was picked and inoculated in 5 mL of LB medium. After incubation at 37 °C for overnight (shaking at 350 rpm and 5% CO₂), the bacteria culture was then diluted 1:100 in the M9 minimal growth medium. After incubation at 37 °C for 2 hours, the bacteria suspensions were carried out during all experiments.

Toxicity assessments of FPCs on *E. coli* bacteria in solution and on surface

Bacterial cultures were prepared overnight from stock cultures inoculated in M9 growth medium. The overnight culture of bacteria was diluted 1:1000 in M9. 150 µL of bacterial solution were placed in each well of a 96 well Falcon Polystyrene Flat Bottom Plate. Three types of FPC⁺ and FPC⁻ solutions were added into the *E. coli* solution to reach final concentration of 4.0x10⁻⁶ M. Each plate contained three repeats of the same concentration. One control with only bacteria and one blank with only M9 growth medium were also prepared. 70 µL of mineral oil were added to each well in order to avoid evaporation. Samples were incubated in a plate reader (Perkin Elmer Victor3 1420 Multilabel Plate Counter) at 37 °C in the dark. The growth of the cells was monitored every nine minutes by reading the optical density (OD@600 nm). The experiments lasted for over 18 hours.

Three types of FPC LbL films and a blank glass slide were immersed in 1:100 dilutions of overnight cultured bacteria, respectively. Then incubated at 37 °C, recorded the OD@600 nm after 2 hours and 3.5 hours.

Bacteria detection

2 µL bacteria suspensions (1.1 - 5.5x10⁷ cells/mL) were introduced onto each FPC LbL film surface, allowed to incubate for 10 minutes at room temperature to settle onto the surface, and then washing step was performed with M9 culture medium twice. Finally, 2 µL fresh M9 medium was added on each surface, and a clean glass slide was used as a coverslip and observed under microscope. Meanwhile, the controls were carried out for each sample by adding 2 µL M9 medium instead of bacteria suspension.

Image analysis

A series of images from different samples were analyzed using NIH (National Institutes of Health) recommended image processing software, Image J.

References

- [1] P. R. Shorten, A. B. Pleasants and T. K. Soboleva. Estimation of microbial growth using population measurements subject to a detection limit. *Int. J. Food Microbiol.* 2006, **108**, 369-375.
- [2] H. Wang, Y. Zhou, X. Jiang, B. Sun and Y. He, *et al.* Simultaneous capture, detection, and inactivation of bacteria as enabled by a surface-enhanced raman scattering multifunctional chip. *Angew. Chem. Int. Ed.* 2015, **54**, 5132-5136.
- [3] C. L. Ventola. The Antibiotic Resistance Crisis: Part 1: Causes and Threats. *P&T*, 2015, **40(4)**, 277-283.
- [4] S. Sengupta, MK. Chattopadhyay and HP. Grossart. The multifaceted roles of antibiotics and antibiotic resistance in nature. *Front Microbiol*, 2013, **4(47)**, 1-13.
- [5] IM. Gould and AM. Bal. New antibiotic agents in the pipeline and how they can help overcome microbial resistance. *Virulence*. 2013, **4(2)**, 185-191.
- [8] O. Lazcka, F. J. Del Campo and F. X. Muñoz. Pathogen detection: A perspective of traditional methods and biosensors. *Biosens. Bioelectron.*, 2007, **22**, 1205-1217.
- [9] M. Nayak, A. Kotian, S. Marathe and D. Chakravorty. Detection of microorganisms using biosensors – A smarter way towards detection techniques. *Biosens. Bioelectron.*, 2009, **25**, 661-667.
- [10] A. Taylor, J. Ladd, Q. Yu, S. Chen and S. Jiang, *et al.* Quantitative and simultaneous detection of four foodborne bacterial pathogens with a multi-channel SPR sensor. *Biosens. Bioelectron.*, 2006, **22**, 752-758.
- [11] Z. He and F. Mansfeld. Exploring the use of electrochemical impedance spectroscopy (EIS) in microbial fuel cell studies. *Energy Environ. Sci.*, 2009, **2**, 215-219.
- [12] M. D. Disney, J. Zheng, T. M. Swager and P. H. Seeberger. Detection of bacteria with carbohydrate-functionalized fluorescent polymers. *J. Am. Chem. Soc.*, 2004, **126 (41)**, 13343-13346.
- [13] R. L. Phillips, O. R. Miranda, C. C. You, V. M. Rotello and U. H. F. Bunz. Rapid and efficient identification of bacteria using gold – nanoparticle - poly(*para*-phenyleneethynylene) constructs. *Angew. Chem. Int. Ed.*, 2008, **47**, 2590-2594.
- [14] Y. Wan, Y. Sun, P. Qi, P. Wang and D. Zhang. Quaternized magnetic nanoparticles - fluorescent polymer system for detection and identification of bacteria. *Biosensors and Bioelectronics*, 2014, **55**, 289-293.
- [15] K. Ariga, J. P. Hill and Q. Ji. Layer-by-layer assembly as a versatile bottom-up nanofabrication technique for exploratory research and realistic application. *Phys. Chem. Chem.*

Phys., 2007, **9**, 2319-2340.

[16] Y. Xiang, S. Lu and S. Jiang. Layer-by-layer self-assembly in the development of electrochemical energy conversion and storage devices from fuel cells to supercapacitors. *Chem. Soc. Rev.*, 2012, **41**, 7291-7321.

[17] G. Decher. Fuzzy nanoassemblies: toward layered polymeric multicomposites. *Science*, 1997, **277**, 1232-1237.

[18] C. Grazon, J. Rieger, P. Beaunier, R. Méallet-Renault and G. Clavier. Fluorescent core-shell nanoparticles and nanocapsules using comb-like macromolecular RAFT agents: synthesis and functionalization thereof. *Polym. Chem.*, 2016, **7**, 4272-4283.

[19] C. Grazon, J. Rieger, R. Méallet-Renault, B. Charleux and G. Clavier. Ultrabright fluorescent polymeric nanoparticles made from a new family of BODIPY monomers. *Macromolecules*, 2013, **46**, 5167-5176.

[20] C. Grazon, J. Rieger, B. Charleux, G. Clavier and R. Méallet-Renault. Ultrabright BODIPY-tagged polystyrene nanoparticles: study of concentration effect on photophysical properties. *J. Phys. Chem. C*, 2014, **118**, 13945-13952.

[21] C. Grazon, J. Rieger, R. Méallet-Renault, G. Clavier and B. Charleux. One-pot synthesis of pegylated fluorescent nanoparticles by RAFT minoemulsion polymerization using a phase inversion process. *Macromol. Rapid Commun.*, 2011, **32**, 699-705.

[22] K. Knop, R. Hoogenboom, D. Fischer and U. S. Schubert. Poly(ethylene glycol) in drug delivery: pros and cons as well as potential alternatives. *Angew. Chem., Int. Ed.*, 2010, **49**, 6288-6308.

[23] W. Qin, T. Rohand, M. Baruah, A. Stefan, M. V. Auweraer, W. Dehaen and N. Boens. Solvent-dependent photophysical properties of borondipyrromethene dyes in solution. *Chemical Physics Letters*, 2006, **420**, 562-568.

[24] M. Ferreira and M. F. Rubner. Molecular-level processing of conjugated polymers. 1. Layer-by-layer manipulation of conjugated polyions. *Macromolecules*, 1995, **28**, 7107-7114.

[25] B. A. Wolf. Coil overlap in moderately concentrated polyelectrolyte solution: effects of self-shielding as compared with salt-shielding as a function of chain length. *RSC Adv*, 2016, **6**, 38004-38011.

[26] D. Yoo, S. S. Shiratori and M. F. Rubner. Controlling bilayer composition and surface wettability of sequentially adsorbed multilayers of weak polyelectrolytes. *Macromolecules*, 1998, **31**(13), 4309-4318.

[27] T. T. Vu, M. Dvorko, E. Y. Schmidt, J. F. Audibert and R. Méallet-Renault, *et al.* Understanding the spectroscopic properties and aggregation process of a new emitting boron

dipyrrromethene (BODIPY). *J. Phys. Chem. C*, 2013, **117**, 5373-5385.

[28] S. Karamdoust, B. Yu, C. V. Bonduelle, Y. Liu and E. R. Gilles, *et al.* Preparation of antibacterial surfaces by hyperthermal hydrogen induced cross-linking of polymer thin films. *J. Mater. Chem.*, 2012, **22**, 4881-4889.

[29] C. E. M. Krämer, W. Wiechert and D. Kohlheyer. Time-resolved, single-cell analysis of induced and programmed cell death via non-invasive propidium iodide and counterstain perfusion. *Sci. Rep.*, 2016, **6**, 32104 (1-13).

[30] C. Dumas-Verdes, F. Miomandre, E. Lepicier, O. Galangau and P. Audebert. *et al.* BODIPY-Tetrazine multichromophoric derivatives. *Eur. J. Org. Chem.*, 2010, 2525-2535.

Chapter 3

Single fluorescent layer LbL film based on metal-enhanced fluorescence (MEF) for bacteria detection

Chapter 3 Single fluorescent layer LbL film based on metal-enhanced fluorescence (MEF) for bacteria detection

A plasmon is generally defined as a quantum of plasma oscillation in physics. As it is well known from our daily life, most metals are highly reflective in visible range of electromagnetic (EM) radiation. In most metals, the plasma frequency is in the ultraviolet. In such cases the electrons shield the electric field if light frequencies lie below the plasma frequency. Therefore low frequencies electromagnetic waves are reflected by these metals and make them shiny in visible range. However, some metals, such as copper and gold, have electronic interband transitions in the visible range, whereby specific light energies are absorbed, yielding their distinct color. With the development of nanotechnology, nanomaterials with different morphologies and properties are widely studied. Noble metal nanostructures result in new near-field optical properties as compared to their bulk material counterpart. Such behavior is due to the collective oscillation of the electrons in the conduction band, known as the surface plasmon oscillation [1].

Surface plasmon can play a role in surface-enhanced fluorescence [2]. The term “Metal-Enhanced Fluorescence (MEF)” was first introduced by Lakowicz and Geddes in 2002 [3]. MEF is a physical effect that occurs when fluorophores are positioned in the near-field, typically at nanometric distances from metallic surfaces. It is characterized by increased fluorescence intensity, quantum yield and a decreased fluorescence lifetime. MEF shows strong distance-dependency, and takes place only over a certain distance range from the metallic surface. It has been reported that the emission is quenched due to the excited fluorophores damping when fluorophore molecules are adsorbed directly on the surface [4]. Under suitable conditions, *i.e.* when the distance between the fluorophore and metal surface is in the 5 to 50 nm range, the excited fluorophores strongly interact with surface plasmons resulting in a dramatic improvement of the fluorescence properties [5]. Many applications based on MEF have attracted interest. However, the actual MEF mechanism is still discussed and debated today. Two mechanisms as usually proposed: (1) enhanced electromagnetic field, metal particles on the surface display strong interactions with incident light and provide selective excitation intensity for fluorophore; (2) increased radiative decay rate of the fluorophore. In the second mechanism, it has been demonstrated that the free space conditions can be influenced by nearby conducting electrons of the metallic surface (Scheme 3.1). Fluorescence lifetime (τ_0) and quantum yield (Φ_0) of a fluorophore are interrelated as defined below [6]:

$$\tau_0 = \frac{1}{\Gamma + \kappa_{nr}} \quad (\text{eq. 3.1})$$

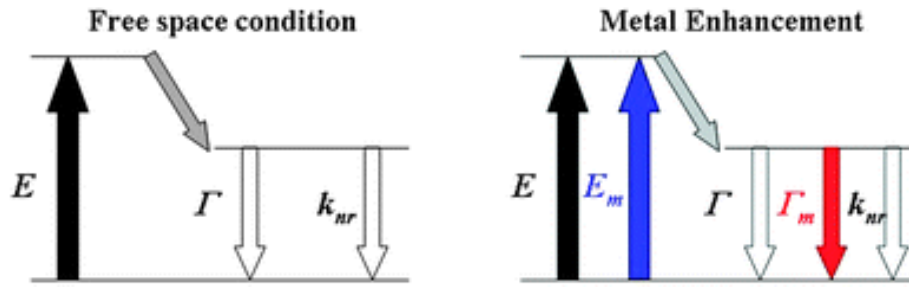
$$\Phi_0 = \frac{\Gamma}{\Gamma + \kappa_{nr}} = \tau_0 \times \Gamma \quad (\text{eq. 3.2})$$

where Γ is the radiative rate and κ_{nr} is the non-radiative rate. From the equation (1) and (2), when the radiative rate increases, the fluorescence quantum yield increases and the lifetime decreases. When the fluorophore is introduced close to a metallic surface, the radiative decay rate increases and becomes $\Gamma + \Gamma_m$, therefore, the fluorescence quantum yield and lifetime are given by:

$$\tau_m = \frac{1}{\Gamma + \Gamma_m + \kappa_{nr}} \quad (\text{eq. 3.3})$$

$$\Phi_m = \frac{\Gamma + \Gamma_m}{\Gamma + \Gamma_m + \kappa_{nr}} = \tau_m \times (\Gamma + \Gamma_m) \quad (\text{eq. 3.4})$$

where Γ_m is the additional radiative rate in the presence of a metallic surface. After addition of this new radiative rate, the fluorescence quantum yield increases thus producing a higher fluorescence signal. In addition, the nature of the electronic interband transition of the metallic surface is dependent on the nature, size and shape of nanoparticles. Consequently, the MEF effect depends on the surface features (nature, density, size and shape of nanoparticles, *etc.*) and the distance between fluorophores and the surface [7].



Scheme 3.1. Classical Jablonski diagram for the free-space condition and the modified form in the presence of a metallic surface. E : excitation rate, E_m : metal enhanced excitation rate, and Γ_m : radiative rate in the presence of a metal. From Geddes and Lakowicz [3].

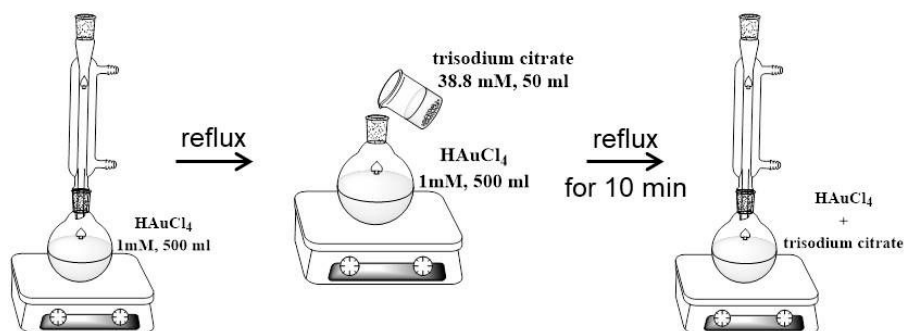
In order to improve the sensitivity of the fluorescent GFPC⁻ (Green Fluorescent Polymer Chains) LbL surface for bacteria detection, we deposited GFPC⁻ layer on gold spherical nanoparticles (Au NPs) surface. We aim at combining good stability and non-toxicity of FPC to produce amplified fluorescence signals based on the MEF.

Firstly, I will introduce the synthesis, modification and the characterizations of spherical Au NPs. The synthesis of GFPC⁻ and two oppositely charged “blank” polymers (PC⁺ and PC⁻) will be described. And then different LbL films containing Au NPs and GFPC⁻ with various layers of PC⁺/PC⁻ were prepared and investigated. Finally, all Au NPs/PCs/GFPC⁻ surfaces were employed for *E. coli* detection.

3.1 Au nanoparticles (Au NPs) and modified Au NPs preparation

3.1.1 Au nanoparticles (Au NPs) synthesis

To fabricate the nanostructured sensitive detection system, we started with synthesis of gold nanoparticles (Au NPs; Scheme 3.2). Glassware was cleaned using aqua regia (3 parts HCl, 1 part HNO₃) for a minimum of 4 hours. After discarding the aqua regia, the glassware was rinsed with Milli-Q water and dried with nitrogen. Aqueous HAuCl₄ (1 mM, 500 mL) solution and trisodium citrate solution (38.8 mM, 50 mL) were prepared. Both salts are highly hygroscopic and so they were weighed quickly and transferred to their flasks. A condenser was attached to the round-bottom flask containing the HAuCl₄ solution which was then placed in a water bath with magnetic stirring and warmed. When the reflux was observable, the trisodium citrate solution was added quickly and vigorous stirring of the solution continued. The pale yellow color of the gold solution quickly turned to dark purple and within 15 mins turned to a dark ruby red characteristic of spherical gold nanoparticles. The solution was left to reflux for another 15 minutes. The AuNP solution was then cooled to room temperature. The solution was finally stored in a refrigerator [8]. This synthesis method produces spherical particles with negative surface charge due to the presence of the citrate ligands.



Scheme 3.2. Au NPs synthetic procedure

3.1.2 Polymer coating of Au NPs (Au NPs@PAH)

Since the AuNPs will be deposited directly on the glass surface which is negatively charged, it was necessary to modify their surface charges from anionic to cationic. A polymer bearing amine side-groups, poly(allylamine hydrochloride), was thus coated on the surface of the AuNPs. The concentration of the polymer coating around the Au NPs was varied to analyze its subsequent effect on the zeta potential of the coated particle and its ability to adsorb on the glass surface.

Two concentrations of PAH solutions were prepared in water: 1 mg/mL and 2 mg/mL (Scheme 3.3). To each solution, 4 mL of Au NPs solution were added while under magnetic stirring and left one hour for coating. The solutions were then centrifuged to precipitation for 40 mins at 10,000 RPM and re-dispersed using Milli-Q water. The centrifuging and washing were

done twice and then the nanoparticles re-dispersed in 4 mL of Milli-Q water and stored in a refrigerator [9].



Scheme 3.3. Chemical structure of poly(allylamine hydrochloride) (PAH) (left) and schematic diagram of the procedure for Au NPs coating with PAH (right).

3.2 Characterization of Au NPs and Au NPs@PAH

3.2.1 Photophysical study of Au NPs and Au NPs@PAH in solution

The absorption spectra of bulk solution of nanoparticles (with and without PAH) are shown in Figure 3.1. A gold plasmon band is observed whatever the sample. The maximum absorbance of Au NPs@2 mg/mL PAH is similar to the bare Au NPs at 524 nm, while it is red-shifted at 536 nm for the Au NPs@1 mg/mL PAH. This is probably due to a lower density of PAH coating around the Au NPs@1 mg/mL PAH compared to the modified Au NPs prepared with a higher concentration of PAH. Less charged surface on Au NPs@PAH leads to aggregation which induces a red-shift on the plasmonic band. In addition, the whole absorption spectrum of Au NPs@2 mg/mL PAH has a larger band on the red edge due to a smaller contribution from aggregates. In addition, from the maximum absorbance, we can deduce the Au NPs size of each sample is between 22 nm and 48 nm according to the literature [10].

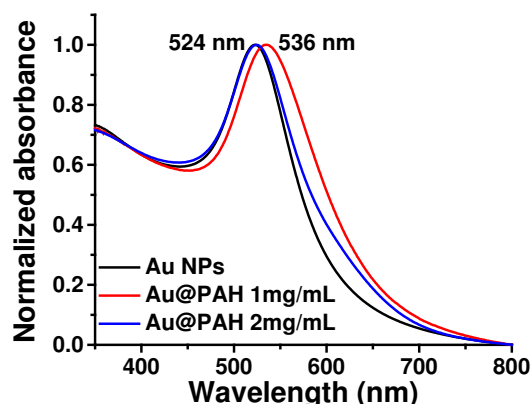


Figure 3.1. Normalized absorption spectra of as synthesized Au NPs and Au NPs@PAH in water.

3.2.2 Zeta potential of Au NPs and Au NPs@PAH in solution

The zeta potentials of Au NPs and modified Au NPs in solution were determined and the results are shown in Table 3.1. The bare Au NPs have a charge of -40.1 mV due to the presence of the citrate ligands introduced during the preparation: it is a stable colloidal solution. The modified Au NPs are positively charged: there is a charge inversion compared to the bare Au NPs. It means that the PAH successfully coated Au NPs surface by electrostatic interactions. In addition, the zeta potential of both Au NPs@1 mg/mL PAH and Au NPs@2 mg/mL PAH is greater than +30 mV. With respect to colloidal stability, both are thus stable. The zeta potential of the Au NPs@1 mg/mL PAH (+37.2±0.9) is lower than that of the Au NPs@2 mg/mL PAH (+47.2±0.3). This means that Au NPs@2 mg/mL PAH experience more electrostatic repulsion. This explains why the formation of aggregates is limited in the latter case. Au NPs@1 mg/mL PAH, shows a lower zeta potential: it allows aggregation to occur. This is in accordance with the plasmon band position (bathochromic shift for Au NPs@1 mg/mL PAH - see Figure 3.1). Based on zeta potential results, any modified Au NPs are likely to bind on activated glass surface through electrostatic attraction. Au NPs@2 mg/mL PAH are expected to have a stronger adsorption affinity.

Table 3.1. Zeta potentials (ζ) of the Au NPs and modified Au NPs@PAH

	Au NPs	Au NPs@1 mg/mL PAH	Au NPs@2 mg/mL PAH
ζ^a / mV	-40.1±1.0	+37.2±0.9	+47.2±0.3

^aZeta potentials (ζ) were recorded in Milli-Q water at 25 °C.

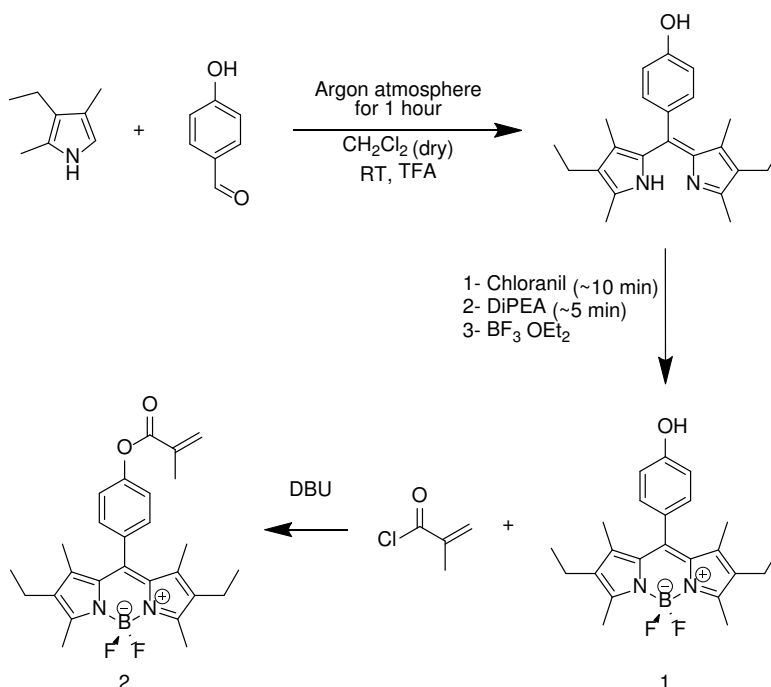
We have demonstrated that PAH is adsorbed on AuNPs. We need now to develop cationic and anionic fluorescent and non-fluorescent polymer chains to build up LbL films with modified Au NPs.

3.3 Synthesis of polycation, polyanion and fluorescent GFPC⁻

The thickness of ultrathin film can be easily adjusted by controlling the number of repeating cycles of polyelectrolyte deposition in the Layer-by-layer (LbL) assembly. The distance between the Au NPs and the fluorescent polymer GFPC⁻ will be controlled by inserting non fluorescent cationic (PC⁺) and anionic (PC⁻) polymer chains in between. All three types of polymer chains have been synthesized and characterized prior to LbL film preparation.

3.3.1 Synthesis of fluorescent P(APEG-co-GBDPMA-co-AA) (GFPC⁻)

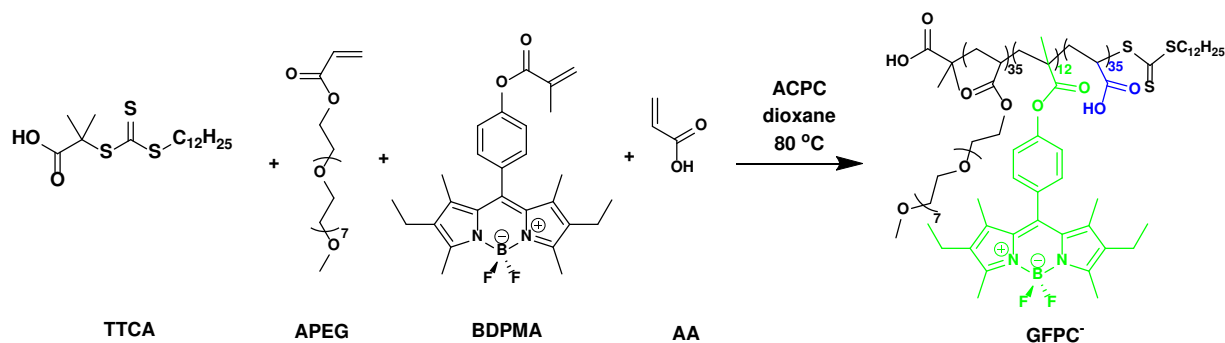
3.3.1.1 Synthesis of BODIPY monomer



Scheme 3.4. Synthetic pathway for *BODIPY methacrylate*.

The negatively charged green fluorescent polymer chains (GFPC⁻) of well-defined chain lengths will be prepared *via* a RAFT polymerization. It is thus necessary to prepare a BODIPY that bears a polymerizable methacrylate function (BDPMA). The synthetic pathway for BDPMA is shown in scheme 3.4 [11, 12]. BODIPY monomer was synthesized starting from a BODIPY bearing a phenol function on the *meso* (8) position. BODIPY-phenol **1** was prepared according to a standard procedure. To obtain the monomer, a classical esterification of the BODIPY phenol **1** was performed in presence of methacryloyl chloride to obtain the monomer BDPMA **2**.

3.3.1.2 Synthesis of P(APEG-*co*-GBDPMA-*co*-AA) (GFPC⁻)

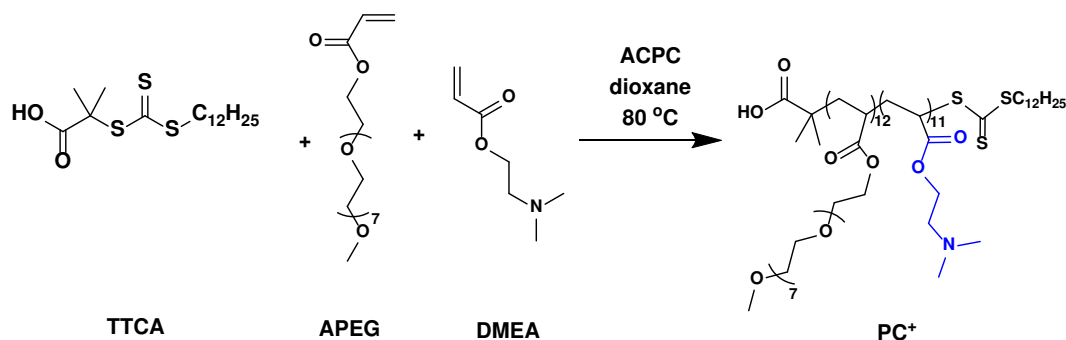


Scheme 3.5. Synthetic scheme employed for the RAFT synthesis of *P(APEG-co-GBDPMA-co-AA)* (GFPC⁻).

The obtained fluorescent BODIPY monomer was copolymerized with poly(ethylene glycol) methyl ether acrylate (APEG) and acrylic acid (AA) in the presence of chain transfer agent TTCA using ACPC as initiator (Scheme 3.5). After a reaction time of 44 hours, the polymerization was terminated at 50.5% conversion. The polymer molecular weight was estimated based on NMR total monomer conversion, and found to be 25000 g/mol.

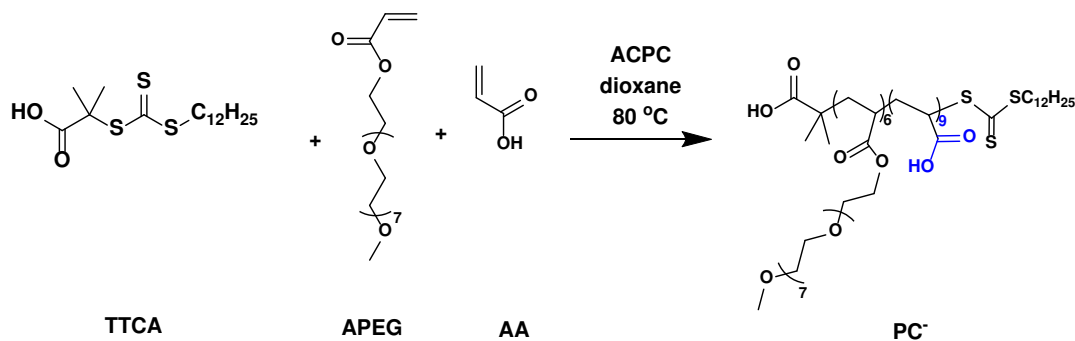
3.3.2 Synthesis of P(APEG-co-DMEA) (PC^+)

The polymerization of poly(ethylene glycol) methyl ether acrylate (APEG) and 2-(dimethylamino)ethyl acrylate (DMEA) under the same experimental condition as for GFPC⁻ was performed (Scheme 3.6) to give PC^+ . The polymerization was terminated at 90% conversion after 4 hours and the reaction mixture immersed into an ice bath. PC^+ was purified by multiple precipitations into cold cyclohexane. The polymer molecular weight was calculated based on NMR total monomer conversion, and found to be 7700 g/mol.



Scheme 3.6. Synthetic scheme employed for the RAFT synthesis of P(APEG-co-DMEA) (PC^+).

3.3.3 Synthesis of P(APEG-co-AA) (PC^-)



Scheme 3.7. Synthetic scheme employed for the RAFT synthesis of P(APEG-co-AA) (PC^-).

The other non-fluorescent polyelectrolyte also has a hydrophilic as well as biocompatible APEG repeating unit and a negatively charged acrylic acid (AA) repeating unit. PC^- was synthesized following the same procedure as for PC^+ (Scheme 3.7). After 4 hours polymerization, the reaction was stopped by immersing the reaction mixture into ice bath. PC^- was purified by multiple precipitations into cold cyclohexane. The polymer molecular weight was calculated based on NMR total monomer conversion, and found to be 3700 g/mol.

3.4 Characterization of the polyelectrolytes

3.4.1 Spectroscopic properties of BDPMA and GFPC⁻

Absorption and fluorescence spectra of the BODIPY monomer recorded in toluene and GFPC⁻ measured in water are shown in Figure 3.2 and their spectroscopic properties are given in Table 3.2. The BDPMA monomer in toluene shows standard spectral features for a BODIPY fluorophore with an intense band in the visible region located at 528 nm and a vibrational shoulder at higher energy in its absorption spectrum [13]. The absorption spectrum of GFPC⁻ exhibits a little bit broad, it can be related to the presence of several conformation of GFPC⁻. Both molecules exhibit very similar fluorescence spectra with a maximum of fluorescence emission at 540 nm. Fluorescence quantum yield of GFPC⁻ is 14% while that of BDPMA in toluene is 70%. The decrease may be due to solvent effect (BODIPY fluorescence quantum yield decreases in polar solvent) [14] and/or quenching from BODIPY aggregation along the polymer chain. Fluorescence lifetime of GFPC⁻ in water was slightly increased. This is likely due to the BODIPY fluorophore protection from solvent interactions by polymer chains.

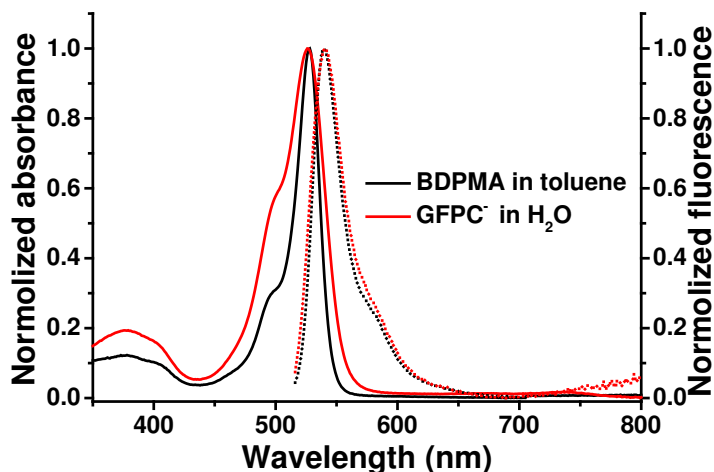


Figure 3.2. Absorption (full lines) and fluorescence spectra (dotted lines, $\lambda_{ex} = 495$ nm) of the BODIPY monomer (BDPMA) recorded in toluene (black) and GFPC⁻ recorded in H₂O (red).

Table 3.2. Spectroscopic properties and zeta potentials of the BDPMA and GFPC⁻

	BDPMA	GFPC ⁻
solvent	toluene	water
λ_{\max} (abs) / nm	528	526
λ_{\max} (em) / nm	540	540
Φ_F ^a	70 %	14 %
$\langle\tau\rangle$ ^b / ns	4.9	5.2

^a Relative fluorescence quantum yields were determined using Rhodamine 590 ($\Phi_F = 0.95$ in ethanol) as a reference. ^b Average fluorescent lifetime recorded for the GFPC⁻ in water and BDPMA in toluene ($\lambda_{\text{ex}} = 495$ nm, $\lambda_{\text{em}} = 540$ nm); decay fitted with a monoexponential function for BDPMA and a multiexponential function for FPCs.

3.4.2 Zeta potential of polyelectrolytes

Table 3.3. Zeta potentials (ζ) of the different polyelectrolytes

	PC ⁺		PC ⁻		GFPC ⁻
pH	8.5	5.4	3.7	9.5	5.7
ζ ^a / mV	5.5±0.4	30.2±0.9	-0.0±0.3	-44.3±0.2	-38.9±0.8

^a Zeta potentials (ζ) were recorded in Milli-Q water at 25 °C, [PC⁺] = 8.2×10⁻⁵ M, [PC⁻] = 4.15×10⁻⁴ M and [GFPC⁻] = 3.1×10⁻⁶ M.

Since the Layer-by-Layer assembly depends on the electrostatic attraction of each polyelectrolytes in the film fabrication, the optimization of deposition solutions were verified with zeta potential measurements. These three polymers are all weak polyelectrolytes; therefore the pH will greatly affect the degree of dissociation of the ionic groups and the charge density of each polymer. As shown in Table 3.3, the natural pH of the PC⁺ dissolved in water is 8.5, due to the amine functional group. pH is 3.7 (acidic suspension) for the PC⁻ as a result of the carboxylic functional group contribution. We investigated the isoelectric points of fluorescent weak polyelectrolytes SW FPC⁺ and SW FPC⁻ in chapter 2. The zeta potential of SW FPC⁺ is close to 0 mV when pH is 8.6 while the isoelectric point was found at pH=3.4 for SW FPC⁻. Because both SW FPC and PC consist of the same ionic units, probably they have similar isoelectric point which explains the near zero zeta potential values of PC⁺ and PC⁻ when directly dissolved in water. Upon changing the pH, more stable colloidal solutions were obtained. When the pH of the

aqueous solution of PC^+ and PC^- were adjusted to 5.4 and 9.5 respectively, the degree of ionization of these two weak polyelectrolytes is enough for the further multi-layer assembly process (absolute value of zeta potential > 30 mV). The zeta potential of the GFPC $^-$ was found to be -38.9 mV at pH = 5.7 which is high enough to allow binding on a positively charged layer through electrostatic attraction.

3.5 Preparation and characterization of Au NPs@PAH surfaces

Negatively charged activated glass slides prepared according to the procedure described in chapter 2 were individually immersed in the Au NPs@1 mg/mL and 2 mg/mL PAH solutions. After washing three times to remove the unbound Au NPs@PAH and drying with a nitrogen flow, the Au NPs@PAH surfaces were obtained.

Their absorbance spectra were recorded (Figure 3.3). The figure shows that the spectrum for the Au NPs@2 mg/mL PAH film has a more intense band centered at a maximum of 525 nm that is similar to the maximum band of Au NPs@2 mg/mL PAH in solution (524 nm), whereas the Au NPs@1 mg/mL PAH has a wider red-shifted absorption band centered at 544 nm (compared to 536 nm in solution). Probably Au NPs@1 mg/mL PAH are aggregated in solution and thus deposit as such on glass leading to broad red shifted plasmon band while the Au NPs@2 mg/mL PAH are well dispersed in solution and thus stay as such on glass.

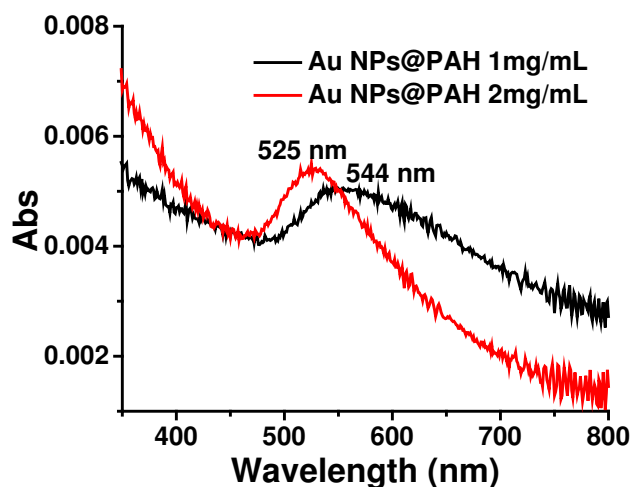


Figure 3.3. Absorbance spectra of Au NPs@PAH deposited on activated glass substrate (Au NPs@PAH films).

The scanning electron microscope (SEM) images in Figure 3.4 suggest that the Au NPs were uniformly and randomly distributed on the substrate. This is favorable to get an efficient MEF effect [15]. In addition, the Au NPs@2mg/mL PAH surface has higher coverage ($22 \text{ NP}/\mu\text{m}^2$)

compared to the Au NPs@1mg/mL PAH surface ($20 \text{ NP}/\mu\text{m}^2$); this confirms that the higher surface charge promotes better adsorption affinity of the particles with the activated glass surface. From the SEM images, we can see that the Au NPs surface with different coverage can be prepared in a controllable way using the LbL assembly by adjusting the charge density of the Au NPs surface. The obtained Au NPs surfaces are suitable for MEF studies, because of their large surface area and will induce increased radiative rates for the fluorophores due to an increase in the local electric field.

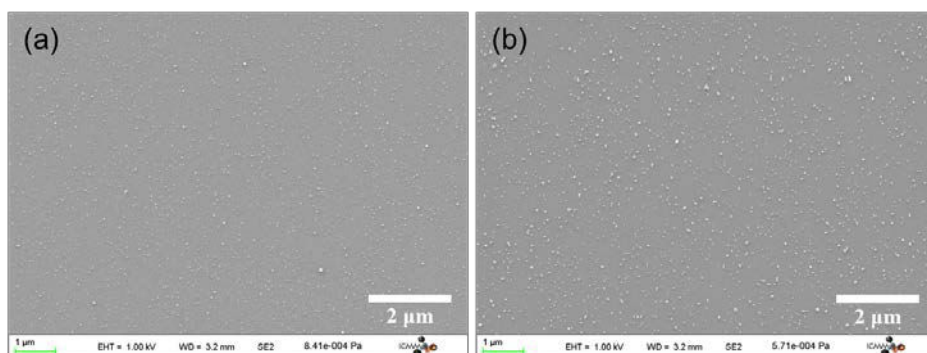
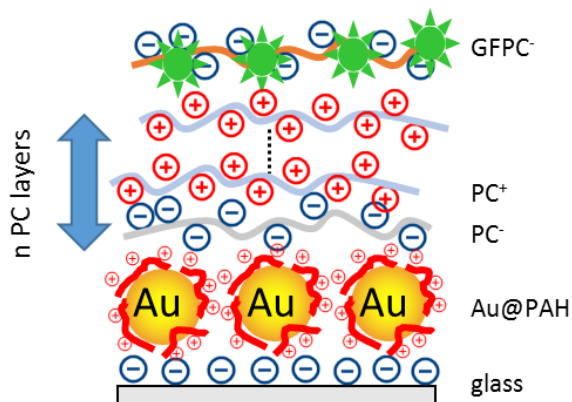


Figure 3.4. Surface morphologies of (1) Au NPs@1mg/mL PAH film surface and (2) Au NPs@1mg/mL PAH film surface as observed by SEM.

3.6 Fabrication and spectroscopic study of Au NPs/PCs/GFPC⁻ LbL surfaces

3.6.1 Fabrication of Au NPs/PCs/GFPC⁻ LbL films

To investigate and optimize the MEF effects of the Au NPs surfaces on GFPC⁻, a film was fabricated by inserting various layers of PC⁻/PC⁺ between the Au NPs substrates and the GFPC⁻ outmost layer (scheme 3.8). Based on the zeta potential investigation for each polyelectrolyte and in order to obtain a thin film, the optimal deposition conditions for each polyelectrolyte is shown in Table 3.4. For each Au NPs@PAH substrate, 4 films were prepared with 0, 2, 4 and 6 PC⁻/PC⁺ layers topped with 1 GFPC⁻ layer.



Scheme 3.8. Schematic representation of the Au NPs/PCs/GFPC⁻ LbL films.

Table 3.4. Optimal composition for polymer deposition solutions

Solution	Concentration (mol/L)	pH	Ionic strength (mol/L)
PC ⁻	4.2×10^{-4}	9.5	0.005
PC ⁺	8.2×10^{-5}	5.4	0.005
GFPC ⁻	5.0×10^{-7}	5.5	0.005

3.6.2 Spectroscopy study of Au NPs/PCs/GFPC⁻ LbL films

3.6.2.1 Absorption and fluorescence spectra of Au NPs/PCs/GFPC⁻ LbL films

Figure 3.5 shows the absorption and fluorescence spectra of the various films prepared with 0, 2, 4 and 6 PC/PC⁺ layers. The absorbance spectrum of each sample shows the clear contribution of the plasmonic band of Au NPs (at 524 nm and 544 nm for Au NPs@2mg/mL PAH and Au NPs@1mg/mL PAH respectively) and absorbance from GFPC⁻ (at 526 nm) (Figure 3.5a and c). The fluorescence measurements display a dramatic intensity dependence on the number of PC layers (thus on Au NP – GFPC⁻ distances) (Figure 3.5b and d).

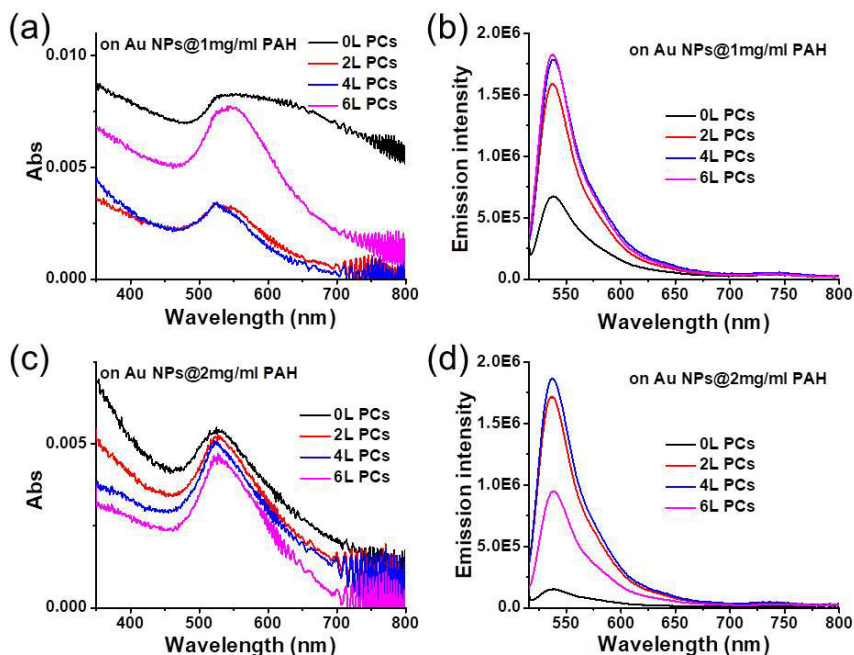


Figure 3.5. (a and c) Absorbance and (b and d) fluorescence spectra of GFPC⁻ on Au NPs surfaces with different PAH coverage: a and b 1 mg/mL PAH and c and d 2 mg/mL PAH with 0, 2, 4 and 6 PC layers in between. The excitation wavelength was 495 nm.

Figure 3.6 summarizes the fluorescence intensity variation as a function of the number of PC layers on the surfaces with different density of Au NPs. The fluorescence intensity is quenched when the PCs layer is 0 in both samples. The quenching efficiency on Au NPs@2 mg/mL PAH surface (fluorescence intensity is 1.51×10^5) is higher than on Au NPs@1 mg/mL PAH surface (fluorescence intensity is 6.7×10^5). This is likely coming from the larger quantity of Au NPs on the Au NPs@2 mg/mL PAH surface. In addition, the maximum fluorescence intensity that was achieved with the 1 mg/mL PAH modified Au NPs was at 6 PCs layers with an intensity value of 1.83×10^6 and tended to level off, while the 2 mg/mL PAH modified Au NPs was able to achieve maximum enhancement fluorescence intensity (1.87×10^6) with 4 PCs layers. The surface with Au NPs@2 mg/mL PAH shows a larger amplitude in fluorescence variation which is more suited for further applications (the variation of intensity in the presence of bacteria should be larger and thus sensing more efficient). This may be related to the high density of particles on the substrate, because the MEF effects are largely dependent on the size and shape of the Au nanostructures. After this preliminary investigation, we chose the surface with the highest density of Au NPs (Au NPs@2 mg/mL PAH surface) for subsequent MEF measurements and application.

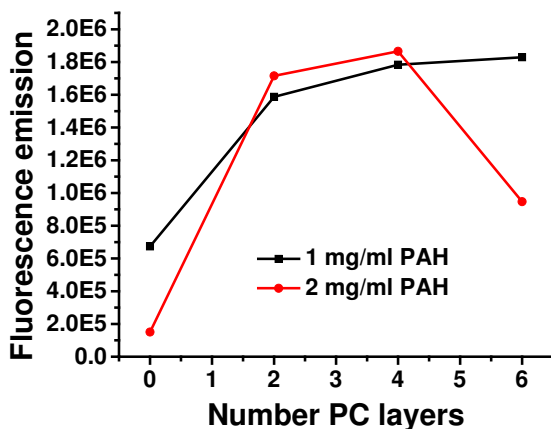


Figure 3.6. Variation of the maximum fluorescence intensity at 538 nm as a function of the number of PC layers. The excitation wavelength was 495 nm.

3.6.2.2 Optimization of MEF effect on Au NPs@2 mg/mL PAH surface

Since the distance between the fluorophore and the Au NPs plays an important role in determining the MEF effect of the Au NPs we adjusted the distances by controlling the numbers of PCs layers. The quantity of polymer chain deposited is also related to the concentration of the deposition solutions. We thus adjusted finely the thickness of each PC⁻/PC⁺ layers to obtain a better control of the MEF effect through slightly reducing the concentration of each PC deposition solution (Table 3.5). We produced a series of Au NPs/PCs/GFPC⁻ LbL films with 0, 2,

4, 6 and 8 PCs layers. We also prepared a $\text{PC}^+/\text{GFPC}^-$ LbL film on bare activated glass substrate as a reference.

Table 3.5. Modified polymer deposition solution composition for fine distance adjustment

Solution	Concentration (mol/L)	pH	Ionic strength (mol/L)
PC^-	3.1×10^{-4}	9.5	0.005
PC^+	6.2×10^{-5}	5.4	0.005
GFPC^-	5.0×10^{-7}	5.5	0.005

As shown in Figure 3.7, the fluorescence of GFPC^- changes on the Au NPs surface that are covered with PCs interlayer films. The fluorescence intensity is maximized for 6 layers which is two more than on the previous sample demonstrating that each layer thickness was indeed decreased. Additionally, a significant quenching of the fluorescence was observed when the GFPC^- layer is directly in contact with Au NPs. Therefore, we concluded that the fluorescence is more intense in the presence of Au NPs than without and it is, as expected, distance dependent. The fluorescence can be enhanced or quenched by adjusting the layers thickness and/or number between the nanoparticle and the fluorophore. It can be used for sensing because if the interaction of bacteria with the film changes the GFPC^- -Au NPs distance then fluorescence will be detected.

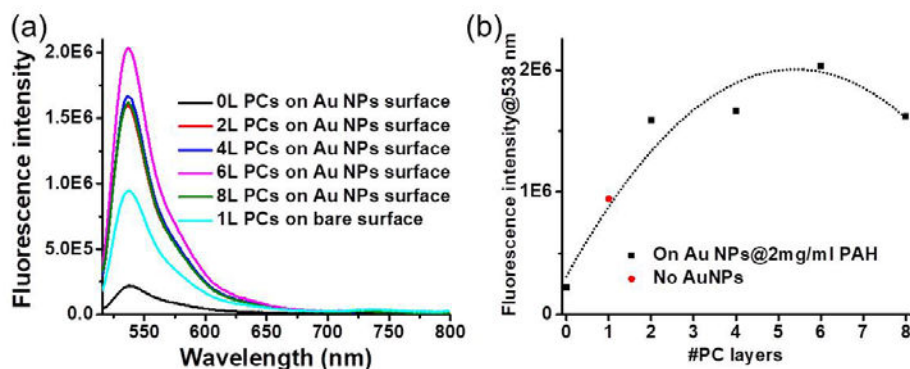


Figure 3.7. (a) Influence of PCs layers number on the fluorescence of the GFPC^- on the Au NPs surface and the control on the bare glass surface and (b) variation of the maximum fluorescence intensity at 538 nm as a function of the number of PC layers (black squares), fit with a second order polynomial model (black line) and intensity of the reference sample (red circles). The excitation wavelength was 495 nm.

3.6.2.3 Time-correlated single photon counting (TCSPC) analysis of Au NPs/PCs/GFPC⁻ LbL surface

In literature, it is reported that the increased intensity of the fluorophores can be attributed to the interaction with the plasmonic nanoparticles nearby and is always accompanied with a lifetime decrease [16, 17]. Thus we measured the fluorescence decays of each film using a single photon counting setup (Figure 3.8). The results were not straightforward as no clear trend could be observed. For the maximum quenched fluorescence film (Au NPs/0 layer PCs/GFPC⁻), decay is much shorter than the one for PC⁺/GFPC⁻ reference film while at the maximum fluorescence enhancement - from intensity data- (Au NPs/6 layers PCs/GFPC⁻ film) the decay is only slightly shorter. On the other hand it is longer for the Au NPs/ PCs/GFPC⁻ films with 2, 4 and 8 PC layers.

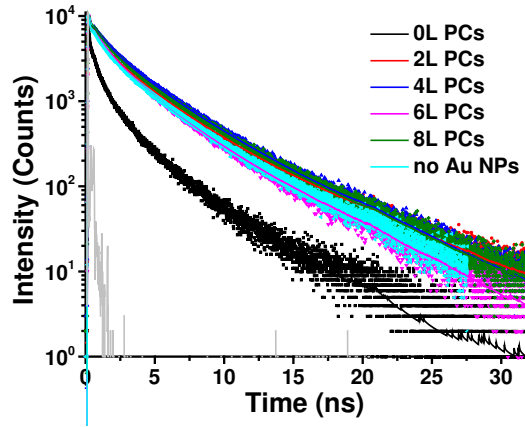


Figure 3.8. Fluorescent lifetime measurements of GFPC⁻ on the Au NPs surface with various PCs layers and the reference on the bare surface. The excitation wavelength was 495 nm and emission wavelength was 540 nm.

In order to gain a better understanding of the photophysical data we calculated the surface of the fluorescence spectra. We can assume that the change in steady state fluorescence intensities is due to changes in the radiative decay rate. The sum of the radiative and non-radiative decay rates were calculated from the fluorescence lifetimes (equation 3.1).

$$\tau = \frac{1}{\Gamma + \kappa_{nr}} \quad (\text{eq. 3.1})$$

where Γ is the radiative rate, κ_{nr} is the non-radiative rate, and their relative variation defined as:

$$\Delta[\kappa_r + \kappa_{nr}] = \frac{\tau_0}{\tau_i} \quad (\text{eq. 3.5})$$

The fluorescence quantum yield is defined as:

$$\Phi = \frac{\text{\#photons emitted}}{\text{\#photons absorbed}} = \frac{\Gamma}{\Gamma + \kappa_{nr}} \quad (\text{eq. 3.2})$$

Then from these results we can determine the relative change in fluorescence quantum yield for each film with Au NPs by comparison with the reference film:

$$\Delta\Phi = \frac{S_F^i}{S_F^0} = \Delta \left[\frac{\Gamma}{\Gamma + \kappa_{nr}} \right] \quad (\text{eq. 3.6})$$

where S_F^i is the area of the fluorescence spectra of the film with i layers and S_F^0 the area of the fluorescence spectrum of the reference sample, and the relative change in radiative rate with the equation:

$$\Delta\Gamma = \Delta\Phi \times \frac{\tau_0}{\tau_i} \quad (\text{eq. 3.7})$$

where τ_i is the average fluorescence lifetime of the film with i layers and, τ_0 the average fluorescence lifetime of the reference sample.

As shown in Table 3.6, the presence of Au NPs incorporated into the film has a direct impact on the radiative decay rate of GFPC⁻, achieving a 1.95 increase in the radiative decay rate and a 1.87 increase in the quantum yield.

Table 3.6. Changes in relative quantum yields and radiative decay rates for GFPC⁻ with and without Au NPs

PCs Layers	S_F^a	$\Delta\Phi$	τ (ns) ^b	$\Gamma + \kappa_{nr}$ (ns ⁻¹)	$\Delta[\Gamma + \kappa_{nr}]$	$\Delta\Gamma$
0	1.55×10 ⁷	0.26	2.02	0.50	1.62	0.43
2	8.74×10 ⁷	1.49	3.6	0.28	0.91	1.36
4	8.94×10 ⁷	1.53	3.63	0.28	0.90	1.38
6	1.10×10 ⁸	1.87	3.15	0.32	1.04	1.95
8	8.57×10 ⁷	1.46	3.58	0.28	0.92	1.34
No Au	5.86×10 ⁷	/	3.28	0.30	/	/

^a Calculated area for the fluorescence spectra. ^b Average fluorescence lifetime calculated from fitted decay with multiexponential function for films ($\lambda_{ex} = 495$ nm, $\lambda_{em} = 540$ nm).

MEF and distance dependence are demonstrated through lifetime and quantum yield analysis.

3.7 The Au NPs/PCs/GFPC⁻ LbL surfaces for bacteria detection

Based on the above investigation, the MEF effect in Au NPs/PCs/GFPC⁻ films is distance dependent. It means that probably the system is a kind of sensor and able to detect bacteria. The interaction of the bacteria with the film will have an effect on the structure and thus change the distance between Au NPs and the GFPC⁻. Thus one can expect that when introducing the bacteria on the outmost GFPC⁻ layer, its fluorescence intensity will be changed. Considering the swelling behavior of the polymer in the presence of M9 culture medium in the biological experiment, the Au NPs/4 layers PCs/GFPC⁻, Au NPs/6 layers PCs/GFPC⁻ and Au NPs/8 layers PCs/GFPC⁻ films were selected for the bacteria detection and should experience the most dramatic fluorescence variation.

We investigated the fluorescence response of GFPC⁻ on each Au NPs/PCs/GFPC⁻ film after incubation with *E. coli* in comparison with a control where only M9 was present. After introducing 2 μ L *E. coli* or M9 on each surface and 10 min. incubation, washing with M9 was done twice. Then surfaces were observed by microscopy. ImageJ was used for image analysis. The fluorescence intensity for each surface in the presence and the absence of *E. coli* are shown in Figure 3.9.

Controls were run on "old samples" prepared almost one year ago. GFPC⁻ layer evolved and it seems to be quenched after this period: therefore the fluorescence intensity is quite low, compared to the one with *E. coli*. The fluorescence intensity of Au NPs/4 layers PCs/GFPC⁻ and Au NPs/6 layers PCs/GFPC⁻ films shows fluorescence increase, compared to the film without Au NPs. Therefore, this Au NPs/PCs/GFPC⁻ film act as a sensor for the bacteria detection but a more systematic study shall be carried out. This system probably also has the potential for the bacteria growth detection because the distance between GFPC⁻ and Au NPs will be compressed when the number of bacteria increases, and then the fluorescence will be decreased.

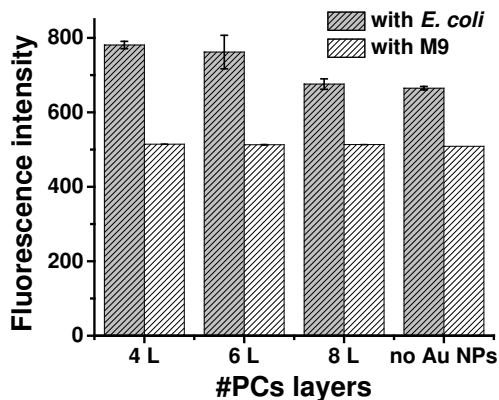


Figure 3.9. Fluorescence intensity of GFPC⁻ layer on Au NPs/PCs/GFPC⁻ and PCs/GFPC⁻ platforms after incubation with *E. coli* and the control with M9 culture medium. The excitation wavelength was 475 nm.

However, if we focus on the bioimaging of the bacteria on Au NPs/PCs/GFPC⁻ film surface, it is clear that *E. coli* can be targeted by GFPC⁻ on Au NPs/4 layers PCs/GFPC⁻ and Au NPs/8 layers PCs/GFPC⁻ surfaces (Figure 3.10). But the detection phenomenon on these two surfaces is different: *E. coli* on Au NPs/4 layers PCs/GFPC⁻ surface is fluorescently visible and brighter than the background while the area around the targeted bacteria became dark on the Au NPs/8 layers PCs/GFPC⁻ surface. Figure 3.11 shows the magnified microscope images on these two surfaces and the fluorescence intensity of the targeted bacteria, surface background and dark zone (for the surface with 8 layers PCs). We proved in Chapter 2 that fluorescent polymer chains were inside the bacteria and proposed that they “ate” the polymer chains and became fluorescent. The result we observed on Au NPs/8 layers PCs/GFPC⁻ surface confirmed the proposed bacteria detection mechanism. There is a single layer of fluorescent polymer chains, the next to the last layer is an uncolored polymer chain: when the bacteria "ate" the top luminescent polymer chains, the fluorescence around the bacteria turned to dark, the contrast between the brighter bacteria and the dark background obviously indicates their presence.

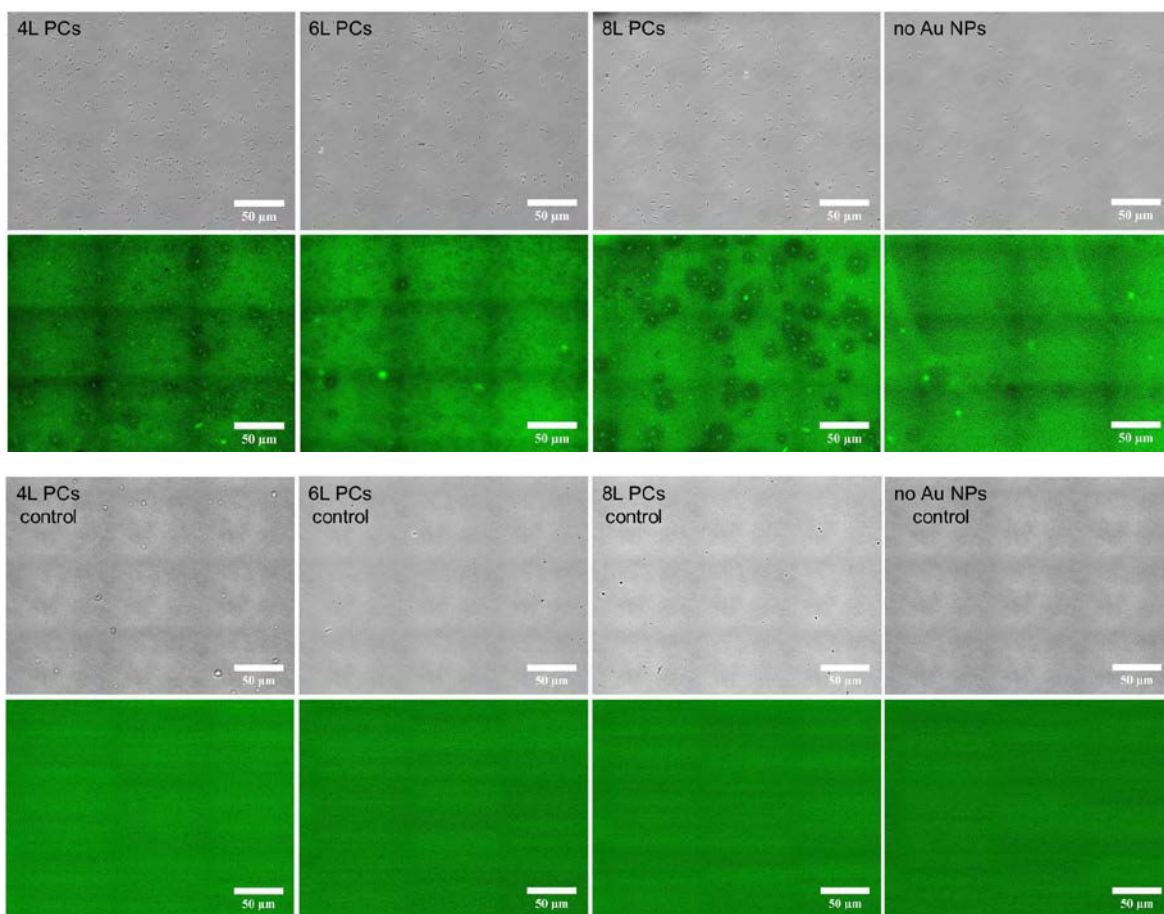


Figure 3.10. Bright field and fluorescence images of Au NPs/PCs/GFPC⁻ and PCs/GFPC⁻ platforms after incubation with *E. coli* (top) and control with M9 (bottom). The excitation

wavelength was 475 nm.

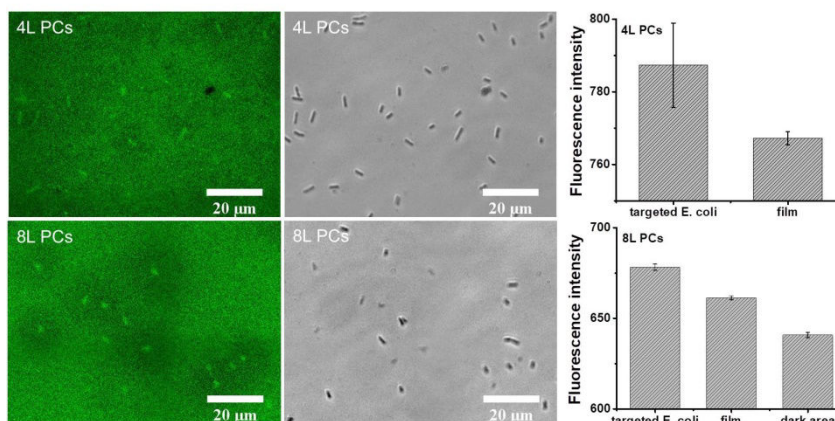


Figure 3.11. Microscope images of *E. coli* bacteria on Au NPs/4 layers PCs/GFPC⁻ film and Au NPs/8 layers PCs/GFPC⁻ film and fluorescence intensity analysis for each zone on the surface. The excitation wavelength was 475 nm.

3.8 Conclusion

In conclusion, we successfully prepared a metal enhanced fluorescence (MEF) LbL film and tested the bacteria detection. Firstly, the synthesis and surface modification of spherical gold nanoparticles was conducted. We found out that the density of the adsorbed Au NPs on the glass surface could be adjusted by changing the concentration of the polymer that is used to coat the Au NPs. Based on the conclusion from Chapter 2, the weak polyelectrolyte and long chain fluorescent polymer (GFPC⁻) was selected as the fluorophore in this system. Different films containing Au NPs and GFPC⁻ were fabricated and the distance between the Au NPs and GFPC⁻ was easily adjusted by changing the number of layers with two oppositely charged polymers (PC⁺ and PC⁻). The surface with Au NPs@2 mg/mL PAH shows larger amplitude in fluorescence variation. Such surface was chosen for further investigations. The spectroscopy study indicated that the presence of Au NPs incorporated into the film have a direct impact on the radiative decay rate of GFPC⁻, achieving a 1.95 increase of the radiative decay rate and a 1.87 increase of the quantum yield. Finally, the Au NPs@2 mg/mL PAH films (Au NPs/4 layers PCs/GFPC⁻, Au NPs/6 layers PCs/GFPC⁻ and Au NPs/8 layers PCs/GFPC⁻ films) were chosen for bacteria detection. The results shows that this Au NPs/PCs/GFPC⁻ film work as a sensor for the bacteria detection but there is a need for a more systematic study to gain a better understanding of the detection mechanism. However, if we focus on the bioimaging of the bacteria on the Au NPs/PCs/GFPC⁻ film surfaces both Au NPs/4 layers PCs/GFPC⁻ and Au NPs/8 layers PCs/GFPC⁻ surfaces indicated that *E. coli* can be targeted by GFPC⁻, especially for the Au NPs/8 layers PCs/GFPC⁻ surface. The contrast between the brighter bacteria and the dark background clearly indicates their presence.

Materials and methods

Materials

Gold (III) chloride trihydrate (Sigma, $\text{HAuCl}_4 \cdot 3\text{H}_2\text{O}$), trisodium citrate (Sigma), Poly(allylamine hydrochloride) (average $M_w = \sim 17\,500$ g/mol, Sigma), Poly(ethylene glycol) methyl ether acrylate (Sigma-Aldrich, $M_n = 454$ g mol⁻¹, APEG), 2-methyl-2-[(dodecylsulfanylthiocarbonyl)sulfanyl] propanoic acid (97%, Strem, TTCA), acrylic acid (99%, Aldrich, AA), 2-(Dimethylamino)ethyl acrylate (98%, Sigma, DMEA), 4,4'-Azobis(4-cyanopentanoic acid) (98%, Sigma, ACPC) were used as received without further purification. Solvents were of synthetic grade and purified according to standard procedures. 18 M Ω Millipore water was used throughout and further pH-adjusted with either HCl or NaOH. All solvents were dried on an automatic M. Braun SPS-800 instrument.

Characterization techniques

All nuclear magnetic resonance (NMR) spectra were recorded in CDCl_3 on a JEOL ECS (400 MHz) spectrometer. All chemical shifts are in ppm and referenced to tetramethylsilane (TMS).

Zeta potentials (ζ) were performed on a Zetasizer Nanoseries (Malvern) apparatus. The dispersant RI value was 1.330. Samples were analyzed in DTS 1060 plastic cells, at 25 °C. Three measurements of at least ten scans were performed for each sample.

pH measurements were performed using a glass electrode connected to PHM210 Standard pH meter from Mettler Toledo.

Contact angles were performed on an advanced surface technology (AST) video contact angle measuring device. A 1 μL droplet of deionized water was deposited on the samples.

Absorption measurements were performed using Varian Cary 100 and Cary 500 from Agilent Technologies.

Emission spectra were performed using Fluorolog FL3-221 spectrofluorimeter from Horiba Jobin-Yvon. A front-face configuration was used.

The SEM images were obtained using Zeiss Supra 55 VP fitted with a Field Emission Gun in ICMMO laboratory (CNRS UMR8182).

The fluorescence decay curves were obtained with a time-correlated single-photon-counting method using a titanium-sapphire laser (82 MHz, repetition rate lowered to 4 MHz thanks to a pulse-peaker, 1 ps pulse width, a doubling crystals is used to reach 495 nm excitation) pumped by an argon ion laser from Spectra Physics (Mountain View, CA, USA). The Levenberg-Marquardt algorithm was used for non-linear least square fit as implemented in the Globals software (Globals Unlimited, Villa Grove, USA). In order to estimate the quality of the fit, the

weighted residuals were calculated. In the case of single photon counting, they are defined as the residuals, i.e. the difference between the measured value and the fit, divided by the square root of the fit. χ^2 is equal to the variance of the weighted residuals. A fit was said appropriate for χ^2 values between 0.8 and 1.2.

Microscope images were taken on an epifluorescence microscopy (Nikon inverted microscope ECLIPSE TI-E). Transmission images were captured with an emCCD camera. Objectives 60 \times (CFI S Plan Fluor ELWD, NA 0.7) was used in this work.

Synthesis

Preparation of Au NPs [8]. All glassware was cleaned using aqua regia (3 parts HCl, 1 part HNO₃) for a minimum of 4 hours. After discarding the aqua regia, the glassware was rinsed with Milli-Q water and dried with nitrogen. The HAuCl₄ (1 mM, 50 mL) solution and the sodium citrate solution (38.8 mM, 5 mL) were prepared. Both salts are highly hygroscopic and so the mass was weighed quickly and transferred to their flasks. The round-bottom flask containing the HAuCl₄ solution was attached to the refluxing apparatus and placed in a water bath with magnetic stirring. When the refluxing solution was observable, the sodium citrate solution was added quickly and the vigorous stirring of the solution continued. The pale yellow colour of the gold solution turned to dark purple and within 15 mins had turned to a dark ruby red characteristic of spherical gold nanoparticles. The solution was left to reflux for another 15 minutes. The AuNPs solution was then left to cool to room temperature. Solution was finally stored in the refrigerator. This synthesis method produces spherical particles with negative surface charge due to the presence of the citrate ligands.

Polymer coating of AuNPs (AuNPs@PAH) [9]. Two concentrations of PAH solution were prepared in water (1 mg/mL and 2 mg/mL). To each solution, 4 mL of Au NPs solution was added while under magnetic stirring and left one hour for mixing. The solution was then centrifuged to precipitation for 40 mins, RPM 10,000 and re-dispersed using Milli-Q water. The centrifuging and washing was done twice and then the nanoparticles re-dispersed in 4 mL of Milli-Q water and stored in the refrigerator.

Synthesis of BODIPY (BODIPY phenol) [11]. A few drops of trifluoroacetic acid were added to a dichloromethane solution of kryptopyrrole (1.0 g, 2 equiv.) and 4-hydroxybenzaldehyde (500 mg, 1 equiv.). The dark reaction mixture was stirred at room temperature until total disappearance of the aldehyde. The oxidising agent (chloranil, 1 equiv.), then 5 min later DIPEA (7 equiv.) and finally trifluoroborate etherate (11 equiv.) were successively added. The mixture was filtered through a pad of silica or used crude. The filtrate was concentrated and the residue purified by chromatography on silica gel or by automatic chromatography to afford BODIPY.

¹H NMR (400 MHz, CDCl₃): δ (ppm) = 0.98 (t, J = 7.5, 6H, CH₂CH₃), 1.35 (s, 6H, CH₃), 2.31

(q, $J = 7.5$ Hz, 4H, CH_2CH_3), 2.53 (s, 6H, CH_3), 6.95 (d, $J = 8.24$ Hz, 2 H_{ar}). ^{13}C NMR (100 MHz, CDCl_3): δ (ppm) = 12.12, 12.76, 14.90, 17.35, 116.29 (C_{ar}), 128.17, 129.93 (C_{ar}), 131.39, 132.97, 138.64, 140.54, 153.79, 156.48. ^{19}F NMR (376 MHz, CDCl_3): δ (ppm) = -145.68 (q, $J = 32$ Hz, BF_2). ^{11}B NMR (128 MHz, CDCl_3): δ (ppm) = -0.13 (t, $J = 32$ Hz).

Synthesis of BODIPY Methacrylate [12]. BODIPY phenol (1 equiv. 1.2 mmol, 475 mg) is dissolved in 50 mL of anhydrous dichloromethane under argon. Then DBU (2 equiv., 2.4 mmol, 365 mg) is slowly added with a syringe to the solution and methacryloyl chloride (1.5 equiv., 1.8 mmol, 190 mg) is added to the dark solution. The mixture is stirred at room temperature during 24 h, until disappearance of the BODIPY phenol trace on TLC. The mixture is concentrated and the residue purified by chromatography on silica gel (dichloromethane/petroleum ether: 70/30), affording 432 mg of product.

^1H NMR (400 MHz, CDCl_3): δ (ppm) = 0.97 (t, $J = 7.6$ Hz, 6H), 1.33 (s, 6H), 2.08 (s, 3H), 2.29 (q, $J = 7.6$ Hz, 4H), 2.52 (s, 6H), 5.80 (s, 1H), 6.39 (s, 1H), 7.27 (d, $J = 8.7$ Hz, 2H), 7.32 (d, $J = 8.7$ Hz, 2H); ^{13}C NMR (100 MHz, CDCl_3): δ (ppm) = 165.69, 154.01, 151.44, 139.22, 138.45, 135.78, 133.32, 133.00, 130.90, 129.53, 127.68, 122.58, 18.46, 17.15, 14.68, 12.60, 11.92. ^{19}F NMR (376 MHz, CDCl_3): δ (ppm) = -145.68 (q, $J = 32.9$ Hz, BF_2). ^{11}B NMR (128 MHz, CDCl_3): δ (ppm) = -0.15 (t, $J = 32.9$ Hz).

Synthesis of P(APEG-co-GBDPMA-co-AA) (GFPC $^{\text{--}}$). Negative fluorescent polymer chain P(APEG₃₁-co-GBDPMA₁₈-co-AA₃₁) was synthesized in 1,4-dioxane at 75 °C under argon atmosphere. APEG (1.07 g, 2.22 mmol), AA (0.16 g, 2.22 mmol), RAFT agent TTCA (0.026 g, 0.07 mmol), DMF (0.08 g, 1.15 mmol) and ACPA (1.3 mg, 0.0048 mmol) were dissolved in 2.0 mL of 1,4-dioxane at room temperature. The mixture solution was then purged with argon for 30 min in an ice bath. It was then immersed into an oil bath at 75 °C to start the polymerization. Samples were periodically withdrawn from the polymerization medium for analyses. To study the kinetics, monomer conversion was determined by ^1H NMR spectroscopy. DMF, which has no influence on the free radical process, was used as internal reference. After 44 h, the flask was quenched in ice bath to terminate the polymerization. After removing all the solvents under reduced pressure, the residues were dissolved in THF and then precipitated into an excess of ethyl ether. This purification cycle was repeated twice. The final polymer was obtained as a red solid.

Synthesis of P(APEG-co-AA) (PC $^{\text{--}}$). Negative polymer chain P(APEG₁₄-co-AA₁₄) was synthesized in 1,4-dioxane at 75 °C under argon atmosphere. APEG (1.46 g, 3.33 mmol), AA (0.24 g, 3.33 mmol), RAFT agent TTCA (0.132 g, 0.233 mmol), DMF (0.135 g, 1.85 mmol) and ACPA (5.2 mg, 0.018 mmol) were dissolved in 3.5 mL of 1,4-dioxane at room temperature. The mixture solution was then purged with argon for 30 min in an ice bath. It was then immersed into an oil bath at 75 °C to start the polymerization. Samples were periodically withdrawn from the polymerization medium for analyses. To study the kinetics, monomer conversion was determined

by ^1H NMR spectroscopy. DMF, which has no influence on the free radical process, was used as internal reference. After 4 h, the flask was quenched in ice bath to terminate the polymerization. After removing all the solvents under reduced pressure, the residues were dissolved in THF and then precipitated into an excess of cold cyclohexane. The final polymer was obtained as a yellow viscous solid.

Synthesis of P(APEG-co-DMEA) (PC^+). Positive polymer chain $\text{P(APEG}_{12}\text{-co-DMEA}_{12})$ was synthesized in 1,4-dioxane at $75\text{ }^\circ\text{C}$ under argon atmosphere. APEG (0.57 g, 1.23 mmol), DMEA (0.18 g, 1.23 mmol), TTCA RAFT agent (0.038 g, 0.105 mmol), DMF (0.037 g, 0.50 mmol) and ACPA (2.0 mg, 0.007 mmol) were dissolved in 2.5 mL of 1,4-dioxane at room temperature. The mixture solution was then purged with argon for 30 min in an ice bath. It was then immersed into an oil bath at $75\text{ }^\circ\text{C}$ to start the polymerization. Samples were periodically withdrawn from the polymerization medium for analyses. To study the kinetics, monomer conversion was determined by ^1H NMR spectroscopy. DMF, which has no influence on the free radical process, was used as internal reference. After 4 h, the flask was quenched in ice bath to terminate the polymerization. After removing all the solvents under reduced pressure, the residues were dissolved in THF and then precipitated into an excess of cold cyclohexane. This purification cycle was repeated twice. The final polymer was obtained as a yellow viscous solid.

Preparation of Au NPs@PAH/PCs/GFPC $^-$ LbL film

Activated glass slides: The glass slides were immersed in piranha solution ($\text{H}_2\text{O}_2/\text{H}_2\text{SO}_4=1:3$ v/v) for 30 min, washed three times with deionized water, and then dried under a gentle stream of nitrogen gas. (*CAUTION: "Piranha" solution reacts violently with organic materials; it must be handled with extreme care.*)

Au NPs surface: A glass slide was removed from the storage dish, dried completely with compressed air, and placed in the Au NPs@PAH (individually prepared in 1 mg/mL and 2 mg/mL PAH solution) solution for 10 minutes. After the glass slide was washed three times for 1 minute each with Milli-Q water, then dried with compressed air. Au NPs surface was obtained.

LbL film fabrication: The positively charged Au NPs film was alternatively immersed in charged PC^- solution (12 mL, 4.2×10^{-4} mol/L, $[\text{NaCl}] = 0.005\text{ M}$, $\text{pH} = 9.5$) and PC^+ solution (12 mL, 8.2×10^{-5} mol/L, $[\text{NaCl}] = 0.005\text{ M}$, $\text{pH} = 5.4$) for 10 min. The final layer was prepared by immersing in GFPC $^-$ (12 mL, 5.0×10^{-7} mol/L, $[\text{NaCl}] = 0.005\text{ M}$, $\text{pH} = 5.5$), and the thickness between Au NPs and GFPC $^-$ was adjusted by changing the number of deposition cycles of PC^- and PC^+ .

Bacteria culture

Bacteria strain used in this research was *Escherichia coli* (K-12, BW25113). The strain was

firstly streaked onto Luria-Bertani (LB) agar plates, and then incubated at 37 °C for overnight. An isolated colony of each strain was picked and inoculated in 5 mL of LB medium. After incubation at 37 °C for overnight (shaking at 350 rpm and 5% CO₂), the bacteria culture was then diluted 1:100 in the M9 minimal growth medium. After incubation at 37 °C for 2 hours, the bacteria suspensions were carried out during all experiments.

Bacteria detection on Au NPs@PAH/PCs/GFPC⁻ LbL surface

Bacteria detection: 2 µL bacteria suspensions ($1.1 - 5.5 \times 10^7$ cells/mL) were introduced onto each Au NPs@PAH/PCs/GFPC⁻ LbL film surface with 4, 6 and 8 PC layers and on GFPC⁻ film surface with no AuNPs, allowed to incubate for 10 minutes at room temperature to settle onto the surface, and then washing step was performed with M9 culture medium twice. Finally, 2 µL fresh M9 medium was added on each surface, and a clean glass slide was used as a coverslip and observed under microscope. Meanwhile, the controls were carried out for each sample by adding 2 µL M9 medium instead of bacteria suspension.

Image analysis: A series of images from different sensing regions were analyzed using NIH (National Institutes of Health) recommended image processing software, Image J.

References

- [1] S. Eustis and M. A. El-Sayed. Why gold nanoparticles are more precious than pretty gold: Noble metal surface plasmon resonance and its enhancement of the radiative and nonradiative properties of nanocrystals of different shapes. *Chem. Soc. Rev.*, 2006, **35**, 209-217.
- [2] C. D. Geddes, H. Cao, I. Gryczynski, Z. Gryczynski and J. R. Lakowicz, *et al.* Metal-Enhanced Fluorescence (MEF) Due to Silver Colloids on a Planar Surface: Potential Applications of Indocyanine Green to in Vivo Imaging. *J. Phys. Chem. A*, 2003, **107**(18), 3443-3449.
- [3] C. D. Geddes and J. R. Lakowicz. Metal-enhanced fluorescence. *J. Fluoresc.*, 2002, **12**(2), 121-129.
- [4] C. D. Geddes and J. R. Lakowicz. Radiative Decay Engineering. 2007, Springer, New York.
- [5] K. Ray and J. R. Lakowicz. Metal-Enhanced Fluorescence Lifetime Imaging and Spectroscopy on a Modified SERS Substrate. *J. Phys. Chem. C*, 2013, **117**, 15790-15797.
- [6] J. R. Lakowicz. Radiative Decay Engineering: Biophysical and Biomedical Applications. *Anal. Biochem.*, 2001, **298**, 1-24.
- [7] C. D. Geddes, Metal-enhanced fluorescence. 2010, Wiley-Blackwell, Oxford.
- [8] Storhoff, J. J., Elghanian, R., Mucic, R. C., Mirkin, C. A. and Letsinger, R. L. One-pot colorimetric differentiation of polynucleotides with single base imperfections using gold nanoparticle probes. *J. Am. Chem. Soc.*, 1998, **120**, 1959-1964.
- [9] Zyuzin, M. V. *et al.* Influence of temperature on the colloidal stability of polymer coated gold nanoparticles in cell culture media. *Small*, 2016, **12**, 1723-1731.
- [10] S. Link and M. A. El-Sayed. Size and temperature dependence of the plasmon absorption of colloidal gold nanoparticles. *J. Phys. Chem. B*, 1999, **103**, 4212-4217.
- [11] C. Dumas-Verdes, F. Miomandre, E. Lepicier, O. Galangau and P. Audebert. *et al.* BODIPY-Tetrazine multichromophoric derivatives. *Eur. J. Org. Chem.*, 2010, 2525-2535.
- [12] C. Gazon, J. Rieger, R. Meallet-Renault, G. Clavier and B. Charleux. One-pot synthesis of pegylated fluorescent nanoparticles by RAFT minoemulsion polymerization using a phase inversion process. *Macromol. Rapid Commun.*, 2011, **32**, 699-705.
- [13] A. Loudet, K. Burgess. BODIPY dyes and their derivatives: syntheses and spectroscopic properties. *Chem. Rev.*, 2007, **107**, 4891-932.
- [14] W. Qin, M. Baruah, M. Van Der Auweraer, F. C. De Schryver and N. Boens. Photophysical properties of borondipyrromethene analogues in solution. *J. Phys. Chem. A*, 2005, **109**, 7371-7384.

- [15] N. Ma, F. Tang, X. Wang, F. He and L. Li. Tunable metal-enhanced fluorescence by stimuli-responsive polyelectrolyte interlayer films. *Macromol. Rapid Commun.*, 2011, **32**, 587-932.
- [16] K. Ray, R. Badugu and J. R. Lakowicz. Polyelectrolyte layer-by-layer assembly to control the distance between fluorophores and plasmonic nanostructures. *Chem. Mater*, 2007, **19**, 5902-5909.
- [17] W. Deng, F. Xie, H. T. M. C. M. Baltar and E. M. Goldys. Metal-enhanced fluorescence in the life sciences: here, now and beyond. *Phys. Chem. Chem. Phys.*, 2013, **15**, 15695-15708.

Chapter 4

“Click”-based Layer-by-Layer Antibody Nanostructured Surface for Selective Bacteria Detection

Chapter 4 “Click”-based Layer-by-Layer Antibody Nanostructured Surface for Selective Bacteria Detection

Antibodies have outstanding molecular recognition properties. It prompted research to use them as bio-therapeutics for various diseases (e.g., cancer) [1-3]. They also play important roles as targeting moieties for specific detection [4-7]. Specific detection of bacteria is vital to clinical diagnostics, food safety, water quality control, and biodefense [8, 9]. Immunological methods are based on the antigen-antibody reaction principle with the advantages of simple operation and fast response [10-12]. In order to improve the specificity and sensitivity of immunosensors for bacteria, antibodies are usually immobilized on the surface to fully exploit their recognition sites [13-15]. Developing a nanostructured antibody-functionalized surface to achieve a high binding sites density still remains a significant challenge in material science.

The copper-catalyzed azide-alkyne cycloaddition reaction (CuAAC), often referred to as “click chemistry”, has become one of the most powerful tools in material science, synthesis, and modification of surfaces since the introduction of the “click” concept in 2001 by Sharpless and coworkers [16, 17]. Because the click chemistry provides a promising and powerful biofunctionalization method due to its high efficiency, simplicity, orthogonality, and tolerance of reaction conditions even in the presence of cellular systems [18, 19], the combination of synthetic polymers with biological materials (e.g. nucleic acids [20, 21], peptides [22, 23], sugars [24], proteins [25, 26] or even viruses [27] and cells [28]) under different synthetic strategies have been widely investigated. However, due to the cytotoxicity of the copper catalyst, CuAAC has been restricted to applications that are insensitive to the presence of trace amounts of the toxic metal ion. Bertozzi and co-workers have developed several strained cyclooctynes to achieve copper-free click chemistry under mild conditions, through the so called strain-promoted azide-alkyne cycloaddition (SPAAC) [29]. Nanostructured antibody-functionalized surfaces have been constructed on a functionalized polymer surface by the self-assembly of protein-polymer conjugates based on SPAAC. Therefore, the fabrication of well-defined nanostructured functionalized polymer surfaces with high packing density is challenging.

The LbL film surface can be modified after assembly when functional groups are present [30]. Nonetheless, to the best of our knowledge, clickable polyelectrolytes have not been synthesized previously as a functional material for the bottom-up assembly of nanostructured polymer surfaces. However, the combination of reversible addition-fragmentation chain transfer polymerization (RAFT) techniques and click chemistry was already shown to offer viable routes for surface modification [31, 32]. Modifying the reversible addition fragmentation technique chain transfer agent (RAFT TTCA) at the chain-end for precise functionalization with 4-dibenzocyclooctynol (DIBO) by esterification reaction makes it possible to rapidly prepare a functional polymer from a common polymeric precursor thereby offering exciting opportunities

to fine-tune the properties of materials [33].

In this chapter, we report for the first time the elaboration of a nanostructured surface functionalized with an antibody for bacteria-selective detection. This is achieved thanks to a simple modification of poly(acrylic acid-co-poly(ethylene glycol) methyl ether acrylate) by 4-dibenzocyclooctynol. The two polyelectrolytes poly(2-(dimethylamino)ethyl acrylate-co-poly(ethylene glycol) methyl ether acrylate) (PC^+) and DIBO- PC^- were simply assembled on activated glass slides through LbL assembly. The DIBO moiety of the DIBO- PC^- can then react with azido anti-*E.coli* antibody by metal-free cycloaddition under mild aqueous conditions, so that the activity of antibody is preserved.

I will introduce the synthesis of DIBO, modified RAFT TTCA agent with DIBO, PC^+ and DIBO- PC^- . The preparation of DIBO- PC^- surface was carried out through LbL assembly and then the surface characterization of DIBO- PC^- film was performed. Azide-modified antibody was prepared and anchored on DIBO- PC^- surface by click chemistry. After the surface passivation, the antibody surface was used for bacteria detection. The influence of various parameters such as fluidic condition and concentration of antibody on the sensitivity of the antibody surface for bacteria detection was investigated. Finally, the selectivity of the antibody functionalized surface was tested.

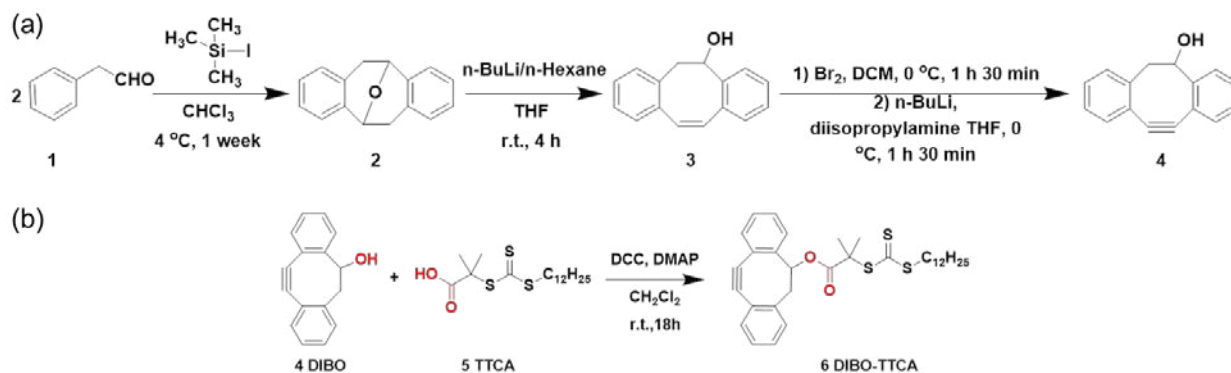
4.1 Synthesis of 4-dibenzocyclooctynol functionalized poly(acrylic acid-co-poly(ethylene glycol) methyl ether acrylate) (DIBO- PC^-) and poly(2-(dimethylamino)ethyl acrylate-co-poly(ethylene glycol) methyl ether acrylate) (PC^+)

4.1.1 Synthesis of DIBO- PC^-

4-dibenzocyclooctynol (DIBO, compound **4**) was chosen since it is ideal for labeling functional structures with azides. Indeed aromatic rings are expected to impose additional ring strain and conjugate with the alkyne, thereby increasing its reactivity in metal-free [2+3] cycloadditions with azides (SPAAC). The compound also has excellent stability because the *ortho* hydrogen atoms of the aromatic rings shield the alkyne from nucleophilic attack. Furthermore, the hydroxyl group in **4** provides a handle for further functionalization [34]. Compound **4** could be prepared from the commercially available phenylacetaldehyde (**1**) in four steps using published procedures (Scheme 4.1a) with an overall yield of 10.3%.

Trithiocarbonates are versatile chain transfer agents (CTAs) that offer a good control of the polymerization as well as high hydrolytic stability. Commercially available 2-(dodecylthiocarbonothioylthio)-2-methylpropionic acid (TTCA, **5**) was used as the starting material for the synthesis of the clickable RAFT agent **6** (Scheme 2b). TTCA (**5**) was connected to DIBO (**4**) through an ester linkage in high yield using *N,N'*-dicyclohexylcarbodiimide (DCC)

and 4-dimethylaminopyridine (DMAP). The product **6** was isolated as an orange oil, which solidified upon standing in 71% yield. NMR spectrometry confirmed the structure of the product (Figure 4.1).



*Scheme 4.1. Synthetic route for 4-dibenzocyclooctynol (DIBO) **4** and preparation of the cyclooctyne-containing RAFT agent DIBO-TTC **6**.*

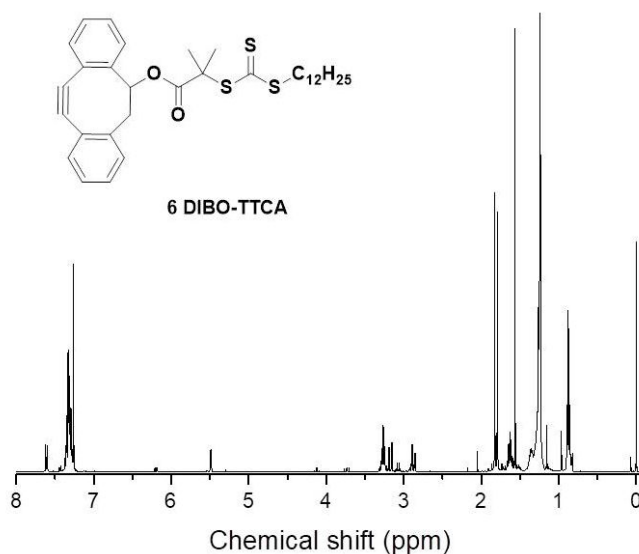
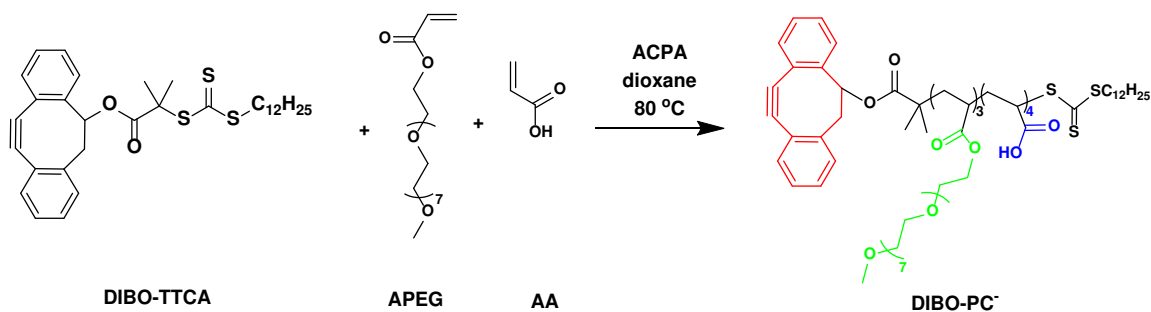


*Figure 4.1. NMR spectrum of DIBO-TTCA **6**.*

With the DIBO-modified RAFT agent in hand, it was engaged in the copolymerization reaction of poly(ethylene glycol) methyl ether acrylate (APEG) and acrylic acid (AA) under standard conditions using 1,4-dioxane as the solvent and 4,4'-Azobis(4-cyanopentanoic acid) (ACPA) as the initiator at 80 °C (Scheme 4.2). After a reaction time of 66.5 hours, the conversion rate leveled at 31% as determined by monitoring the disappearance of the ethylenic protons in the crude mixture by ^1H NMR spectrometry. The end-functionalized DIBO-PC⁻ was isolated by precipitation into cold diethyl ether and tangential flow filtration. ^1H NMR spectrum

of the resulting polymer showed successful installation of a DIBO moiety due to the bands in the aromatic region (Figure 4.2).



Scheme 4.2. Synthetic scheme for the RAFT synthesis of P(APEG-co-AA) (DIBO-PC⁻).

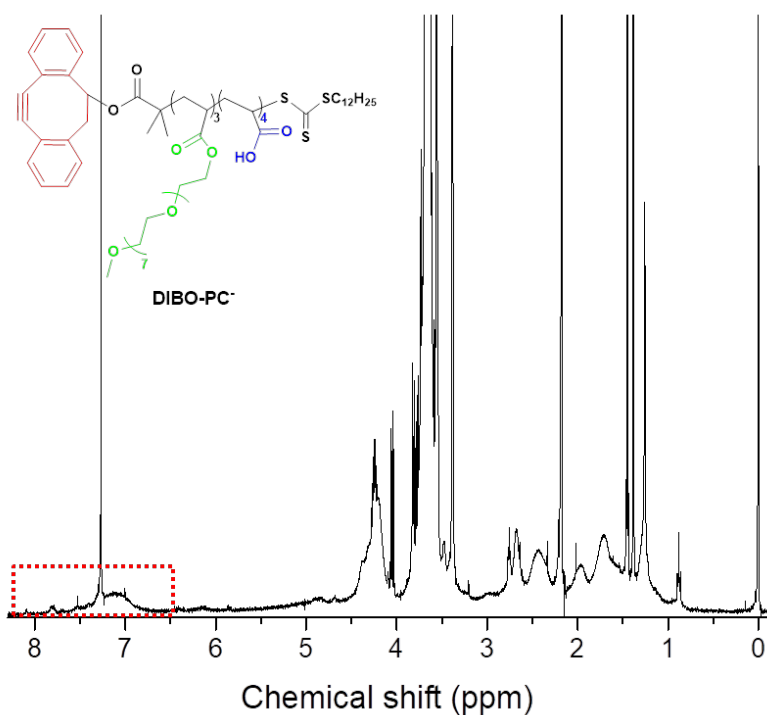
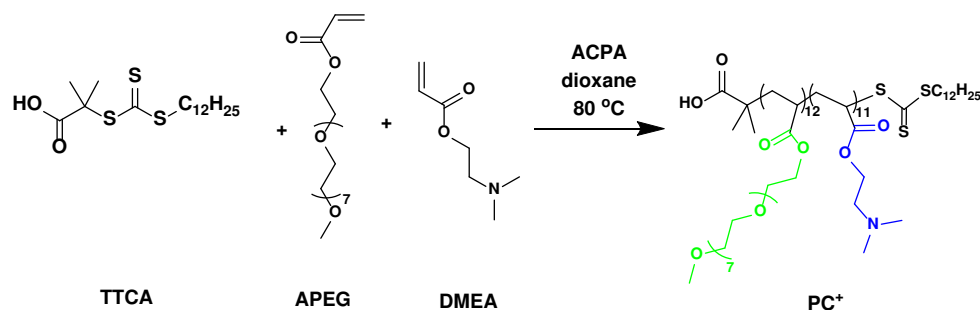


Figure 4.2. NMR spectrum of DIBO-PC⁻.

4.1.2 Synthesis of PC⁺

In order to prepare the DIBO-PC⁻ surface by Layer-by-layer (LbL) assembly, a positively charged polymer was necessary. Poly(ethylene glycol) methyl ether acrylate (APEG) and 2-(dimethylamino)ethyl acrylate (DMEA) were copolymerized by RAFT technique following the same experimental conditions than for DIBO-PC⁻ (scheme 4.3). The conversion rate reached 90% after 1.5 hours as determined by monitoring the disappearance of the ethylenic protons in

the crude mixture by ^1H NMR spectrometry. The polymerization was stopped by immersing the reaction mixture into an ice bath. PC^+ was isolated by repeated precipitation into cold cyclohexane.



Scheme 4.3. Synthetic scheme for the RAFT synthesis of $P(\text{APEG-co-DMEA})$ (PC^+).

4.2 Preparation and characterization of DIBO- PC^- surface

The zeta potential of the PC^+ was found to be 5.5 mV at pH 8.52. After adjusting the pH of the PC^+ solution at 5.43, the value reached 30.2 mV which is high enough to allow them to bind on activated glass slides through electrostatic attraction (Table 4.1). For the negatively charged DIBO- PC^- , the initial zeta potential is -33.2 mV at pH 3.64. The zeta-potential reached -43.6 mV when the pH of the DIBO- PC^- solution was set at 5.28. The results show that the layer-by-layer assembly can be conducted with the positively charged PC^+ with a zeta-potential of 30.2 mV and the negatively charged DIBO- PC^- with a zeta-potential of -33.2 mV when the pH of the solutions are approximately 5.4.

Table 4.1. Zeta potentials (ζ) of the PC^+ and DIBO- PC^-

	PC^+		DIBO- PC^-	
pH	8.52	5.43	3.64	5.28
ζ^a / mV	5.5±0.4	30.2±0.9	-33.2±0.3	-43.6±0.2

^aZeta potentials (ζ) were recorded in Milli-Q water at 25 °C, $[\text{PC}^+] = 8.2 \times 10^{-5}$ M, $[\text{DIBO-PC}^-] = 5.1 \times 10^{-4}$ M.

PC^+ and DIBO- PC^- were used to build LbL films. Noting that ionic strength has a great influence on the conformation of the polyelectrolyte [35], 0.005M NaCl was added to the 8.2×10^{-5} M PC^+ and 5.1×10^{-4} M DIBO- PC^- aqueous solutions. Contact angles using ultra-pure water (18.2 M Ω cm) as the probe fluid were measured as a qualitative indication of the surface modification and quantitative measurement of the surface wettability. Five replicate

measurements were taken for each sample, and the average and standard deviation are reported in Table 4.2. The contact angle for the bare activated glass slide is 1.8° , indicating a super-hydrophilic surface. After the activated glass slide was immersed into the PC^+ solution for 20 min, washed with water three times and dried with a stream of nitrogen, the corresponding contact angle was 25.3° . The surface is thus hydrophilic. This means that the glass slide has been modified and covered with PC^+ chains. Next the PC^+ film was immersed into the oppositely charged solution (DIBO- PC^-) for 20 min, then the surface was washed and dried. The film became more hydrophobic (contact angle 30.3°) because of the DIBO functional group in the polymer chains but still hydrophilic enough for our purpose. The results indicate that the LbL assembly has been successfully applied for thin film fabrication and the DIBO- PC^- surface is sufficiently hydrophilic.

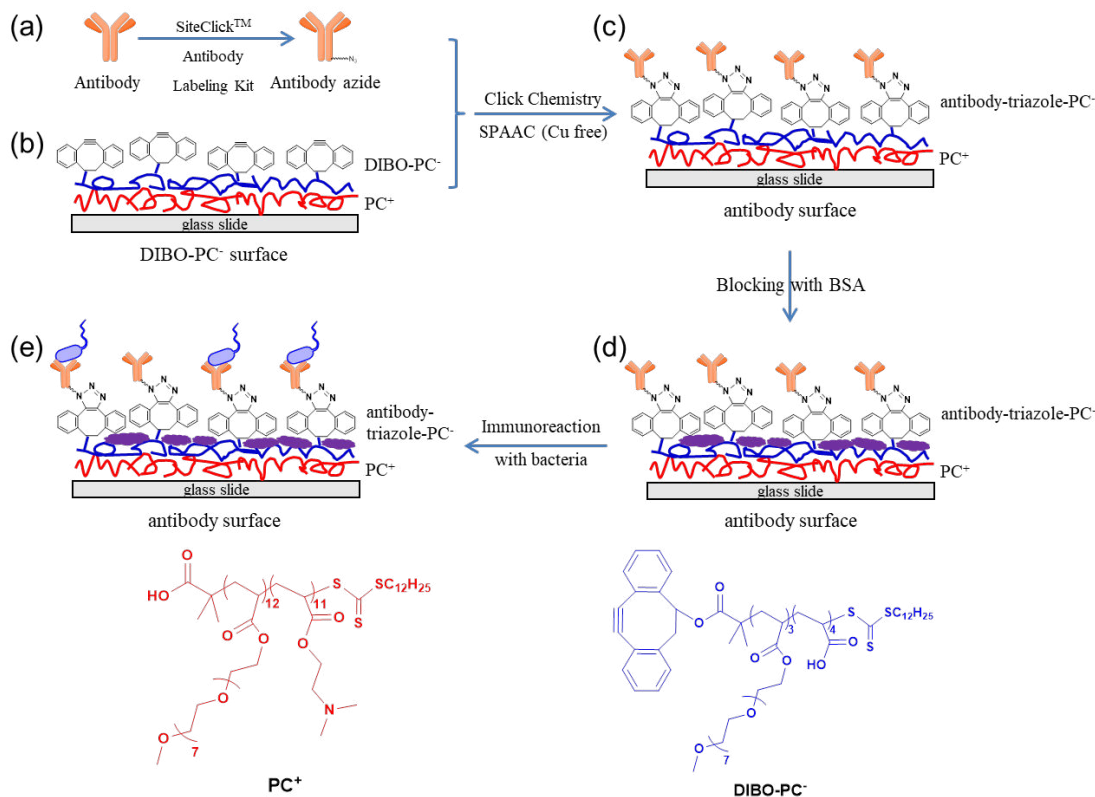
Table 4.2. Contact angle of different surfaces

	Activated glass slide	PC^+	$PC^+/DIBO-PC^-$
Contact angle	$1.8^\circ \pm 0.1$	$25.3^\circ \pm 0.2$	$30.3^\circ \pm 2.2$

4.3 Specific bacteria detection based on immunoassay between anti-*E. coli* antibody surface and *E. coli*

The principle for the selective detection of the targeted bacteria based on an immunoassay approach between the antibody and bacteria is schematically described in scheme 4.4. One of the main steps for the development of the sensors is the synthesis of an antibody azide. We used a commercial SiteClickTM antibody labeling kit with a two-step reaction (scheme 4.4a). Antibody consists of two regions: Fab containing the specific antigen-binding sites and Fc region that can bind to cell receptors and complement proteins. To avoid interfering with the recognition ability of antibodies, the modification site should be on the Fc region of the antibodies. The terminal galactose residues in the Fc region of antibody were modified by galactosidase, which readily undergoes condensation reaction with an azide-containing sugar. Subsequently, azide modified antibodies were obtained after purification. In the present work IgG antibody which is specific for *E. coli* was selected. The DIBO- PC^- surface (Scheme 4.4b) was immersed in a solution containing the azide modified Anti-*E. coli* antibody to achieve the strain-promoted azide-alkyne cycloadditions (SPAAC) reaction in mild aqueous conditions (Scheme 4.4c). Surface passivation was performed using a solution of 20 mg/mL bovine serum albumin (BSA) for 2 hours at $37^\circ C$ in order to decrease nonspecific binding on the antibody modified surface (Scheme 4.4d). Finally, in this study *E. coli* was used as a model bacterium (gram-negative) for selective bacteria detection assay by introducing *E. coli* onto the passivated anti-*E. coli* antibody modified surface (Scheme 4.4e). Finally *E. coli* bacteria were flown into a microfluidic channel and landed on the

anti-*E. coli* antibody modified surface. Then unbound (non-specific) bacteria were washed away by fluidic force, the remaining bacteria were counted. The influence of the fluidic condition and the quantity of antibody was investigated. Finally, gram-positive *B. subtilis* was used to evaluate the specificity of the anti-*E. coli* antibody modified surface.



*Scheme 4.4. Schematic illustration of the structured film of polycation (PC⁺) and polyanion (DIBO-PC⁻) and the mechanism of antibody surface grafting for specific bacteria detection assay. (a) Introduction of the azide on the Fc region of the IgG antibody (anti-*E. coli* antibody) using the SiteClick™ kit. (b) DIBO-PC⁻ surface prepared with PC⁺ and DIBO-PC⁻ via LbL assembly. (c) Surface functionalized with the antibody by click chemistry. (d) Surface passivation performed using a solution of 20 mg/mL BSA for 2 hours at 37 °C. (e) Binding of the targeted bacteria by the passivated antibody modified surface.*

4.4 Azide-modified antibody preparation and anti-*E. coli* antibody surface preparation in a microfluidic set up

Anti-*E. coli* antibody, which belongs to IgG fraction, recognizes a unique molecule of the harmful agent (called an antigen) *via* the Fab's variable region. The ability of an antibody to communicate with the other components of the immune system is mediated *via* its Fc region, which contains a conserved glycosylation site involved in these interactions. Antibody azide was synthesized using a commercial SiteClick™ antibody labeling kit with a two-step reaction on

the Fc region of the antibodies. In the first step of SiteClick™ modification (Figure 4.3), terminal galactose residues on the N-linked sugars in the Fc region of the antibody were removed by β -Galactosidase. The azide-containing sugar, GalNAz, was then added to the modified carbohydrate domain of the antibody *via* the β -1,4-galactosyltransferase (Gal-T)-catalyzed reaction targeting the terminal GlcNAc residues. Subsequently, azide-modified antibodies were obtained by following a purification procedure provided by the supplier. The procedure ensures that the specific functionalization maintained the integrity of the antigen binding site of the antibody.

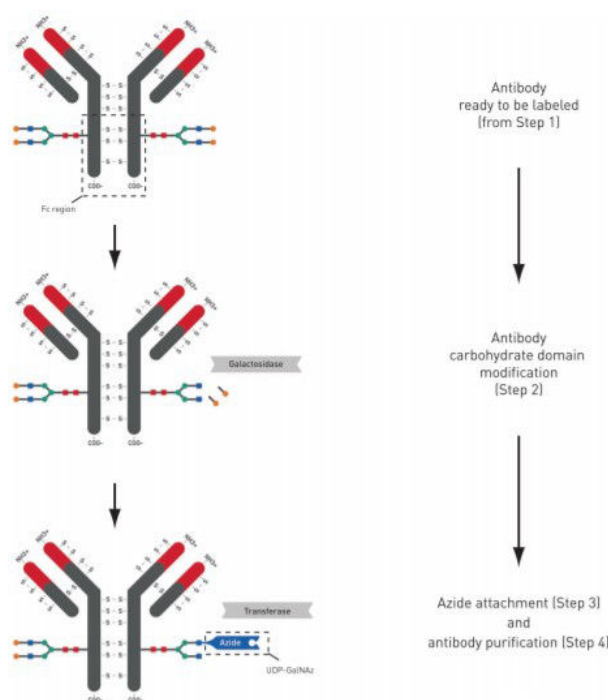


Figure 4.3. SiteClick™ conjugation procedure: in the first step, terminal galactose residues on the N-linked sugars in the Fc region of the antibody are removed by β -Galactosidase. The azide-containing sugar, GalNAz, is then added to the modified carbohydrate domain of the antibody via the β -1,4-galactosyltransferase (Gal-T)-catalyzed reaction targeting the terminal GlcNAc residues. This specific targeting maintains the integrity of the antigen binding site of the antibody (from [36]).

The choice of the commercial Sticky-Slide VI 0.4 (bottomless blank slide, Figure 4.4) from IBIDI company as microfluidic device was dictated by a combination of advantageous parameters. It is a bottomless 6 channels slide with a self-adhesive underside that can be fitted to many surfaces including glass and compatible with cell culture. Each channel has a volume of 30 μ l. It is thus possible to quickly build a set-up with 6 parallel channels on a single surface for biological assays that requires smaller sample/reagent quantities (especially azide-modified

antibodies) and offers a precise control of shear stress.

After depositing subsequently a layer of PC^+ and one of $DIBO-PC^-$ on a treated glass surface, the μ -Slide channels was stuck to it and azide-modified antibodies could be loaded into the channel. Subsequent SPAAC copper-free click reaction occurred between azide-modified antibodies and $DIBO-PC^-$ surface under mild condition at room temperature. Excess azide-modified antibodies were removed by washing the channel with fresh PBS buffer. The anti-*E. coli* antibody surface was stored by immersing the channel with PBS buffer.

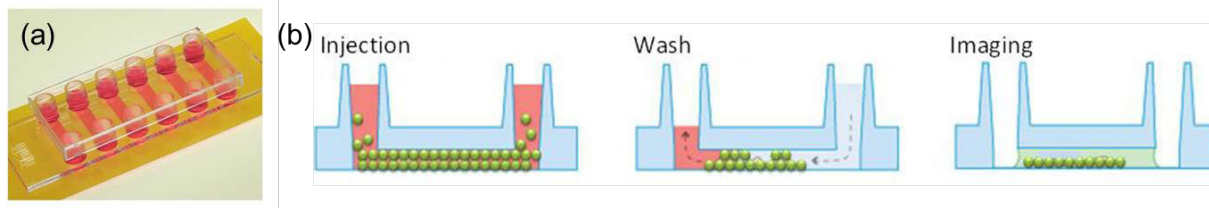


Figure 4.4. (a) Image of the Sticky-Slide VI 0.4 from IBIDI. (b) Preparation procedure of functionalized surface in the device.

4.5 Surface passivation with bovine serum albumin (BSA)

In order to prevent cell adhesion on the anti-*E. coli* antibody surface through nonspecific binding and improve the accuracy and selectivity of the bacteria detection, passivation of the surface and channel walls has to be done. A 20 mg/mL Bovine Serum Albumine (BSA) solution was flown into the channel for at least one hour at 37 °C. First, we tested the effect of BSA passivation on the $DIBO-PC^-$ surface alone (Figure 4.5).

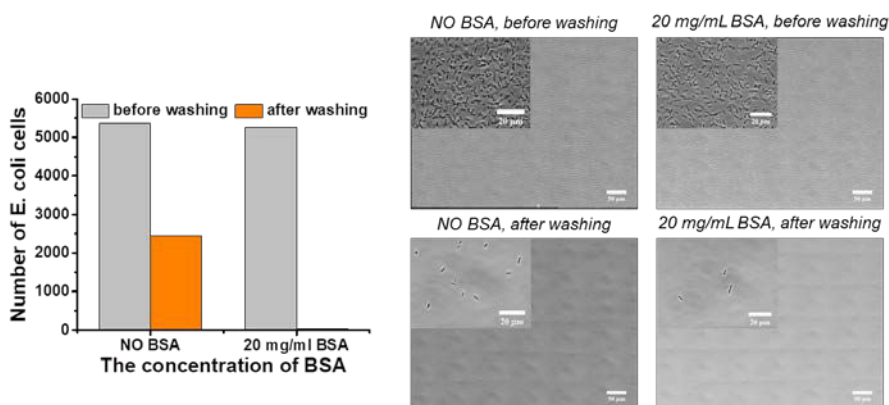


Figure 4.5. Effect of BSA passivation on the $DIBO-PC^-$ surface: (left) *E. coli* cells counted by image analysis of the surface (0.25 mm²) before and after washing and (right) corresponding bright field microscopy images.

The number of *E. coli* cells on the passivated $DIBO-PC^-$ surface is dramatically decreased after washing with PBS, comparing to the untreated $DIBO-PC^-$ surface (Figure 4.5). For the anti-

E. coli antibody surface, the same passivation protocol was employed to eliminate the possibility of nonspecific binding on the surface.

4.6 Effect of fluidic conditions on the stability and sensitivity of the anti-*E. coli* antibody surface for *E. coli* detection

After the incubation step, almost all solid-phase immunoassays perform a washing step to remove nonspecifically bound analyte and reduce the background signal. Ideally, the washing step should expose the assay labels to forces stronger than the strongest non-specific interaction, but weaker than the weakest binding affinity. In addition, the non-specific interactions have been demonstrated to be at least an order of magnitude weaker than specific antibody-antigen bonds [37, 38]. In brief, the unbound cells can be removed by rinsing under fluid flow shear. In the used microfluidic system, the shear stress (τ , $\frac{\text{dyn}}{\text{cm}^2}$), can be calculated by the following formula:

$$\tau = \eta \cdot 97.1 \cdot \Phi \quad (\text{eq. 4.1})$$

where η is the buffer dynamical viscosity ($\frac{\text{dyn}\cdot\text{s}}{\text{cm}^2}$) and Φ the flow rate ($\frac{\text{ml}}{\text{min}}$). For PBS buffer, the dynamical viscosity is 1.05 cP (equal to $0.0105 \frac{\text{dyn}\cdot\text{s}}{\text{cm}^2}$) at room temperature. The flow rate was set at 100, 150, 200, 250, 300 and 400 $\mu\text{L}/\text{min}$, corresponding to shear stress of 0.102, 0.153, 0.204, 0.255, 0.306 and 0.408 dyn/cm^2 , respectively.

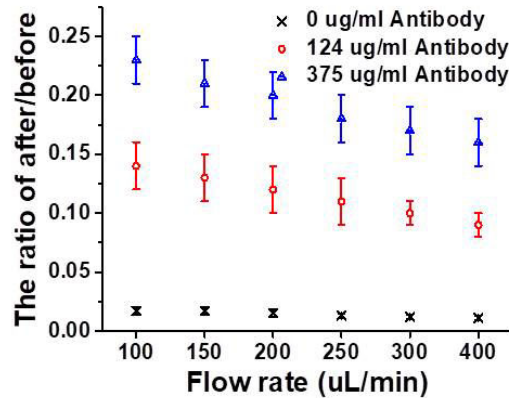


Figure 4.6. Flow rate effect on the *E. coli* “capture” capability of anti-*E. coli* antibody surface: ratio of the number of *E. coli* on the surface after and before washing step as a function of flow rate.

Figure 4.6 clearly indicates that the non-specifically bound bacteria on the passivated surface (control, no antibody) were removed by rinsing under low fluid flow shear ($0.102 \text{ dyn}/\text{cm}^2$) and exhibited a good signal-to-noise background. Shear stress equal to or greater than $0.102 \text{ dyn}/\text{cm}^2$,

when applied to the bacteria, can therefore be expected to be sufficient to remove non-specifically bound bacteria on the 124 $\mu\text{g/ml}$ and 375 $\mu\text{g/ml}$ anti-*E. coli* antibody surface. When further increasing the shear stress to 0.255 dyn/cm^2 , the bacteria detachment from the target surface tended to reach a plateau for each surface. Even when the fluid flow shear was 0.408 dyn/cm^2 , there was still a large quantity of *E. coli* remaining on the anti-*E. coli* antibody surface which is attributed to the good stability of the “click”-based LbL antibody nanostructured surface. In order to improve the sensitivity of anti-*E. coli* antibody surface for selective bacteria detection, the shear stress in the microfluidic channel was fixed at 0.102 dyn/cm^2 for further study.

4.7 Effect of the concentration of anti-*E. coli* antibody on the sensitivity of the anti-*E. coli* antibody surface for *E. coli* detection

Next, we investigated whether the sensitivity for bacteria detection of anti-*E. coli* antibody surface can be improved by increasing the concentration of the antibody solution used for the SPAAC reaction on the surface. 60 μL of azido anti-*E. coli* antibody solutions corresponding to 124 and 375 $\mu\text{g/mL}$ were injected into two different channels, meanwhile, one control with 60 μL 1 \times Tris was introduced into a third channel. The surface preparation with different quantities of anti-*E. coli* antibody followed the protocol described earlier (washing then BSA passivation and washing were performed) and the reference channel was also passivated with BSA.

The obtained passivated anti-*E. coli* antibody surfaces with various concentration of antibody (0, 124 and 375 $\mu\text{g/mL}$) were loaded with diluted *E. coli* ($\text{OD} = 0.115$) to test the “capture” capability of the surfaces. The bacteria settled on each surface after 1 hour incubation and then each surface was washed to remove all non-specifically bound bacteria cells. Thanks to imaging we could observe that a significant number of bacteria was present on both of the passivated antibody functionalized surfaces, while the passivated DIBO-PC⁻ reference surface exhibited neglectful cells number (Figure 4.7).

The number of *E. coli* cells remaining on the anti-*E. coli* antibody functionalized surface with the highest concentration (375 $\mu\text{g/mL}$) was about twice higher than the one with the lower concentration (124 $\mu\text{g/mL}$). On one hand, LbL assembled nanostructured DIBO-PC⁻ surface supplied large specific surface area and sufficient active binding sites (DIBO moiety) for antibody-polymer conjugation. So, in our case the highest the antibody number, the more bacteria cells could be captured. On the other hand, the azide-modified antibody was initially exposed to the DIBO-PC⁻ surface followed by the click conjugation from the surface. Because antibody *in situ* immobilization involved minimized steric hindrance for antibody-polymer conjugation on the surface, significantly higher grafting densities could be achieved. It is noteworthy that we did not tested higher concentration of antibody-azide in order to determine the highest number that can be immobilized on the surface because of the availability and cost of

the starting material.

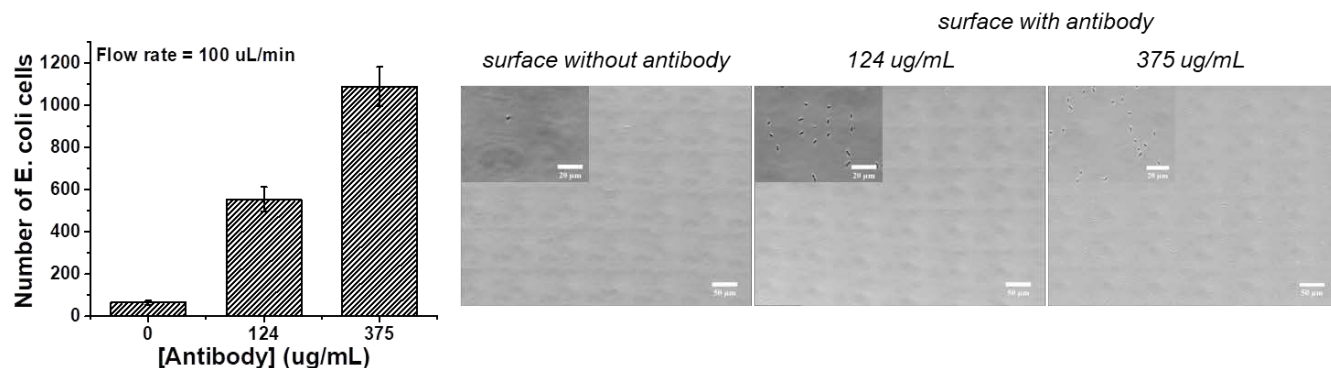


Figure 4.7. Effect of the quantity of anti-*E. coli* antibody (0, 124 and 375 $\mu\text{g/mL}$) on the sensitivity of the passivated anti-*E. coli* antibody surface for *E. coli* detection: (left) *E. coli* cells number obtained by image analysis (0.25 mm^2) after washing and (right) corresponding bright filed microscopy images.

Thus the antibody surface display outstanding recognition property after facile and effective SPAAC click chemistry. In subsequent experiments, we utilized the anti-*E. coli* antibody solutions at 375 $\mu\text{g/mL}$ for surface functionalization.

4.8 Specificity evaluation

In order to determine the selective targeting capability of anti-*E. coli* antibody surface toward *E. coli* (gram-negative type), we conducted a control experiment by injecting a gram-positive bacteria (*B. subtilis* NCIB 3610) onto the surface and then compared the number of attached cells. The specificity was defined as the value of the ratio of the number of bacteria cells on the anti-*E. coli* antibody surface after and before washing divided by the ratio on the surface without antibody, this also can be expressed by the below formula:

$$\text{Specificity} = \frac{\left(\# \text{bacteria} \left(\frac{\text{after}}{\text{before}} \right) \text{washing} \right)_{\text{on antibody surface}}}{\left(\# \text{bacteria} \left(\frac{\text{after}}{\text{before}} \right) \text{washing} \right)_{\text{without antibody surface}}} \quad (\text{eq. 4.2})$$

After the washing step at 100 $\mu\text{L/min}$, only *E. coli* remained on the anti-*E. coli* antibody surface (375 $\mu\text{g/mL}$) with a significant number of cells observed. According to the formula, the specificity of anti-*E. coli* antibody surface for *E. coli* is 14 times higher than for *B. subtilis* (Figure 4.8) which demonstrates that the anti-*E. coli* antibody surface can differentiate efficiently the targeted bacteria from a different type.

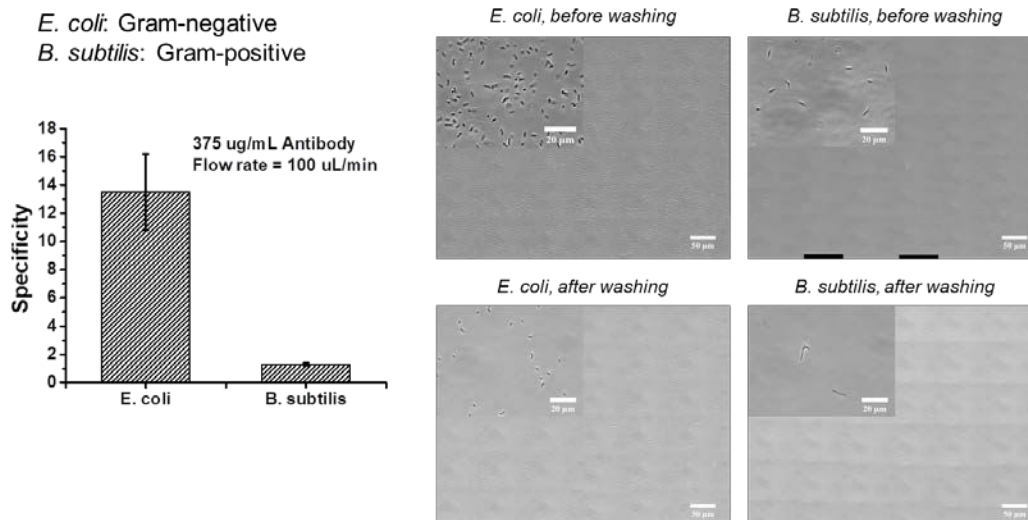


Figure 4.8. Specificity of anti-*E. coli* antibody surface (375 $\mu\text{g/mL}$) for *E. coli* and *B. subtilis* detection (left). Microscope images of the bacteria binding on the surface (0.25 mm^2) after and before washing step at 100 $\mu\text{L/min}$ (right).

Our antibody surface is a novel approach that has a great potential for bacteria detection in real samples. It is also possible to envision constructing selective surfaces for bioassays by introducing other targeting agents.

4.9 Conclusion

We developed a new, simple and convenient layer-by-layer functional surface *via* immunoassay between antibody and antigen for rapid, effective and specific detection of bacteria (*E. coli*). The polyanion and polycation with DIBO functional group were straightforward to synthesize and simply assembled on activated glass slides using electrostatic attraction. Then anti-*E. coli* antibody azide was efficiently introduced on the surface in a single step using strain-promoted azide-alkyne cycloaddition (SPAAC) reaction. In addition, unlike traditional antibody-based targeting methods that are temperature sensitive and undergo irreversible antibody denaturation, the “click”-based LbL surface offers a novel approach to construct convenient, effective, specific, and stable platforms for bioassays, holding great potential for pathogenic bacteria detection in food and water samples.

Materials and methods

Materials

Phenylacetaldehyde (Sigma), Trimethylsilyl iodide (97%, Sigma), n-butyllithium solution (1.6 M in hexanes, Sigma), Bromine (99.6%, Acros), N,N'-Dicyclohexylcarbodiimide (99%, Sigma, DCC), 4-(Dimethylamino)pyridine (99%, Sigma, DMAP), Poly(ethylene glycol) methyl ether acrylate (Sigma-Aldrich, $M_n = 454 \text{ g mol}^{-1}$, APEG), 2-methyl-2-[(dodecylsulfanylthiocarbonyl)sulfanyl] propanoic acid (97%, Strem, TTCA), acrylic acid (99%, Aldrich, AA), 2-(Dimethylamino)ethyl acrylate (98%, Sigma, DMEA), 4,4'-Azobis(4-cyanopentanoic acid) (98%, Sigma, ACPA) were used as received without further purification. Solvents were of synthetic grade and purified according to standard procedures. 18 M Ω Millipore water was used throughout and further pH-adjusted with either HCl or NaOH.

Characterization

All nuclear magnetic resonance (NMR) spectra were recorded in CDCl₃ on a JEOL ECS (400 MHz) spectrometer. All chemical shifts are in ppm and referenced to tetramethylsilane (TMS).

Zeta potentials (ζ) were performed on a Zetasizer Nanoseries (Malvern) apparatus. Samples were prepared at a concentration of 3.1×10^{-6} M in pure distilled water. Samples were analyzed in DTS 1060 plastic cells, at 25 °C. Three measurements of at least ten scans were performed for each sample.

pH measurements were performed using a glass electrode connected to PHM210 Standard pH meter from Mettler Toledo.

Contact angle measurements were performed on an advanced surface technology (AST) video contact angle measuring device. A 1 μ L droplet of deionized water was deposited on the samples.

Microscope images were taken on an epifluorescence microscopy (Nikon inverted microscope ECLIPSE TI-E) equipped with a syringe pump. Transmission images were captured with an emCCD camera. Objectives 60 \times (CFI S Plan Fluor ELWD, NA 0.7) was used in this work.

Synthesis

Synthetic scheme employed for the clickable RAFT agent (DIBO-TTCA) is shown in Scheme 1 and the RAFT polymerization of P(APEG-co-AA) (DIBO-PC⁻) and P(APEG-co-DMEA) (PC⁺) is shown in Scheme 2.

Synthesis of 2,3: 6,7-Dibenzo-9-oxabicyclo[3.3.1]nona-2,6-diene (2) [39]. In round flask was added phenylacetaldehyde (6.25 g, 52.0 mmol) dissolved in 26 mL chloroform (anhydrous). The flask was kept under argon atmosphere and cooled in an ice bath. Trimethylsilyl iodide (8.75 mL,

12.3 g, 61.5 mmol) was added to this solution and the reaction was vigorously stirred at 4 °C for 1 week. After warming the reaction to room temperature, the reaction was quenched with 1 M sodium thiosulfate in water (50 mL) and diluted with dichloromethane (50 mL); the two-phase mixture was stirred until the iodine color disappeared. The organic phase was separated and dried over anhydrous Na₂SO₄ and the solvent was evaporated *in vacuo*. The crude product was purified by silica gel column chromatography eluting with chloroform to afford the white crystalline ether (2.387 g, 41%).

¹H NMR (400 MHz, CDCl₃): δ(ppm) = 2.75 (d, *J* = 16.0 Hz, 2H, CH₂), 3.56 (dd, *J* = 16.5 Hz, 2H, CH₂), 5.30 (d, *J* = 6.0 Hz, 2H, CH), 7.09 (m, 8H); ¹³C NMR (100 MHz, CDCl₃): δ(ppm) = 36.24, 69.68, 125.29, 126.10, 127.00, 129.22, 131.73, 137.90.

Synthesis of 5-Hydroxy-1,2:5,6-dibenzocycloocta-1,5,7-triene (3) [39]. The reaction was kept under argon atmosphere. To a solution of the ether (1) (1.28 g, 5.8 mmol) in anhydrous THF (40 mL), was added dropwise a solution of *n*-butyllithium 1.6 M in *n*-hexane (7.21 mL, 11.5 mmol). The reaction was stirred at room temperature for 4 h. Subsequently, the mixture was quenched by slowly addition of water and then extracted with chloroform (2×30 mL). The combined organic layers were washed with brine (30 mL), dried over anhydrous Na₂SO₄, and the solvent was evaporated to give the crude product. The compound was purified by silica gel column chromatography, eluting first with chloroform, to remove impurities and later with ethyl acetate to afford the pure alcohol (0.96 g, 75%).

¹H NMR (400 MHz, CDCl₃): δ(ppm) = 3.35 (m, 2H, CH₂), 5.29 (q, *J* = 6.1 Hz, 1H, CHOH), 6.86 (q, *J* = 2.7 Hz, 2H, CH), 7.10-7.26 (m, 7H), 7.47 (m, 1H); ¹³C NMR (100 MHz, CDCl₃): δ(ppm) = 42.7, 74.7, 125.9, 126.1, 127.2, 127.3, 128.8, 129.3, 129.9, 130.3, 131.7, 131.8, 134.6, 136.3, 136.9, 140.9.

Synthesis of 4-dibenzocyclooctynol (DIBO) (4) [39]. Dibenzocyclooctene (2) (0.30 g, 1.3 mmol) was dissolved in 7 mL anhydrous dichloromethane at 0 °C. After a few minutes stirring, the bromine (0.07 mL, 1.4 mmol) was added dropwise. The reaction mixture was stirred for 1.5 h at 0 °C. And then the reaction was stopped with the addition of a sodium thiosulfate saturated aqueous solution. The aqueous phase was extracted twice with dichloromethane. The combined organic phases were washed twice with brine, and then dried over MgSO₄. The crude product was directly used in the subsequent step without purification.

Diisopropylamine (0.75 mL, 5.3 mmol) was placed under an argon atmosphere with 8 mL anhydrous THF at 0 °C. The *n*-butyllithium (1.6 M in THF) (3.3 mL, 5.3 mmol) was added dropwise to form lithium diisopropylamide (LDA). The mixture was stirred for 30 min at 0 °C. The dibrominated compound (1.3 mmol) was dissolved in 8 mL anhydrous THF, subsequently was added to the LDA. The reaction mixture was stirred for 1.5 h. The reaction was stopped with the addition of ammonium chloride saturated aqueous solution. The aqueous phase was extracted twice with ethyl acetate. The combined organic phases were dried over MgSO₄. The crude

product was purified by column chromatography on pre-packed silica (gradient: petroleum ether to petroleum ether/AcOEt (9:1, v/v) over 30 min) to obtain the white solid compound (82 mg, 33.5%).

^1H NMR (400 MHz, CDCl_3): $\delta(\text{ppm}) = 2.95$ (dd, $J = 11.2, 3.6$ Hz, 1H, CHH), 3.12 (dd, $J = 12.4, 2.3$ Hz, 1H, CHH), 4.66 (dd, $J = 3.7, 2.1$ Hz, 1H, CHOH), 7.50-7.25 (m, 8H, CH_{ar}), 7.76 (d, $J = 7.8$ Hz, 1H, CH_{ar}); ^{13}C NMR (100 MHz, CDCl_3): $\delta(\text{ppm}) = 48.8, 75.4, 110.8, 113.0, 121.4, 123.9, 124.3, 124.7, 126.2, 126.8, 126.9, 127.9, 128.2, 129.8, 151.7, 155.7$.

Synthesis of P(APEG-co-AA) clickable RAFT agent (DIBO-TTCA) [40]. A solution of DCC (153 mg, 0.74 mmol) in CH_2Cl_2 (2.7 mL) was added drop wise to a stirred solution of 2-(dodecylthiocarbonothioylthio)-2-methylpropionic acid (272 mg, 0.74 mmol), 4-dibenzocyclooctynol (82 mg, 0.37 mmol), and DMAP (11 mg, 0.09 mmol) in CH_2Cl_2 (2.7 mL) and the resulting mixture was stirred for 18 h at room temperature. Upon the completion of the reaction, the mixture was filtered to remove dicyclohexylurea and the filtrate was concentrated under reduced pressure. The resulting residue was purified by column chromatography on silica gel using a gradient of 0 to 20% EtOAc in petroleum ether as an eluent to give pure DIBO-TTCA (132 mg, 71%) as a yellow oil.

^1H NMR (400 MHz, CDCl_3): $\delta(\text{ppm}) = 0.88$ (t, $J = 7.0$ Hz, 3H, CH_3CH_2), 1.24-1.28 (m, 18H, $\text{CH}_3(\text{CH}_2)_9$), 1.61-1.63 (m, 2H, $\text{CH}_2\text{CH}_2\text{S}$), 1.79 (s, 3H, CH_3C), 1.83 (s, 3H, CH_3C), 2.89 (dd, $J = 15.1, 4.0$ Hz, 1H, CHHCHO), 3.15 (dd, $J = 15.1, 2.0$ Hz, 1H, CHHCHO), 3.26 (app dt, $J = 7.3, 4.2$ Hz, 2H, CH_2S), 5.49 (br s, 1H, CH_2CHO), 7.25-7.33 (m, 7H, $7\times\text{CH}_{\text{ar}}$), 7.60 (d, $J = 8.0$ Hz, 1H, CH_{ar}); ^{13}C NMR (100 MHz, CDCl_3): $\delta(\text{ppm}) = 14.3$ (CH_2CH_3), 22.8 (CH_2CH_3), 25.5 (CH_3), 25.9 (CH_3), 28.0 ($\text{CH}_2\text{CH}_2\text{S}$), 29.1 (CH_2), 29.2 (CH_2), 29.5 (CH_2), 29.6 (CH_2), 29.7 (CH_2), 29.8 ($2\times\text{CH}_2$), 32.0 (CH_2), 37.1 (CH_2S), 46.1 (CH_2CHO), 56.1 ($\text{C}(\text{CH}_3)_2$), 77.9 (OCHCH_2), 109.5 ($\text{C}\equiv\text{C}$), 113.1 ($\text{C}\equiv\text{C}$), 121.3 (C_{ar}), 123.6 (CH_{ar}), 124.3 (C_{ar}), 125.9 (CH_{ar}), 126.3 (C_{ar}), 127.2 (CH_{ar}), 127.3 (CH_{ar}), 128.0 (CH_{ar}), 128.3 (CH_{ar}), 130.4 (CH_{ar}), 151.1 ($2\times\text{C}_{\text{ar}}$), 171.7 ($\text{C}=\text{O}$), 220.9 ($\text{SC}=\text{S}$).

Synthesis of P(APEG-co-AA) (DIBO-PC $^\bullet$). DIBO modified negative polymer chain P(APEG₁₄-co-AA₁₄) was synthesized in 1,4-dioxane at 80 °C under argon atmosphere. APEG (1.46 g, 3.33 mmol), AA (0.24 g, 3.33 mmol), DIBO-TTCA clickable RAFT agent (0.132 g, 0.233 mmol), DMF (0.135 g, 1.85 mmol) and ACPA (5.2 mg, 0.018 mmol) were dissolved in 3.5 mL of 1,4-dioxane at room temperature. The mixture solution was then purged with argon for 30 min in an ice bath. It was then immersed into an oil bath at 80 °C to start the polymerization. Samples were periodically withdrawn from the polymerization medium for analyses. To study the kinetics, monomer conversion was determined by ^1H NMR spectroscopy. DMF, which has no influence on the free radical process, was used as internal reference. After 20 h, the flask was quenched in ice bath to terminate the polymerization. After removing all the solvents under reduced pressure, the residues were dissolved in THF and then precipitated into an excess of

ethyl ether. This purification cycle was repeated twice. And the product was purified by tangential flow filtration. The final polymer was obtained as a yellow viscous solid.

Synthesis of P(APEG-co-DMEA) (PC⁺). Positive polymer chain P(APEG₁₂-co-DMEA₁₂) was synthesized in 1,4-dioxane at 80 °C under argon atmosphere. APEG (0.57 g, 1.23 mmol), DMEA (0.18 g, 1.23 mmol), TTCA RAFT agent (0.038 g, 0.105 mmol), DMF (0.037 g, 0.50 mmol) and ACPA (2.0 mg, 0.007 mmol) were dissolved in 2.5 mL of 1,4-dioxane at room temperature. The mixture solution was then purged with argon for 30 min in an ice bath. It was then immersed into an oil bath at 80 °C to start the polymerization. Samples were periodically withdrawn from the polymerization medium for analyses. To study the kinetics, monomer conversion was determined by ¹H NMR spectroscopy. DMF, which has no influence on the free radical process, was used as internal reference. After 4 h, the flask was quenched in ice bath to terminate the polymerization. After removing all the solvents under reduced pressure, the residues were dissolved in THF and then precipitated into an excess of ethyl ether. This purification cycle was repeated twice. The final polymer was obtained as a yellow viscous solid.

Preparation of PC⁺/DIBO-PC⁻ LbL film

Activated glass slides: The glass slides were immersed in piranha solution (H₂O₂/H₂SO₄=1:3 v/v) for 30 min, washed three times with deionized water, and then dried under a gentle stream of nitrogen gas. (*CAUTION: “Piranha” solution reacts violently with organic materials; it must be handled with extreme care.*)

Film preparation: The activated glass slides were alternatively immersed in charged PC⁺ solution (30 mL, 8.2×10⁻⁵ mol/L, [NaCl] = 0.005 M, pH = 5.43) and DIBO-PC⁻ solution (30 mL, 5.1×10⁻⁴ mol/L, [NaCl] = 0.005 M, pH = 5.28) for 20 min. The final layer was DIBO-PC⁻.

Preparation of anti-*E. coli* antibody surface

Commercial microfluidic devices: The commercial sticky-slide VI^{0.4} allows to perform biological experiments with the DIBO-PC⁻ film which was deposited on the glass slides. The self-adhesive (“sticky”) underside of the bottomless blank slide is easily adapted to the specific substrate by pressing on by hand. The sticky-slide VI^{0.4} can also be connected to a pump and enables the experiment to observe under flow conditions.

Azido anti-*E. coli* antibody: anti-*E. coli* antibody (IgG) was functionalized by azide according to standard protocol recommended by supplier of commercially available SiteClickTM Antibody Labeling Kit (Thermofisher, USA) to prepare azide attachment to the antibody [36].

Anti-*E. coli* antibody surface: Varying concentration of azido anti-*E. coli* antibody (60 μL, 0 - 375 μg/mL in 1×Tris) were incubated on the DIBO-PC⁻ surface at room temperature for

overnight, and then rinsed with PBS twice to remove the unreacted antibodies.

Surface passivation: The passivation of the anti-*E. coli* antibody surface was performed using a solution of 20 mg/mL bovine serum albumin (BSA) in water for 2 hours at 37 °C, and then rinsed with PBS twice [41].

Bacteria culture

All bacteria strains used in this research were *Escherichia coli* (K-12, BW25113) and *Bacillus subtilis* (NCIB 3610). *E. coli* was selected as target bacteria; meanwhile *B. subtilis* was selected as control group for selective bacteria detection. All above strains were firstly streaked onto Luria-Bertani (LB) agar plates, and then incubated at 37 °C for overnight. An isolated colony of each strain was picked and inoculated in 5 mL of LB medium. After incubation at 37 °C for overnight (shaking at 350 rpm and 5% CO₂), the bacteria culture was then diluted 1:100 in the M9 minimal growth medium. After incubation at 37 °C for 2 hours, the bacteria suspensions were carried out during all experiments.

Bacteria capture on anti-*E. coli* antibody surface

Bacteria capture: 60 µL bacteria suspensions ($1.1 - 5.5 \times 10^7$ cells/mL) were introduced into each channel, allowed to incubate for 1 hour at room temperature to settle onto the surface, and then washing step was performed with PBS buffer solution.

Fluidic conditions: The flow rate during the washing step was controlled by a syringe pump. Each commercial sticky-slide VI^{0.4} channel is depth $h=400$ µm, length $L=17$ mm and width $w=3.8$ mm. Using the syringe pump in infusion mode, the volumetric flow rates were between 100 and 400 µL/min for 10 min. It should be noted that fluidic force was likely completed in the first 30 seconds to 1 minute, but additional washing was required to clear out all residual non-specifically bound bacteria. Following each washing step, the images were recorded from all sensing regions [42].

Image analysis: A series of images from different sensing regions were analyzed using NIH (National Institutes of Health) recommended image processing software, Image J. The number of bacteria cells is determined by setting a binary threshold to delineate the cells.

References

- [1] Mark X. Sliwkowski and Ira Mellman. Antibody therapeutics in cancer. *Science*, 2013, **341**, 1192-1198.
- [2] Ravi V. J. Chari. Targeted Cancer Therapy: Conferring Specificity to Cytotoxic Drugs. *Acc. Chem. Res.*, 2008, **41(1)**, 98-107.
- [3] George J. Weiner. Building better monoclonal antibody-based therapeutics. *Nat. Rev. Cancer*, 2015, **15**, 361-370.
- [4] Ryou Kubota and Itaru Hamachi. Protein recognition using synthetic small-molecular binders optical protein sensing *in vitro* and in live cells. *Chem. Soc. Rev.*, 2015, **44**, 4454-4471.
- [5] Guntur Fibriansah, Joanne L. Tan, Scott A. Smith, Ruklanthi de Alwis and Shee-Mei Lok, *et al.* A highly potent human antibody neutralizes dengue virus serotype 3 by binding across three surface proteins. *Nat. Commun.*, 2015, **6**: **6341**, doi: 10.1038/ncomms7341.
- [6] Xue-Hui Dong, Allie C. Obermeyer and Bradley D. Olsen. Three-Dimensional Ordered Antibody Arrays Through Self-Assembly of Antibody-Polymer Conjugates. *Angew. Chem. Int. Ed.*, 2017, **56**, 1273-1277.
- [7] Hongfei Gao, Shijia Yang, Jing Han, Jie Xiong and Zhifeng Fu, *et al.* Double-site recognition of pathogenic bacterial whole cells based on an antibiotic-affinity strategy. *Chem. Commun.*, 2015, **51**, 12497-12500.
- [8] Sue Binder, Alexandra M. Levitt, Jeffrey J. Sacks and James M. Hughes. Emerging infectious Diseases: Public Health Issues for the 21 st Century. *Science*, 1999, **284**, 1311-1313.
- [9] Carl A. Batt. Food Pathogen Detection. *Science*, 2007, **316**, 1579-1580.
- [10] Wen Ju, Xiuling Song, Gang Yan, Kun Xu and Juan Li, *et al.* Layer-by-layer assembly of polyoxometalate-pyrene-decorated fluorescent microspheres for the suspension immunoassay of *Listeria monocytogenes*. *J. Mater. Chem. B.*, 2016, **4**, 4287-4294.
- [11] Shana O. Kelley, Chad A. Mirkin, David R. Walt, Rustem F. Ismagilov and Edward H. Sargent, *et al.* Advancing the speed, sensitivity and accuracy of biomolecular detection using multi-length-scale engineering. *Nature Nanotechnology*, 2014, **9**, 969-980.
- [12] Wonjae Lee, Donghoon Kwon, Woong Choi, Gyoo Yeol Jung and Sangmin Jeon, *et al.* 3D-Printed Microfluidic Device for the Detection of Pathogenic Bacteria Using Size-based Separation in Helical Channel with Trapezoid Cross-Section. *Scientific Reports*, 2015, **5**, 7717; DOI: 10.1038/srep07717.
- [13] Sandeep Kumar Vashist, Edmond Lam, Sabahudin Hrapovic, Keith B. Male and John H. T. Luong. Immobilization of Antibodies and Enzymes on 3-Aminopropyltriethoxysilane-Functionalized Bioanalytical Platforms for Biosensors and Diagnostics. *Chem. Rev.*, 2014,

114(21), 11083-11130.

[14] Kara Yamada, Won Choi, Inae Lee, Byoung-Kwan Cho and Soojin Jun. Rapid detection of multiple foodborne pathogens using a nanoparticle-functionalized multi-junction biosensor. *Biosensors and Bioelectronics*, 2016, **77**, 137-143.

[15] Wenli Zhang, Kush Patel, Andrew Schexnider, Shirin Banu and Adarsh D. Radadia. Nanostructuring of Biosensing Electrodes with Nanodiamonds for Antibody Immobilization. *ACS Nano*, 2014, **8(2)**, 1419-1428.

[16] Weixian Xi, Timothy F. Scott, Christopher J. Kloxin and Christopher N. Bowman. Click chemistry in Materials Science. *Adv. Funct. Mater.*, 2014, **24**, 2572-2590.

[17] Hartmuth C. Kolb, M. G. Finn, and K. Barry Sharpless. Click chemistry: Diverse Chemical Function from a Few Good Reactions. *Angew. Chem. Int. Ed.*, 2001, **40**, 2004-2021.

[18] Karen Alt, Brett M. Paterson, Erik Westein, Stacey E. Rudd and Christoph E. Hagemeyer, *et al.* A Versatile Approach for the Site-Specific Modification of Recombinant Antibodies Using a Combination of Enzyme-Mediated Bioconjugation and Click chemistry. *Angew. Chem. Int. Ed.*, 2015, **54**, 7515-7519.

[19] Ivana Nikic, Jun Hee Kang, Gemma Estrada Girona, Iker Valle Aramburu and Edward A Lemke. Labeling proteins on live mammalian cells using click chemistry. *Nature Protocols*, 2015, **10**, 780-791.

[20] Afaf H. El-Sagheer and Tom Brown. Click chemistry with DNA. *Chem. Soc. Rev.*, 2010, **39**, 1388-1405.

[21] Chuan Zhang, Liangliang Hao, Colin M. Calabrese, Yu Zhou and Chad A. Mirkin, *et al.* Biodegradable DNA-Brush Block Copolymer Spherical Nucleic Acids Enable Transfection Agent-Free Intracellular Gene Regulation. *Small*, 2015, **11 (40)**, 5360-5368.

[22] Wen Tang and Matthew L. Becker. "Click" reactions: a versatile toolbox for the synthesis of peptide-conjugates. *Chem. Soc. Rev.*, 2014, **43**, 7013-7039.

[23] Yan Pang, Jinyao Liu, Yizhi Qi, Xinghai Li and Ashutosh Chilkoti. A Modular Method for the High-Yield Synthesis of Site-Specific Protein- Polymer Therapeutics. *Angew. Chem. Int. Ed.*, 2016, **55**, 10296-10300.

[24] K. Jono, M. Nagao, T. Oh, S. Sonoda, Y. Hoshino and Y. Miura. Controlling the lectin recognition of glycopolymers via distance arrangement of sugar blocks. *Chem. Commun.*, 2018, **54**, 82-85.

[25] Isidro Cobo, Ming Li, Brent S. Sumerlin and Sebastien Perrier. Smart Hybrid materials by conjugation of responsive polymers to biomacromolecules. *Nature Materials*, 2015, **14**, 143-159.

[26] Yan Lyu, Xu Zhen, Yansong Miao and Kanyi Pu. Reaction-Based Semiconducting Polymer

Nanoprobes for Photoacoustic Imaging of Protein Sulfenic Acids. *ACS Nano*, 2017, **11**(1), 358-367.

[27] C. A. Hommersom, B. Matt, A. van der ham, J. J. L. M. Cornelissen and N. Katsonis. Versatile post-functionalization of the external shell of cowpea chlorotic mottle virus by using click chemistry. *Org. Biomol. Chem.*, 2014, **12**, 4065-4069.

[28] Jia Niu, David J. Lunn, Anusha Pusuluri, Justin I. Yoo and Craig J. Hawker, *et al.* Engineering live cell surfaces with functional polymers via cytocompatible controlled radical polymerization. *Nature Chemistry*, 2017, **9**, 537-545.

[29] Nicholas J. Agard, Jennifer A. Prescher and Carolyn R. Bertozzi. A Strain-Promoted [3+2] Azide-Alkyne Cycloaddition for Covalent Modification of Biomolecules in Living Systems. *J. Am. Chem. Soc.*, 2004, **126**(46), 15046-15047.

[30] Xi Qiu Liu and Catherine Picart. Layer-by-Layer Assemblies for Cancer Treatment and Diagnosis. *Adv. Mater.*, 2016, **28**, 1295-1301.

[30] Maren E. Buck, Jingtao Zhang and David M. Lynn. Layer-by-Layer Assembly of Reactive Ultrathin Films Mediated by Click-Type Reactions of Poly(2-Alkenyl Azlactone)s. *Adv. Mater.*, 2007, **19**, 3951-3955.

[31] Rajesh Ranjan and William J. Brittain. Combination of Living Radical Polymerization and Click Chemistry for Surface Modification. *Macromolecules*, 2007, **40**, 6217-6223.

[32] Rajesh Ranjan and William J. Brittain. Synthesis of High Density Polymer Brushes on Nanoparticles by Combined RAFT Polymerization and Click Chemistry. *Macromol. Rapid Commun.*, 2008, **29**, 1104-1110.

[33] Hakan Durmaz, Amitav Sanyal, Gurkan Hizal and Umit Tunca. Double click reaction strategies for polymer conjugation and post-functionalization of polymers. *Polym. Chem.*, 2012, **3**, 825-835.

[34] X. Ning, J. Guo, M. Wolfert and G. Boons. Visualizing metabolically labeled glycoconjugates of living cells by copper-free and fast huisgen cycloadditions. *Angew. Chem. Int. Ed.*, 2008, **47**, 2253-2255.

[35] G. Decher and J. Schmitt. Fine-tuning of the film thickness of ultrathin multilayer films composed of consecutively alternating layers of anionic and cationic polyelectrolytes. *Prog. Colloid Polym. Sci.*, 1992, **89**, 160-164.

[36] <https://tools.thermofisher.com/content/sfs/manuals/mp10469.pdf>.

[37] G. U. Lee, L. A. Chrisey and R. J. Colton. Direct measurement of the forces between complementary strands of DNA. *Science*, 1999, **283**, 1727-1730.

[38] S. W. Metzger, M. Natesan, C. Yanavich, J. Schneider and G. U. Lee. Development and

characterization of surface chemistries for microfabricated biosensors. *J. Vac. Sci. Technol. A*, 1999, **17**, 2623-2628.

[39] Jukuan Zheng, Kaiyi Liu, Darrell H. Reneker, and Matthew L. Becker. Post-assembly derivatization of electrospun nanofibers via strain-promoted azide alkyne cycloaddition. *J. Am. Chem. Soc.* 2012, **134**, 17274-17277.

[40] Petr A. Ledin, Nagesh Kolishetti, Manish S. Hudlikar, and Geert-Jan Boons. Exploring strain-promoted 1,3-dipolar cycloadditions of end functionalized polymers. *Chem. Eur. J.* 2014, **20**, 8753-8760.

[41] J. Sheats, B. Sclavi, M. C. Lagomarsino, P. Cicuta and K. D. Dorfman. Role of growth rate on the orientational alignment of *Escherichia coli* in a slit. *R. Soc. Open sci.* **4**: 170463.

[42] B. Raja, C. Pascente, J. Knoop, D. Shakarisaz, T. Sherlock, S. Kemper, K. Kourentzi, R. F. Renzi, A. V. Hatch, J. Olano, B. H. Peng, P. Ruchhoeft and R. Willson. An embedded microretroreflector-based microfluidic immunoassay platform. *Lab Chip*, 2016, **16**, 1625-1635.

Chapter 5

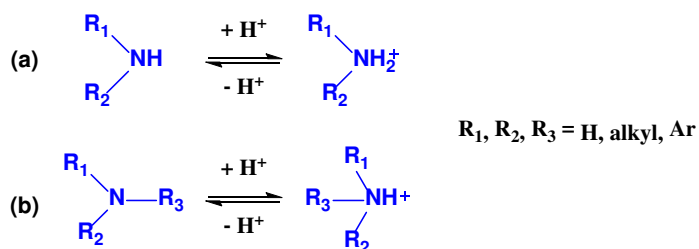
**pH sensitive Layer-by-Layer film surface
for bacteria growth detection**

Chapter 5 pH sensitive Layer-by-Layer film surface for bacteria growth detection

In the previous chapters we provided a new approach for bacteria detection on thin film. However, rapid, accurate and simple detection of bacterial growth still remains a challenge. It is a key step for further real sample analysis in the antimicrobial resistance study.

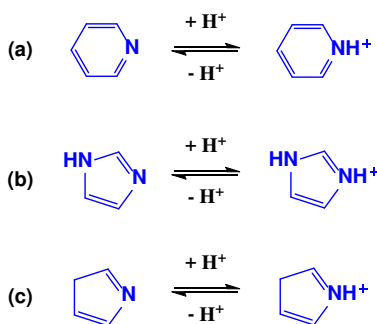
The growth of bacteria is often associated with a pH decrease of the growth medium due to a release of acidic metabolites such as acetic acid, lactic acid and CO_2 [1]. Consequently, developing an accurate, rapid and stable pH sensitive LbL surface is a reasonable and practical goal for the detection of bacterial growth. Over the past decades, different fluorophores (fluorescein-based pH indicators, benzoxanthene dyes and cyanine-based pH indicators) have been widely used in fluorescence-based pH sensing since the fluorescence properties were modified with a change of concentration of the hydrogen ions (pH). Yoon [2] described the different principles for the hydrogen ion detection with fluorescent probes.

(1) pH probes based on reversible protonation of amines. Alkyl and aromatic amines participate in rapid acid-base equilibrium reactions (Scheme 5.1). As a result, amine moieties have been widely employed as sites for acid-base reactions of the fluorescent pH probes [3, 4].



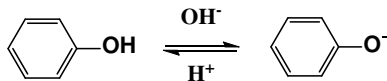
Scheme 5.1. Reversible protonation of alkyl amines and aromatic amines.

(2) pH probes based on protonation of N-heterocycles. N-heterocycles, such as pyrrole, indole, imidazole, pyridine or quinolone, have been applied to construct pH probes due to the generation of the corresponding cations by reversible protonation under acidic conditions (Scheme 5.2) [5, 6].



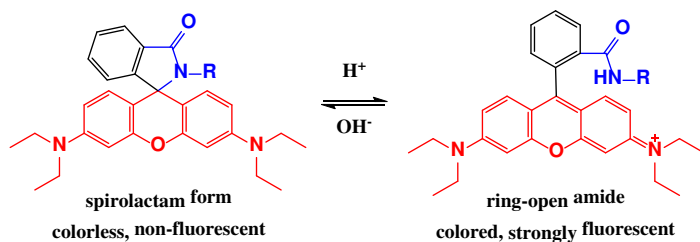
Scheme 5.2. Protonation of N-heterocycles.

(3) pH probes based on phenols. An aqueous solution of phenol is weakly acidic and it can be deprotonated in basic (high pH) environments to form the phenolate ion (Scheme 5.3). Because of this character, the phenol moiety has been used as a basis for development of pH probes [7, 8].



Scheme 5.3. Deprotonation of phenol.

(4) pH probes based on ring-opening of rhodamine. Commonly, the rhodamine spirolactam form is colorless and non-fluorescent in many solvents, whereas it opens in the presence of acid to give the ring-opened amide form which is strongly fluorescent (Scheme 5.4). Therefore, rhodamine derivatives are often used as pH fluorescent probes [9, 10].



Scheme 5.4. pH probe based on ring-opening of rhodamine.

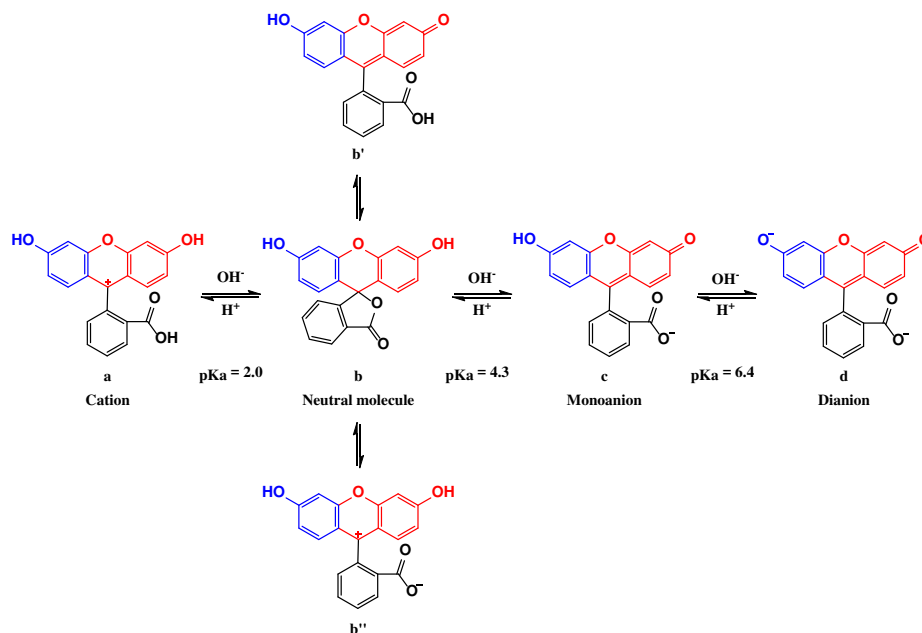
Other types of pH probes have been designed on the basis of chemical reactions such as addition or isomerization processes [11, 12]. In different applications, pK_a value is crucial for the pH indicators and it should be located at the center of the measurable pH range. pH of the growth medium can be changed from 7 to 5 during *E. coli* growth. Carboxyfluorescein is a phenol based pH probe with different pK_a values depending on the form of carboxyfluorescein in solution.

Table 5.1. Photophysical properties of different forms of Carboxyfluorescein (from [13])

Species	λ_{abs} (nm)	λ_F (nm)	ϵ ($10^3 \cdot L \cdot mol^{-1} \cdot cm^{-1}$)	Φ_F	τ (ns)
F _{b'}	434	/	11	~ 0	/
F _c	472	520-540	29	0.37	3.0
F _d	490	520	77	0.93	4.1

Carboxyfluorescein in aqueous solution exist as a cation (a), a neutral quinonoid molecule (b'), a neutral lactonic molecule (b), a monoanion (c) or a dianion (d), depending on the pH (Scheme 5.5) [13, 14]. Its fluorescence property and pK_a are strongly pH dependent and only the dianionic form is highly fluorescent (Table 5.1). Furthermore, the pK_a of carboxyfluorescein

from monoanion form to dianion transformation is about 6.4, which is suitable for the detection of pH changes in bacterial growth.



Scheme 5.5. Different forms of Carboxyfluorescein depending upon pH and their pK_a .

pH sensor can be designed as single-signal detection, and ratiometric sensor is an alternative. Ratiometric detection is sensor concentration independent by introducing at least two emission or excitation wavelengths [15]. Ratiometric sensor consists of two dyes: one is pH sensitive and the other is insensitive or both of them are pH sensitive with opposite direction, which induce the ratio change in fluorescence wavelength or intensity. The intensity-based ratiometric sensor either enables or disables Fluorescence resonance energy transfer (FRET) leading to shift of emission intensities [16]. In addition, the measure of ratio between two fluorescence signals allows to get rid of artifacts due to instrument (changes in focus, variations in laser intensity), or bleaching.

Herein we present a rather simple and novel method to introduce carboxyfluorescein as a pH probe on the LbL film surface by copper-free click chemistry. Two single-signal pH sensitive surfaces containing fluorescein and one ratiometric pH sensitive surface combining fluorescein with insensitive BODIPY were designed and prepared with different features, the photophysical properties were studied and the bacterial growth detection were performed on each surface.

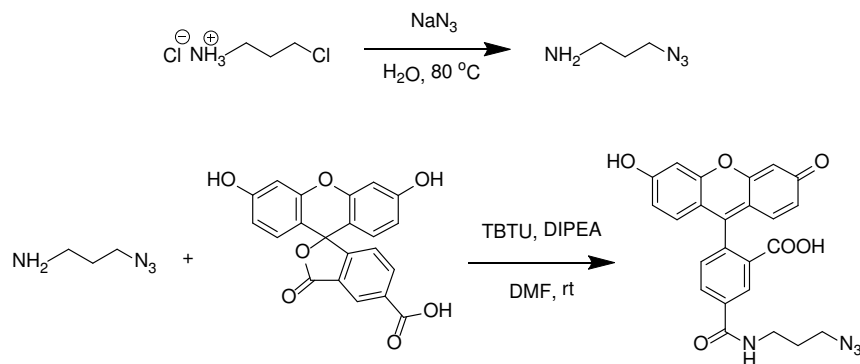
Firstly, I will introduce the synthesis and the characterizations of fluorescein azide (FA), relatively short and long polyanions with DIBO moiety (DIBO-SWPC⁻ and DIBO-LWPC⁻), red fluorescent polyanion (RFPC⁻) and positively charged polyelectrolyte (PC⁺). And then the preparations and characterizations of different types of pH sensitive surfaces (DIBO-SW PC⁻/FA,

DIBO-LW PC⁻/FA and (DIBO-LW PC⁻ + RFPC⁻)/FA surface) will be described. Finally, all pH sensitive surfaces were tested for *E. coli* growth detection.

5.1 Synthesis of fluorescein azide, polyanion and polycation

5.1.1 Synthesis of fluorescein azide (FA)

Fluorescein was selected as a pH-sensitive fluorophore for the bacteria growth detection because of its very high molar absorptivity at the wavelength of the argon laser (488 nm) and large fluorescence quantum yield [13]. In addition, fluorescein in aqueous solution appears in cationic, neutral, anionic and dianionic forms [14] making its absorption and fluorescence properties strongly pH dependent. Moreover the pK_a of the anion/dianion form is about 6.4, which is suitable to measure changes in pH in biological media as already stated earlier [1]. Preparation of fluorescein azide was performed thanks to a general procedure for the synthesis of amides *via* the direct condensation of carboxylic acids and amines using TBTU as coupling agent (Scheme 5.6) [17, 18].



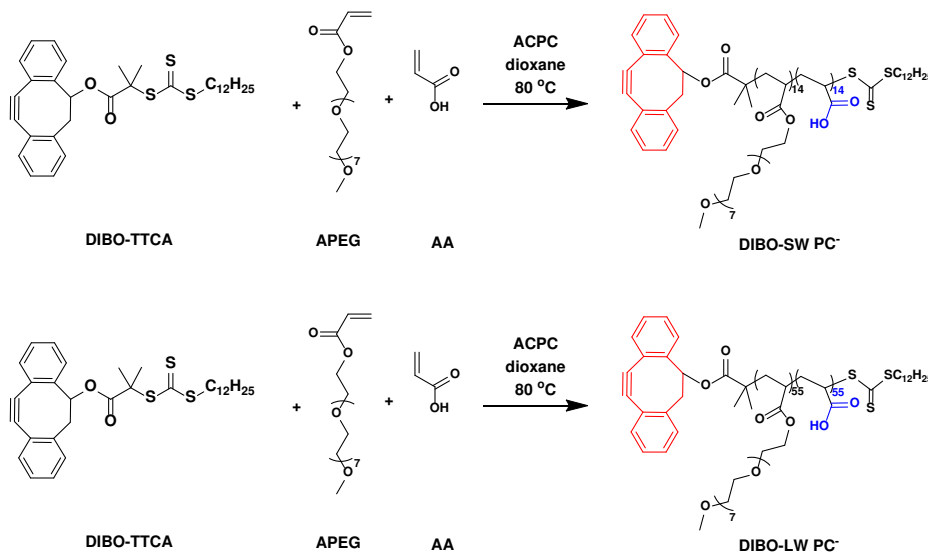
Scheme 5.6. Preparation of the fluorescein azide (FA-N₃).

5.1.2 Synthesis of polyanion

5.1.2.1 Synthesis of DIBO-SW PC⁻ and DIBO-LW PC⁻

The synthesis of DIBO functionalized RAFT agent TTCA-DIBO has been described in Chapter 4, we designed two polyanions with relatively high and low molecular weights for the further study. Different ratio of monomers and chain transfer agent DIBO-TTCA (APEG:AA:DIBO-TTCA = 14:14:1 or 55:55:1) were introduced into each polymerization reaction under standard conditions using 1,4-dioxane as the solvent and 4,4'-Azobis(4-cyanopentanoic acid) (ACPC) as the initiator at 80 °C (Scheme 5.7). The polymer with the ratio of APEG:AA:DIBO-TTCA (14:14:1) was labeled as DIBO-SWPC⁻, the other polyanion was called DIBO-LWPC⁻. After a reaction time of 66.5 hours or 88 hours, the polymerization of DIBO-SWPC⁻ and DIBO-LWPC⁻ reached 31% conversion and 72% conversion, respectively.

The end-functionalized DIBO-PC⁻ were isolated by multiple precipitations into cold diethyl ether and tangential flow filtration. ¹H NMR spectra of the resulting polymers showed successful introduction of a DIBO moiety due to the bands in the aromatic region (Figure 5.1). The number average molecular weight ($M_n(\text{NMR})$) was calculated based on NMR total monomer conversion. The estimated molecular weights of DIBO-SWPC⁻ and DIBO-LWPC⁻ are 2800 g/mol and 20600 g/mol, respectively.



Scheme 5.7. Synthetic scheme employed for the RAFT synthesis of P(APEG-co-AA) with different repeating units, relatively low molecular weight DIBO-SWPC⁻ and high molecular weight DIBO-LWPC⁻.

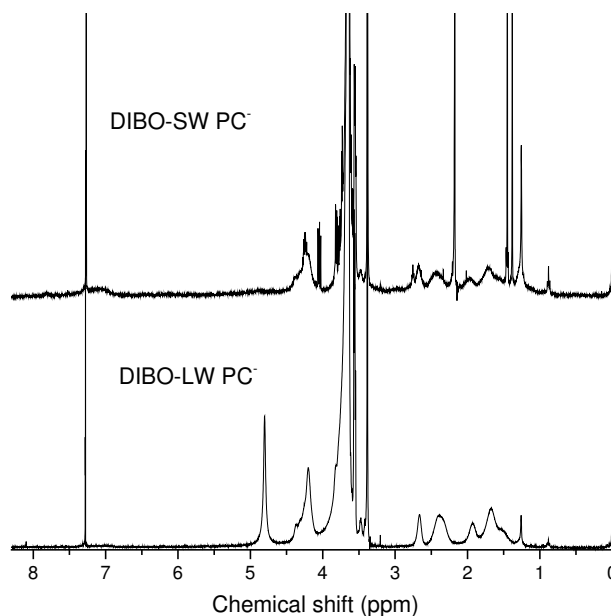
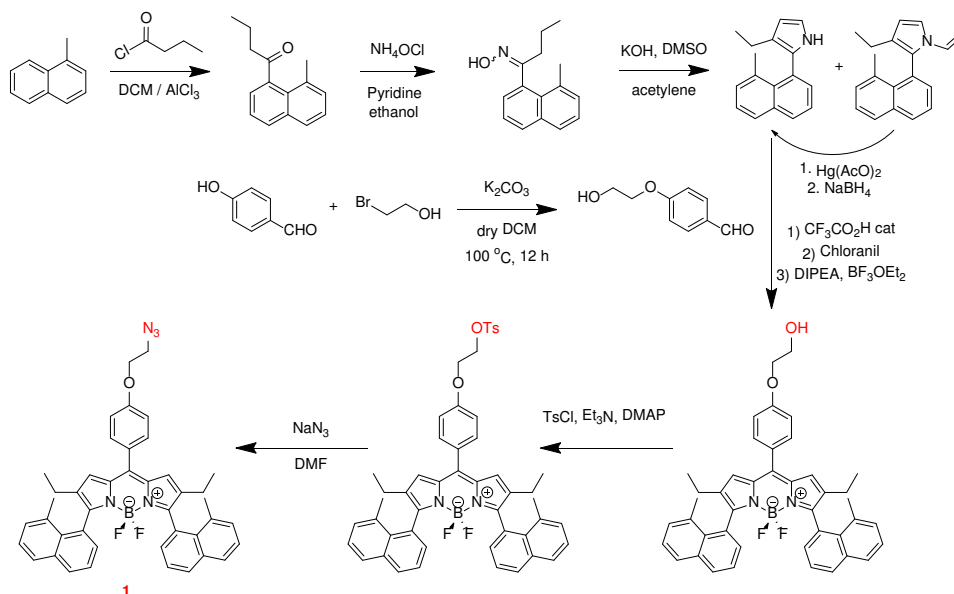


Figure 5.1. ¹H NMR spectra of DIBO-SWPC⁻ and DIBO-LWPC⁻.

5.1.2.2 Synthesis of red fluorescent polymer (RFPC)

Boron-dipyrromethene (BODIPY) derivatives are interesting because of their very good spectroscopic properties, as described in previous chapters. They are also relatively insensitive to the polarity and pH of the environment. Moreover small modifications of their structures enable tuning of their fluorescence features (emission spectrum tunable from green to red) [19, 20]. Therefore, BODIPY was selected as a reference fluorophore in the ratiometric sensor.

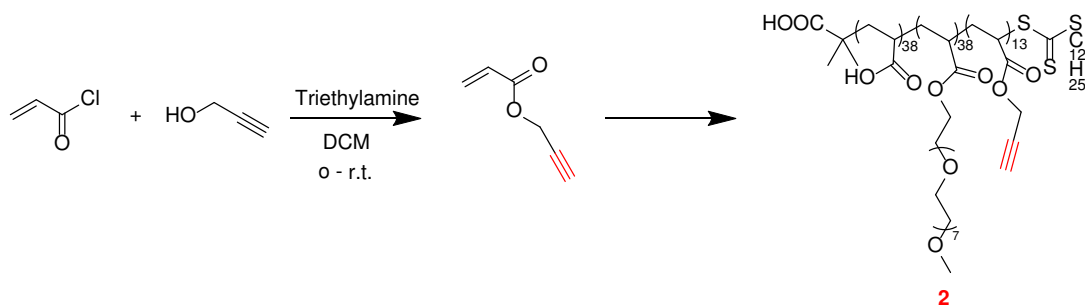


Scheme 5.8. Synthesis of methylnaphthyl BODIPY monomer (BODIPY- N_3).

Since the maximum emission wavelength of pH sensitive fluorophore (fluorescein) is around 520 nm (green-emitting pH probe), a polymer carrying BODIPY derivative that acts as a red-emitting reference dye was designed. Based on the former PhD student Chloé GRAZON's work, methylnaphthyl BODIPY is known to emit around 610 nm [21]. We first synthesized methylnaphthyl BODIPY azide as BODIPY monomer and an alkyne functionalized polyanion for further polymer modification and LbL film fabrication. In the end, methylnaphthyl BODIPY polyanion could be obtained by linking (click chemistry) the methylnaphthyl BODIPY azide and alkyne functional polyanion.

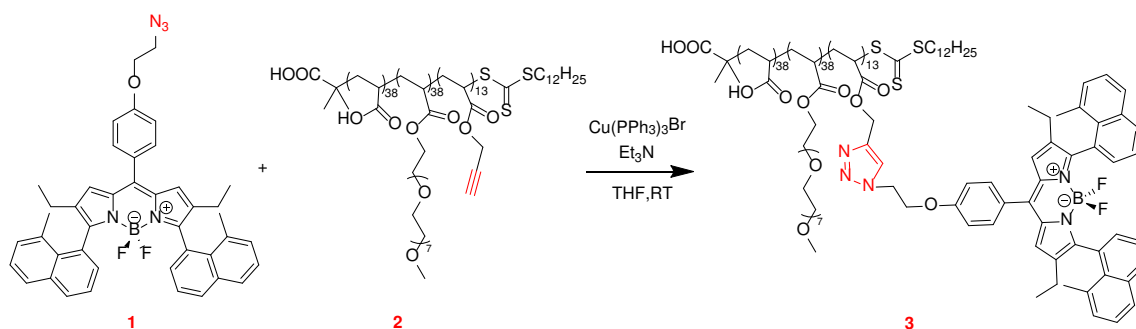
BODIPY can be synthesized from pyrroles using a standard three-step procedure via a condensation of two pyrroles with an aldehyde followed by aromatization and final complexation with boron trifluoride [22]. Most commonly in the literature, BODIPY derivatives with high emission wavelength are synthesized starting from pyrroles substituted with phenyl groups. Furthermore, functional groups may be introduced before or after the BODIPY formation from pyrrole and substituted benzaldehyde or benzoyl chloride. Therefore, (8-methylnaphthyl)pyrrole

was obtained by the Trofimov reaction (Scheme 5.8) [23]. In order to decrease the steric hindrance of the BODIPY and improve the click reaction efficiency, we chose to introduce a functional group in the meso (8) position of the BODIPY [24, 25] and the obtained methylnaphthyl BODIPY was post-modified to afford methylnaphthyl BODIPY azide (Scheme 5.8).



Scheme 5.9. Synthetic scheme employed for the RAFT synthesis of P(APEG-co-ProA-co-AA) with alkyne functional group.

The polymer functionalized with an alkyne side chain was synthesized by RAFT polymerization (Scheme 5.9) [26]. After a reaction time of 38 hours, the polymerization was reached 83% conversion (NMR). The end-functionalized alkynyl PC⁻ was isolated by precipitation into cold diethyl ether. The number average molecular weight (M_n (NMR)) was calculated based on NMR total monomer conversion to be 18900 g/mol.

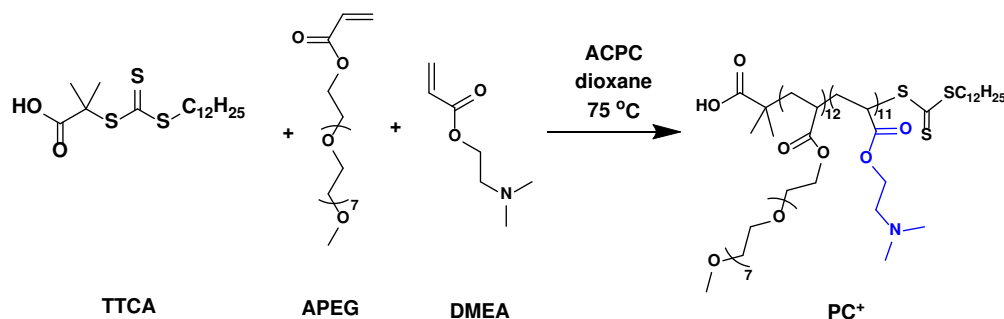


Scheme 5.10. Synthesis of the methylnaphthyl BODIPY fluorescent anionic polymer using CuAAC click chemistry.

After obtaining the clickable alkyne functional polymer and methylnaphthyl BODIPY azide, the copper catalyzed alkyne/azide cycloaddition (CuAAC) click reaction was carried out under mild conditions with $[(PPh_3)_3CuBr]$ as the catalyst, in the presence of Et_3N (Scheme 5.10) [27]. The methylnaphthyl fluorescent polyanion (RFPC⁻) was purified by precipitation into cold diethyl ether and washing with H_2O .

5.1.3 Synthesis of poly(2-(dimethylamino)ethyl acrylate-co-poly(ethylene glycol) methyl ether acrylate) (PC⁺)

Positively charged polyelectrolytes (PC⁺) are necessary as a bridge to bind the negatively charged glass slide and the functional polyanion using the Layer-by-layer (LbL) assembly. The polymerization of poly(ethylene glycol) methyl ether acrylate (APEG) and 2-(dimethylamino)ethyl acrylate (DMEA) under the same experimental condition as for DIBO-PC⁻ was performed (Scheme 5.11). The polymerization reached 90% conversion after 4 hours and was stopped by immersing the reaction mixture into an ice bath. PC⁺ was purified by precipitation into cold cyclohexane. The number average molecular weight (M_n (NMR)) was estimated to be 7700 g/mol based on NMR total monomer conversion.



Scheme 5.11. Synthetic scheme employed for the RAFT synthesis of P(APEG-co-DMEA) (PC⁺).

After describing the different synthetic pathways, we will continue with the characterizations of the polyions and fluorescent dye.

5.2 Characterization of fluorescein azide, polyanion and polycation

5.2.1 Spectroscopic properties of fluorescein azide and RFPC⁻ in solution

UV-vis absorption and fluorescence emission spectra of fluorescein azide and RFPC⁻ dissolved in water are depicted in Figure 5.2. The maximum of absorption and fluorescence emission of fluorescein azide are found at 478 nm and 521 nm in water, a usual value for fluorescein. In addition, the main absorption band of RFPC⁻ at 552 nm is attributed to the 0-0 vibrational band of a strong $S_0 \rightarrow S_1$ transition; the band in the 460-350 nm range at the short wavelength side of the spectrum is assigned to the $S_0 \rightarrow S_2$ transition. The fluorescence emission of RFPC⁻ is in the red range at 594 nm. These two fluorophores can be combined to form a ratiometric sensor since they absorb and emit in different parts of the visible spectra.

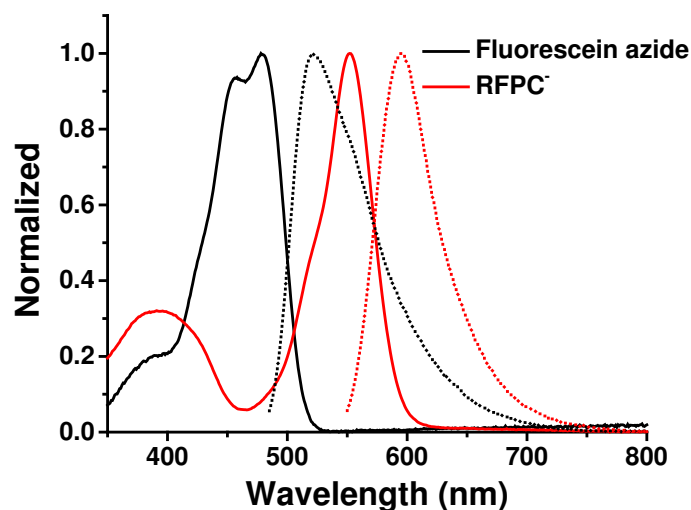


Figure 5.2. Normalized absorption (full lines) and fluorescence (dotted lines, $\lambda_{ex} = 478$ nm for fluorescein and $\lambda_{ex} = 540$ nm for RFPC⁻) spectra of fluorescein azide and RFPC⁻ in water.

5.2.2 Zeta potential of DIBO-SW PC⁻, DIBO-LW PC⁻ and RFPC⁻

Since the Layer-by-Layer assembly depends upon the electrostatic attraction of each polyelectrolytes, the optimization of the deposition solutions was verified by zeta potential measurements. These four polymers are all weak polyelectrolytes; therefore the pH will greatly affect the degree of dissociation and the charge density of each polymer. The zeta potentials of each polyelectrolyte in water were determined and the result is shown in Table 5.2. The natural pH of the PC⁺ dissolved in water is basic, due to the amine functional group whereas it is acidic for all polyanions as a result of the carboxylic functional group. The natural pH of three polyanions is different probably due to different concentrations of the polyanions solutions. For the long chain polyelectrolytes, the concentration is crucial for the conformation of the polymer in solution and has a great influence on its zeta potential in solution. For instance, when the concentration of DIBO-LW PC⁻ is 5.0×10^{-4} M, 5.0×10^{-5} M and 5.0×10^{-6} M, the zeta potential is -24.4 mV, -32.5 mV and -26.6 mV at pH around 5.5, respectively. We suppose that DIBO-LW PC⁻ chains are in a coiled conformation and the charged units are screened by the other part of the chain, therefore a low zeta potential (-24.4 mV) is measured when the concentration of DIBO-LW PC⁻ is high (5.0×10^{-4} M). When the concentration of DIBO-LW PC⁻ chains is low (5.0×10^{-6} M) even though they are extended and more charges are exposed, the zeta potential (-26.6 mV) is still not high enough. At the intermediate concentration (5.0×10^{-5} M), a stable colloidal solution was obtained (zeta potential -32.5 mV). Following the same procedure, we found out that the optimal concentration for RFPC⁻ is 4.8×10^{-7} M.

Table 5.2. Zeta potentials (ζ) of the polyelectrolytes

	PC ⁺		DIBO-SWPC ⁻		DIBO-LWPC ⁻		RFPC ⁻	
pH	8.5	5.4	3.6	5.3	4.1	5.6	5.0	6.6
ζ^a / mV	5.5±0.4	30.2±0.9	-33.2±0.3	-43.6±0.2	-26.0±0.6	-32.5±0.4	-27.9±0.2	-39.1±0.4

^aZeta potentials (ζ) were recorded in Milli-Q water at 25 °C, [PC⁺] = 8.2×10⁻⁵ M, [DIBO-SWPC⁻] = 5.1×10⁻⁴ M, [DIBO-LWPC⁻] = 5.0×10⁻⁵ M and [RFPC⁻] = 4.8×10⁻⁷ M.

Upon changing the pH, more stable colloidal solutions were achieved. When the pH was adjusted to 5.4 for PC⁺, 5.3 for DIBO-SW PC⁻, 5.6 for DIBO-LW PC⁻ and 6.6 for RFPC⁻, the degree of ionization of these four weak polyelectrolytes is high enough for the further multi-layer assembly process through electrostatic attraction.

5.3 pH sensitive surface preparation

5.3.1 DIBO-SW PC⁻ / fluorescein surface preparation by click chemistry

Table 5.3. Optimal conditions for polymer deposition solutions

Solution	Concentration (mol/L)	pH	Ionic strength (mol/L)
PC ⁺	8.2×10 ⁻⁵	5.4	0.005
DIBO-SWPC ⁻	5.1×10 ⁻⁴	5.3	0.005
FA	5.4×10 ⁻⁴		5% DMSO

To investigate the pH effect on the surface, the fluorescein was introduced on the outmost DIBO-SWPC⁻ layer by click chemistry and the interlayer was built with PC⁺ through LbL assembly. Based on the zeta potential investigation for each polyelectrolyte and in order to obtain a thin film, optimal deposition conditions for each polyelectrolyte was used as shown in Table 5.3. After obtaining the PC⁺/DIBO-SWPC⁻ film, it was immersed in a FA-N₃ solution at room temperature without any other catalyst. A relatively high concentration of fluorescein azide was used to ensure that sufficient FA is available for the clickable DIBO-PC⁻ surface. The FA coverage was thus only dependent on the quantity of binding sites available on the DIBO-PC⁻ surface. The fluorescein film was obtained after 2 hours by copper-free strain promoted alkyne-azide cycloaddition (SPAAC) click reaction. A reference film with DIBO-SW PC⁻ but without the FA was also prepared for comparison.

5.3.2 DIBO-LW PC⁺ / fluorescein surface preparation by click chemistry

The PC⁺ layer was first introduced in the same conditions as for the film with the DIBO-SW PC⁺ film on activated glass and then the DIBO-LW PC⁺ in the condition described in table 5.4. FA grafting on the surface was finally carried out using 1 equivalent of FA per polymer chain.

Table 5.4. Optimal conditions for polymer deposition solutions

Solution	Concentration (mol/L)	pH	Ionic strength (mol/L)
PC ⁺	8.2×10^{-5}	5.4	0.005
DIBO-LWPC ⁺	5.0×10^{-5}	5.6	0.005
FA	5.4×10^{-4}		5% DMSO

In summary, a film was obtained with DIBO-LW PC⁺ which will provide a more stable top layer but a relatively lower quantity of fluorescein compared to the one prepared in the previous paragraph.

5.3.3 (DIBO-LW PC⁺ + RFPC⁺) / fluorescein surface preparation by click chemistry

Table 5.5. Optimal conditions for polymer deposition solutions

Solution	Concentration (mol/L)	pH	Ionic strength (mol/L)
PC ⁺	8.2×10^{-5}	5.4	0.005
DIBO-LWPC ⁺	$5.0 \times 10^{-5} / 1.5 \times 10^{-4}$	6.6	0.005
RFPC ⁺	$4.8 \times 10^{-7} / 1.4 \times 10^{-6}$	6.6	0.005
FA	3.0×10^{-6}		5% DMSO

A ratiometric LbL film was fabricated very simply by preparing a mixture deposition solution containing both DIBO-LWPC⁺ and RFPC⁺ and then introducing fluorescein by copper-free click chemistry. The ratio of fluorescence intensity from fluorescein and RFPC⁺ on LbL film at the same excitation wavelength can be adjusted by changing the ratio of DIBO-LWPC⁺ and RFPC⁺ in the deposition solution, because the quantity of fluorescein depends on the quantity of DIBO-

LWPC⁻ on the film. We choose a 104/1 ratio between DIBO-LWPC⁻ and RFPC⁻ (Table 5.5). The total concentration of these two polyanions was adjusted to improve the total fluorescence intensity of the fluorescent LbL film. Two concentrations of the mixture deposition solution were prepared. Two (DIBO-LW PC⁻ + RFPC⁻) / fluorescein surfaces (deposited from relatively high concentration and low concentration mixture deposition solutions) were obtained.

5.4 Characterization of DIBO-SW PC⁻/FA, DIBO-LW PC⁻/FA and (DIBO-LW PC⁻ + RFPC⁻)/FA surface

5.4.1 Fluorescence emission analysis of the LbL films

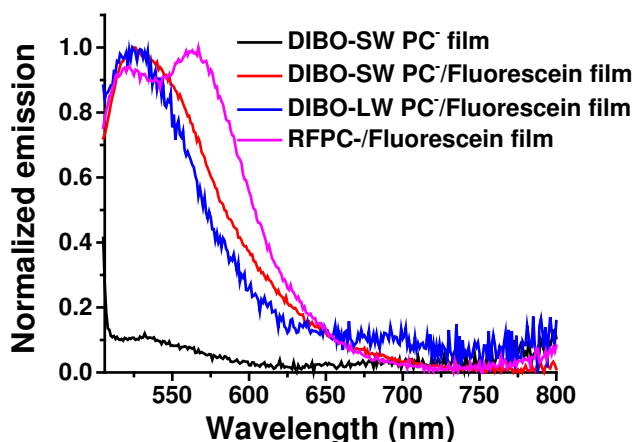


Figure 5.3. Fluorescence spectra ($\lambda_{ex} = 478$ nm) of the different LbL films: the outmost layer is DIBO-SW PC⁻ (as a reference), DIBO-SWPC⁻/fluorescein, DIBO-LWPC⁻/fluorescein and ratiometric RFPC⁻/fluorescein, respectively. All spectra were taken in air (no solution).

The fluorescence emission spectra of the different films where the outmost layer is DIBO-SW PC⁻ (reference), DIBO-SWPC⁻/fluorescein, DIBO-LWPC⁻/fluorescein and ratiometric DIBO-LWPC⁻/fluorescein are shown in Figure 5.3. No visible emission from the blank LbL film before modification can be seen. A maximum emission band at around 522 nm for the LbL films modified with fluorescein is observed which is typical of the emission of the dianionic form of the fluorescein. Those two facts indicate that the post-functionalization of LbL films was successful. An additional emission band with a maximum at 567 nm was observed for the RFPC⁻/fluorescein film. This second emission can be attributed to the BODIPY units. It is blue shifted compared to the solution spectra possibly because of the highly polar environment. The ratio of the fluorescence intensity at 522 nm and 567 nm is 0.95. We successfully introduced two fluorophores on one nanostructured LbL film surface and their ratio was easily controlled to get similar fluorescence intensity.

5.4.2 Fluorescence imaging of LbL films

The fluorescence of each DIBO-PC⁻/fluorescein surface was observed under microscope. Figure 5.4 shows that both DIBO-SWPC⁻/fluorescein and DIBO-LWPC⁻/fluorescein surfaces are homogeneous. The fluorescence intensity of each surface was analyzed with ImageJ. The fluorescence intensity from DIBO-SWPC⁻/fluorescein surface (0.25 mm²) is around 738, while it is lower (around 507) for DIBO-LWPC⁻/fluorescein surface as expected from the ratio of DIBO moiety and acrylic acid units in both polymer chains.

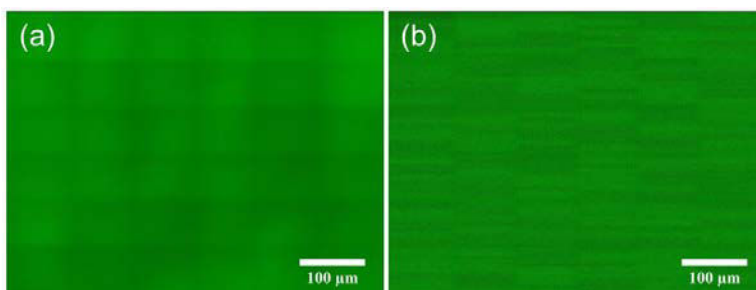


Figure 5.4. Fluorescence images of DIBO-SWPC⁻/fluorescein (a) and DIBO-LWPC⁻/fluorescein (b) surfaces (0.25 mm²) in the presence of M9. The excitation wavelength was 475 nm.

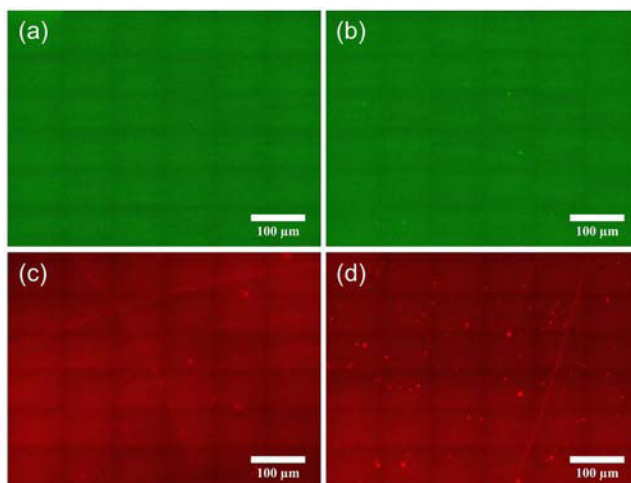


Figure 5.5. Green (top) and red channels (bottom) fluorescence images of ratiometric RFPC⁻/fluorescein surfaces (0.25 mm²) prepared at relatively low (a and c) and high (b and d) concentrations of the deposition solutions in the presence of M9 culture medium. The excitation wavelength was 475 nm (a and c) and 542 nm (b and d), respectively.

The ratiometric RFPC⁻/fluorescein surfaces were prepared with different concentrations of the mixed deposition solution. Figure 5.5 indicates that the ratiometric RFPC⁻/fluorescein surface (Figure 5.5a and c) that were prepared with a lower concentration solution ([DIBO-LWPC⁻] = 5.0×10^{-5} M and [RFPC⁻] = 4.8×10^{-7} M) seems more homogeneous, compared to the one (Figure

5c and d) prepared with a higher concentration ($[DIBO-LWPC^-] = 1.5 \times 10^{-4}$ M and $[RFPC^-] = 1.4 \times 10^{-6}$ M). Indeed brighter spots appeared in the red channel (Figure 5.5d). It means that high concentration of $RFPC^-$ leads to BODIPY aggregation. In addition, there are also few green bright spots indicative of aggregation of FA as well (Figure 5.5b) on the high concentration surface. In this deposition condition, the conformation of the polymers is probably coiled.

5.5 Study of surface pH sensitivity

5.5.1 pH effect on DIBO-SWPC⁻/fluorescein surface

pH sensitive properties of (modified) fluorescein in multiple architectures has been widely investigated in solution. However, there are few reports on the pH sensitivity of FA on surface or in solid state.

pH effect on DIBO-SWPC⁻/fluorescein surface was studied first by adding 1 M HCl or 1M NaOH aqueous solution directly on the surface. Fluorescence spectra of the surface were recorded after each addition. Figure 5.6 left shows that the initial fluorescence intensity of DIBO-SWPC⁻/fluorescein surface was 9.1×10^4 . The fluorescence intensity increased when the base was added (cycle 2) and subsequently the fluorescein emission was quenched in the presence of acid (cycle3). Most notably, the DIBO-SWPC⁻/fluorescein surface displayed reversible ability when base and acids were subsequently added (cycle 4 and 5 respectively). However, the pH effect experiment was performed under high acidic or basic environment which is not adapted to mimic the pH changes in biological media. The pH change ranges from 7 to 5 upon bacterial grow. We thus designed a new protocol to study the pH effect on the DIBO-SWPC⁻/fluorescein surface. Different modified M9 media were prepared with pH values 5, 6 and 7 and were separately deposited onto DIBO-SWPC⁻/fluorescein surface. A clean glass slide was used as a coverslip and the films observed by confocal microscopy. The fluorescence images of DIBO-SWPC⁻/fluorescein surfaces in the presence of different pH modified M9 medium are shown in Figure 5.6 right. The decrease of fluorescence brightness could be observed when the pH of modified M9 medium was reduced from 7 to 5. The bright spots remaining at pH 5 maybe because some aggregated fluorescein are not affected.

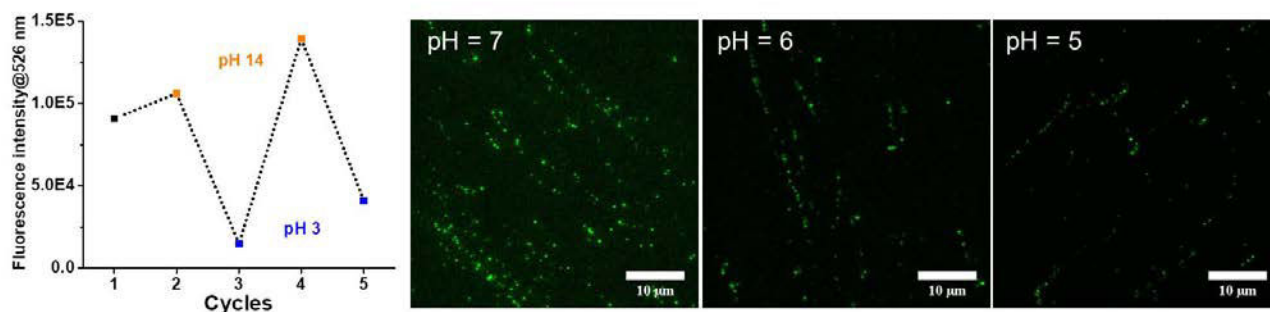


Figure 5.6. pH effect on the DIBO-SWPC/fluorescein surface: plot of the fluorescence intensity at 526 nm recorded with a fluorolog3 versus pH ($\lambda_{ex} = 478$ nm), pH of the surface adjusted by aqueous 1M NaOH and 1M HCl directly (left). Fluorescence images of the surface in the presence of modified M9 to adjust the pH recorded by confocal microscopy ($\lambda_{ex} = 488$ nm) (right).

5.5.2 pH effect on RFPC/fluorescein surface

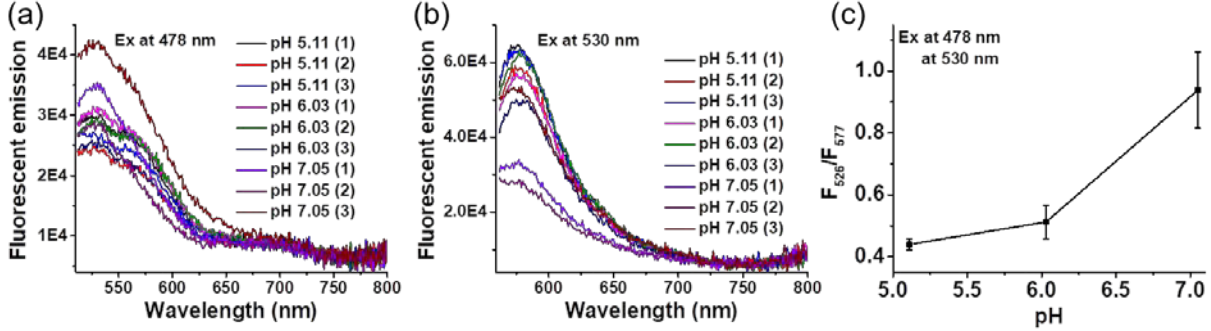


Figure 5.7. (a) and (b) Emission spectra of the RFPC/fluorescein surface in the presence of different pH M9 culture medium. (c) pH effect on the RFPC/fluorescein surface: plot of F_{526}/F_{577} versus pH value. F_{526} and F_{577} indicate the fluorescence intensity at 526 nm ($\lambda_{ex} = 478$ nm) and 577 nm ($\lambda_{ex} = 530$ nm), respectively.

Several modified M9 culture media at different pH (5, 6 and 7) were prepared and separately added onto RFPC/fluorescein surface. A clean glass slide was used as a coverslip. Fluorescence spectra of each surface were recorded with a Fluorolog-3 spectrofluorimeter (Figure 5.7a and b). As shown in Figure 5.7c, the emission ratio at 526 nm ($\lambda_{ex} = 478$ nm) to that at 577 nm ($\lambda_{ex} = 530$ nm), F_{526}/F_{577} increased from 0.44 to 0.94 upon increasing the pH of the medium from 5.11 to 7.05.

5.6 Study of bacterial growth on the pH sensitive surfaces

5.6.1 Real-time detection of *E. coli* growth in modified M9 minimal medium

Growth of *E. coli* bacteria with glucose results in the production of CO_2 and acetic acid. Therefore, a decrease in the pH of the growth medium is observed [1]. We initially studied the pH change in the growth medium during the bacterial growth. A growth medium with an initial pH of 6.8 and an initial *E. coli* bacteria concentration of 2×10^6 CFU/mL (OD = 0.025) was incubated at 37 °C. The growth of the cells was monitored every 30 min by measuring the optical density at 600 nm using a spectrophotometer and the pH of the suspension was measured concomitantly with a pH meter. Figure 5.8 shows that the pH of the growth medium initially at 6.8, started to decrease when the bacteria began to grow. When the bacterial concentration

increased to 8×10^7 CFU/mL (OD = 0.88), the pH of the growth medium decreased to 5.3. Theoretically, the pH decrease of the growth medium from 6.8 to 5.3 when bacteria grow can be detected by the pH sensitive surface.

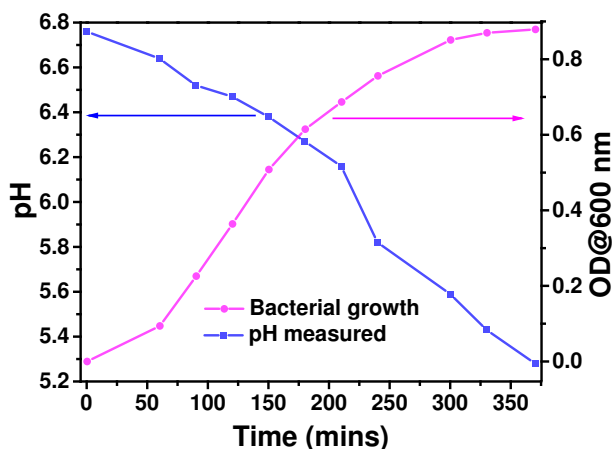


Figure 5.8. Real-time bacterial growth curve (circle line) and the corresponding pH evolution as measured by a pH meter (square line).

5.6.2 Study of *E. coli* growth on pH sensitive DIBO-SW PC⁻/fluorescein surface

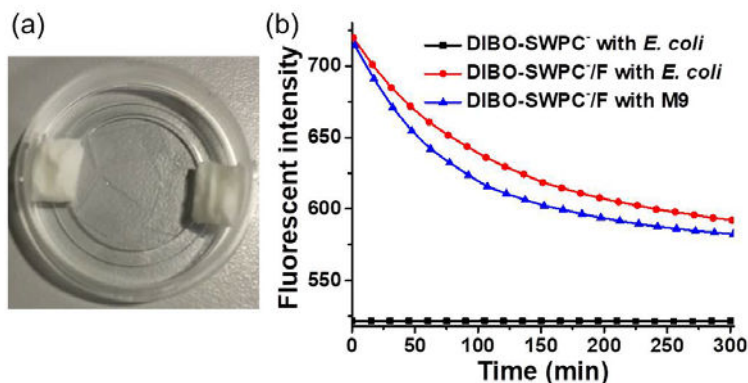


Figure 5.9. (a) Bacteria growth detection on pH sensitive surface in Ibidi μ -Dish with wet tissue; (b) Fluorescence intensity of DIBO-SWPC⁻/fluorescein surface in the presence of *E. coli* bacteria (red line and circles) as a function of time. Two controls were also recorded, blank DIBO-SWPC⁻ surface in the presence of *E. coli* bacteria (black line and squares) and DIBO-SWPC⁻/fluorescein surface in the presence of modified M9 minimal medium (blue line and triangles). The excitation wavelength was 475 nm.

In order to test the pH sensitive DIBO-SW PC⁻/fluorescein surface for *E. coli* growth detection, we put the sample in an Ibidi μ -Dish with a wet tissue to control the humidity during

bacterial growth (Figure 5.9a). Meanwhile, two controls were recorded: a blank DIBO-SWPC⁻ surface in the presence of *E. coli* bacteria and a DIBO-SWPC⁻/fluorescein surface in the absence of bacteria. Microscope images of each sample were recorded by wide-field microscopy in time-lapse mode for 300 min upon incubation at 30 °C. Figure 5.9b shows that the fluorescence intensity of the DIBO-SW PC⁻/fluorescein surface in the presence of *E. coli* decreased from 719 to 592 over 300 min (the microscope images are shown in Figure 10). However, the fluorescence intensity of the DIBO-SW PC⁻/fluorescein surface in the absence of *E. coli* also decreased from 714 to 582 over 300 min (the microscope images are shown in Figure 5.12). It means that photobleaching is likely to occur. Another hypothesis is that the stability of DIBO-SW PC⁻/fluorescein surface is reduced.

Moreover, the number of bacteria cells on the DIBO-SWPC⁻/fluorescein surface and on the control DIBO-SWPC⁻ surface (microscope images in Figure 5.11) were counted with ImageJ at 0, 120 and 300 min (Table 5.6). We found out that the number of *E. coli* increased from 421 to 1623 and 710 to 2391 on the DIBO-SWPC⁻/fluorescein surface and the control DIBO-SWPC⁻ surface respectively, indicating *E. coli* indeed split on the surface and that the third generation appeared after 300 min incubation. We measured the OD and pH of the initial bacteria suspension when we introduced the bacteria onto each surface, therefore, the OD could be calculated according the number of *E. coli* and then the pH could be deduced from Figure 8. The theoretical pH on DIBO-SWPC⁻/fluorescein surface after 300 min should be 5.8. The surface should respond to such pH change by a measurable fluorescence decrease. In conclusion, the DIBO-SWPC⁻/fluorescein surface was biocompatible for *E. coli* growth, but the stability of the film was an issue and shall be optimized for instance by using longer chains.

Table 5.6. Evolution of the number of bacteria on each surface during the time-lapse experiment

		0 min	120 min	300 min
DIBO-SWPC ⁻ /fluorescein surface	# <i>E. coli</i> ^a	421	1023	1628
	OD	0.198 ^b	0.481 ^c	0.766 ^c
	pH	~ 6.6 ^b	~ 6.4 ^c	~ 5.8 ^c
DIBO-SWPC ⁻ surface	# <i>E. coli</i> ^a	710	1692	2391
	OD	0.198 ^b	0.472 ^c	0.667 ^c
	pH	~ 6.6 ^b	~ 6.4 ^c	~ 6.2 ^c

^a the number of *E. coli* on the surface (0.25 mm²) was counted with ImageJ; ^b the parameter was measured by spectrophotometer or pH meter; ^c the parameter was calculated according to figure 5.8.

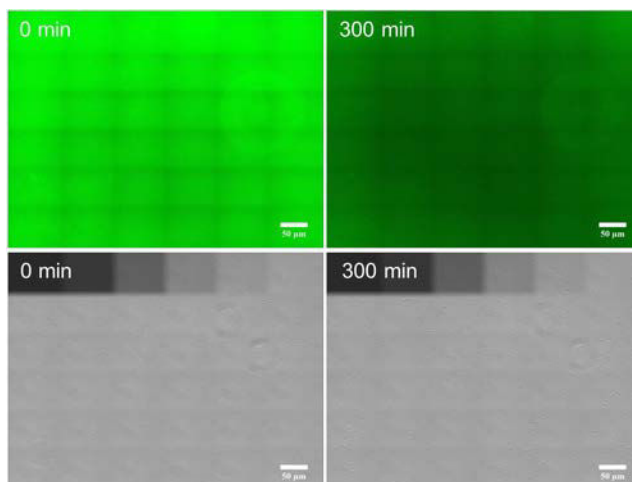


Figure 5.10. Microscope images of DIBO-SWPC/fluorescein surface in the presence of *E. coli* bacteria before and after time-lapse. The excitation wavelength was 475 nm.

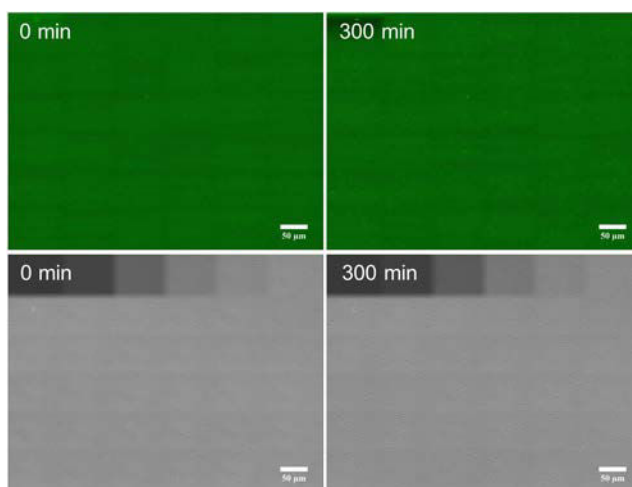


Figure 5.11. Microscope images of DIBO-SWPC surface in the presence of *E. coli* bacteria before and after time-lapse. The excitation wavelength was 475 nm.

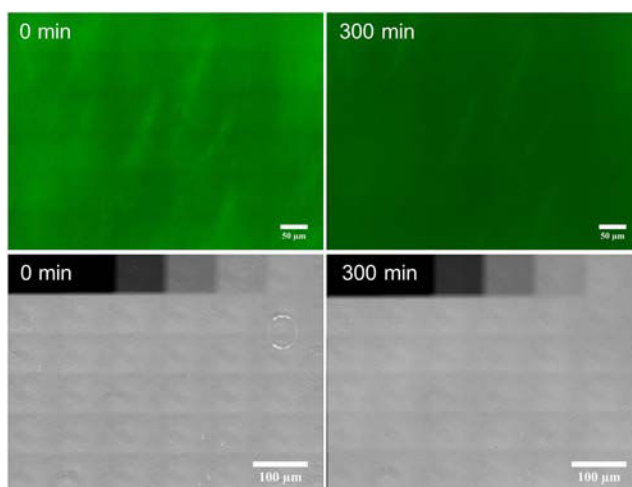


Figure 5.12. Microscope images of DIBO-SWPC/fluorescein surface in the presence of modified *E. coli* bacteria before and after time-lapse. The excitation wavelength was 475 nm.

M9 only before and after time-lapse. The excitation wavelength was 475 nm.

5.6.3 Study of *E. coli* growth on pH sensitive DIBO-LW PC⁻/fluorescein surface

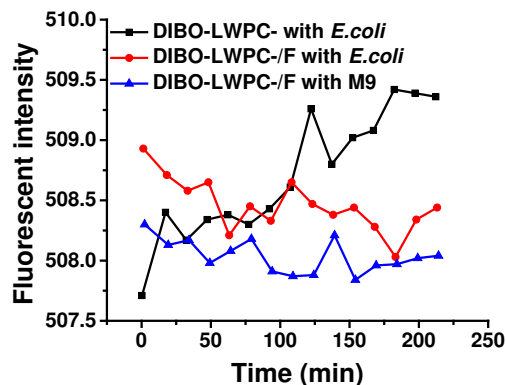


Figure 5.13. Fluorescence intensity of DIBO-LWPC⁻/fluorescein surface in the presence of *E. coli* bacteria (red line and circles) as a function of time for bacterial growth. Two controls were also recorded, blank DIBO-LWPC⁻ surface in the presence of *E. coli* bacteria (black line and squares) and DIBO-LWPC⁻/fluorescein surface in the presence of modified M9 minimal medium (blue line and triangles). The excitation wavelength was 475 nm.

Considering the stability of DIBO-SWPC⁻/fluorescein surface for *E. coli* growth detection, the more stable DIBO-LWPC⁻/fluorescein surface was tested to detect the *E. coli* growth following the same protocol as for the DIBO-SWPC⁻/fluorescein surface. The recorded fluorescence intensity of each surface over time is shown in Figure 5.13. The signal from DIBO-LWPC⁻/fluorescein surface with or without *E. coli* was random and tended to a constant average value. This is due to the low fluorescence intensity of the surface. In addition, the fluorescence intensity of the blank DIBO-SWPC⁻ surface slightly increased: this is likely to come from the auto-fluorescence of bacteria.

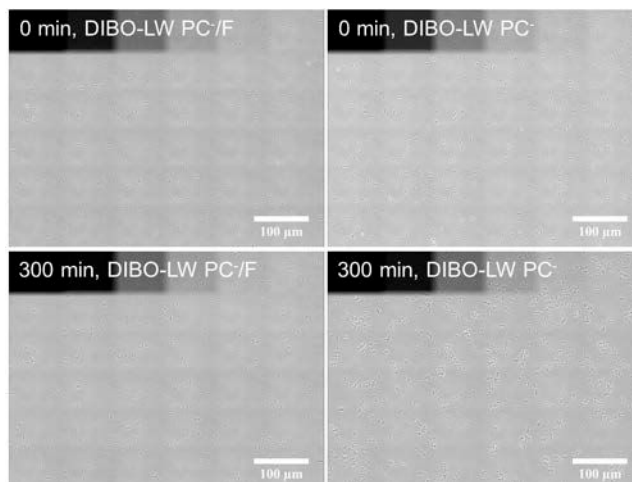


Figure 5.14. Microscope images of DIBO-LWPC⁻/fluorescein surface (left) and DIBO-LWPC⁻ surface (right) in the presence of *E. coli* before and after time-lapse.

The bright field images of DIBO-LWPC⁻/fluorescein and DIBO-LWPC⁻ surfaces in the presence of *E. coli* are shown in Figure 5.14. The number of *E. coli* on each surface (0.2 mm²) before and after time-lapse was estimated. The number of *E. coli* increased from 194 to 328 on the DIBO-LWPC⁻/fluorescein surface and from 332 to 1367 on the DIBO-LWPC⁻ surface, indicating that both surfaces were biocompatible for *E. coli* growth.

5.6.4 Study of *E. coli* growth on pH sensitive RFPC⁻/fluorescein ratiometric surface

Using the same set-up with previous samples (Figure 5.9a), 2 μ L growth medium with an initial concentration of *E. coli* bacteria of 1.0×10^7 CFU/mL (OD \sim 0.2) was introduced onto the RFPC⁻/fluorescein films prepared in a mixt solution of relatively low ([DIBO-LWPC⁻] = 5.0×10^{-5} M and [RFPC⁻] = 4.8×10^{-7} M) and high ([DIBO-LWPC⁻] = 1.5×10^{-4} M and [RFPC⁻] = 1.4×10^{-6} M) concentration. Meanwhile, a control was also recorded on both RFPC⁻/fluorescein surfaces in the presence of modified M9 minimal medium only. The fluorescence and bright field microscope images were recorded at regular time intervals to monitor the fluorescence intensity of each surface (Figure 5.15) and the growth of cells (Figure 5.16).

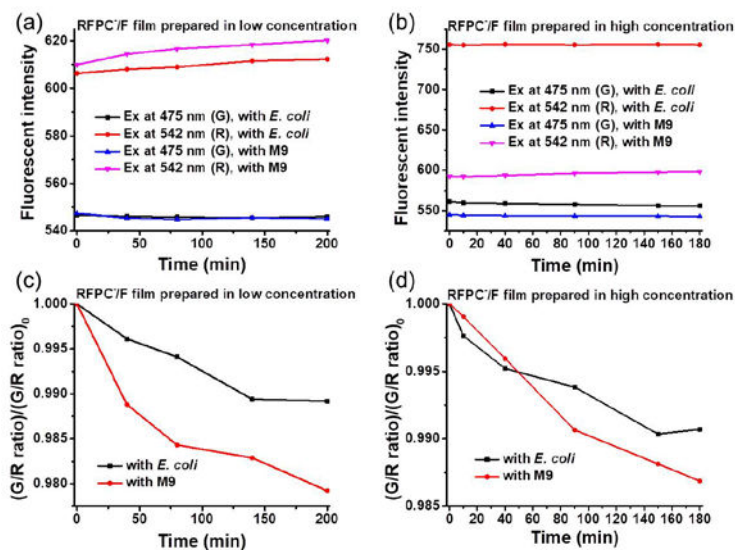


Figure 5.15. Fluorescence intensity of RFPC⁻/fluorescein surface that were prepared with low (a) and high (b) concentration deposition solutions in the presence of *E. coli* bacteria as a function of time. A control was also recorded: RFPC⁻/fluorescein surface in the presence of modified M9 minimal medium. The excitation wavelength was 475 nm or 542 nm. (c and d) Normalized Green/Red fluorescence ratio of the RFPC⁻/fluorescein surface as a function of time. Green and Red indicate the fluorescence intensity of the ratiometric surface at λ_{ex} = 475 nm and 542 nm, respectively.

The fluorescence intensity (Figure 5.15a and b) and the corresponding *Green/Red* ratio (Figure 5.15c and d) of each RFPC⁻/fluorescein surface as a function of time is shown in Figure 5.15. It was found that the green and red fluorescence intensity of RFPC⁻/fluorescein surface prepared at high concentration is more intense than for the film prepared at low concentration. This means that fluorescence intensity can be increased to a certain extent by controlling the deposition condition. There is almost no decrease in the green channel for both of surfaces after 3 hours of bacterial growth (Figure 5.15a and b). When we focus on the ratiometric fluorescence (*Green/Red* ratio) change on each surface (Figure 5.15c and d), the decrease in the percentage of the G/R ratio of RFPC⁻/fluorescein surface in the absence of *E. coli* is higher than for the surface in the presence of *E. coli*. However, we could still observe the bacterial growth on each surface by counting the number of *E. coli* (area = 0.2 mm²) before and after time-lapse (Figure 5.16). The number of *E. coli* increased from 285 to 698 on RFPC⁻/fluorescein surface prepared at low concentration and from 572 to 1886 on the surface prepared at high concentration, indicating that both surfaces are biocompatible with *E. coli* growth.

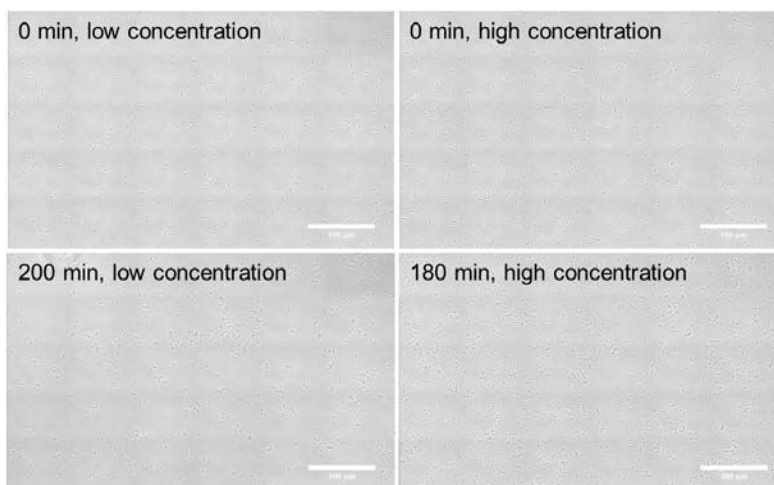


Figure 5.16. Microscope images of RFPC⁻/fluorescein surfaces prepared in mixt solutions of low (left) and high (right) concentrations in the presence of *E. coli* bacteria before and after time-lapse.

5.7 Conclusion

In conclusion, we successfully prepared different types of pH sensitive LbL film and tested the bacterial growth detection. Firstly, the synthesis of different functionalized polyanions (short and long chain DIBO-PC⁻ and red fluorescent polymer) was presented. Then three types of pH sensitive surfaces containing fluorescein were prepared using a combination of LbL assembly and copper-free SPAAC click chemistry: a DIBO-SWPC⁻/fluorescein surface containing high fluorescein content; a more stable DIBO-LW PC⁻/fluorescein surface and a ratiometric RFPC⁻

/fluorescein surface. The spectroscopic properties, fluorescence image of each surface and pH effect of DIBO-SWPC/fluorescein and ratiometric RFPC/fluorescein surfaces were investigated and the results indicated that: i) the fluorescein was successfully introduced on each surface by click chemistry between the fluorescein azide and DIBO moiety on the LbL surface and ii) its fluorescence intensity changes with pH. Finally, the three pH sensitive surfaces were tested for bacteria growth detection. All of the surfaces were biocompatible, the number of *E. coli* increased after several hours incubation on each surface. Unfortunately, the decrease in the percentage of the fluorescence intensity of each surface in the absence of *E. coli* was higher than for the surfaces in the presence of *E. coli*. Maybe we observed the photobleaching of fluorescein. Another possible explanation is that the low fluorescence intensity on the pH sensitive surfaces leads to a low signal to noise ratio.

Materials and methods

Materials

Phenylacetaldehyde (Sigma), Trimethylsilyl iodide (97%, Sigma), n-butyllithium solution (1.6 M in hexanes, Sigma), Bromine (99.6%, Acros), N,N'-Dicyclohexylcarbodiimide (99%, Sigma, DCC), 4-(Dimethylamino)pyridine (99%, Sigma, DMAP), 3-chloropropylamine hydrochloride (98%, Aldrich), sodium azide (99%, Acros), 5-carboxyfluorescein (99%, Sigma-Aldrich), O-(Benzotriazol-1-yl)-1,1,3,3-tetramethyluronium tetrafluoroborate (TBTU, Sigma-Aldrich), N,N-diisopropylethylamine (99.5%, Sigma-Aldrich, DIPEA), 1-methylnaphthalene (95%, Aldrich), butyryl chloride (98%, Aldrich), hydroxylamine hydrochloride ($\geq 96\%$, Sigma), mercury acetate ($\geq 99\%$, Sigma-Aldrich), 4-hydroxybenzaldehyde (98%, Aldrich), 2-bromoethanol (95%, Aldrich), acryloyl chloride (97%, Aldrich), propargyl alcohol (99%, Aldrich), triethylamine ($\geq 99\%$, Sigma-Aldrich), Bromotris(triphenylphosphine)copper(I) (98%, Aldrich, $(\text{PPh}_3)_3\text{CuBr}$), tetrachlorol-1,4-benzoquinone (99%, Aldrich, Chloranil), boron trifluoride diethyletherate (2 M in diethyl ether, Aldrich), methacryloyl chloride ($\geq 97\%$, Sigma-Aldrich), 1,8-diazobicyclo[5,4,0]undec-7-ene ($\geq 98\%$, Fluka, DBU), Poly(ethylene glycol) methyl ether acrylate (Sigma-Aldrich, $M_n = 454 \text{ g mol}^{-1}$, APEG), 2-methyl-2-[(dodecylsulfanylthiocarbonyl)sulfanyl] propanoic acid (97%, Strem, TTCA), acrylic acid (99%, Aldrich, AA), 2-(Dimethylamino)ethyl acrylate (98%, Sigma, DMEA), 4,4'-Azobis(4-cyanopentanoic acid) (98%, Sigma, ACPC) were used as received without further purification. Solvents were of synthetic grade and purified according to standard procedures. 18 M Ω Millipore water was used throughout and further pH-adjusted with either HCl or NaOH. All solvents were dried on an automatic M. Braun SPS-800 instrument.

Characterization techniques

All nuclear magnetic resonance (NMR) spectra were recorded in CDCl_3 on a JEOL ECS (400 MHz) spectrometer. All chemical shifts are in ppm and referenced to tetramethylsilane (TMS).

Zeta potentials (ζ) were performed on a Zetasizer Nanoseries (Malvern) apparatus. The dispersant RI value was 1.330. Samples were analyzed in DTS 1060 plastic cells, at 25 °C. Three measurements of at least ten scans were performed for each sample.

pH measurements were performed using a glass electrode connected to PHM210 Standard pH meter from Mettler Toledo.

Contact angles were performed on an advanced surface technology (AST) video contact angle measuring device. A 1 μL droplet of deionized water was deposited on the samples.

Absorption measurements were performed using Varian Cary 100 and Cary 500 from Agilent Technologies.

Fluorescence emission spectra were performed using Fluorolog-3 spectrofluorimeter from Horiba Jobin-Yvon. A front-face configuration was used for film measurement.

Microscope images were taken on a confocal laser scanning microscope (Leica TCS SP5) or epifluorescence microscope (Nikon inverted microscope ECLIPSE TI-E).

Synthesis

Synthesis of 3-azidopropan-1-amine [17]. Sodium azide (1.5 g, 23.14 mmol) was added into a solution of 3-chloropropyl-1-amine hydrochloride (1.0 g, 7.71 mmol) in water (7.7 mL), and the mixture was refluxed for 7 hours. After cooling down to room temperature, half solvent was evaporated. KOH (0.4 g) was added to the residual solution at 0 °C, and the mixture was extracted with Et₂O (15×3 mL), the combined organic layers were dried over Na₂SO₄, evaporated to give the product as pale yellow and volatile oil.

¹H NMR (400 MHz, DMSO-d₆): δ(ppm) = 1.60 (m, 2H, CH₂CH₂CH₂), 2.61 (t, 2H, CH₂NH₂), 3.38 (t, 2H, CH₂N₃). ¹³C NMR (100 MHz, DMSO-d₆): δ (ppm) = 32.9, 39.5, 49.3.

Synthesis of fluorescein azide (FA) [18]. 5-Carboxyfluorescein (28 mg, 0.074 mmol), DIPEA (40 μL, 0.23 mmol) and TBTU (36 mg, 0.11 mmol) were added into a solution of 3-azidopropan-1-amine (11 mg, 0.11 mmol) in dry DMF (0.6 mL) at room temperature under argon atmosphere. The mixture was stirred for 2 hours under the same conditions, diluted with AcOEt/Et₂O (1/1, 10 mL), and acidified with 10% aqueous HCl (5 mL). The mixture was extracted with AcOEt/Et₂O (1/1, 2×10 mL), the combined organic layers were dried over Na₂SO₄, evaporated to give the crude material, which was purified on a silica gel column chromatography (CHCl₃/MeOH = 49:1 to 29:1 to 19:1) to give the title compound an orange solid.

¹H NMR (400 MHz, CD₃OD): δ(ppm) = 1.91 (quint, 2H, *J* = 6.7 Hz), 3.44 (t, 2H, *J* = 6.7 Hz), 3.50 (t, 2H, *J* = 6.7 Hz), 6.53 (dd, 2H, *J* = 8.7, 2.3 Hz), 6.59 (d, 2H, *J* = 8.7 Hz), 6.67 (d, 2H, *J* = 2.3 Hz), 7.29 (t, 1H, *J* = 7.9 Hz), 8.18 (dd, 1H, *J* = 8.2, 1.5 Hz), 8.41 (d, 1H, *J* = 1.5 Hz).

Synthesis of 4-(2-hydroxy-ethoxy)-benzaldehyde [15, 28]. To a solution of 4-hydroxybenzaldehyde (5.0 g, 40.9 mmol) in dry DMF (40 mL), K₂CO₃ (11.3 g, 81.9 mmol) and 2-bromoethanol (6.1 g, 49.1 mmol) were added. The reaction mixture was heated to 100 °C for 1 hours with monitoring by TLC. The resulting solution was filtrated and removed the precipitate, and then extracted with ethyl acetate (3×40 mL) and dried over anhydrous MgSO₄. The solvents of the combined organic layer were removed under reduced pressure.

¹H NMR (400 MHz, CDCl₃): δ(ppm) = 4.02 (t, *J* = 4.1 Hz, 2H, CH₂CH₂), 4.19 (t, *J* = 4.1 Hz, 2H, CH₂CH₂), 7.04 (d, *J* = 8.7 Hz, 2H_{ar}), 7.84 (d, *J* = 8.7 Hz, 2H_{ar}), 9.90 (s, 1H, CHO). ¹³C NMR (100 MHz, CDCl₃): δ (ppm) = 61.3, 69.6, 114.9, 130.3, 132.2, 163.8, 191.0.

Synthesis of methylnaphthyl BODIPY phenol (BODIPY-OH). A few drops of trifluoroacetic

acid were added to a dichloromethane solution of methylnaphthyl pyrrole (2.8 g, 12.0 mmol, 2 equiv.) and 4-(2-hydroxyethoxy)-benzaldehyde (1.0 g, 6.0 mmol, 1 equiv.). The dark reaction mixture was stirred at room temperature until total disappearance of the aldehyde. The oxidising agent (chloranil, 1 equiv.), then 5 min later DIPEA (7 equiv.) and finally trifluoroborate etherate (11 equiv.) were successively added. The mixture was filtered through a pad of silica or used crude. The filtrate was concentrated and the residue purified by automatic chromatography on silica gel (dichloromethane/petroleum ether: 80/20) to afford BODIPY.

^1H NMR (400 MHz, CDCl_3): $\delta(\text{ppm}) = 0.93$ (m, 6H, CH_2CH_3), 1.96 (m, 2H, CH_2CH_3), 2.09 (m, 2H, CH_2CH_3), 2.63 (s, 6H, CH_3), 3.89 (t, 2H, CH_2CH_2), 4.02 (t, 2H, CH_2CH_2), 6.85 (m, 2H, CH), 7.1-7.6 (m, 12H, H_{ar}), 7.90 (d, 2H, H_{ar}), 7.97 (d, 2H, H_{ar}). ^{13}C NMR (100 MHz, CDCl_3): $\delta(\text{ppm}) = 14.2, 14.3, 19.3, 19.7, 61.4, 69.4, 114.5, 124.4, 125.6, 125.7, 126.0, 126.8, 128.2, 132.1, 134.5, 135.6, 137.3, 155.6, 160.4$. ^{19}F NMR (376 MHz, CDCl_3): $\delta(\text{ppm}) = -126.3$ (m, 0.8F), -137.3 (q, 2F, $J_{\text{F-B}} = 32.3$ Hz), -147.1 (m, 0.8F). ^{11}B NMR (128 MHz, CDCl_3): $\delta(\text{ppm}) = -0.21$ (t, $J_{\text{B-F}} = 29.5$ Hz).

Synthesis of methylnaphthyl BODIPY tosylate (BODIPY-OTs). To a stirred solution of BODPY-OH (1.93 g, 2.90 mmol, 1.0 equiv.) in anhydrous CH_2Cl_2 (58 mL) was added 4-toluenesulfonyl chloride (0.83 g, 4.34 mmol, 1.5 equiv.), Et_3N (0.88 g, 8.69 mmol, 3.0 equiv.) and DMAP (0.07 g, 0.58 mmol, 0.2 equiv.) under Argon. The reaction mixture was stirred for overnight at 4 °C and quenched with a saturated aqueous NH_4Cl (12 mL). The aqueous layer was extracted with CH_2Cl_2 and the organic layer was washed with H_2O , dried over MgSO_4 and concentrated in vacuo. The residue was purified by column chromatography on silica gel (dichloromethane/petroleum ether: 70/30) to afford 1.8 g of product.

^1H NMR (400 MHz, CDCl_3): $\delta(\text{ppm}) = 0.94$ (m, 6H, CH_2CH_3), 2.00 (m, 2H, CH_2CH_3), 2.10 (m, 2H, CH_2CH_3), 2.62 (s, 6H, CH_3), 3.73 (t, 2H, CH_2CH_2), 4.09 (t, 2H, CH_2CH_2), 6.85 (m, 2H, CH), 7.1-7.6 (m, 12H, H_{ar}), 7.90 (d, 2H, H_{ar}), 7.97 (d, 2H, H_{ar}). ^{13}C NMR (100 MHz, CDCl_3): $\delta(\text{ppm}) = 14.3, 14.4, 19.4, 19.7, 21.8, 65.5, 68.3, 114.5, 124.4, 125.6, 125.7, 126.0, 126.8, 128.2, 130.0, 132.1, 133.08, 134.5, 135.6, 137.3, 145.1, 155.6, 159.9$. ^{19}F NMR (376 MHz, CDCl_3): $\delta(\text{ppm}) = -126.3$ (m, 0.8F), -137.3 (q, 2F, $J_{\text{F-B}} = 32.3$ Hz), -147.1 (m, 0.8F). ^{11}B NMR (128 MHz, CDCl_3): $\delta(\text{ppm}) = -0.21$ (t, $J_{\text{B-F}} = 29.5$ Hz).

Synthesis of methylnaphthyl BODIPY azide (BODIPY- N_3). To a stirred solution of BODPY-OTs (1.89 g, 2.30 mmol, 1.0 equiv.) in anhydrous CH_2Cl_2 (10 mL) and DMF (46 mL) was added sodium azide (0.18 g, 2.77 mmol, 1.2 equiv.). The reaction mixture was stirred for overnight at 100 °C and quenched with H_2O . The mixture was washed with H_2O and extracted with CH_2Cl_2 , dried over MgSO_4 and concentrated in vacuo. The residue was purified by column chromatography on silica gel (dichloromethane/petroleum ether: 40/60) to afford 0.9 g of product.

^1H NMR (400 MHz, CDCl_3): $\delta(\text{ppm}) = 0.97$ (m, 6H, CH_2CH_3), 1.92 (m, 2H, CH_2CH_3), 2.04 (m, 2H, CH_2CH_3), 2.63 (s, 6H, CH_3), 3.62 (t, 2H, CH_2CH_2), 4.20 (t, 2H, CH_2CH_2), 6.79 (m, 2H, CH), 7.1-7.7 (m, 12H, H_{ar}), 7.89 (d, 2H, H_{ar}), 7.91 (d, 2H, H_{ar}). ^{13}C NMR (100 MHz, CDCl_3): $\delta(\text{ppm}) = 14.2, 14.3, 19.3, 19.7, 22.8, 50.1, 67.2, 114.5, 124.4, 125.6, 125.9, 126.0, 126.8, 128.2, 132.0, 132.3, 134.4, 135.7, 137.2, 155.7, 159.9$. ^{19}F NMR (376 MHz, CDCl_3): $\delta(\text{ppm}) = -126.3$ (m, 0.8F), -137.3 (q, 2F, $J_{\text{F-B}} = 32.3$ Hz), -147.1 (m, 0.8F). ^{11}B NMR (128 MHz, CDCl_3): $\delta(\text{ppm}) = -0.21$ (t, $J_{\text{B-F}} = 29.5$ Hz).

Synthesis of propargyl acrylate (ProA) [19]. A solution of propargyl alcohol (0.5 g, 8.90 mmol, 1.0 equiv.), Et_3N (1.0 g, 10.70 mmol, 1.2 equiv.) and DCM (41 mL) was cooled in ice-water bath. Acryloyl chloride (0.97 g, 10.70 mmol, 1.2 equiv.) was added dropwise in 20 min. The reaction mixture was stirred in ice-water bath for 1 hour and at room temperature for 15 hour. The reaction was quenched with saturated aqueous NaHCO_3 . The organic layer was washed with 10% HCl (3 \times 3.1 mL), saturated aqueous NaHCO_3 (3 \times 3.1 mL) and H_2O (2 \times 3.1 mL). The mixture was dried over MgSO_4 and filtrated through neutral Al_2O_3 . The solvent was removed by rotary evaporation. Then, propargyl acrylate was obtained by further vacuum distillation.

^1H NMR (400 MHz, CDCl_3): $\delta(\text{ppm}) = 2.50$ (s, 1H, $\text{C}\equiv\text{CH}$), 4.77 (s, 2H, $\text{OCH}_2\text{C}\equiv\text{CH}$), 5.90 (d, 1H, $\text{CHH}=\text{CH}$), 6.16 (q, 1H, $\text{CHH}=\text{CH}$), 6.50 (d, 1H, $\text{CH}_2=\text{CH}$).

Synthesis of P(APEG-co-ProA-co-AA) (alkynyl PC $^-$). Negatively alkynyl polymer chain P(APEG $_{38}$ -co-ProA $_{13}$ -co-AA $_{38}$) was synthesized in 1,4-dioxane at 75 °C under argon atmosphere. APEG (3.47 g, 7.23 mmol), AA (0.52 g, 7.23 mmol), RAFT agent TTCA (69 mg, 0.19 mmol), DMF (0.25 g, 3.39 mmol) and ACPA (3.55 mg, 0.013 mmol) were dissolved in 4.0 mL of 1,4-dioxane at room temperature. The mixture solution was then purged with argon for 30 min in an ice bath. It was then immersed into an oil bath at 75 °C to start the polymerization. Samples were periodically withdrawn from the polymerization medium for analyses. To study the kinetics, monomer conversion was determined by ^1H NMR spectroscopy. DMF, which has no influence on the free radical process, was used as internal reference. After 38 h, the flask was quenched in ice bath to terminate the polymerization. After removing all the solvents under reduced pressure, the residues were dissolved in THF and then precipitated into an excess of cold ethyl ether. This purification cycle was repeated nine times. The final polymer was obtained as a yellow viscous solid.

Synthesis of P(APEG-co-BODIPY-co-AA) (RFPC $^-$) by click chemistry. Negative red fluorescent polymer chain P(APEG $_{38}$ -co-BODIPY $_{13}$ -co-AA $_{38}$) was synthesized through the click chemistry between P(APEG-co-ProA-co-AA) (alkynyl PC $^-$) and methylnaphthyl BODIPY azide (BODIPY- N_3). A solution of alkynyl PC $^-$ (80.6 mg, 0.0043 mmol), BODIPY- N_3 (32.5 mg, 0.0471 mmol) and Et_3N (0.22 mg, 0.0021 mmol) in THF (2.13 mL) was degassed by bubbling nitrogen for 10 min. $[(\text{PPh}_3)_3\text{CuBr}]$ (0.79 mg, 0.0009 mmol) was then added and nitrogen was

bubbled into the resulting solution for further 5 min. The clear solution was stirred at ambient temperature for 3 days with monitoring by TLC [20]. After removing all the solvents under reduced pressure, the residues were dissolved in THF and then precipitated into an excess of cold Et₂O, and then washing with water was carried out. The aqueous phase was concentrated in vacuo. The final polymer was obtained as a red viscous solid.

Synthesis of P(APEG-co-AA) (DIBO-PC⁻). DIBO modified negative polymer chain P(APEG₁₄-co-AA₁₄) and P(APEG₅₅-co-AA₅₅) were synthesized in 1,4-dioxane at 75 °C under argon atmosphere. APEG (1.46 g, 3.33 mmol or 7.49 g, 16.49 mmol), AA (0.24 g, 3.33 mmol or 1.19 g, 16.49 mmol), DIBO-TTCA clickable RAFT agent (0.132 g, 0.233 mmol or 0.17 g, 0.300 mmol), DMF (0.135 g, 1.85 mmol or 0.48 g, 6.60 mmol) and ACPA (5.2 mg, 0.018 mmol or 5.6 mg, 0.020 mmol) were dissolved in 3.5 mL or 16.0 mL of 1,4-dioxane at room temperature. The mixture solution was then purged with argon for 30 min in an ice bath. It was then immersed into an oil bath at 75 °C to start the polymerization. Samples were periodically withdrawn from the polymerization medium for analyses. To study the kinetics, monomer conversion was determined by ¹H NMR spectroscopy. DMF, which has no influence on the free radical process, was used as internal reference. After 66.5 hours (or 88 hours), the flask was quenched in ice bath to terminate the polymerization. After removing all the solvents under reduced pressure, the residues were dissolved in THF and then precipitated into an excess of cold ethyl ether. This purification cycle was repeated twice. And the product was purified by tangential flow filtration. The final polymers were obtained as a yellow viscous solid.

Synthesis of P(APEG-co-DMEA) (PC⁺). Positive polymer chain P(APEG₁₂-co-DMEA₁₂) was synthesized in 1,4-dioxane at 75 °C under argon atmosphere. APEG (0.57 g, 1.23 mmol), DMEA (0.18 g, 1.23 mmol), TTCA RAFT agent (0.038 g, 0.105 mmol), DMF (0.037 g, 0.50 mmol) and ACPA (2.0 mg, 0.007 mmol) were dissolved in 2.5 mL of 1,4-dioxane at room temperature. The mixture solution was then purged with argon for 30 min in an ice bath. It was then immersed into an oil bath at 75 °C to start the polymerization. Samples were periodically withdrawn from the polymerization medium for analyses. To study the kinetics, monomer conversion was determined by ¹H NMR spectroscopy. DMF, which has no influence on the free radical process, was used as internal reference. After 4 h, the flask was quenched in ice bath to terminate the polymerization. After removing all the solvents under reduced pressure, the residues were dissolved in THF and then precipitated into an excess of cold cyclohexane. This purification cycle was repeated twice. The final polymer was obtained as a yellow viscous solid.

Preparation of pH sensitive surface

Activated glass slides: The glass slides were immersed in piranha solution (H₂O₂/H₂SO₄=1:3 v/v) for 30 min, washed three times with deionized water, and then dried under a gentle stream of nitrogen gas. (*CAUTION: "Piranha" solution reacts violently with organic materials; it must be*

handled with extreme care.)

Fluorescein LbL film surfaces fabrication: The negatively charged glass slide substrate was alternatively immersed in charged PC⁺ solution (12 mL, 8.2×10^{-5} mol/L, [NaCl] = 0.005 M, pH = 5.4) and DIBO-PC⁻ solution (12 mL, 5.1×10^{-4} mol/L or 5.0×10^{-5} mol/L, [NaCl] = 0.005 M, pH = 5.5) for 20 min. The final layer was prepared by immersing in a stirring fluorescein azide aqueous solution (15 mL, 5.4×10^{-4} mol/L, 5% DMSO) for 2 hours. As a control, the film surface without fluorescein (PC⁺/DIBO-PC⁻) was prepared.

RFPC⁻ + Fluorescein LbL film surfaces fabrication: The negatively charged glass slide substrate was alternatively immersed in charged PC⁺ solution (12 mL, 8.2×10^{-5} mol/L, [NaCl] = 0.005 M, pH = 5.4) and the mixture solution of DIBO-PC⁻ solution and RFPC⁻ for 20 min. The final layer was prepared by immersing in a stirring fluorescein azide aqueous solution for 2 hours. As a control, the film surface without fluorescein (PC⁺/(DIBO-PC⁻ + RFPC⁻)) was prepared.

Modified M9 minimal medium

M9 Minimal Medium is a microbial growth medium used for the culture of *E. coli*. This buffered minimal microbial medium contains only salts and nitrogen, so it is traditionally supplemented with glucose, amino acids and vitamins as needed. We use a Modified M9 minimal medium with a lower concentration of phosphate salts in order to decrease the buffering capacity of the growth medium and thus obtain a more sensitive measure of bacterial growth from the response of the pH sensitive surface. The modified M9 minimal medium contains 5.9 mM Na₂HPO₄·2H₂O, 4.4 mM KH₂PO₄, 3.7 mM NH₄Cl, 1.7 mM NaCl, 2 mM MgSO₄, 0.1 mM CaCl₂, 19.6 μM tryptophan, 20.6 μM thymidine, 0.5% casamino acids, 22.2 mM glucose.

Bacteria culture

Bacteria strain used in this research was *Escherichia coli* (K-12, BW25113). The strain was firstly streaked onto Luria-Bertani (LB) agar plates, and then incubated at 37 °C for overnight. An isolated colony of each strain was picked and inoculated in 5 mL of LB medium. After incubation at 37 °C for overnight (shaking at 350 rpm and 5% CO₂), the bacteria culture was then diluted 1:100 in the modified M9 minimal growth medium. After incubation at 37 °C for 2 hours, the bacteria suspensions were carried out during all experiments.

Bacteria growth detection on different fluorescein LbL surface

Bacteria growth detection: 2 μL bacteria suspensions ($1.1 - 5.5 \times 10^7$ cells/mL) were introduced onto different types of fluorescein LbL surface and a surface without fluorescein as a control.

Meanwhile, 2 μ L fresh modified M9 medium was added onto fluorescein LbL surface as control. These films were placed as coverslip in a Ibidi μ -Dish with wet tissue to control the humidity of the chamber and observed under the epifluorescence microscope at 30 °C. The fluorescence images of each film surface were recorded under time-lapse mode of the microscope during the bacteria growth.

Image analysis: A series of images and the corresponding fluorescence intensity from different film surface during the time-lapse were analyzed using NIH (National Institutes of Health) recommended image processing software, Image J.

References

- [1] Y. Si, C. Gazon, G. Clavier, J. Rieger and R. Méallet-Renault, *et al.* Rapid and accurate detection of *Escherichia coli* growth by fluorescent pH-sensitive organic nanoparticles for high-throughput screening applications. *Biosensors and Bioelectronics*, 2016, **75**, 320-327.
- [2] J. Yin, Y. Hu and J. Yoon. Fluorescent probes and bioimaging: alkali metals, alkaline earth metals and pH. *Chem. Soc. Rev.*, 2015, **44**, 4619-4644.
- [3] A. P. de Silva and R. A. D. D. Rupasinghe. A new class of fluorescent pH indicators based on photo-induced electron transfer. *J. Chem. Soc., Chem. Commun.*, 1985, 1669-1670.
- [4] F. Galindo, M. I. Burguete, L. Vigara, S. V. Luis and D. A. Russell, *et al.* Synthetic macrocyclic peptidemimetics as tunable pH probes for the fluorescence imaging of acidic organelles in live cells. *Angew. Chem.*, 2005, **117**, 6662-6666.
- [5] B. Tang, F. Yu, P. Li, L. Tong and X. Wang, *et al.* A near-infrared neutral pH fluorescent probe for monitoring minor pH changes: imaging in living HepG2 and HL-7702 cells. *J. Am. Chem. Soc.*, 2009, **131** (8), 3016-3023.
- [6] Z. Yang, W. Qin, J. W. Y. Lam, S. Chen and B. Z. Tang, *et al.* Fluorescent pH sensor constructed from a heteroatom-containing luminogen with tunable AIE and ICT characteristics. *Chem. Sci.*, 2013, **4**, 3725-3730.
- [7] L. Albertazzi, B. Storti, L. Marchetti and F. Beltram. Delivery and subcellular targeting of dendrimer-based fluorescent pH sensors in living cells. *J. Am. Chem. Soc.*, 2010, **132** (51), 18158-18167.
- [8] L. Gao, X. Li, S. Wang, S. Li and G. Yang, *et al.* A novel nanogel-based fluorescent probe for ratiometric detection of intracellular pH values. *Chem. Commun.*, 2014, **50**, 8787-8790.
- [9] J. Hu, X. Zhang, D. Wang, X. Hu and S. Liu, *et al.* Ultrasensitive ratiometric fluorescent pH and temperature probes constructed from dye-labeled thermoresponsive double hydrophilic block copolymers. *J. Mater. Chem.*, 2011, **21**, 19030-19038.
- [10] M. H. Lee, J. H. Han, J. H. Lee, N. Park, and J. S. Kim, *et al.* Two-color probe to monitor a wide range of pH values in cells. *Angew. Chem. Int. Ed.*, 2013, **52**, 6206-6209.
- [11] L. Fan, Q. Liu, D. Lu, H. Shi and S. Shuang, *et al.* A novel far-visible and near-infrared pH probe for monitoring near-neutral physiological pH changes: imaging in live cells. *J. Mater. Chem. B*, 2013, **1**, 4281-4288.
- [12] S. Chen, Y. Hong, Y. Liu, C. W. T. Leung and B. Z. Tang, *et al.* Full-range intracellular pH sensing by an aggregation-induced emission-active two-channel ratiometric fluorogen. *J. Am. Chem. Soc.*, 2013, **135** (13), 4926-4929.
- [13] R. Sjöback, J. Nygren and M. Kubista. Absorption and fluorescence properties of fluorescein.

Spectrochimica Acta Part A, 1995, **51**, L7-L21.

[14] M. M. Martin and L. Lindqvist. The pH dependence of fluorescein fluorescence. *Journal of Luminescence*, 1975, **10**, 381-390.

[15] J. Y. Han and K. Burgess. Fluorescent indicators for intracellular pH. *Chem. Rev.*, 2010, **110**, 2709-2728.

[16] D. Andina, J. C. Leroux and P. Luciani. Ratiometric fluorescent probes for the detection of reactive oxygen species. *Chem. Eur. J.*, 2017, **23**, 13549-13573.

[17] A. Horatscheck, S. Wagner, J. Ortwein, B. G. Kim and J. Rademann, *et al.* Benzoylphosphonate-based photoactive phosphopeptide minetics for modulation of protein tyrosine phosphatases and highly specific labeling of SH2 domains. *Angew. Chem. Int. Ed.*, 2012, **51**, 9441-9447.

[18] K. Onizuka, A. Shibata, Y. Taniguchi and S. Sasaki. Pin-point chemical modification of RNA with diverse molecules through the functionality transfer reaction and the copper-catalyzed azide-alkyne cycloaddition reaction. *Chem. Commun.*, 2011, **47**, 5004-5006.

[19] A. Loudet and K. Burgess. BODIPY dyes and their derivatives: synthesis and spectroscopic properties. *Chem. Rev.*, 2007, **107**, 4891-4932.

[20] T. E. Wood and A. Thompson. Advances in the chemistry of dipyrins and their complexes. *Chem. Rev.*, 2007, **107**, 1831-1861.

[21] C. Grazon. Élaboration de nanoparticules fluorescentes à base de BODIPY par polymérisation RAFT en miniémulsion: synthèse, caractérisation et fonctionnalisation de surface. (Cachan, Ecole normale supérieure, 2012).

[22] T. T. Vu, S. Badré, C. Dumas-Verdes, J. J. Vachon and R. Méallet-Renault. New hindered BODIPY derivatives: solution and amorphous state fluorescence properties. *J. Phys. Chem. C*, 2009, **113**, 11844-11855.

[23] B. A. Trofimov, E. Y. Schmidt, N. V. Zorina, E. Y. Senotrusova and G. Clavier. A short-cut from 1-acetyl adamantane to 2-(1-adamantyl)pyrroles. *Tetrahedron Letters*, 2008, **49**, 4362-4365.

[24] N. T. Chandrika, S. K. Shrestha, H. X. Ngo and S. Garneau-Tsodikova. Synthesis and investigation of novel benzimidazole derivatives as antifungal agents. *Bioorg. Med. Chem.*, 2016, **24**, 3680-3686.

[25] G. S. Sun, X. Xu, S. H. Jin, L. Lin and J. J. Zhang. Ovicidal and Insecticidal Activities of Pyripropoxyfen Derivatives with an Oxime Ester Group. *Molecules*, 2017, **22**, 958-968.

[26] B. Y. Zhang, W. D. He, W. T. Li, L. Y. Li and H. Zhang, *et al.* Preparation of block-brush PEG-*b*-P(NIPAM-*g*-DMAEMA) and its dual stimulus-response. *Polymer*, 2010, **51**, 3039-3046.

- [27] V. Ladmiral, G. Mantovani, G. J. Clarkson, S. Cauet and D. M. Haddleton, *et al.* Synthesis of Neoglycopolymers by a Combination of “Click Chemistry” and Living Radical Polymerization. *J. Am. Chem. Soc.*, 2006, **128**, 4823-4830.
- [28] X. D. Wang, R. J. Meier and O. S. Wolfbeis. Fluorescent pH-sensitive nanoparticles in an agarose matrix for imaging of bacterial growth and metabolism. *Angew. Chem. Int. Ed.*, 2013, **52**, 406-409.

General conclusion and perspectives

General conclusion and perspectives

My PhD work aimed at developing fluorescent and sensitive nanostructured polymer films on surface for bacterial detection.

A series of functionalized LbL polymer films were designed for the detection of bacteria: three types of BODIPY-based fluorescent LbL films for the first generation study; Au NPs/GFPC LbL film based on MEF for the sensitive bacteria detection; “Click”-based LbL antibody nanostructured surface for selective bacteria detection and pH sensitive LbL film surface for bacterial growth detection. All these LbL surfaces have proved to be biocompatible to *E. coli*.

At the beginning, first generation of nanostructured fluorescent LbL films were designed and fabricated for bacterial detection (*E. coli*). Among these three pairs of polyelectrolytes (SW, SS and LW FPCs), Short chains and Weak polyelectrolytes (SW FPCs) were chosen as the model for the investigation of the concentration of deposition solution to obtain a homogenous LbL film. Thanks to the LbL assembly, the activated glass slides were able to adsorb FPCs from very low concentration solutions (5.0×10^{-7} M) and gave homogeneous film surfaces. In addition, from the effect of the concentration of the deposition solution on *E. coli* bacteria detection with SW FPC LbL films, we have demonstrated that the *E. coli* bacteria became labeled on the SW FPC film when the concentration of the deposition solution is increased from 5.0×10^{-7} M to 1.3×10^{-4} M. Moreover, the effect of the nature of FPCs on *E. coli* bacteria detection indicated that the *E. coli* bacteria can be detected by the LW FPC LbL film surfaces more effectively under quite low concentration of the FPCs solutions compared to the others (5.0×10^{-7} M). Finally, we have demonstrated that the LW FPC LbL film can not only detect but also kill or inactivate bacteria. Such achievement is likely to lead to future advances for pathogenic bacteria detection.

Based on the emission spectra of FPC LbL films, the fluorescence intensity of the LbL film decreased when the number of bilayers increased. For the purpose of obtaining a bright FPC LbL film, only one layer of fluorescent polymer should be deposited for further study in our work. In addition, we observed that the concentrated polycation containing ammonium groups ($\geq 8.0 \times 10^{-5}$ M) exhibited cytotoxicity. Therefore, polyanion should be assembled as the outermost layer.

The effort to increase the films' sensitivity by using the metal-enhanced fluorescence (MEF) principle was performed. The particle size of spherical gold nanoparticles between 22 nm and 48 nm was deduced from the maximum absorbance which was suitable for the MEF effect. We found out that the density of the adsorbed Au NPs on the glass surface could be adjusted by changing the concentration of the polymer that is used to coat the Au NPs. Based on the conclusion from Chapter 2, the fluorescent weak and long chain polyanion (GFPC⁻) was selected as the fluorophore in this system. Different films containing Au NPs and GFPC⁻ were fabricated and the distance between the Au NPs and GFPC⁻ was easily adjusted by changing the number of

layers with two oppositely charged polymers (PC^+ and PC^-). The surface with Au NPs@2 mg/mL PAH shows larger amplitude in fluorescence variation. Such surface was chosen for further investigations. The spectroscopy study indicated that the presence of Au NPs incorporated into the film have a direct impact on the radiative decay rate of GFPC⁻, achieving a 1.95 increase of the radiative decay rate and a 1.87 increase of the quantum yield. Finally, the Au NPs@2 mg/mL PAH films (Au NPs/4 layers PCs/GFPC⁻, Au NPs/6 layers PCs/GFPC⁻ and Au NPs/8 layers PCs/GFPC⁻ films) were tested for sensor and bioimaging in the presence of bacteria. The results shows that this Au NPs/PCs/GFPC⁻ film works as a sensor for the bacteria detection but there is a need for a more systematic study to gain a better understanding of the detection mechanism. However, if we focus on bacteria imaging on Au NPs/PCs/GFPC⁻ film surfaces both Au NPs/4 layers PCs/GFPC⁻ and Au NPs/8 layers PCs/GFPC⁻ surfaces indicated that *E. coli* can be targeted by GFPC⁻, especially for the Au NPs/8 layers PCs/GFPC⁻ surface. The contrast between the brighter bacteria and the dark background clearly indicates their presence.

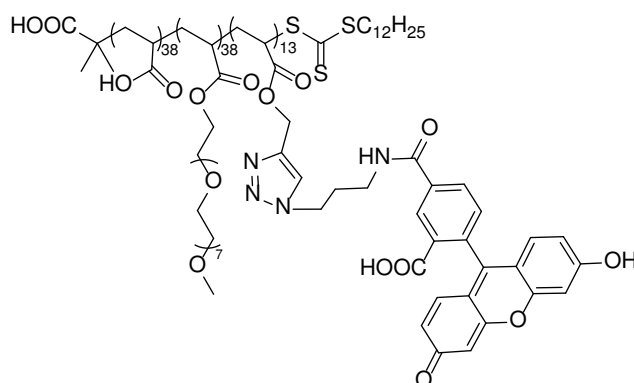
In order to achieve the selectivity of LbL films for bacteria detection, recognition element (antibody) was introduced on the surface of the film. The polyanion and polycation with DIBO functional group were straightforward to synthesize and simply assembled on activated glass slides using electrostatic attraction. Then anti-*E. coli* antibody azide was efficiently introduced on the surface in a single step using strain-promoted azide-alkyne cycloaddition (SPAAC) reaction. The surface passivation was carried out with 20 mg/mL BSA to eliminate the possibility of nonspecific binding on the surface. Subsequently, we tested the anti-*E. coli* antibody surface for *E. coli* detection under different fluidic condition during the washing step, anti-*E. coli* antibody surface shows good stability. In addition, the number of *E. coli* captured on the surface was shown to be dependent on the amount of antibody on the surface. The specificity of anti-*E. coli* antibody surface for *E. coli* is 14 times higher than for *B. subtilis*.

An alternative approach to detect bacterial growth on thin LbL film by introducing pH sensitive fluorophore (fluorescein) was presented. We successfully prepared two single-signal pH sensitive surfaces containing fluorescein and one ratiometric pH sensitive surface combining fluorescein with insensitive BODIPY and tested the bacterial growth detection. Firstly, the different functionalized polyanions (short and long chain DIBO-PC⁻ and red fluorescent polymer) was synthesized. Then three types of pH sensitive surfaces containing fluorescein were prepared using a combination of LbL assembly and copper-free SPAAC click chemistry: a DIBO-SWPC⁻/fluorescein surface containing high fluorescein content; a more stable DIBO-LW PC⁻/fluorescein surface and a ratiometric RFPC⁻/fluorescein surface. The spectroscopic properties, fluorescence image of each surface and pH effect of DIBO-SWPC⁻/fluorescein and ratiometric RFPC⁻/fluorescein surfaces were investigated and the results indicated that: i) the fluorescein was successfully introduced on each surface by click chemistry between the fluorescein azide and DIBO moiety on the LbL surface and ii) its fluorescence intensity changes with pH. Finally, the three pH sensitive surfaces were tested for bacteria growth detection. All of

the surfaces were biocompatible, the number of *E. coli* increased after several hours incubation on each surface. Unfortunately, the decrease in the percentage of the fluorescence intensity of each surface in the absence of *E. coli* was higher than for the surfaces in the presence of *E. coli*. Such preliminary experiments lead us to develop some perspectives:

For the bacterial growth detection, as mentioned earlier there are several approaches.

(1) single-signal pH sensitive surfaces containing fluorescein. In order to improve the fluorescence intensity of fluorescein surface, fluorescein derivative is proposed to introduce into polymer as monomer. The molecule structure is shown below;



(2) Prepare a new ratiometric pH sensitive surface by using another pH sensor (e.g., SNARF-4F (5-(and 6-)-carboxylic acid)) which is a long-wavelength fluorescent pH indicator ($\lambda_{em} = \sim 580$ nm) and the pKa is around 6.4 and couple with green fluorescence BODIPY-based polyanion ($\lambda_{em} = \sim 527$ nm).

The above ratiometric approaches introduce the second fluorescence emission by a “physical mixture”. Therefore, the performance of ratiometric sensing is associated with the experimental conditions and probably leads to inaccurate data acquisition. Another possible strategy is the development of a ratiometric sensor by coupling two fluorescence emissions into a polymer. For example, designing a dual-single polyanion consists of four repeating units: APEG, AA, red BODIPY and fluorescein.

Subsequently, the selectivity antibody functionalized LbL surface can combine with the obtained pH sensitive polymer to give a selective and sensitive LbL surface and test for the sensitive bacterial growth detection in the presence of a smaller number of bacteria (also can test with food and water samples) by combining with microfluidic device. And then drug resistance can test by measuring bacterial growth on the functionalized surface. On the other hand, pathogenic bacteria detection can be designed by using another specific antibody.

Acknowledgements

The past over four years in the laboratory of PPSM, LBPA and ISMO have been impactful and special experience in my life. I want to express my great appreciation to these who have helped and supported me so much during my PhD study.

First and foremost, I would like to thank my supervisors: Dr. Gilles Clavier, Prof. Rachel Méallet-Renault and Dr. Bianca Sclavi for giving me the opportunity to pursue my research in their laboratories. They always have lots of ideas for my PhD research, are always very patient to help me understand the goal and always ready to give suggestions for the tricky problems in the study. They also help me so much for the administrative procedure throughout my PhD studies and offer me many opportunities to participate in conferences. Their knowledge in many areas has always broadened my horizon and the way to consider problems impressed me. Their character and personality indeed affect me. It is their great patient, encouragement and all kinds of help, which made this dissertation possible.

For this dissertation I would like to thank my reviewers: Prof. Eléna ISHOW, Dr. Andrey KLYMCHENKO for their time to read my dissertation and helpful comments. I would also like to thank the jury members Prof. Marie ERARD and Prof. Donal O'SHEA of my oral defense, for their time and insightful questions, and for all the suggestions.

I want to express my deeply thanks to Dr. Yang SI, who helps me to get familiar with the lab and Cachan, taught me for the biological experiments and also recommended the good restaurant to me. I also want to thank for Rachael Taitt's nice work in the Chapter 3 and she could always give me some ideas to improve this part of work after the discussion. I am very grateful to Jean-Frederic Audibert, who was very experienced in microscope and he provides great assistant for my microscopy experiments, thanks to his useful discussion, patience and inspiration. I would like to express my great thanks to Dr. Jérémy Malinge, who taught me how to do the organic synthesis, in addition, always gave me very useful suggestions and help me solve the problems during my synthesis. I also want to thank Dr. Qui Xuan, who is always very patient to help me analyze NMR spectra, give me very useful suggestions for my synthesis. And always share the funny experiences with me. I am very thankful to Yangyang Qu for the fruitful discussions about experiences, synthesis and my PhD work and always willing to help me. I am grateful for the preparation of some polymers from Dr. Roland Geagea. Special thanks go to Dr. Naresh Kumar for the guidance for the synthesis and let me obtain my first polymer. I am truly grateful Dr. Alexis Depauw for all the help during my synthesis and always make our lab clean. Thanks to Dr. Stéphane Maisonneuve for the NMR spectra and HPLC measurements and always very friendly discussion. I also want to thank Arnaud Brosseau for the fluorescence lifetime measurement. Special thanks go to Rasta Ghasemi in IDA for Scanning Electron Microscopy

experiment and sputter coating.

Furthermore, I would like to express my thanks to Dr. Christian Marlière for the AFM measurement and Dr. Karine Steenkeste for the training of confocal microscope in ISMO. Thanks Gabriela Moran so much for sharing plenty of nice time, knowledge and interesting and fruitful discussion with me. I want to thank Dr. Qing Zhang for the guidance in the biological experiments and helpful discussion in biology in LBPA.

I would like to acknowledge all the members in PPSM: Dr. Laurent Galmiche, Dr. Fabien Miomandre, Prof. Pierre Audebert, Dr. Clemence Allain, Dr. Galina Dubacheva, Dr. Isabelle Leray, Dr. Cédric Mongin, Dr. Jean-Pierre Lefevre, Prof. Keitaro Nakatani, Dr. Rémi Metivier, Dr. Guillaume Laurent, Prof. Joanne Xie, Dr. Nicolas Bogliotti and Prof. Robert Pansu who helped me during my whole stay in Cachan. Thank you for your helpful suggestions and constant encouragement. I would like to express my thanks to Mrs. Andrée Husson and Mr. Christian Jean-Baptiste for their administrative help. I appreciate Mr. Jacky Fromont for installing the software and handling my computer problems.

Over the past years, I would like to thank all the former and current members of the PPSM: Jia, Na for kindly help when I just arrived in France, Yuan, Claire, Corentin, Charlotte, Marine, Paul, Clarisse, Chaoqi, Antonio, Zhenyu, Etienne, Leticia, Linh, Yahdi, Luca, Tuan... I appreciate your warm help and kind assistance.

My deep gratitude goes to Prof. Xike TIAN for the recommendation of the PhD position and constant supporting and helping during my PhD. I also want to thank all my dear beloved friends in my life: Longlong Ma, Ye Zhang, Huilin Tu, Yan Long, Yufei Hao for always listening and sharing anytime.

Nothing is more important for me than the members of my family. I would like to express my deepest gratitude to my family, who always respect my decisions, always love me and never pressure me to get married.

I also want to thank myself for the passion and constant love for the PhD research during these four years. And all of the experiences I got from my experiments, the affection of the French culture and the knowledge in history, culture and science. In addition, the good international relationship between China and France that creates a friendly atmosphere for our studying and research.

25-07-2018

Cachan

Titre : Elaboration de nouveaux films fluorescents par dépôt couche par couche (LbL) et fonctionnalisation pour la détection sensibles de bactéries.

Mots clés : film couche par couche; polymère; fluorescence; BODIPY; detection bacterienne

Résumé : Les antibiotiques ont été utilisés pour le traitement des infections bactériennes depuis plus de 70 ans, sauvant des millions de vies. Cependant, leur mauvaise et sur-utilisation ont conduit à l'émergence de la résistance bactérienne. Outre le développement de nouvelles familles d'antibiotiques, la détection rapide et sensible de bactéries est très importante pour le diagnostic médical. Les polymères fluorescents représentent un grand potentiel, car ils sont faciles à fonctionnaliser, synthétiser et greffer. Les films sont plus pratiques, faciles à manipuler et peuvent être réutilisés, ce qui n'est pas le cas des méthodes de détection en solution. L'objectif de ce travail est de développer un film de polymère nanostructuré fluorescent et sensible sur des surfaces de verre pour la détection bactérienne. Sur la base de la méthode de polymérisation radicalaire par transfert de chaîne réversible par addition-fragmentation (RAFT), trois types de polyélectrolytes fluorescents à base de BODIPY (FPC) ont été synthétisés : des chaînes relativement courtes à caractère polyélectrolyte faible (SW FPC), des chaînes courtes à caractère polyélectrolyte fort (SS FPC) et enfin des chaînes longues à caractère polyélectrolyte faible (FPC LW). Les films FPC LbL ont été élaborés sur des lames en verre par interaction électrostatique. Les propriétés photophysiques et de surface des FPC LbL ont été contrôlées en ajustant les conditions de dépôt. Les films FPC LbL à base de BODIPY ont été utilisés comme dispositif de première génération pour la détection de *E. coli*.

Dans l'étape suivante, la sensibilité des films a été augmentée en utilisant le principe de fluorescence exaltée par plasmon (Metal Enhanced Fluorescence MEF). Un film LbL - MEF a été préparé et testé pour la détection de bactéries. Des nanoparticules d'or sphériques (Au NPs) ont été synthétisées et recouvertes de poly(chlorhydrate d'allylamine) (PAH). Le FPC LW a été sélectionné comme couche fluorescente. Différents films contenant des Au NPs et LW FPC⁻ ont été fabriqués. La distance

entre les NPs Au et LW FPC⁻ a été ajustée par l'ajout de deux polymères de charge opposée (PC⁺ et PC⁻). Les deux surfaces de AuNP / 4 couches PC / LW FPC⁻ et Au NPs / 8 couches PC / LW FPC⁻ ont montré que *E. coli* peut être ciblée par LW FPC⁻.

La sélectivité des films LbL a été ajoutée en introduisant un anticorps comme site de reconnaissance spécifique. Le polyanion et le polycation avec le groupe fonctionnel 4-dibenzocyclooctynol (DIBO) ont été assemblés sur des lames de verre activées. L'anticorps anti-*E. coli* a ensuite été introduit sur la surface en une seule étape via la réaction de cycloaddition azide-alcyne (SPAAC). Le nombre d'*E. coli* capturées dépend de la concentration d'anticorps sur la surface. La surface a montré une sélectivité significative pour *E. coli*, comparée à *B. subtilis*.

La croissance bactérienne peut être détectée sur un film mince LbL en introduisant un fluorophore sensible au pH (fluorescéine). En effet, la croissance des bactéries est souvent associée à une diminution du pH du milieu due à une libération de métabolites acides. Nous avons préparé avec succès différents types de films LbL sensibles au pH. Dans un premier temps, la synthèse de différents polyanions fonctionnalisés (chaîne courte et longue de DIBO-PC et polymère fluorescent rouge) a été achevée. Ensuite, trois types de surfaces sensibles au pH contenant de la fluorescéine (DIBO-SWPC⁻ / fluorescéine, DIBO-LW PC⁻ / fluorescéine et ratiométrique RFPC⁻ / fluorescéine) ont été préparés sur la base d'assemblage LbL et de chimie click. Enfin, trois surfaces sensibles au pH ont été étudiées pour la détection de la croissance des bactéries. Toutes les surfaces étaient biocompatibles, le nombre de *E. coli* augmentait même après plusieurs heures d'incubation sur chaque surface. La détection par le changement de fluorescence est en cours de développement.

Title : Elaboration of new layer-by-layer (LbL) fluorescent thin films and their functionalization for the sensitive detection of bacteria

Keywords : layer-by-layer film; polymer; fluorescence; BODIPY; bacteria detection

Abstract : Antibiotics have been used for the treatment of bacterial infections for over 70 years, saving millions of lives. The current antibiotic resistance crisis has been attributed to the overuse and misuse of these medications. Therefore, the prevention of infection transmission by the rapid and sensitive detection of antibiotic resistant strains is needed in managing this crisis. Fluorescent polymers show great potential for bacteria detection, because they are easy to functionalize, reproduce and graft. Compared with the methods used for bacterial detection in liquid, bacterial detection on a film surface is more convenient, easier to handle and is applied in devices that can be easily reused. The goal of my PhD work is to develop fluorescent and sensitive nanostructured polymer films on surfaces for bacterial detection.

Three types of BODIPY-based fluorescent polyelectrolytes (FPC) with different features were synthesized based on reversible addition-fragmentation transfer (RAFT) polymerization: relatively Short chains and Weak polyelectrolytes (SW FPCs), Short chains and Strong polyelectrolytes (SS FPCs) and Long chains and Weak polyelectrolytes (LW FPCs). FPC LbL films were fabricated on activated glass slides by means of electrostatic attraction. The photophysical and surface properties of FPC LbL films were easily controlled by adjusting the deposition conditions.

The following step aimed at increasing the films' sensitivity by using the metal-enhanced fluorescence (MEF) principle. A MEF based LbL film was prepared and tested for bacteria detection. Spherical gold nanoparticles (Au NPs) were synthesized and coated with poly(allylamine hydrochloride) (PAH). The LW FPC- was selected as the fluorescent layer. Different films containing Au NPs and LW FPC⁻ were fabricated and the distance between the Au NPs and LW FPC⁻ was adjusted by changing the numbers of layers with two oppositely charged polymers (PC⁺ and PC⁻). Both Au NPs/4 layers PCs/LWFPC⁻ and Au NPs/8 layers PCs/LWFPC⁻ surfaces indicated that *E. coli* can be detected by LW FPC⁻.

The selectivity of LbL films was added by introducing an antibody on the surface of the film to provide specific recognition of a chosen bacterial strain. This LbL surface achieved a rapid, effective and specific detection of *E. coli* bacteria. The polyanion and polycation with a 4-dibenzocyclooctynol (DIBO) functional group were assembled on the activated glass slides and an anti-*E. coli* antibody containing an azide group was efficiently introduced on the surface in a single step based on the azide-alkyne cycloadditions (SPAAC) reaction. The number of *E. coli* captured on the surface was shown to be dependent on the amount of antibody on the surface. The anti-*E. coli* antibody surface showed significant selectivity for *E. coli*, compared with *B. subtilis*.

An alternative approach is to detect bacterial growth on thin LbL film by introducing pH sensitive fluorophore (fluorescein). The growth of bacteria is often associated with a decrease in pH of the growth medium due to a release of acidic metabolites. Different types of pH sensitive LbL film were prepared and tested for the detection of bacterial growth. Firstly, the synthesis of different functionalized polyanions (short and long chain of DIBO-PC⁻ and red fluorescent polymer) was carried out. Three types of pH sensitive surfaces containing fluorescein (DIBO-SWPC⁻/fluorescein, DIBO-LW PC⁻/fluorescein and ratiometric RFPC⁻/fluorescein surfaces) were prepared based on the combination of LbL assembly and copper-free click chemistry. Finally, three pH sensitive surfaces were studied for bacteria growth detection. All the surfaces were shown to be biocompatible, the number of *E. coli* increased after several hours of incubation on each surface, as detected by brightfield microscopy imaging. The application for the fluorophore-dependent detection of bacterial growth remains to be developed.

